UNIVERSITY OF CRETE

Department of Chemistry

Development of Photosensitive Nanostructured Hybrid Devices

by

Minas M. Stylianakis

A dissertation submitted to the faculty of

The University of Crete

In fulfillment of the requirements for the degree of

Doctor of Philosophy

In Chemistry

Heraklion 2015

The present dissertation has been written under the direction of

Professor Spiros H. Anastasiadis

and has been approved by:

1. Spiros H. Anastasiadis

2. Emmanuel Koudoumas

3. Pantelis N. Trikalitis

4. Emmanuel Kymakis

5. Athanassios G. Coutsolelos

6. Nikos Tagmatarchis

7. Benoit Loppinet

European Union
European Social Fund
OPERATIONAL PROGRAMME
EDUCATION AND LIFELONG LEARNING
investing in knowledge society
MINISTRY OF EDUCATION, LIFELONG LEARNING AND RELIGIOUS AFFAIRS
MANAGING AUTHORITY
NSRF 2007-2013
programme for development
EUROPEAN SOCIAL FUND
Co- financed by Greece and the European Union

Dedicated to the memory of

Prof. John A. Mikroyannidis

ABSTRACT OF THE DISSERTATION

Development of Photosensitive Nanostructured Hybrid Devices

By ***Minas M. Stylianakis***

The extraordinary mechanical, electric and optical properties of graphene and its derivatives, along with the need for low-cost and solution-processed materials, ideal for electronic applications, have experienced particular attention in global scientific research, over the past decade. Graphene-based nanostructured materials appear to be attractive alternatives in a range of new energy devices, including organic photovoltaic cells, lithium batteries, fuel cells and supercapacitors.

In organic photovoltaic applications, graphene-based materials have been introduced as transparent conductive electrodes (TCE), buffer layers, as well as electron donor/acceptor materials to improve the architecture and the photovoltaic performance, replacing the conventional existing materials. Therefore, new insights into "graphene chemistry" have been rapidly developed, leading to novel graphene derivatives, by innovative synthetic routes and new fabrication methods. Graphene-based OPVs seem to be perspectives, due to their promising and appealing properties, reaching to comparable or higher efficiencies to the traditional OPVs, which are summarized to an exponentially growing literature.

In this thesis, novel graphene-based materials have been designed and synthesized for bulk heterojunction (BHJ) photosensitive nanostructured hybrid devices development. The resulting graphene-based materials have been incorporated into the photoactive layer of OPV devices and have been applied as electron-acceptor materials, replacing the most used fullerene derivative $PC_{71}BM$ and moreover have been used as electron-cascade donor materials, constituting the third component to a ternary organic blend, along with polymer/fullerene composites. Finally, the structures of the graphene-based materials used, as well as the optimization of the fabricated OPVs have been evaluated by utilizing various spectroscopy and microscopy analyses, alongside with complementary photovoltaic measurements.

ΠΕΡΙΛΗΨΗ ΤΗΣ ΔΙΑΤΡΙΒΗΣ

Ανάπτυξη Φωτοευαίσθητων Νανοδομημένων Υβριδικών Διατάξεων

*Από το **Μηνά Μ. Στυλιανάκη***

Οι εξαιρετικές μηχανικές, ηλεκτρικές και οπτικές ιδιότητες του γραφενίου και των παραγώγων του, σε συνδυασμό με την ανάγκη για εξεύρεση φτηνών υλικών που μπορούν να επεξεργαστούν σε διάλυμα, ιδανικά για ηλεκτρονικές εφαρμογές, έχουν συγκεντρώσει την προσοχή της παγκόσμιας επιστημονικής έρευνας, κατά την τελευταία δεκαετία. Νανοδομημένα υλικά με βάση το γραφένιο φαίνεται ότι μπορούν να αποτελέσουν ελκυστικά εναλλακτικά υλικά σε μια σειρά από νέες ενεργειακές συσκευές, συμπεριλαμβανομένων των οργανικών φωτοβολταϊκών διατάξεων, των μπαταριών λιθίου, των κυψελών καυσίμου και των υπερπυκνωτών.

Στις οργανικές φωτοβολταϊκές διατάξεις, τα υλικά με βάση το γραφένιο έχουν εισαχθεί ως διάφανα αγώγιμα ηλεκτρόδια, ρυθμιστικές στιβάδες μεταφοράς οπών ή/και ηλεκτρονίων, αλλά και ως υλικά δότες/δέκτες ηλεκτρονίων, ώστε να βελτιώσουν την αρχιτεκτονική και τη φωτοβολταϊκή απόδοση τους, αντικαθιστώντας τα υπάρχοντα συμβατικά υλικά. Ως εκ τούτου, νέες ιδέες αναπτύχθηκαν γρήγορα στη ‘’Χημεία του Γραφενίου’’, οδηγώντας σε νέα παράγωγα του γραφενίου, με καινοτόμες συνθετικές πορείες και μεθόδους παρασκευής. Τα οργανικά φωτοβολταϊκά με βάση το γραφένιο δείχνουν να έχουν προοπτική εξέλιξης, χάρη στις υποσχόμενες και ελκυστικές ιδιότητές τους, αποδίδοντας εξίσου ή και υψηλότερα με τα κλασικά οργανικά φωτοβολταϊκά, όπως συνοψίζεται σε μια εκθετικά αυξανόμενη βιβλιογραφία.

Στην παρούσα διατριβή, συντέθηκαν καινοτόμα υλικά με βάση το γραφένιο, για την ανάπτυξη αποδοτικών φωτοευαίσθητων νανοδομημένων υβριδικών διατάξεων, τύπου διεσπαρμένης ετεροεπαφής. Τα υλικά που συντέθηκαν, με βάση το γραφένιο, εισήχθησαν μέσα στη φωτοενεργή στιβάδα των οργανικών φωτοβολταϊκών διατάξεων και αποτέλεσαν τα υλικά δέκτες ηλεκτρονίων, αντικαθιστώντας το πιο συνηθισμένο παράγωγο φουλερενίου, το $PC_{71}BM$. Επίσης, χρησιμοποιήθηκαν ως βοηθητικά υλικά δότες, για τη σύζευξη των ενεργειακών επιπέδων ροής των ηλεκτρονίων, αποτελώντας τον τρίτο παράγοντα σε ένα τριμερές οργανικό μείγμα, μαζί με σύνθετα

πολυμερούς/φουλερενίου. Τέλος, οι δομές των υλικών με βάση το γραφένιο που συντέθηκαν, όπως και η βελτιστοποίηση των οργανικών φωτοβολταϊκών διατάξεων που κατασκευάστηκαν, πιστοποιήθηκαν με τη χρήση διαφόρων φασματοσκοπικών και μικροσκοπικών αναλύσεων, παράλληλα με συμπληρωματικές φωτοβολταϊκές μετρήσεις.

Acknowledgements

I would like to express my sincere gratitude to my PhD supervisor Prof. Spiros H. Anastasiadis, for his continuous support, guidance, and collaboration during my PhD dissertation. Moreover, I would like to thank Prof. Emmanuel Koudoumas, for writing the proposal for my fellowship of Heraclitus II and Prof. Pantelis N. Trikalitis for the excellent cooperation as a member of my three member advisory committee.

I would also like to express my appreciation for the fellow-students and friends that we were working side-by-side at the Lab of Nanomaterials & Organic Electronics (NANO) at TEI of Crete, over the past three years, for all the support and creating a joyful environment to work in. Special thanks to George Kakavelakis, Dimitris Konios, Anna Orfanoudaki, Eva Vasilaki and Pavlos Tzourbakis. At this point, I would like to make a special mention of two exceptional friends-collaborators. I feel very lucky to have worked with George Spyropoulos and George Viskadouros, for their great friendship, support, help and suggestions during the entire process. I enjoyed the discussions about the research projects and beyond. I'm also really grateful to my family and my friends for their continuous support and encouragement.

My deepest gratitude goes to Prof. Emmanuel Kymakis and Dr. Emmanuel Stratakis for their friendship, collaboration and guidance. Their enthusiasm and optimism, as well as their ideas have made my research experience truly enjoyable and were the main reasons that I have returned to Heraklion and joined the Nanomaterials & Organic Electronics (NANO) Group, five years ago.

Finally, this thesis is dedicated to the memory of Prof. John A. Mikroyannidis, who died just a few months ago. I have no words to express my gratefulness to the man who had made me fall in love with chemistry. He has been a great mentor academically, professionally and personally, providing me with invaluable advice over the years, as well as freedom and support to pursue my research interests.

This research has been cofinanced by the European Union (European Social Fund, ESF) and Greek national funds through the Operational Program "Education and Lifelong Learning" of the National Strategic Reference Framework (NSRF) Research Funding Program: Heracleitus II. Investing in knowledge society through the European Social Fund.

Table of Contents

Chapter 2

Chapter 3

Chapter 4

Chapter 5

Chapter 6

List of tables

List of figures

Chapter 1

Chapter 2

Chapter 3

Figure 7. Field-emission scanning electron microscopy (FE-SEM) images of GO-PITC in (a) plane tree leaves, (b) wrapped graphene-based sheets, and (c) AFM image of GO-PITC.

Figure 8. Normalized UV-vis absorption spectra of P3HT (red line) and of the P3HT:GO-PITC (black line) composite in thin films onto quartz substrates.

Figure 9. Photoluminescence (PL) spectra of P3HT (red line) and P3HT:GO-PITC 20% (black line) in thin film on a Si substrate at an excitation wavelength of 325 nm.

Figure 10. AFM images of (a) P3HT and (b) P3HT:GO-PITC 20% thin films.

Figure 11. (a) Schematic of the photovoltaic device with P3HT:GO-PITC thin film as the active layer and the structure ITO/PEDOT:PSS(30 nm)/P3HT:GO-PITC(110 nm)/Al(80 nm). (b) Experimental J−V curves of the photovoltaic devices based on P3HT (red curve) and P3HT:GO-PITC composites (blue curve, 10 wt %; black curve, 20 wt %) after post fabrication thermal annealing at 160 °C for 20 min.

Chapter 4

Figure 1. (Top) The chemical synthesis of solution-processed GO-EDNB by functionalization of GO and (bottom) presentation of pure GO and GO-EDNB solutions in *o*-DCB after a week. The GO-EDNB (brown) remains as solution, while the pure GO (gray) precipitates.

Figure 2. FT-IR spectra of pure GO and GO-EDNB in transmission mode.

Figure 3. Normalized UV–vis absorption spectra of pure GO and GO-EDNB in solid thin film prepared by spin-coating on quartz substrate.

Figure 4. (a) Normalized UV-Vis absorption spectra of P3HT and P3HT:GO-EDNB blend in *o*-DCB solution (10^{-5} M) and (b) in thin film on a quartz substrate.

Figure 5. PL spectra of P3HT and P3HT:GO-EDNB thin films on Si.

Figure 6. Raman spectra of GO and GO-EDNB. The inset shows the 2D peak of GO-EDNB.

Figure 7. The TGA graphs of GO and GO-EDNB obtained under inert atmosphere of N_2, with heating rate 10 °C/min. The inset displays the TGA graph of the initial EDNB.

Figure 8. X-ray diffraction patterns from GO and GO-EDNB samples.

Figure 9. SEM images of unpurified GO-EDNB a) in a graphene neurons structure, b) and c) wrapped graphene-based sheets, (d) a vermiculite-like structure; SEM and (e) AFM images of purified GO-EDNB graphene sheets.

Figure 10. Dependence of the most probable sheet size (a) and maximum sheet thickness (b) on the number of purification steps.

Figure 11. GO-EDNB sheet size distribution following a series of five purification steps. Sheet sizes were determined using a number of SEM and AFM images.

Figure 12. AFM image of a single GO-EDNB sheet.

Figure 13. (a) Schematic of the device with P3HT/GO-EDNB thin film as the active layer and the structure ITO/PEDOT:PSS (30 nm)/P3HT:GO-EDNB (110 nm)/Al (80 nm) (b) J–V curves of PV devices based on P3HT:GO-EDNB active layer with different graphene content (5, 10, and 15 wt%) after annealing at 160 ^{o}C for 20 min.

Chapter 5

Figure 1. Schematic display of the spontaneous acylation of graphene oxide and (Bottom) the spontaneous grafting of ethylenediaminedinitrobenzoyl (EDNB), induced by pulsed laser.

Figure 2. Schematic of the experimental setup used for the photochemical synthesis of LGO-EDNB.

Figure 3. The Proposed Reaction Mechanisms of (a) Acylation (b) Amide bond Mechanism.

Figure 4. (a) XPS survey spectra of GO and LGO-EDNB; (b) high-resolution XPS C1s spectra of GO (top) and LGO-EDNB (bottom); (c) high-resolution N1s XPS spectra.

Figure 5. (a) The ^{1}H NMR spectra in DMSO d_6 solution of GO-EDNB. The solvent peak is denoted by an asterisk. The spectrum displays upfield signals at 9.06 and 8.92 ppm assigned to the aromatic protons ortho and meta to nitro groups, labeled ‘‘c’’ and ‘‘b’’, respectively. The aliphatic protons ‘‘a’’ gave signals at 4.00 ppm, associated with the alkyl -CH_2-CH_2- linking groups. (b) Fourier transform infrared (FT-IR) spectra of LGO-EDNB. The spectrum of the functionalized dinitro graphene-based material exhibits two new bands at 1543 and 1345 cm^{-1}, which are characteristic of the symmetric and asymmetric stretching modes of the NO_2 group. The observed lowering of the OH characteristic peak at ~3400 cm^{-1} indicates reduction of the initial GO lattice.

Figure 6. Raman spectra of GO (black) and LGO-EDNB (red).

Figure 7. (a) GO reduction and functionalization levels as a function of Np; (b) the evolution of the HOMO and LUMO levels as a function of irradiation time. The HOMO-LUMO levels of GO-EDNB are also shown for comparison.

Figure 8. The absorption UV-vis spectra of LGO-EDNB as a function of irradiation time.

Figure 9. The voltammetric behavior of LGO-EDNB (prepared at 10mw, 100 pulses) in CH_3CN using 0.1 M Tetrabutylammonium hexafluorophosphate ($TBAPF_6$) as the electrolyte, at a scan rate of 10 mV s^{-1}, between the potential sweep window of 1.7 V to −1.7 V. A well-defined reversible reduction peak was observed at −1.0 V (R1) and −0.8 V (R2), while an oxidation peak was appeared at 0.7 V.

Figure 10. The HOMO-LUMO levels separation of LGO-EDNB as a function of irradiation time. The corresponding evolution of the N_{1s}/C_{1s} intensity ratio is also

shown. The bandgap, decreases with increased exposure time most likely due to a synergetic effect of the EDNB-functionalization and the partial reduction processes.

Figure 11. The TGA graphs of LGO-EDNB, prepared using Np=10 pulses, and GO-EDNB obtained under inert atmosphere of N_2, with heating rate 10 °C/min.

Figure 12. (a) Schematic illustration of BHJ OSC device with LGO-EDNB as the electron acceptor (b) The energy level diagram depicting the relevant energy levels under flat conditions of all materials used in OSCs c) J-V characteristics of OSCs with different LGO-EDNB concentrations.

Figure 13. (a) Dependence of the most probable sheet size on the number of purification steps; (b) LGO-EDNB sheet size distribution following a series of five purification steps. Sheet sizes were determined using a number of TEM a representative of which is shown in Figure 13.

Figure 14. Representative TEM image of LGO-EDNB flakes.

Chapter 6

Figure 1. Schematic representation of the chemical synthesis.

Figure 2. Characterization of GO (black line) and GO-TPP (red line). a) FT-IR spectra, b) UV-vis spectra including the UV-vis spectrum of TPP-NH_2, c) Room-temperature fluorescence spectra of isoabsorbing (A = 0.24) DMF solutions of TPP-NH_2 (blue line) and GO-TPP (red line) after excitation at 419 nm and d) Raman spectra.

Figure 3. a) Cyclic voltammetry curve of GO-EDNB in CH_3CN using 0.1 M Tetrabutylammonium hexafluorophosphate (TBAPF6) as the electrolyte, at a scan rate of 10 mV s^{-1}. b) Energy levels diagram of photovoltaic device components referenced to the vacuum level.

Figure 4. Thermogravimetric Analysis. TGA curves of GO (black) and GO-TPP (red).

Figure 5. a) Schematic of the photovoltaic device with PCDTBT:PC_{71}BM:GO-TPP thin film as the active layer and the structure ITO/PEDOT:PSS/PCDTBT:PC_{71}BM:GO-TPP/TiO_x/Al (top). b) Experimental *J*−V curves of the photovoltaic devices based on PCDTBT:PC_{71}BM (black curve) and PCDTBT:PC_{71}BM:GO-TPP composites (red curve, 0.1%; green curve, 0.3%); blue curve, 0.5%).

Preface and Thesis Layout

When the global warming and depletion of common energy supplies, such as fossil fuels started threatening the balance of human life, great attention was driven towards the renewable (alternative) energy sources. Among number of alternative sources, such as wind energy, hydroelectric energy, biomass and geothermal energy, solar energy has the highest amount potentially available on earth. A very small fraction of sun power (less than 0.02 %) reaching the earth surface can cover the whole energy demand of the world. Yet, by the end of year 2008, solar technology based sources have been providing only 0.1 % of all the energy consumed by man according to Renewable Energy Policy Network (REN21) report.

Moreover, the increasing demand for energy consumption and the limited energy resources are the two main driving forces for the exploration of new energy-harvesting processes, among which new materials, especially nanomaterials, have been investigated in clean energy applications such as solar cells, solar fuels, lithium-ion batteries (LIBs) and supercapacitors.

Graphene, a 2D sheet composed of sp^2-bonded single-layer carbon atoms with the honeycomb lattice structure, has attracted great research interest in physics, chemistry, materials science, etc. Until now, the electrical, optical, mechanical, thermoelectric, and magnetic properties of graphene have been intensively studied. In order to mass produce high-quality 2D graphene nanosheets for potential applications, various strategies have been developed.

The main goal of this thesis is to design, as well as to synthesize novel, innovative solution-processed graphene-based materials, which can combine the extraordinary properties of graphene, along with some additional optical, mechanical and photovoltaic properties of the linking molecules, for photosensitive nanostructured hybrid devices fabrication; highly efficient organic photovoltaics (OPVs). The studies presented in this thesis tackle the synthesis of graphene-based electron acceptor materials as potentials for the fullerene derivative (PCBM) replacement, into the active layer of an OPV device. In addition, a brief description of the corresponding synthetic routes, step by step, is stated, followed by a detailed report for the OPV devices

fabrication methods, including the preparation and the introduction of the blends into the OPV device for the active layer fabrication.

In the following Chapter 1 is described the theoretical background that is most relevant to the contents of this thesis. The production of graphene and its derivatives by various methods, as well as their properties, are briefly reported. It is aimed to introduce the reader to "the world of graphene", analyzing each method for graphene production separately, and comparing their benefits and disadvantages.

In Chapter 2, several organic reactions are presented which have been applied on graphene up to now affording a large number of derivatives. The organic nature of graphene, allows its functionalization in order to improve the properties that make graphene and graphene-based materials ideal for organic electronics. Covalent, non-covalent and doping reactions take place between graphene and polymers, small molecules as well as gazes, respectively. It is worth mentioned that all these reactions affect the solubility, the light harvesting, the band gap tuning, the charge transportation, the conductivity and the transmittance, which are important factors in the field of organic electronics.

The main focus of the experimental work is described in Chapters 3, 4, 5, 6. Briefly, in Chapter 3 a novel graphene-based material, named GO-PITC is synthesized by the covalent attachment of graphene oxide with the small molecule phenyl isothiocyanate (PITC) by taking advantage of the functional carboxyl groups of graphene oxide. GO-PITC was used as the electron acceptor material in poly-(3-hexylthiophene) (P3HT) bulk heterojunction photovoltaic devices, yielding a power conversion efficiency of 1.02 %.

Chapter 4 describes the synthetic route, by chemical way, of a very promising graphene-based material, named GO-EDNB. The small molecule ethylene-dinitro-benzoyl (EDNB) is covalently linked around to the main graphene oxide sheet via an amide bond. It brings two nitro groups, which make GO-EDNB a strong electron acceptor material and was used as the electron acceptor material in poly-(3-hexylthiophene) (P3HT) bulk heterojunction photovoltaic devices to significantly improve the performance, instead of $PC_{60}BM$, yielding a power conversion efficiency of ~1 %.

The fabrication of the most efficient graphene-based electron acceptors to date, is situated in Chapter 5. The synthesis of the above mentioned graphene-based molecule GO-EDNB was restated using a laser beam for a fast and facile photochemical synthetic route, yielding LGO-EDNB. Moreover, the energy levels of LGO-EDNB can be readily tuned upon fine-tuning of the bandgap, since it is directly related to the irradiation dose applied during the synthesis process. LGO-EDNB was also utilized as the electron acceptor material in organic bulk heterojunction solar cells (OSCs) with the poly(2,7-carbazole) (PCDTBT) as the electron donor, achieving a PCE of 2.41 %.

Chapter 6 includes a different approach in the field of OPVs. The synthesis of a porphyrin-graphene oxide hybrid material (GO-TPP) is discussed and was incorporated in the photoactive layer of bulk heterojunction organic solar cells, as electron-cascade donor material, to fabricate highly efficient ternary blend polymer solar cells, blended with PCDTBT and $PC_{71}BM$. The highest resulting PCE was 5.93 %.

The last Chapter of this dissertation refers the concluding remarks and suggested future work.

Chapter 1

1.1 Introduction

Carbon materials are the leading thread in the unfolding story of nanotechnology, during the last couple of decades. The hybridization of carbon-based materials occurs between 2s and 2p orbitals to form sp^n state, where n is the number of 2p orbitals mixed with the 2s orbital. The ability to exhibit sp^n hybridization gives rise to the formation of a wide variety of molecular and crystalline structures with varied chemical and physical properties. The sp^2 hybridized carbon systems are particularly interesting because carbon molecules with every dimensionality (0 to 3) can be formed. In fact, carbon is the only element in the periodic table which has allotropes from zero to three dimensions (Figure 1).[1] While graphite, a three dimensional sp^2 carbon allotrope, has been known for centuries,[2] discovery of the fullerenes (0D),[3] carbon nanotubes (1D)[4] and graphene (2D)[5] has significantly contributed to shaping the route that science at the nanoscale has taken. These materials have unique and extraordinary optical, electrical, mechanical, and thermal properties arising from their dimensionality and structure.

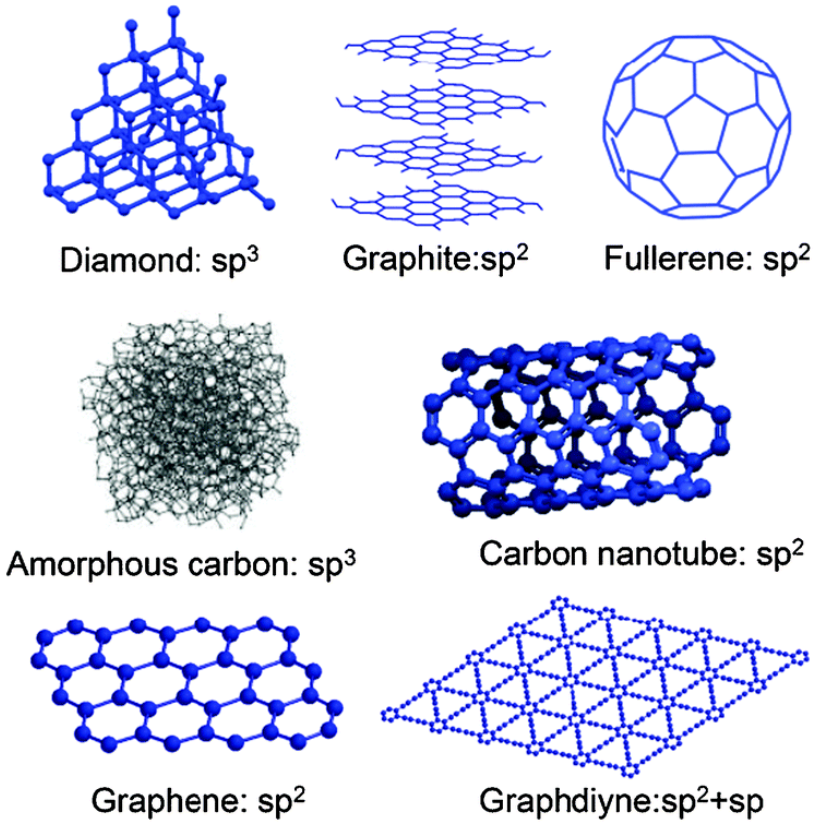

Figure 7. Low-dimensional carbon allotropes with the relevant hybridization.[6]

Graphene is a flat monolayer of carbon atoms tightly packed into a two-dimensional (2D) honeycomb lattice (Figure 2), which can be viewed as both a solid and a macromolecule with molecular weights of more than 10^6-10^7 $gmol^{-1}$. It is a basic building block for all the above mentioned graphitic materials for theoretical reasons and in order to simplify the analysis. It can be wrapped up into 0D fullerenes, rolled into 1D nanotubes or stacked into 3D graphite. It can also be considered as an infinitely large polycyclic aromatic hydrocarbon (see also Figure 1). Graphene was recently isolated by repeatedly peeling highly oriented pyrolytic graphite (HOPG) using scotch tape.[5] Since then, outstanding physical properties predicted and measured for graphene have been explored for practical applications such as field-effect transistors,[5,7,8,9] chemical sensors[10,11,12] and composite reinforcement.[13,14,15] Monolayer graphene possesses high crystallographic quality and ballistic electron transport on the micrometer scale with only ~2.5 % of light absorption.[16,17] Moreover, the combination of its high chemical and thermal stability,[18,19] high stretchability[20,21,22] and low contact resistance with organic materials,[18,23,24] offers tremendous advantages for using graphene as a promising transparent conductor,[19,25,26,27,28] as hole transport layer,[29,30,31] and as electron acceptor material[32,33] in organic electronic devices, e.g. solar cells, organic light emitting diodes (OLEDs),[34,35] liquid crystal displays (LCDs),[18] touch screens,[36] field emitters,[37,38] field effect transistors (FETs),[39,40,41] photodetectors[42,43] and spectroelectrochemistry investigation.[44]

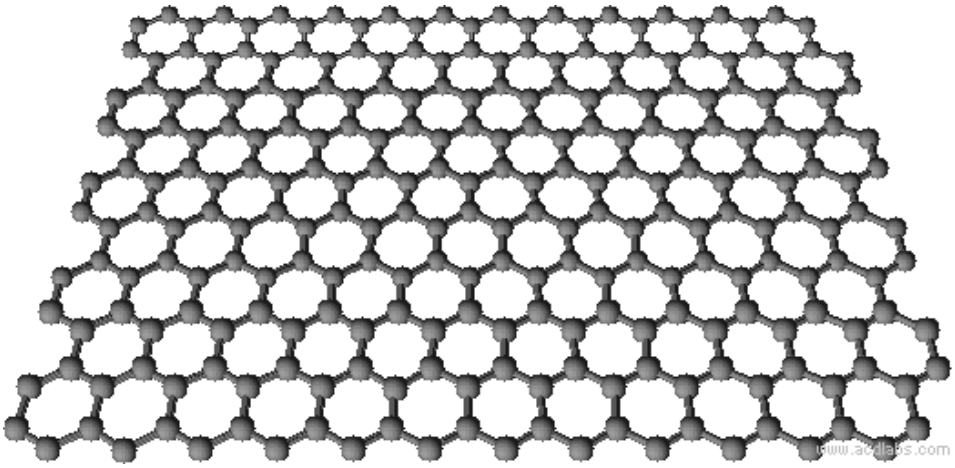

Figure 8. The hexagonal honeycomb crystal lattice of graphene.

1.2 Production of graphene

As graphene presents so many unique physical properties, how to produce such material has become a critical issue. Currently, graphene has mainly been made by different methods, as Figure 3 depicts.

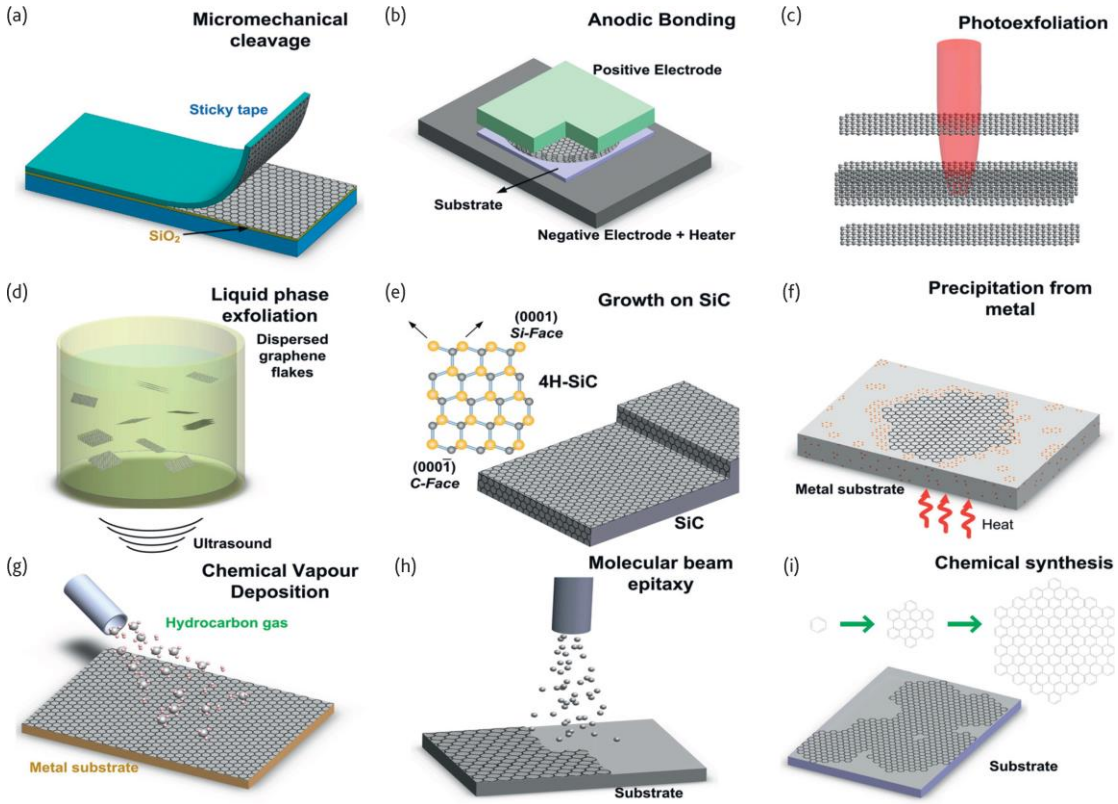

Figure 9. Schematic illustration of the main graphene production techniques. (a) Micromechanical cleavage. (b) Anodic bonding. (c) Photoexfoliation. (d) Liquid phase exfoliation. (e) Growth on SiC. Gold and grey spheres represent Si and C atoms, respectively. At elevated T, Si atoms evaporate (arrows), leaving a carbon-rich surface that forms graphene sheets. (f) Segregation/precipitation from carbon containing metal substrate. (g) Chemical vapor deposition. (h) Molecular Beam epitaxy. (i) Chemical synthesis using benzene as building block.[45]

Dry exfoliation

Dry exfoliation is the splitting of layered materials (LM) into atomically thin sheets via mechanical, electrostatic, or electromagnetic forces in air, vacuum or inert environments.

a) Micromechanical cleavage

Micromechanical cleavage (MC), also known as micromechanical exfoliation, has been used for decades by crystal growers and crystallographers.[46,47] In 1999, reported a controlled method of cleaving graphite,[48] yielding films consisting of several layers of graphene. It was also suggested that "more extensive rubbing of the graphite surface against other flat surfaces might be a way to get multiple or even single atomic layers of graphite plates." This was then firstly demonstrated, achieving single layer graphene (SLG) using a scotch tape, by Novoselov et al, (Fig. 3a).[49] Micromechanical cleavage is now optimized to yield high quality layers, with size limited by the single crystal grains in the starting graphite, of the order of millimeters.[50] The number of layers can be readily identified by elastic[51] and inelastic[52] light scattering. Raman spectroscopy also allows a fast and non-destructive monitoring of doping,[53,54,55] defects,[56,57,58,59] strain,[60,61] disorder,[62] chemical modifications[57,63] and edges.[64,65]

Although, MC is impractical for large scale applications, it is still the method of choice for fundamental studies. Indeed, the vast majority of basic results and prototype devices were obtained using MC flakes. Thus, MC remains ideal to investigate both new physics and new device concepts and remains the best method in terms of electrical and structural quality of the obtained graphene, primarily because it benefits from the high quality of the starting single crystalline graphite source. The size of the deposit is also appreciable, and can be purchased on supporting substrate in the fraction of square millimeter.

b) Anodic bonding

Anodic bonding is widely used in the microelectronics industry to bond Si wafers to glass,[66] to protect them from humidity or contaminations.[67] When employing this technique to produce SLGs,[68,69] graphite is first pressed onto a glass substrate, a high voltage of few kVs (0.5 – 2 kV) is applied between the graphite and a metal back contact (Fig. 3b), and the glass substrate is then heated (~200 °C for ~10 – 20 mins).[68,69] If a positive voltage is applied to the top contact, a negative charge accumulates in the glass side facing the positive electrode, causing the decomposition of Na_2O impurities in the glass into Na^+ and O^{2-} ions.[68,69] Na^+ moves towards the back contact, while O^{2-} remains

at the graphite-glass interface, establishing a high electric field at the interface. A few layers of graphite, including SLGs, stick to the glass by electrostatic interaction and can then be cleaved off;[68,69] temperature (T) and/or an applied voltage can be used to control the number of layers and their size.[68,69] Anodic bonding has been reported to produce flakes up to about a millimeter in width.[68]

c) Laser ablation and photoexfoliation

Laser ablation is the use of a laser beam to remove material from a solid surface.[70] If irradiation results in the detachment of an entire or partial layer, the process is called photoexfoliation.[71]

Laser pulses can in principle be used to ablate/exfoliate graphite flakes (Fig. 3c). Indeed, tuning the laser energy density permits the accurate patterning of graphene.[72] The ablation of a defined number of layers can be obtained exploiting the laser energy density windows required for ablating a SLG[72] and N-layer graphene (NLGs) of increasing number of layers (N).[72] Laser ablation is still in its infancy[72,73] and needs further development. The process is best implemented in inert or vacuum conditions,[74,75] since ablation in air tends to oxidize the graphene layers.[72] Promising results were recently demonstrated also in liquids.[76]

d) Liquid-phase-exfoliation (LPE)

Liquid-phase exfoliation has been considered as one of the most feasible approach for industrial production of graphene due to its scalability and low cost. This approach typically involves sonication of graphite or graphite oxide powders in solvents. Depending on the graphite precursors, liquid-phase exfoliation of graphite has been studied using (1) natural graphite, (2) graphite oxide and (3) graphite intercalation compound (GIC) as displayed in Figure 3d. The liquid-phase exfoliation (LPE) process generally involves three steps: 1) dispersion of graphite in a solvent; 2) exfoliation; 3) “purification”. The third step is necessary to separate exfoliated from un-exfoliated flakes, and is usually carried out via ultracentrifugation.[77]

LPE of graphite

The exfoliation of graphite via chemical wet dispersion followed by ultrasonication in water[78,79,80,81] and organic solvents[77,79,82,83] has been shown to be an efficient and low-cost method to produce oxide-free graphene flakes in solution. The exfoliation process occurs because of the strong interaction between the solvent and the composing layers of graphite. Ultrasound-assisted exfoliation is controlled by hydrodynamic shear-forces, associated with cavitation,[84] i.e., the formation, growth, and collapse of bubbles or voids in liquids due to pressure fluctuations.[84] After exfoliation, the solvent-graphene interaction needs to balance the inter-sheet attractive forces.

Two factors need to be taken into account when graphene is dispersed in organic solvents and/or surfactant solutions: polydispersity and flake size. The first one is related to the nature of the objects present in the solution, i.e. monolayers, bilayers, multilayers, which ideally would need to be separated before film formation. Because of the different buoyant densities of the multilayered graphene compared to mono or bilayer graphene, different strategies based on ultracentrifugation in a uniform medium,[85] or in a density gradient medium (DGM),[86] are used in order to remove the thick flakes. The first is called differential ultracentrifugation (sedimentation based-separation, SBS),[85] while the second is called density gradient ultracentrifugation (DGU).[86] The SBS process separates various particles on the basis of their sedimentation rate in response to centrifugal force acting on them.[85] Sedimentation based separation is the most common separation strategy and, to date, flakes ranging from few nanometers to a few microns have been produced, with concentrations up to a few mg/ml.[87,88] High concentration is desirable for large scale production of composites[77] and inks.[82] Y_M up to ~70 % was achieved by mild sonication in water with SDC, followed by SBS,[81] while Y_M~33 % was reported with NMP.[82] This Y_M difference is related to the difference in flake lateral size. The narrower the dispersivity of the graphene dispersions, the more homogeneous the films obtained, which means significant improvement in transmittance and Rs.[80] The flake size is also an important parameter on the film formation. In general, the small sized graphene sheets are more stable than the large ones in the solution. Thus, in the view of the stability, long-time sonication is normally used to cut the large graphene sheet to small pieces.[89]

Solvents ideal to disperse graphene are those that minimize the interfacial tension [mN/m] between the liquid and graphene flakes (i.e. the force that minimizes the area of the surfaces in contact).[90] In general, interfacial tension plays a key role when a solid surface is immersed in a liquid medium.[90,91,92] If the interfacial tension between solid and liquid is high there is poor dispersibility of the solid in the liquid.[90] In the case of graphitic flakes in solution, if the interfacial tension is high, the flakes tend to adhere to each other and the work of cohesion between them is high (i.e. the energy per unit area required to separate two flat surfaces from contact),[90] hindering their dispersion in liquid. Liquids with surface tension (i.e., the property of the surface of a liquid that allows it to resist an external force, due to the cohesive nature of its molecules) $\gamma \sim 40$ mN/m,[77] are the "best" solvents for the dispersion of graphene and graphitic flakes, since they minimize the interfacial tension between solvent and graphene.

The majority of solvents with $\gamma \sim 40$ mN/m (i.e., NMP, DMF, Benzyl benzoate, GBL, etc.)[77] have some disadvantages. E.g., NMP may be toxic for the reproductive organs,[93] while DMF may have toxic effects on multiple organs.[94] Thus, the main drawback is the low yield and the high (>450 K) boiling points temperature of the organic solvents used for exfoliation, which makes processing complicated. As an alternative, low boiling point solvents,[95] such as acetone, chloroform, isopropanol, etc. can be used. Water, the "natural" solvent, has $\gamma \sim 72$ mN/m, too high (30 mN/m higher than NMP) for the dispersion of graphene and graphite.[96] In this case, the exfoliated flakes can be stabilized against re-aggregation by Coulomb repulsion using linear chain surfactants, e.g. SDBS,[78] or bile salts, e.g. SC[80] and sodium deoxycholate (SDC)[79,81] or polymers, e.g. pluronic,[97] etc. However, depending on the final application, the presence of surfactants/polymers may be an issue, e.g. compromising, decreasing, the inter-flake conductivity.[98]

LPE of graphite oxide

A low cost method of producing graphene on a large scale is to reduce graphene oxide (GO) to graphene. GO is made by oxidizing graphite with strong acids followed by intercalation and exfoliation in water.[99,100] The oxidation of graphite in the presence of potassium chlorate ($KClO_3$) and fuming nitric acid was developed by Brodie in 1859 while investigating the reactivity of graphite flakes.[101] This process involved successive

oxidative treatments of graphite in different reactors.[101] In 1898, Staudenmaier modified Brodie's process by using concentrated sulphuric acid and adding $KClO_3$ in successive steps during the reaction.[102] This allowed carrying out the reaction in a single vessel, streamlining the production process.[103] However, both methods were time consuming and hazardous, as they also yielded chlorine dioxide (ClO_2) gas,[104] which can explosively decompose into oxygen and chlorine. Graphite oxide flakes were already investigated by Kohlschtter and Haenni in 1918,[105] and the first TEM images reported in 1948 by Ruess and Vogt[106] showed the presence of single GO sheets. In 1958, Hummers modified the process using a mixture of sulphuric acid, sodium nitrate and potassium permanganate.[99] Avoiding $KClO_3$ made the process safer and quicker with no explosive byproducts.[99] The downside of this approach is that, after reduction, some places in the sp^2 carbon network can be irreversibly destroyed leaving sp^3 carbons and vacancies which behave as electron traps.[8,107,108] Thus, hydroxyl or epoxide groups are introduced in the basal plane, while carbonyl and carboxylic groups, together with lactone, phenol and quinone attach to the edges (Figure 4). However, the introduction of these functional groups is essential for the GO production and subsequent liquid dispersion. GO flakes can be produced via sonication,[109,110] stirring,[111] thermal expansion,[112] etc., of graphite oxide. The aforementioned functional groups make GO flakes strongly hydrophilic, allowing their dispersion in pure water,[110,113] organic solvents,[111,112,114] aqueous mixtures with methanol, acetone, acetonitrile or 1-propanol and ethylene glycol.[115,116]

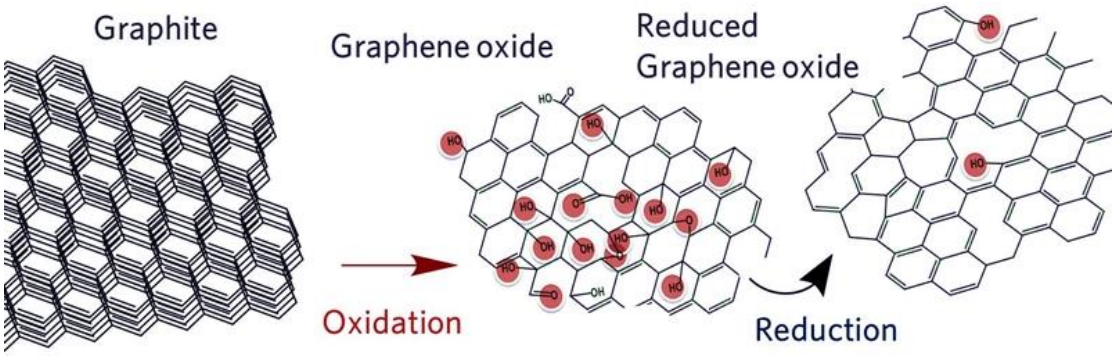

Figure 10. Graphite can be oxidized to give water dispersible Graphene Oxide (GO). Reduction of GO gives nm thick graphitic structures.

However, due to its low cost and easy solution processing, a great number of attempts have been made to improve the electronic properties of the reduced graphene oxide

(RGO), such as the preparation of large-sized GO sheets,[7,117,118,119] chemical doping,[113] and defect repairing.[120,121]

Graphene oxide is electrically insulating material due to its disrupted sp^2 bonding networks. On the other hand, the reduction of the GO can recover the π-network and restore the electrical conductivity of graphene. Thus, graphene oxide sheets became one of the most promising starting materials in the mass production of solution processable graphene sheets through various chemical reduction approaches, e.g. by chemical reduction (using reductants such as hydrazine[7,110,111,122] dimethylhydrazine,[13] hydroquinone[123] and $NaBH_4$),[124,125] by thermal reduction (annealing in argon/hydrogen)[19,112] or by electrochemical reduction.[126]

Thermal treatment of GO is another route used to obtain reduced graphene oxide. Rapid heating (>2.000 °C min^{-1}) up to 1.050 °C exfoliates as well as reduces GO, yielding a black powder.[112,127] The platelets have similar oxygen content to that of hydrazine-reduced graphene oxide, and powder conductivity has been reported in the range of (1 - 2.3) × 10^3 S m^{-1}.[112,127] Although thermal reduction is able to eliminate oxygen-containing groups, the corruption of sp^2 carbon network during the graphite oxidation strongly hampers the properties of ReG. How to mend the defects left on ReG is a key and open question for producing high quality graphene by reducing exfoliated graphite oxide.

The in-plane conductivity in RGO film is much higher than that in the vertical direction.[128] The preparation of ultra-large GO sheets is interesting because of the feasible processing and favorability towards reducing the inter-junction resistance. The Hummers method is modified by replacing the sonication process with shaking. The ultra-large monolayer graphene sheets can be delaminated via centrifugation of the GO dispersion at different centrifugation speeds.[117,118] Freeze-drying has proven to be a very efficient technique to dry the GO colloid, thus facilitating the re-dispersion process.[118] Due to the incorporation of a significant number of water molecules between the GO sheets, freeze-drying of the GO colloid can keep the GO sheets separated from each other, leading to a porous morphology. The absence of post sonication treatment of the dried GO powder is undoubtedly favorable to maintain the size of the initially produced sheets.

LPE of intercalated graphite[129]

Liquid-phase exfoliation of graphite intercalation compound (GICs) for production of graphene was first reported by Viculis et al and has attracted great interest recently.[130,131,132,133] This method begins with intercalation of graphite followed by expansion of graphite via rapid increase in the vapor pressure of the volatile intercalated substance under microwave or thermal treatment (See Figure 5). As non-oxidative agents are applied for intercalation of graphite and microwave or thermal treatment of GIC leads to large expansion of graphite, high-yield production of graphene with high quality can be achieved using this method. For example, it was reported that, by solvothermal-assisted exfoliation of expanded graphite (EG) obtained from GIC in acetonitrile, Qian et al. successfully prepared mololayer and bilayer graphene with 10-12 wt% yield without significant structural defects.[134] However, these recipes are limited by using either poisonous chemical agents[131] or dangerous chemical reactions.[132,133]

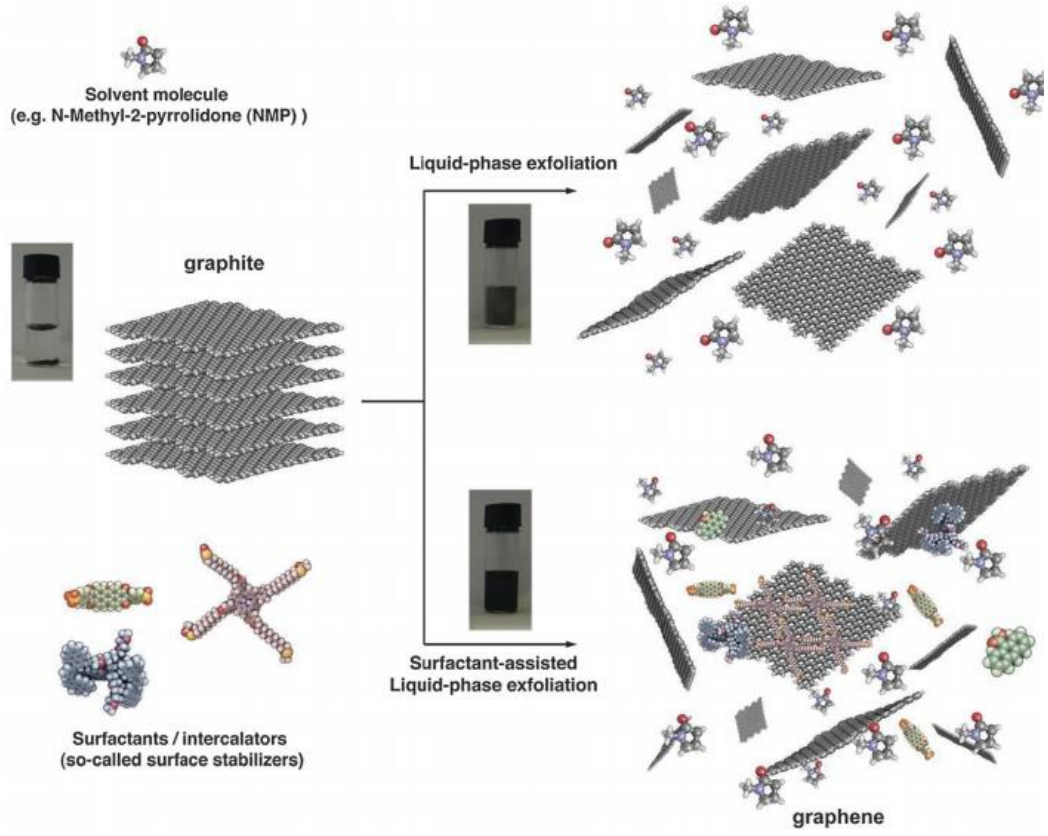

Figure 11. Schematic representation of the liquid-phase exfoliation process of graphite in the absence (top-right) and presence (bottom-right) of surfactant molecules.

e) Growth on SiC (Carbon Segregation)

Graphene can also be produced through carbon segregation from silicon carbide (SiC) following high-temperature annealing.[135,136,137] Acheson reported[136] a method of producing graphite from SiC in as early as 1896. High-quality layers can now be produced on SiC in an argon atmosphere[138] and electronic decoupling from the underlying SiC substrate can be achieved by hydrogen treatment.[139]

The underling method in synthesizing graphene from SiC wafers is to sublime silicon from the wafer surface whereby the remaining carbon will reform into a graphene sheet. The annealing of SiC comes with some simplicity as it avoids the use of metal catalysts and as such is favourable in traditional CMOS processing. However the price of this simplicity is paid by the use of high annealing temperatures (upwards of 1300 °C) and ultra-high vacuum needed to achieve silicon sublimation. In addition, the surface topography of SiC will limit the area of graphene growth as graphene is limited to the horizontal terraces with little growth occurring on vertical edges.

Epitaxial graphene synthesis from SiC was first carried by Von Bommel et al. in 1974,[140] this process was carried out in UHV and at temperatures above 800 °C. From these experiments it was found that the orientation of the crystal plays a principal role in graphene growth, with carbon terminated faces having higher rates of graphene growth then silicon terminated sides.

After Geim's discovery in 2004, Berger et al. were the first to fabricate graphene devices on Si-terminated 6H-SiC wafers. In this work synthesis occurred in UHV conditions and at temperatures ranging from 1250-1450 °C. These conditions produced "ultrathin epitaxial graphite", possibly to say that the films produced were multilayer graphite. Afterwards traditional lithography techniques were applied in patterning devices in which moderate field effect was seen, and thus served as an inspiring proof of concept into a new breed of graphene SiC devices. Studies into graphene synthesis on SiC by Emtsev et al[138] go on to show that graphene defects in sublimed SiC are caused by high silicon sublimation rates seen in UHV synthesis, and that sublimation can better be controlled by utilizing argon at atmospheric pressures. In this way, true monolayer graphene can be synthesized on SiC terraces. The downside of atmospheric annealing in argon is naturally the higher temperatures required (1600 °C) in order to initiate sublimation in ambient pressure argon.

Following in the success approach to controlling silicon sublimation, de Heer et al[141] have recently published a refined synthesis method referred to as confinement controlled sublimation (CCS). In this method SiC wafers are confined in a nonreactive graphite chamber with a small leakage aperture which maintains a higher silicon vapour pressure and thus limits the sublimation rate. The CCS method has be used with both UHV and argon atmospheres and can effectively grow graphene on both the silicon and carbon terminated faces of SiC by tuning both the temperature and size of the leak aperture.

SiC on Si

There are several other divisions in the methods of graphene synthesis from SiC, one of which consists of growing SiC films on silicon via gas source molecular beam epitaxy, followed by an in situ UHV anneal.[142] This method reports marginally lower annealing temperatures in UHV (1200 °C) in comparison to Berger's annealing temperatures that range from 1250-1450 °C, however this demonstrates the utility of SiC synthesis method without relying on expensive SiC wafers.

Etching SiC on Si

All the methods discussed thus far rely on physical sublimation of silicon from the SiC surface, another possibility exists by inducing a chemical reaction that will consume silicon in favour of carbon and thus induce graphene synthesis. This method was first exploited by Moon et al in which a SiC film is first grown on a silicon substrate with mono methyl saline, subsequently the SiC film is exposed to a halogen gas which leads to the de-adsorption of silicon and formation of graphene.[143] The most impressive aspect of this research is that this process is carried out in chemical vapour deposition (CVD) reactor with synthesis temperatures of 850 °C. Further research in this method may show promise as a low temperature solution to synthesizing graphene on silicon substrates.

f) Growth on metals by precipitation

The first reports of synthetic growth of graphite, i.e. not extracted from mines, on transition metals date back to the early 1940s.[144,145] However, the details of the growth process were not elucidated until the 1970s, when Shelton et al. identified, via a combination of Auger and low energy electron diffraction (LEED), SLG formed from carbon precipitation, following high T annealing of Co, Pt, or Ni.[146] Graphite can also be obtained from carbon saturated molten Fe during the formation of steel.[147] In this process, Fe is supersaturated with carbon, and the excess carbon precipitates.[147] This is usually referred to as ”Kish graphite”,[148] derived from the German ”Kies”, used by steel workers to refer to the ”mixture of graphite and slag separated from and floating on the surface of molten pig iron or cast iron as it cools”.[149]

The amount of carbon that can be dissolved in most metals is up to a few atomic percent.[150] In order to eliminate the competition between forming a carbide and graphite/graphene growth, the use of non-carbide forming metals, e.g. Cu, Ni, Au, Pt, Ir, is preferred.[151] Elements like Ti, Ta, Hf, Zr and Si, etc. form thermally stable carbides, as shown by the phase diagram,[152,153,154,155,156] thus are not ”ideal” for graphite/graphene growth. Moreover, all these have a large (>20 %) lattice mismatch with graphene.

Carbon can be deposited on a metal surface by a number of techniques: flash evaporation, physical vapor deposition (PVD), chemical vapor deposition (CVD), spin coating, etc. The carbon source can be a solid,[157,158] liquid[159,160,161] or gas.[162] In the case of a pure carbon source, flash evaporation[163] or PVD,[164] can be used to deposit carbon directly on the substrate of interest, before diffusion at high T followed by precipitation of graphite (graphene) upon cooling. When the solid source is a polymer, it can be spun on the metal substrate at RT, followed by high T annealing and growth[158] as mentioned above.

The growth process on Ni was first investigated in 1974.[146] The authors observed SLG on Ni (111) at T>1000 K by Auger analysis, followed by graphite formation upon cooling. During high T annealing, carbon diffuses into the metal until it reaches the solubility limit. Upon cooling, carbon precipitates forming first graphene, see Fig. 4f, then graphite.[146] The graphite film thickness depends on the metal, and the solubility of

carbon in that metal, the Tat which the carbon is introduced, the thickness of the metal and the cooling rate.

There has been an effort to try and use inexpensive metals to grow large area (cm scale) graphene, such as Ni[165,166,167,168] and Co,[169] while growth on noble metals such as Ir,[170] Pt,[171] Ru,[172,173] and Pd,[171,174] was performed primarily to study the growth mechanism,[175,176,177,178] and/or obtain samples suitable for fundamental studies, e.g. for scanning tunneling microscopy (STM),[173,176,179] requiring a conductive substrate.

Growth of graphene on Ni,[165,166,167,168,180] Co,[169] Ru,[181] etc. was also reported by so-called CVD at high T, using various hydrocarbon precursors.[165,166,167,168,169] However, the CVD process referred to in the aforementioned papers is a misnomer, since graphene is not directly produced on the metal surface by the reaction and deposition of the precursor at the ”growth T”, but rather grows by carbon segregation from the metal bulk, as a result of carbon supersaturation in the solid, as discussed above.[146,162]

For lattice mismatches between graphene and substrate below 2%, commensurate superstructures are formed, where the resulting symmetry (between graphene and substrate) is a doubling of the unit cell along one axis (i.e., 1/2, 0,0).[180] This is the case for Co (0001).[182] Larger mismatches yield incommensurate Moiré superstructures, (i.e. with total loss of symmetry in a particular direction, like (0.528,0,0)), such as in Pt (111),[183] Ir (111),[184] or Ru (0001).[175] E.g., high-T segregation of C on Ru (0001) gives a spread of orientations.[175] Also, the graphene/Ru lattice mismatch[179] gives a distribution of tensile and compressive strains,[185] thus causing corrugation, with a roughness ~2 Å.[185] The Moiré superstructure could be eliminated by adsorption of oxygen,[186] since this weakens the graphene interaction with the substrate.[186]

Growth of graphene by precipitation requires careful control of metal thickness, T, annealing time, cooling rate, and metal microstructure. Reference 181 reported growth on Ni, Co and Ru on sapphire. Through the suppression of grain boundaries, demonstrated uniform growth on Ru by a surface catalyzed reaction of hydrocarbons, but not on Ni and Co.[181] Both SLG and FLG were observed on Ni and Co, presumably due to the higher C solubility and incorporation kinetics in comparison to Ru at the same T.[181] However, graphene was grown on epitaxial Co on sapphire,[187] achieving SLGs, in contrast to FLGs in reference 181. An alternative strategy for SLG growth on high C solubility substrates was proposed,[188] using a binary alloy (Ni-Mo). The Mo

component of the alloy traps all the dissolved excess C atoms, forming molybdenum carbides and suppressing C precipitation.[188] Graphene was also grown on epitaxial Ru (0001) on sapphire.[189]

One of the shortcomings of the growth on metals is that most applications require graphene on an insulating substrate. It is suggested that graphene can be grown directly on SiO_2 by the precipitation of carbon from a Ni film deposited on its surface.[190] This process has promise but needs further refinement.

g) Chemical Vapor Deposition (CVD)

Nickel has been one of the best working catalysts in the prior synthesis of carbon nanotubes and these methods have been adapted in the production of graphene through the use of CVD.[165] Nickel provides a very soluble media in which carbon can diffuse into while at high temperature. Upon cooling the carbon solubility will start to decrease causing the dissolved carbon to escape from the nickel film, ultimately segregating on the surface to form graphite and graphene. While nominal CVD reactions do not involve chemical diffusion, it is believed that diffusion is responsible for CVD graphene synthesis using methane as a source gas.[165] The formation of graphene even in CVD methods is determined by the thermal history of the nickel film, and CVD process using methane at temperatures of 1000 °C will yield 1-10 layers of graphene. During the above process, the evaporated nickel film will undergo recrystallization, forming grains of 20μm, sheets of continuous graphene are ultimately limited to the size of these nickel grains, however by carefully dosing and cooling of samples can produce larger areas of single and few layers of graphene up 85% surface coverage.[191]

Transferring graphene films from nickel is carried out be first applying poly methyl methacrylate (PMMA) over the graphene, followed by selectively etching the underlying nickel with hydrochloric acid. After etching, the PMMA/graphene film can be transferred onto an arbitrary substrate and the PMMA can be subsequently removed with acetone.

Similar CVD methods using copper as catalytic film have also been established.[151] As copper has a limited solubility for carbon, CVD synthesis utilizing methane as a carbon source have been found to be self-limiting, with most of the synthesis area

containing single layer graphene. Unlike nickel, CVD growth on copper is found to be non-temporal and authors report that the synthesis mechanism is a truly catalytic surface reaction unlike the segregation that takes place in nickel. The Exacting details of the copper–carbon reaction mechanism are still unknown. At present CVD on copper provides the largest possible area of synthesized graphene with a graphene yield of 95% and continuous growth over copper grain boundaries.

h) Molecular beam epitaxy

Molecular beam epitaxy (MBE) is widely used and well suited for the deposition and growth of compound semiconductors.[192] It was used to grow graphitic layers with high purity carbon sources (Fig. 3e) on a variety of substrates such as SiC,[193] Al_2O_3,[194,195] Mica,[196,197] SiO_2,[196] Ni,[198] Si,[199] h-BN,[200] MgO,[201] etc., in the 400–1100 °C range. However, these films have a large domain size distribution of defective crystals,[198] with lack of layer control,[198] because MBE is not a self-limited process relying on the reaction between the deposited species.[192] Moreover, the reported μ at RT is thus far very low (~1 $cm^2V^{-1}s^{-1}$).[194] Based on the graphene growth mechanism that we have learned over the past few years on metals,[151,166,180,202,203,204] specifically Cu,[36,151,203] it is unlikely that traditional MBE can be used to grow SLG of high enough quality to compete with other processes discussed above. Since MBE relies on atomic beams of elements impinging on the substrates, it is difficult to prevent, say carbon, from being deposited on areas where graphene has already grown. Therefore, since MBE is a thermal process, the carbon is expected to be deposited in the amorphous or nanocrystalline phase. One might however envisage the use of chemical beam epitaxy (CBE)[205] to grow graphene in a catalytic mode, taking advantage of the CBE ability to grow or deposit multiple materials, such as dielectrics[206] or layered materials, on the top of graphene, to form heterostructures.

Atomic Layer Epitaxy (ALE)

Atomic layer epitaxy (ALE) has by large not been as successful a technique to grow semiconductor materials as MBE is. Atomic layer deposition (ALD),[207] on the other hand, has been extensively used to produce thin layers of nano-crystalline binary metal

nitrides (e.g. TaN, TiN),[208,209] and high-k gate dielectrics such as HfO_2.[210] The ALD process can be used to controllably grown very thin, less than 1nm, films,[207] but to our knowledge, single atomic layers have not been commonly deposited on large areas. Large area graphene can be grown by thermal CVD[36,151,204] and PECVD[211,212] using hydrocarbon precursors. A process dealing with a specific precursor and reactant could in principle be used in the ALE mode. However, to date there are no reports, to the best of our knowledge, of ALE-growth of graphene.

i) Chemical synthesis[213]

Stankovich et al.[110] recently proposed a chemical route for producing large quantity of graphene from graphite. The process involves synthesis of graphite oxide and exfoliation into individual monolayer of graphene oxide. GO can be viewed as graphene sheet with oxygen functional groups attached on the basal plane as well as around the sheet the edges. As-synthesized GO is electrically insulating because oxygen bonding disrupts sp^2 carbon network over which π electrons are delocalized. Reduction of GO partially restores the sp^2 carbon network and renders GO electrically conductive.[13] Reduction can be achieved *via* various routes but thermal annealing and chemical reduction are commonly used. GO sheets can be deposited onto a substrate from aqueous suspensions and lithographically contacted for transport studies as shown in Figure 6a. Figure 6b and c show transition of GO from insulator to conductor with gradual reduction treatment. Complete reduction of GO is generally not achieved and the conductivity of reduced GO is typically more than two orders of magnitude lower than the minimum conductivity of graphene due to residual oxygen and disorder.[8,122] FETs fabricated using reduced GO exhibit graphene-like ambipolar characteristics but the field effect mobility values is on the order of 1-300 $cm^2/V{\cdot}s$, which is significantly lower than those of ideal graphene (Fig. 6d and e).[8,122] The on/off ratio increases with decreasing temperature as in the case of GNRs and values as large as 100 has been observed at low temperatures.[8] The proposed conduction mechanism of reduced GO has been inconsistent due possibly to variability in the oxidation and reduction state of the reported reduced GO devices.[8,122,214,215,216,217] From temperature and field dependence of reduced GO conductivity, activated transport[215,216] thermionic emission[122,214] variable range hopping,[8] and space-charge limited transport[217] have been

proposed as potential conduction mechanisms. Wu et al.[214] indicated that as-synthesized GO is a semiconductor and forms a Schottky barrier at a metal interface. Jung et al.[217] reported that conduction in reduced GO FETs are not contact limited but trap limited. Chua et al.[216] suggested that the transport mechanism may depend on the structure of sp^2 carbon network. It is likely that carrier transport across highly disordered graphene occurs via hopping between intact sp^2 carbon domains. A recent study of hydrogenated graphene, or graphene,[63] demonstrates that variable range hopping (Fig. 6f) becomes the dominant transport mechanism after some of the atoms in the graphene lattice are converted to sp^3 carbon. Further investigation is essential to understand the correlation between the chemical and electronic structure of GO and transport properties.

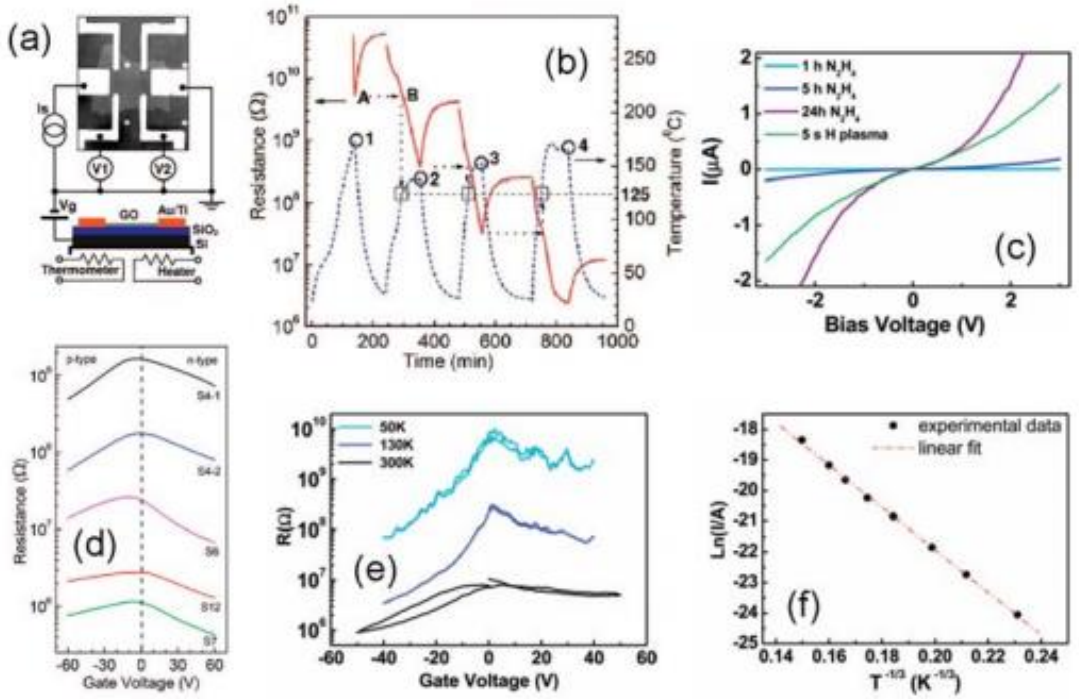

Figure 12. (a) Optical micrograph and device schematic of a reduced GO FET. The heater is used to thermally reduce GO. (b) Resistance of GO as a function of time during several annealing cycles. (c) I-V characteristics of GO with progressive chemical reduction. The results for H plasma reduction are also shown. (d) Transfer characteristics for progressively reduced GO. (e) Transfer characteristics of chemically reduced GO at different temperatures. (f) Current of chemically reduced GO fitted with variable range hopping model. (a,b,d) were reproduced from Ref. 217 and (c,e,f) from Ref. 8.

Chapter 2

2.1 Graphene functionalization and composite[218]

Covalent functionalization of pristine graphene

Graphene is a carbon nanostructure with high chemical stability in general, which is provided by the extended aromatic character of the graphitic lattice. In practice, this stability is usually associated with the influence of chemical substances like gases, acids, or bases under specific conditions determined by chemical processes such as catalytic procedures. On the other hand, several organic reactions have been applied on graphene up to now affording a large number of derivatives. In general the reactions with graphene are divided in two main categories. The first category includes the reactions of the carboxyl, hydroxyl, and epoxy groups that are spread on a graphene oxide (GO) layer as a consequence of their preparation procedure. The second category includes the covalent attachment of organic functional groups directly on sp^2 carbon atoms of pristine graphene or GO and they are described in this chapter.

The chemical reactivity of sp^2 carbon atoms of graphene originates from various sources that are described below. It is known that a number of carbon atoms at the defect sites and at the edges have sp^3 hybridization. The existence of these sp^3 carbon atoms decreases the aromatic character in the areas around the defects and near the edges and consequently increases the reactivity of the neighboring sp^2 carbon atoms or carbon–carbon double (C=C) bonds. In addition, because the direct covalent addition to graphitic carbon atoms changes their hybridization from sp^2 to sp^3, as the reaction proceeds the number of sp^3 carbon atoms of the graphene layer is increased. As a consequence, during the reaction the aromatic character of graphene is decreased continuously and the chemical reactivity is increased. Furthermore, although theoretically graphene has a planar structure, the combination of the large 2D surface area with the minimal thickness creates a number of anomalous – out of planar – curved domain-like folds and wrinkles that induce local strain and hence chemical reactivity to the C=C bonds analogous to the induced reactivity of carbon nanotubes as a result of the curvature of the cylindrical shape.

The organic modification of graphene through covalent bonds with graphitic carbon atoms has advantages and disadvantages. The addition of organic groups on the

graphene surface, which is followed by the transformation of the hybridized carbon atoms from sp^2 to sp^3, disrupts the aromatic systems. This change has an important influence on the electronic and the mechanical properties of the organic graphene derivatives. Usually the extent of this influence depends on the percentage of the carbon atoms that have reacted and the type of reaction as well. The advantages of derivatization are related to the nature of the added organic functionalities, which can enrich graphene with various novel physicochemical properties. Thus, graphene can be functionalized with organophilic or hydrophilic organic groups, chromophores, drugs, biomolecules, or polymers acquiring analogous properties and characteristics. Making the graphene nanoplatelets highly organophilic, its dispersion in organic solvents and subsequent dispersion or mixing with analogous polymers is facilitated. In addition the organic character that is gained after the modification increases the chemical affinity with polymers which is a crucial factor for the enhancement of the mechanical strength in polymer nanocomposites. In general carbon nanostructures–graphene, carbon nanotubes, nanohorns – dispersed in organic solvents can be purified, characterized, and handled much easier than in solid phase. In the case of graphene the absence of a stabilizer in the liquid phase very often leads to the reorganization of graphene monolayers into larger graphitic aggregates or in the absence of the liquid phase, into graphite.

The characterization of the functionalized graphene is usually based on microscopic techniques such as AFM (atomic force microscope), TEM (transmission electron microscope), HRTEM (high-resolution transmission electron microscope) for the identification of graphene and spectroscopic techniques such as UV–vis, FTIR (Fourier transform infrared), Raman, XPS (X-ray photoelectron spectroscopy), photoluminescence spectroscopy, and thermogravimetric analysis (TGA) for its morphology. Free radicals, dienophiles, and other reactive intermediates are the most frequently used organic species in the direct organic functionalization of graphene. The following sections include the description of the most widely used reactions of this category through the presentation of representative examples.

I. Addition of Free Radicals to sp^2 Carbon Atoms of Graphene

Upon heating of a diazonium salt, a highly reactive free radical is produced, which attacks the sp^2 carbon atoms of graphene forming a covalent bond. This reaction has been used by Tour and co-workers to decorate graphene with nitrophenyls.[219,220] The graphene sheets in this work were produced through the chemical unzipping of carbon nanotubes. A measurement of the conductivity of a graphene sheet through a simple device (Figure 7) during chemical functionalization with diazonium salts results in a remarkable decrease in conductivity due to disruption of the aromatic system by transformation of carbon atoms from sp^2 to sp^3 hybridization. The conductivity of the graphene sheets was shown to decrease in a controlled manner, showing that conductivity can be controlled by reaction time (Figure 8).

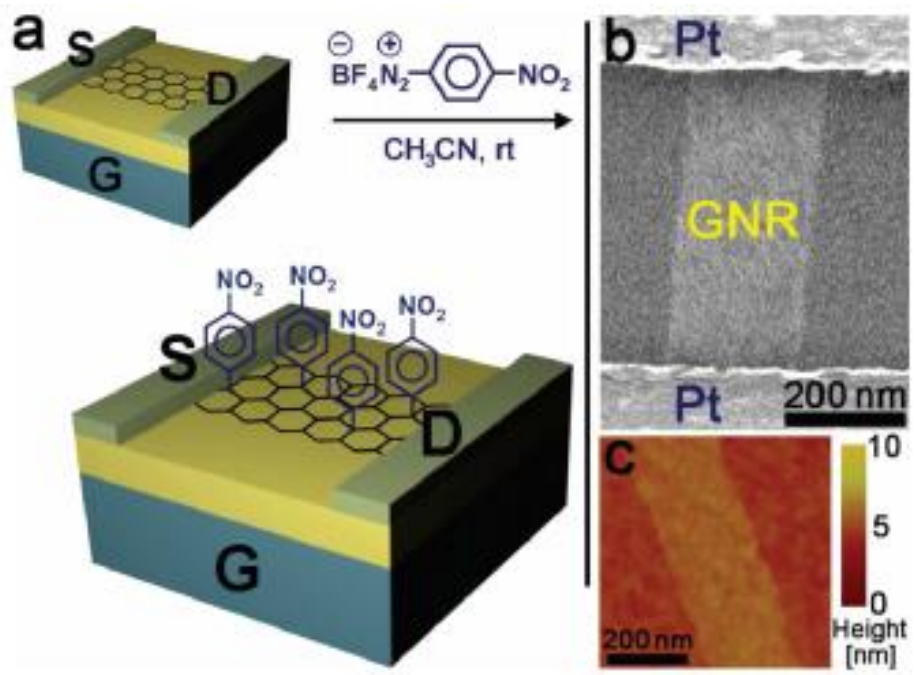

Figure 7. Chemical doping of graphene with 4-nitrophenyl groups: (a) schematic representation; (b) SEM image of a graphene nanoplatelets between Pt electrodes; (c) AFM image of a fragment of a monolayer graphene.[220]

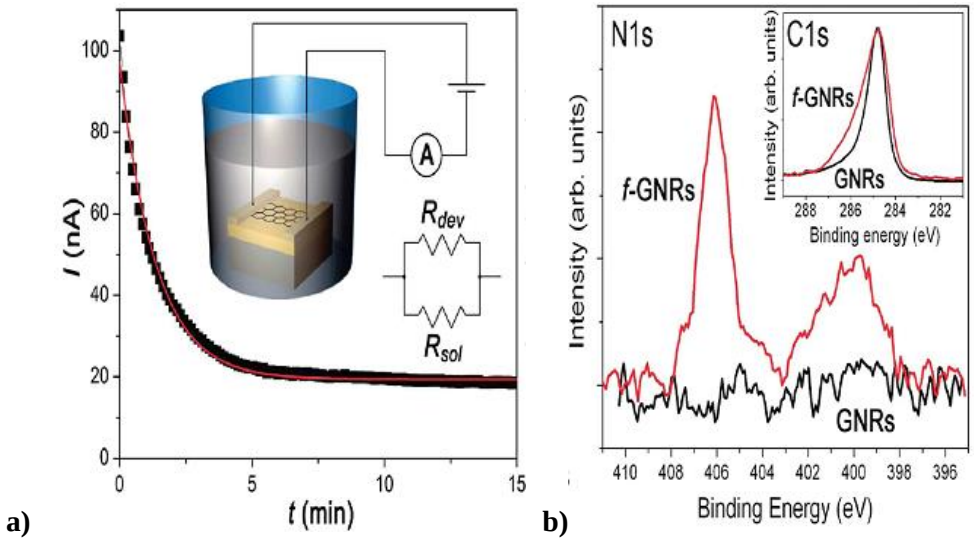

Figure 8. Time dependence of current I: (a) Scheme of the experiment shows the device consisted of two parallel resistances derived from the graphene and the solution, and (b) N1s and C1s XPS spectra of GNRs before and after the functionalization (f-GNRs).[220]

In a similar approach, Niyogi and coworkers[221] showed that the covalent attachment of nitrophenyls to graphene sheets results in the introduction of a band gap, which can be controlled, making the functionalized graphenes potentially useful as semiconducting nanomaterials. The strong covalent binding of the nitrobenzyl group on graphene was detected by X-ray photoelectron spectroscopy (XPS) (Figure 8b). The N1s XPS spectrum of the functionalized graphenes exhibits two peaks at 406 and 400 eV that correspond to the nitrogen of NO_2 and the partially reduced nitrogen of the product, respectively. The reactions with diazonium salts have been applied to the functionalization of chemically or thermally converted graphenes, single graphene sheets obtained by micromechanical cleavage from bulk graphite, and epitaxial graphenes.[111,220,222,223,224,225]

Hydroxylated aryl groups grafted covalently on graphene by the diazonium addition reaction act as initiators for the polymerization of styrene via the atomic transfer radical polymerization (ATRP) method (Figure 9). As a consequence the polymeric chains are covalently grafted on the graphene surface.[226]

The ratio between carbon atoms with sp^2 and sp^3 hybridization in the graphitic lattice is an indication of the degree of oxidation or a covalent functionalization reaction. This ratio is estimated using Raman spectroscopy as the I_D/I_G ratio, where I_D and I_G are the intensities of the peaks at ~1350 and 1580 cm^{-1}, which correspond to the number of sp^3 and sp^2 C atoms, respectively. Graphene is defined as a pristine two-dimensional

sp^2 hybridized carbon sheet; as such the coexistence of sp^3 carbons in the lattice are inherently classified as defects, where these defects can be on the basal edges or inside defects in the plane. For the modification described in Figure 9, the I_D/I_G ratio increased from 1.7 to ~2 after functionalization by diazonium addition.

An alternative free radical addition method includes the reaction of benzoyl peroxide with graphene sheets.[227] Graphene isolated mechanically from Kish graphite was deposited on a silicon substrate and immersed in a benzoyl peroxide/toluene solution. The reaction was initiated photochemically, by focusing an Ar-ion laser beam onto the graphene sheets in the solution. The attachment of the phenyl groups was directly indicated by the appearance of a strong D band at 1343 cm^{-1}. The appearance of this D band is due to the formation of sp^3 carbon atoms in the basal plane of graphene by covalent attachment of phenyl groups (Figure 10). The above reaction was also carried out on a graphene sheet placed in afield effect transistor (FET) device.

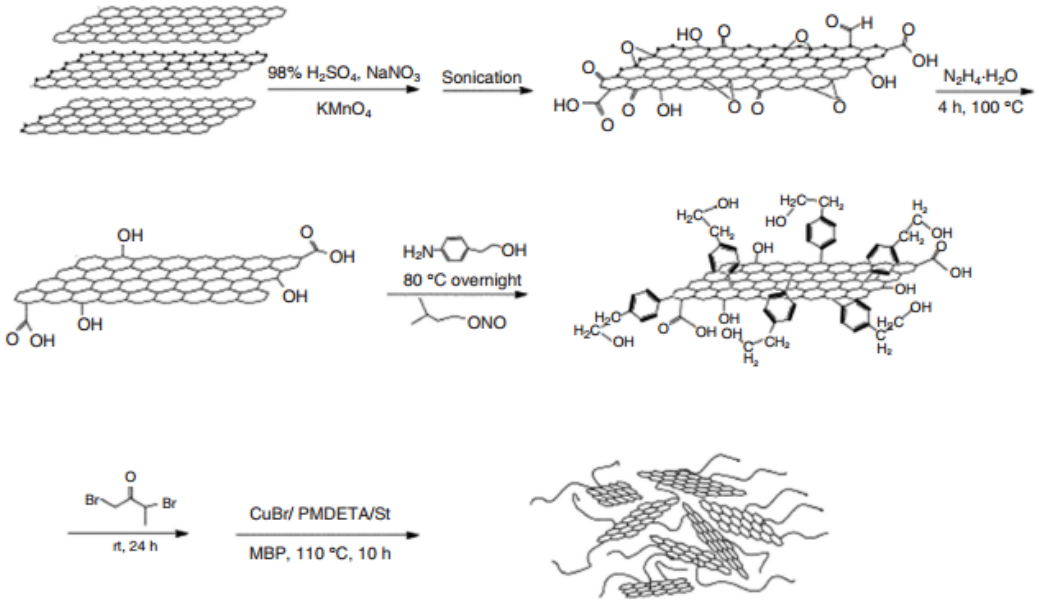

Figure 9. The attachment of aryl groups on graphene nanoplatelets and the formation of polystyrene chains grafted on graphene nanoplatelets.[226]

In this case, apart from the significant decrease in conductivity due to the increase of sp^3 carbon atoms after the covalent addition of phenyl groups, an increase in the level of hole doping was also observed. The increase in the hole doping was attributed to the physisorbed benzoyl peroxide. Regarding the mechanism of radical generation, Liu et al.[227] suggest that a hot electron initiates an electron transfer from photoexcited graphene to the physisorbed benzoyl peroxide. The short-lived benzoyl peroxide radical

anion is then decomposed to produce the phenyl radicals, which react with the sp^2 graphene carbon atoms.

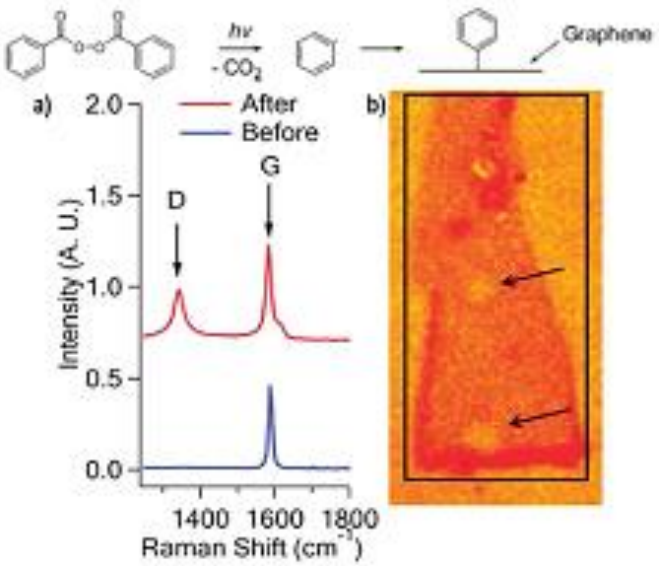

Figure 10. Schematic representation of the radical addition reaction: (a) the appearance of D band in the Raman spectrum of a single layer graphene after the photochemical reaction and (b) optical image of a functionalized single-layer graphene. The arrows indicate holes resulting from prolonged laser exposure.[227]

II. Addition of Dienophiles to Carbon-Carbon Bonds

Apart from free radicals, dienophiles also react with sp^2 carbons of graphene. Azomethine ylide, which reacts through a 1,3-dipolar cycloaddition, is one of the most common dienophiles that have been successfully applied in the functionalization of carbon nanostructures: fullerenes, nanotubes, onions, and nanohorns. This type of reaction affords a variety of organic derivatives, which display interesting applications in several areas; these include polymer composites, biotechnology, nanoelectronic devices, drug delivery, and solar cells.[228,229,230,231,232,233] After the successful production of graphene sheets directly from graphite dispersed in organic solvents,[234] Georgakilas et al.[235] showed that these graphene sheets could be substituted with pyrrolidine rings via a 1,3-dipolar cycloaddition of azomethine ylide. The graphene sheets were decorated with dihydroxyl phenyl groups by pyrrolidine rings that were formed perpendicular to the graphene surface by addition of azomethine ylide precursors (Figure 11)[235] The azomethine ylide was formed by the condensation of 3,4-dihydroxybenzaldeyde and sarcosin. The hydroxyl groups introduced onto a graphene

sheet increase its dispersibility in polar solvents such as ethanol and N,N-dimethyformamide (DMF).

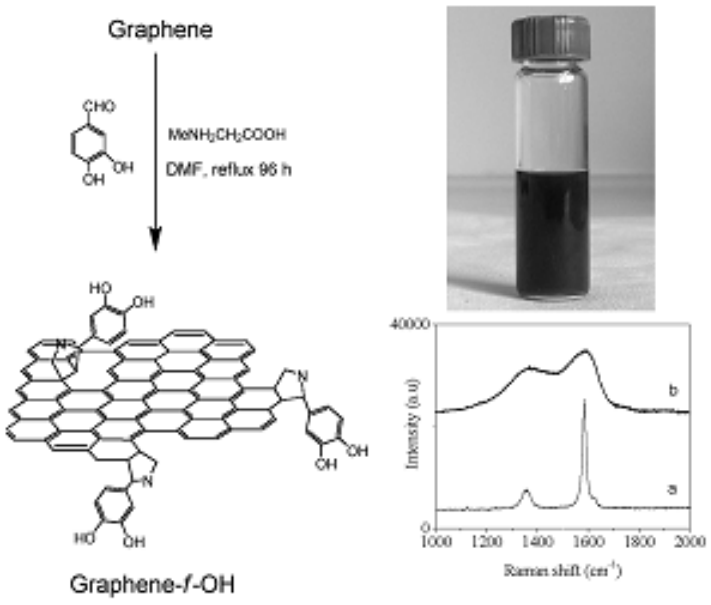

Figure 11. (left) Schematic representation of the 1,3 dipolar cycloaddition of azomethine ylide on graphene. (top, right) Dispersion of functionalized graphene nanoplatelets in ethanol. (bottom, right) Raman spectra of (a) pristine graphene and (b) pyrrolidine functionalized graphene.[235]

The flexibility of this reaction procedure makes it important because one is able to choose among several aldehydes or substitutedα-amino acids as precursors, thus yielding a variety of desirable functional groups. For example, to decorate graphene sheets with tetraphenylporphyrin (TPP) or palladium-TPP, Zhang and co-workers[236] used tetraphenylporphyrin aldehyde (and the Pd analogue) and sarcosin as precursors. Quintana et al.[237] utilized 1,3-dipolar cycloaddition to graphene sheets by employing precursors of paraformaldehyde and a specifically designed NH_2-terminated α-amino acid. These amino groups were shown to selectively bind gold nanorods. Phenyl and alkyl azides react with the C−C bonds of graphene by the formation of the reactive intermediate nitrene. The reaction of organic azides with graphene has been used successfully by several research groups affording a variety of organic graphene derivatives. By thermally and photochemically activating a variety of para-substituted perfluorophenylazides (PFPA), Liu et al.[238] were able to attach various functionalities to the graphene sheet via a three-membered aziridine ring (Figure 12). These

modifications result in varying solubility-dispersibility and surface energy of the modified graphenes.

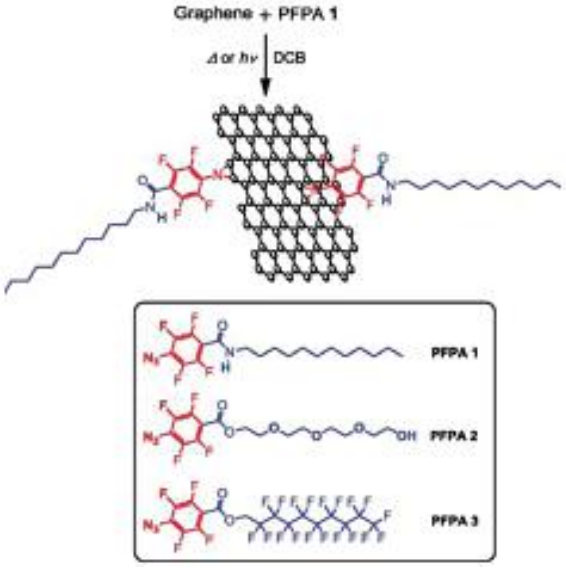

Figure 12. Functionalization of pristine graphene with PFPA.[238]

Nitrene addition has also been used in the functionalization of graphene sheets with phenylalanine. The graphene sheets were reacted with B_{oc}-protected azidophenylalanine in *o*-DCB (Figure 13). The product was determined to have 1 phenylalanine substituent per 13 carbons.[239]

Vadukumpully et al.[240] reported that graphene sheets can be covalently functionalized with alkylazides, where the alkyl chains include several groups such as hexyl, dodecyl, hydroxylundecanyl, and carboxy-undecanyl. The carboxylate groups introduced on the surface facilitated the attachment of Au nanoparticles, which were used as markers to investigate the reactive site distribution. The organically modified graphene sheets showed enhanced dispersibility in common organic solvents such as toluene and acetone. An increase in the I_D/I_G ratio was observed on functionalization, which increased when excess nitrene was added. This indicates that the degree of functionalization is dependent on the amount of nitrene added to the reaction mixture (Figure 14). The appearance of a broad 2D band at 2700 cm^{-1} is characteristic of few layer modified graphene sheets.

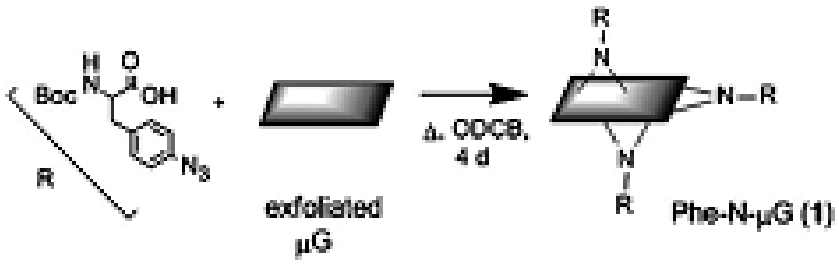

Figure 13. Nitrene addition to graphene sheets using B_{oc}-protected azidophenylalanine.[239]

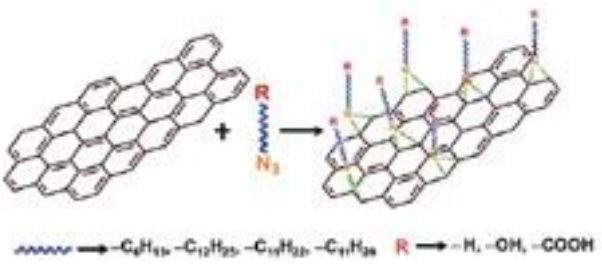

Figure 14. The reaction of alkyl nitrenes with graphene sheets.[240]

The formation of covalent bonds between thermally generated nitrene and epitaxial graphene has been demonstrated by Choi et al.[241] In this case, the formed band gap of the functionalized epitaxial graphene can be controlled by the amount of the added nitrene in the reaction.

Zhong et al.[242] recently described aryne cycloaddition to the graphene surface using 2-(trimethylsilyl)aryl triate as a precursor toward the reactive benzyne intermediate (Figure 15). The reaction resulted in the formation of a four-membered ring that connected the aromatic arene rings to the graphene surface. The aryl-modified graphene sheets were dispersible in DMF, *o*-DCB, ethanol, chloroform, and water. Additionally, the aryl rings can be substituted by several organic groups (i.e., methyl and fluoro), thereby giving a variety of interesting derivatives.

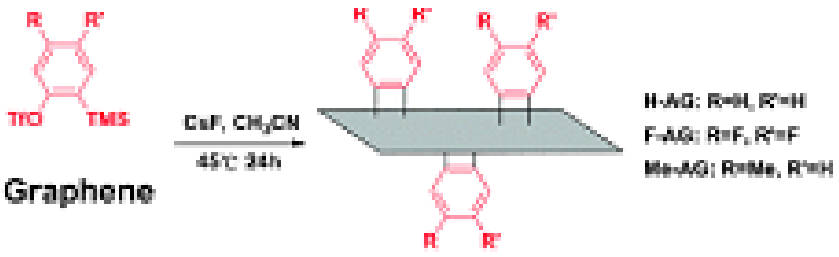

Figure 15. Aryne cycloaddition to graphene sheets.[242]

Covalent functionalization of graphene oxide

GO can be characterized as a single graphitic monolayer with randomly distributed aromatic regions (sp^2 carbon atoms) and oxygenated aliphatic regions (sp^3 carbon atoms) containing hydroxyl, epoxy, carbonyl, and carboxyl functional groups. The epoxy and hydroxyl groups lie above and below each graphene layer and the carboxylic groups exist usually at the edges of the layers; however it should be noted that the chemistry and heterogeneity of graphene oxide is still heavily debated. The presence of oxygen groups on the surface of GO provides a remarkable hydrophilic character and analogous chemical reactivity. GO is prepared either by methods based on the oxidation of graphite with strong acidic media[99] or ozone[243] or the chemical/thermal exfoliation of graphite oxide.[110,112,127,244,245,246] GO forms unstable dispersions in water and polar organic solvents such as ethylene glycol, DMF, NMP, and THF, since the exfoliated GO nanoplatelets tend to aggregate through π-π stacking and form large particles of graphite oxide. Several protective agents have been presented for the stabilization of GO nanoplatelets in the solution such as octadecylamine,[114] 1-octyl-3-methyl-imidazolium,[126] large aromatic molecules,[27] didodecyldimethyl-ammonium bromide,[247] polystyrene,[248] and poly(sodium 4-styrenesulfonate)[249] and also elastomeric silicon foams[250] and DNA.[251] The presence of these stabilizing groups is not favorable however in terms of use of graphenes in technological applications. Theoretically, a simple reduction of GO should remove the oxygen groups and rehybridize the effected sp^3 C atoms to sp^2 C, thereby leaving it aromatic and defect free. However, experimentally, after any reductive treatment of GO a critical number of oxygen groups and defects remain. The reduction of GO has been extensively researched, and the methods ranging from the traditional hydrazine treatment[110] to bacterial treatment[252] have shown to be successful, as well as a variety of other methods.[112,253,254,255,256] These defects affect the properties of the reduced GO (RGO), most importantly its electric conductivity. For this reason, the type of graphene used is usually specified, that is, chemically converted graphene, chemically reduced graphene, RGO, or thermally reduced graphene, in order to discriminate it from pristine graphene.[257] Due to the rich chemistry of hydroxyl, carboxyl, and epoxy groups, GO has been selected very often as the starting material for the formation of graphene derivatives through the covalent attachment of organic groups on its surface. In this type of functionalization where the added groups are linked through the oxygen atoms

of GO, the Raman spectra of the functionalized graphene show no important differences from those of GO, since no further structural perturbation occurred.

III. Addition of Chromophores

Polythiophenes and oligothiophenes are well-known conjugated polymeric materials with potential use in various optoelectronic applications, for example, solar cells, due to high charge mobility arising from the large number of πelectrons delocalized along their molecular chains.[258] Amine-terminated oligothiophenes can be grafted on GO nanoplatelets through covalent amide bonds, as described by Liu et al.[258] (Figure 16). The as-synthesized donor-acceptor material displayed a superior optical limiting effect compared with the standard optical limiting material C_{60} and a control sample consisting of a physical mixture of GO and oligothiophene.

In an analogous approach, Yu et al.[259] reported functionalization of GO with $-CH_2OH$ terminated regioregular poly(3-hexylthiophene) (P3HT) through the formation of ester bonds with the carboxyl groups of GO nanoplatelets (Figure 17). Due to the presence of an abundant number of hydroxyl groups in the added polymer, P3HT-GO was soluble in common organic solvents, facilitating its characterization and device fabrication by solution processing.

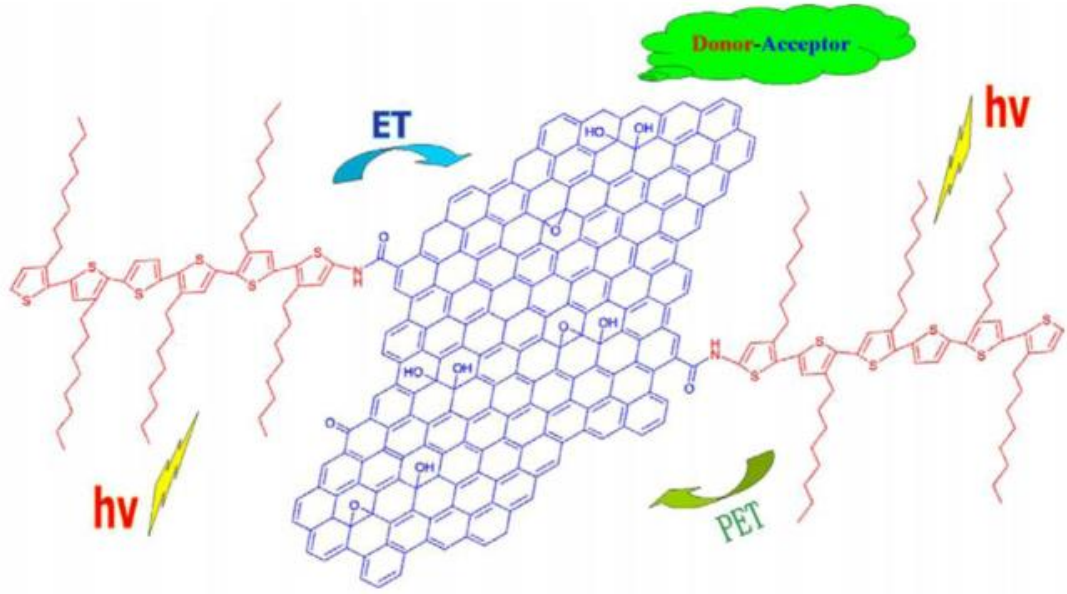

Figure 16. Structure of oligothiophene functionalized GO.[258]

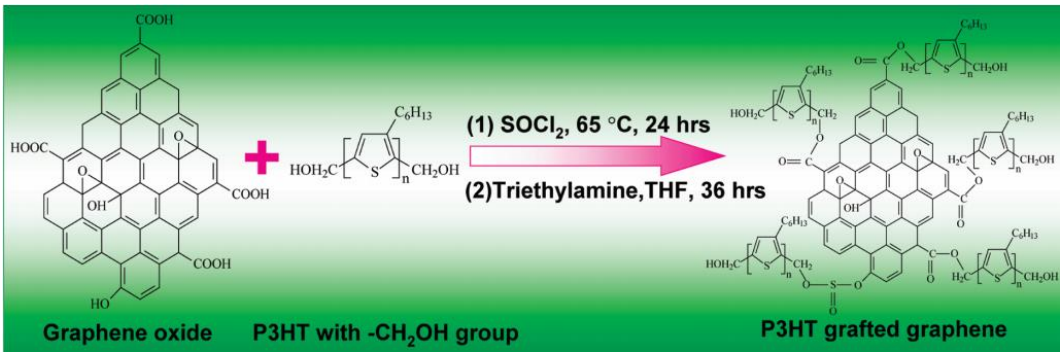

Figure 17. Synthesis procedure for chemical grafting of CH_2OH-terminated P3HT chains onto graphene, which involves the $SOCl_2$ treatment of GO (step 1) and the esterification reaction between acyl-chloride functionalized GO and MeOH-terminated P3HT (step 2).[259]

Apart from the classical esterification and amidation reactions, Melucci et al.[260] covalently attached optically active silane-terminated oligothiophene groups to GO substrates. The advantage of this reaction is that the covalent attachment is completed within a few minutes via microwave radiation, thereby affording GO derivatives soluble in water as well as nonpolar solvents.

Apart from conjugated polymers, simple organic chromophores such as porphyrins, phthalocyanines, and azobenzene with very interesting optoelectronic properties have been covalently attached on graphene nanoplatelets.[261,262,263,264] Due to the large visible light extinction coefficients, porphyrins and phthalocyanines are frequently used as antennas for harvesting energy from photons. GO can be functionalized with porphyrins through the formation of amide bonds between amine functionalized porphyrins and carboxylic groups of GO as shown in Figure 18.[261]

The covalent interaction between the porphyrin and the GO surface resulted in an improvement in the dispersibility in organic solvents and an effective fluorescence quenching after the photoexcitation of the porphyrin.

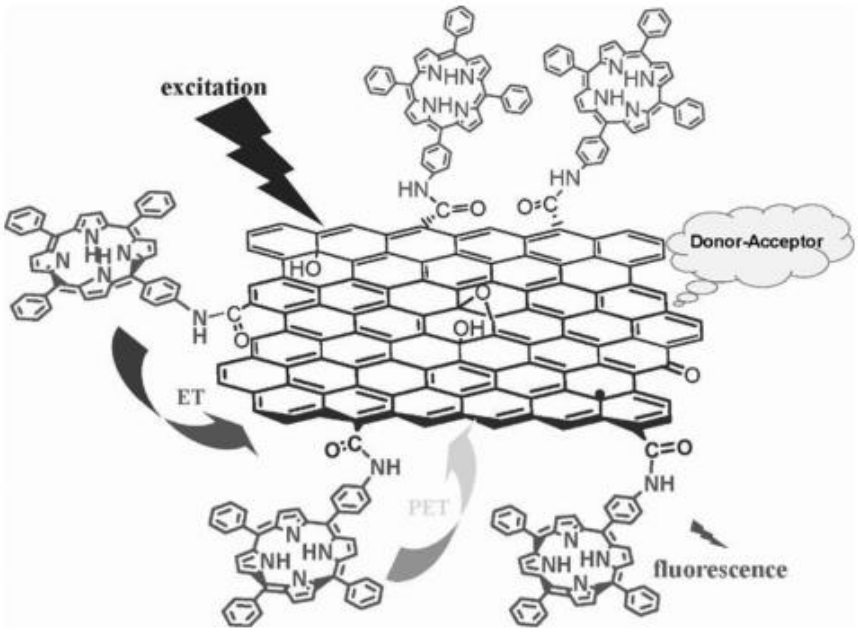

Figure 18. Schematic representation of the product of the reaction between GO and amine-functionalized porphyrin.[261]

IV. Covalent Linkage to Polymers

GO can be grafted to polymeric chains that have reactive species like hydroxyls and amines, that is, poly(ethylene glycol), polylysine, polyallylamine, and poly(vinyl alcohol). These materials combine the properties of their parts; the polymeric part offers dispersibility in certain solvents, mechanical strengthening, and several morphological characteristics, while graphene contributes to the electrical conductivity, chemical reactivity, and reinforcement of the mechanical properties.

Poly(ethylene glycol) (PEG) is a biocompatible superhydrophilic polymer that has been used to cover nanostructures providing them with these basic characteristics. It has found use as a carrier for drug delivery, that is, metallic nanoparticles or carbon nanotubes. Amine-terminated PEG can be grafted onto GO nanoplatelets through amide bond formation. The PEGylated GO is highly dispersible in water, as well as, in contrast to GO, in several aquatic biological solutions such as serum or cell medium. This important characteristic makes PEGylated GO an important candidate for the delivery of hydrophobic drugs in biological systems. As an example, a camptothecin analogue named SN38 (Figure 19), which is highly hydrophobic, can be immobilized on the surface of PEGylated GO through van der Waals interactions, forming a nanostructure with excellent stability in biological solutions.[265] Camptothecin is an

organic aromatic molecule, which displays remarkable anticancer properties. Its main disadvantage in cancer therapy is its low solubility in aqueous media. In further work, Yang et al.[266] studied the behavior of PEGylated GO nanoplatelets in vivo.

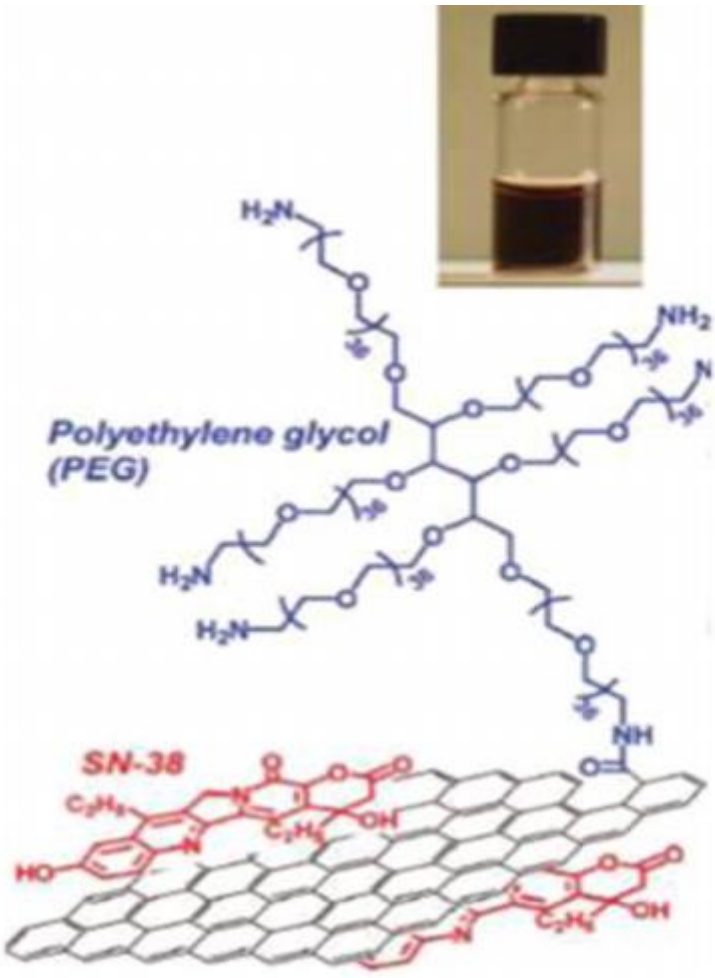

Figure 19. Immobilization of SN38 camptothecin on PEG-GO.[265]

RGO can be made dispersible in biological solution after its functionalization by poly(L-lysine) (PLL) through amidation (Figure 20).[267] Poly(L-lysine) is an attractive biocompatible molecule, with uses in promoting cell adhesion, drug delivery, cell labeling, biofuel cells, and DNA electrochemical sensors. The PLL/RGO nanostructure was used as a biosensor for hydrogen peroxide (H_2O_2) detection exhibiting improved sensing of H_2O_2. The detector device was based on the immobilization of horseradish peroxidase onto the PLL/RGO surface and the deposition of the resulting nanocomposite on a gold electrode.

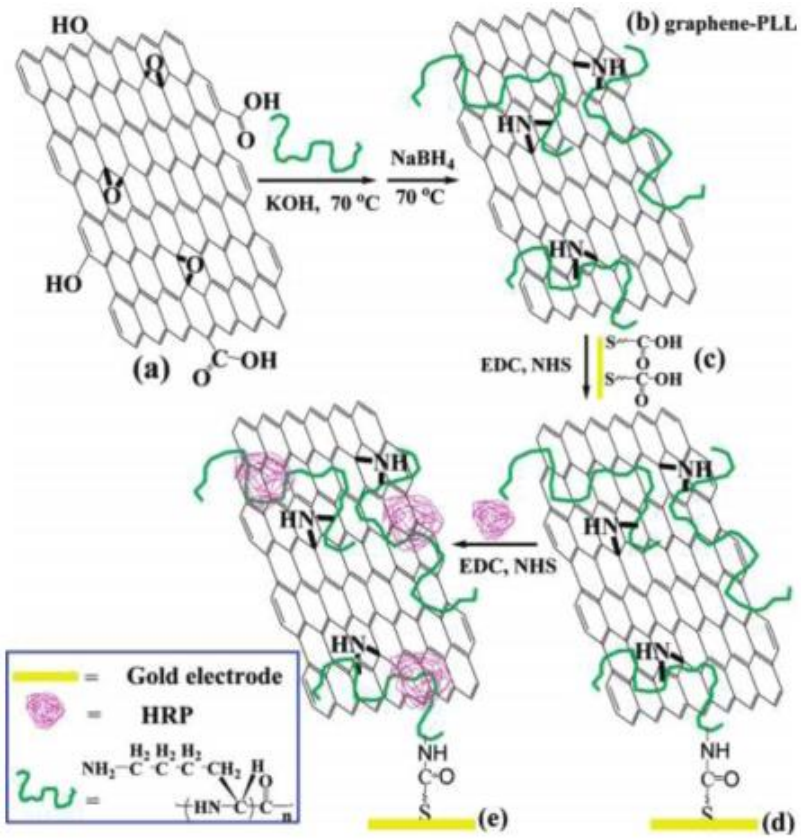

Figure 20. Schematic representation of the formation of the PLL/RGO−horseradish peroxidase and its subsequent deposition on a gold electrode.[267]

Polyallylamine (PAA) can be reacted with GO; in this reaction the numerous amine groups react successfully with the epoxy groups of GO forming an effective cross-linking of the GO sheets (Figure 21). After filtration of a colloidal suspension of PAA/GO through a filter paper, a thin paper-like membrane was formed.[268] Although, the mechanical properties of PAA/GO membrane are not impressively increased in comparison to a GO analogue, the idea of making stiff GO membranes by cross-linking with polymers seems to work successfully.

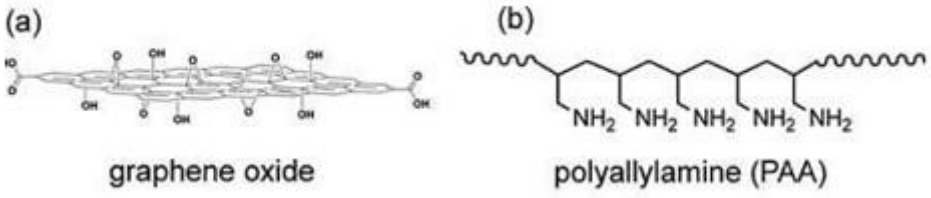

Figure 21. Schematic representation of (a) GO and (b) PAA.[268]

Poly(vinyl alcohol) (PVA) can be grafted onto GO nanoplatelets via ester bonds between the hydroxyl groups of PVA and the carboxylic groups of GO. These covalent bonds can be formed either by direct formation or after the transformation of carboxylates to the more reactive acyl chlorides. The PVA/GO composite was dispersible in DMSO and hot water. In a further step, the PVA/GO composite was partially reduced by hydrazine, affording the PVA/RGO composite.[269] Veca et al.[270] also reported covalent functionalization of graphene nanoplatelets with PVA, affording derivatives readily soluble in aqueous and polar organic solvents for further application.[271,272] Lin et al.[273] demonstrated an efficient method to covalently graft polyethylene (PE) chains onto the surface of GO, which resulted in a high polymer grafting efficiency and a 10 °C increase in the crystallization temperature compared with the pure polymer. Furthermore, the polyethylene-functionalized GO (PE/GO) displays a unique encapsulating structure and can be stably dispersed in toluene.

Lee et al.[274] reported an atom transfer radical polymerization (ATRP) approach to functionalize GO nanoplatelets with polymers. In this method, polymer chains were directly grown from the surface of GO via living radical polymerization. The technique involves the covalent attachment of the initiator followed by the ATRP of various monomers including styrene, methyl methacrylate, or butyl acrylate without damaging the GO structure.[275] The obtained nanocomposites showed significant enhancement in thermal and mechanical properties compared with the pure polymers. Poly(methyl methacrylate) PMMA functionalization of GO was carried out by Goncalves et al.[276] Different PMMA/GO composites were synthesized by changing the percentage of PMMA polymer to GO in the reaction. The resulting composites were readily dispersible in organic solvents and used as reinforcement fillers in the preparation of PMMA composite films.

The formation of covalently bonded polymer-GO nanocomposites, where GO was initially functionalized with octadecylamine (ODA) has been reported by Pramoda et al.[277] These ODA functionalized GO nanoplatelets were subsequently reacted with methacryloyl chloride to incorporate polymerizable –C=C− functionalities at the graphene surfaces. These intermediates were then employed in in situ polymerization of methylmethacrylate to obtain covalently bonded PMMA/GO nanocomposites.

Ramanathan et al.[278] mixed oxygen and hydroxyl-functionalized high-surface-area graphene nanoplatelets with PMMA to yield graphene reinforced PMMA nanocomposites with a significant increase of about 30 °C in the glass transition temperature using only 0.5 wt % functionalized graphene nanoplatelets.

Amide-functionalized graphene nanoplatelets (few layer graphene) were prepared by Das et al.[279] to reinforce PMMA. This functionalization resulted in a significant increase of 70% and 10% in the elastic modulus and the hardness, respectively, of the composites with the addition of 0.6 wt % of graphene nanoplatelets.

Fang et al.[226] demonstrated that polystyrene (PS) chains can be covalently grafted onto the surface of partially RGO nanoplatelets, enhancing the glass transition temperature of the polymer by 15 °C. The initiator molecules were covalently bonded to the RGO surface via a diazonium addition, and the subsequent ATRP of styrene was carried out. With the addition of only 0.9 wt % GO nanoplatelets, the resulting PS/RGO composite film exhibited a prominent reinforcement effect, showing a 57.2% and 69.5% increase in Young's modulus and tensile strength, respectively. The synthesis of PS grafted GO nanoplatelets at room temperature was reported by Sun et al.[280] The obtained functionalized nanoplatelets exhibited good dispersibility in organic solvents. The covalent grafting of polyglycerol onto the surface of GO was reported by Pham et al.[281] while Zhang et al.[282] reported that GO can be functionalized with poly(N-vinylcarbazole) (PVK), where GO acts as an electron acceptor, while PVK acts as the electron donor. This material was characterized by IR, DSC, TGA, UV-vis, CV, XRD, and AFM. A nanocomposite of waterborne polyurethane (WPU) with covalent functionalized graphene nanoplatelets finely dispersed in the polymer matrix improves the conductivity of the WPU.[283,284]

V. Addition of Other Organic Molecules

One of the earliest reports of the functionalization of GO was the formation of amide bonds between octadecylamine (ODA) and the carboxylic groups of GO.[285,286] The functionalized GO product was characterized by Raman, FT-IR, UV spectroscopy, AFM microscopy, and thermogravimetric analysis and was found to be dispersible in THF (0.5 mg/mL), CCl_4, and 1,2-dichloroethane. Water-dispersible GO derivatives have been produced by the attachment of allylamine, p-phenyl sulfonate, and phenylene diamine groups on the graphene surface.[124,287]

GO can also be used as support for the immobilization of enzymes in the preparation of biosensors. As an example, glucose oxidase (GO_x) can be immobilized on GO nanoplatelets through amide bonds (Figure 22).[288]

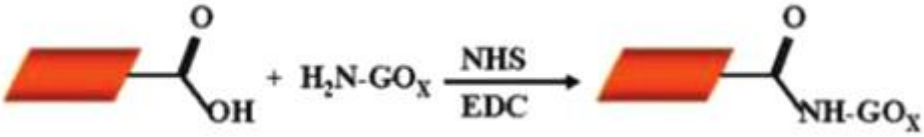

Figure 22. Immobilization of glucose oxidase (H_2N-GO_x) onto GO nanoplatelets.[288]

The GO/GO_x composite has been examined as a biosensor for the determination of glucose and was shown to give a linear response over a broad concentration range and exhibit high sensitivity, reproducibility in measurements, and biocompatibility with human cells. Zhang et al.[289] have reported on the formation of a hybrid material by covalent linking of C_{60} with GO (Figure 23). In this synthesis an amide bond was formed between a pyrrolidine ring modified C_{60} and the carboxyl groups on the GO surface. Analogously to the fullerene derivatives of carbon nanotubes,[290,291] GO-C_{60} hybrids could be useful in many optoelectronic applications due to their remarkable electronic and optical properties. Another interesting modification of partially RGO with imidazolium derivatives was presented by Yang et al.;[292] they showed that 1-(3-aminopropyl)-imidazolium bromide can be attached to the epoxy groups of GO nanoplatelets (Figure 24).

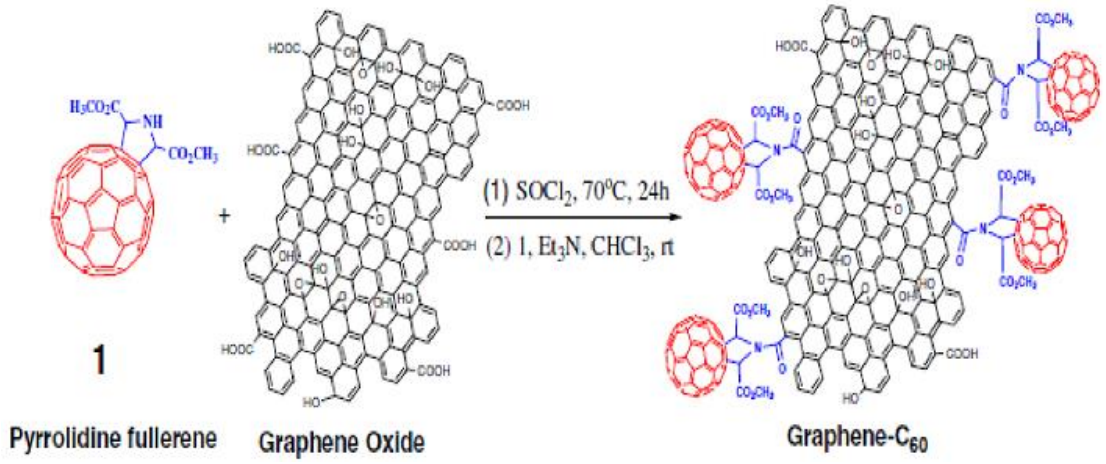

Figure 23. Representation of the formation of the C_{60}−GO composite.[289]

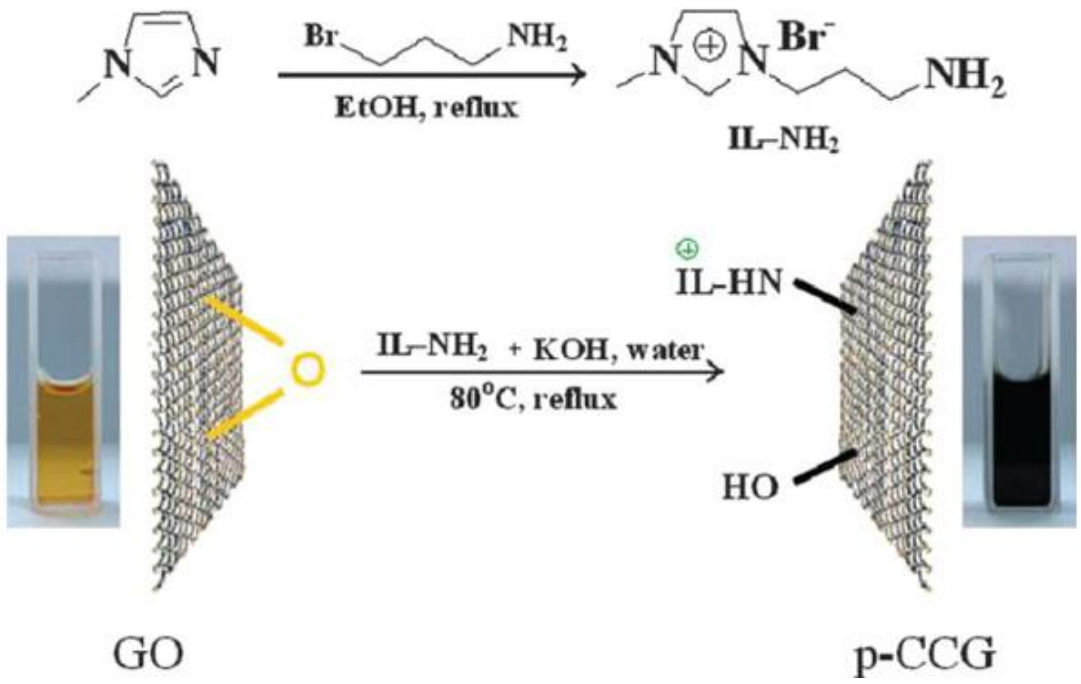

Figure 24. Illustration of the preparation of imidazolium-modified GO.[292]

An organic GO derivative obtained from the covalent attachment of phenyl isocyanate to GO through the formation of an ester bond with the epoxy group has been used in several diverse applications. After this chemical modification, GO nanoplatelets were easily dispersible in organic solvents such as *o*-DBC and DMF; additionally the incorporation of these organically modified GO nanoplatelets into polymers and conjugated polymers for photovoltaics was facilitated. This procedure was initially developed by Stankovich et al.[13] as a general approach for preparation of GO−polymer composites. Phenyl isocyanate-treated GO nanoplatelets were dispersed in PS and other styrenic copolymers, such as acrylonitrile-butadiene-styrene or styrene-butadiene, through solution phase mixing. The modified GO was then chemically reduced in order to improve the electrical conductivity of composites.

This functionalization procedure has been further used by Liu and co-workers[293,294,295] in the fabrication of organic photovoltaic cells. The phenyl isocyanate functionalized graphene was easily dispersed into *o*-DBC, and this was further dispersed in P3HT to form a donor/acceptor system. After the insertion of modified GO into P3HT, a remarkable quenching of the photoluminescence was observed, indicating a strong interaction and electron transfer from P3HT to GO nanoplatelets. This function

makes the formed composite suitable as an active layer in bulk heterojunction photovoltaic cells as represented in Figure 25. A photovoltaic cell containing the P3HT/GO composite showed a power conversion efficiency of 1.1%.[295]

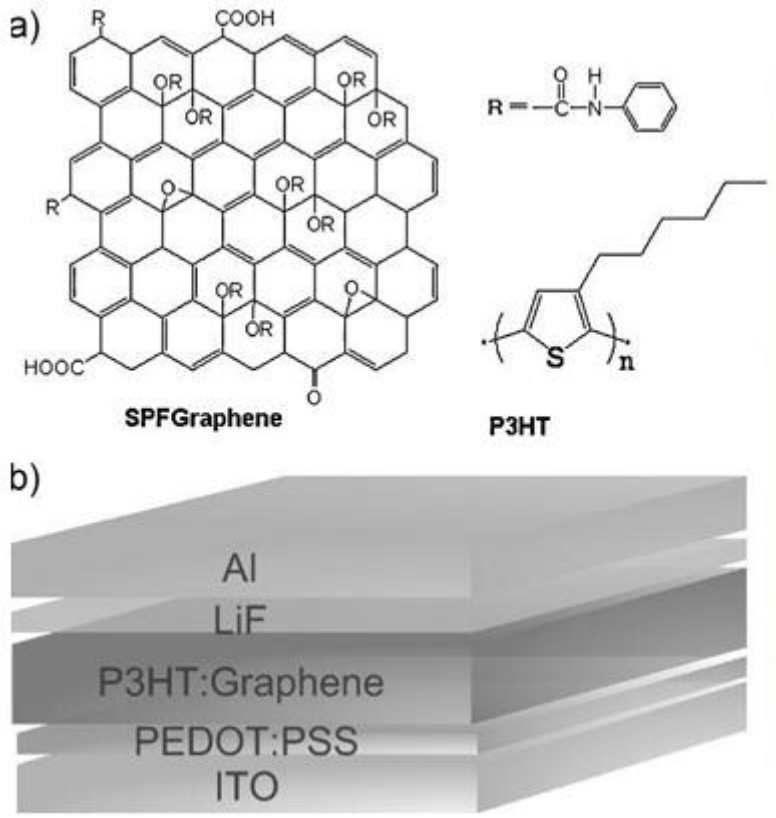

Figure 25. (a) Graphical representation of the modified graphene and P3HT, (b) schematic representation of the bulk heterojunction photovoltaic cells.[295]

Finally, Avinash et al.[296] obtained covalently functionalized GO with ferrocene via a green chemistry approach at room temperature on solid phase alumina. The ferrocene/GO composite material exhibited interesting magnetic properties, with the magnetization of the composite material found to be more than that of both GO and ferrocene.

VI. Starting from Partially Reduced Graphene Oxide

As referred in the introduction of this chapter the complete reduction of GO to graphene via different routes has not been achieved yet. There are always epoxy and hydroxyl functional groups on the basal plane of the RGO.[297] Density functional theory (DFT) investigations of the structure of graphene after deoxygenation confirm that it is impossible to completely remove the oxygen-containing functional groups from the

graphene surface using chemical or thermal reduction or even a combination of these two.[298,299]

In a subsequent DFT study, Ghaderi and Peressi[300] confirmed the presence of hydroxyl groups after reduction. The residual oxygen-containing groups give the RGO a weaker chemical reactivity as regards organic groups that can be grafted onto the graphene surface through oxygen linkers. The chemical functionalization of RGO using residual oxygen groups has been presented by Hsiao et al.[301] This procedure has the advantage that it does not create additional defects on the graphene surface compared with the reaction with C=C bonds. They used a specific polymeric molecule (MA-POA2000), which was grafted onto RGO by two different methods, radical addition and condensation using residual epoxy groups (Figure 26). In the free radical grafting method, initiated by benzoyl peroxide, the radical attacked the sp^2 carbon atoms on the RGO surface. In the second method, the free amine groups reacted with the residual epoxy groups of RGO.

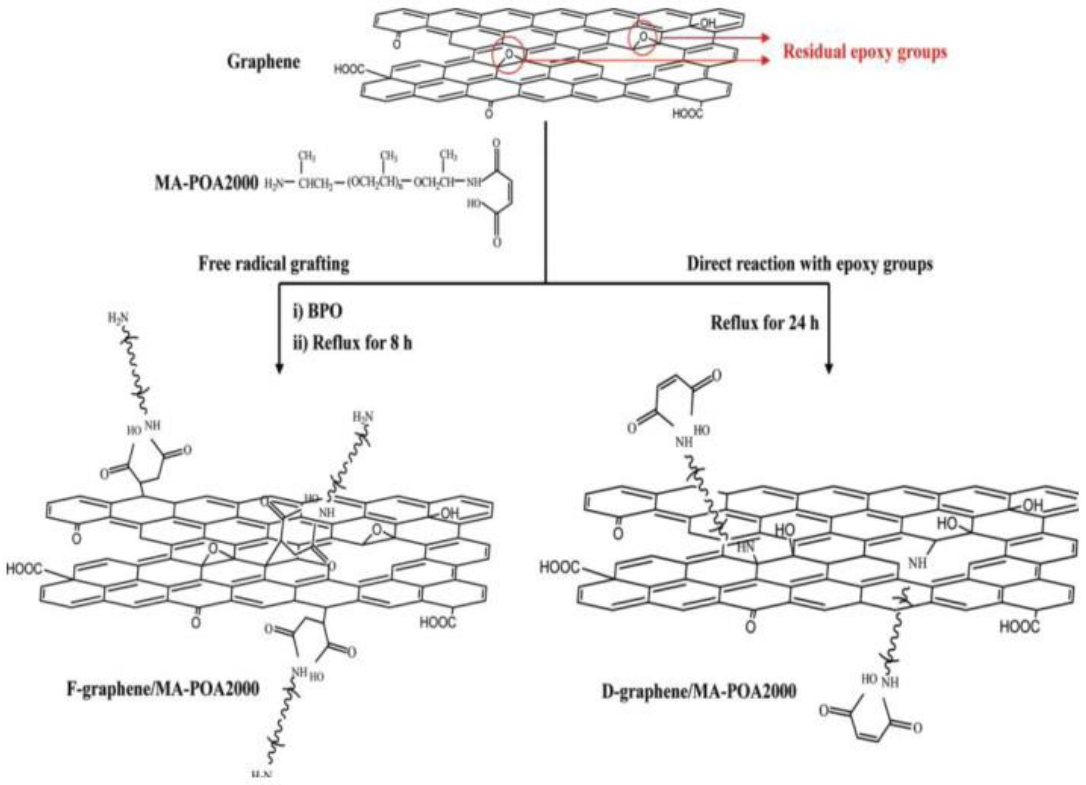

Figure 26. Two different grafting methods from the same organic molecule.[301]

Derivatives of RGO with poly(oxyalkyne)-amine are dispersible in THF (0.25 mg/mL), and the dispersions remain stable for at least two months. RGO was also used by Shen et al.[302] for the preparation of "amphiphilic" graphenes. Here GO was reduced by sodium boron hydride ($NaBH_4$) affording RGO nanoplatelets, which were decorated with PS−polyacrylamide copolymer (PS−PAM) by in situ free radical polymerization, initiated by benzoyl peroxide (Figure 27). The polymerized GO is dispersible in water, due to its hydrophilic PAM component, and simultaneously in xylene due to the hydrophobic PS component. Additionally, by controlling the ratio between the two polymeric components, the hydrophilic-hydrophobic balance of the functionalized graphene can also be controlled.

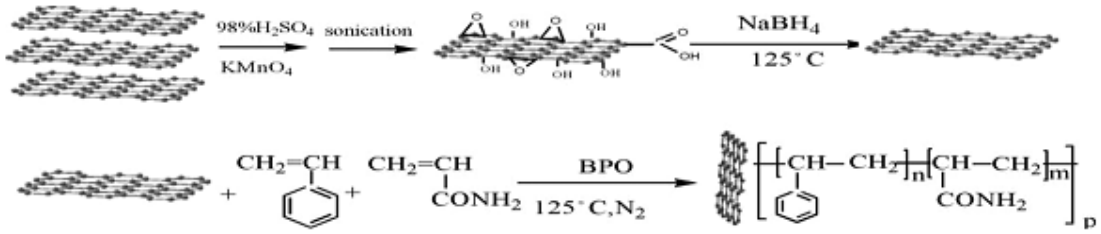

Figure 27. Schematic representation of covalent attachment of PS/PAM copolymer to RGO.[302]

Non-covalent functionalization of pristine graphene

In addition to covalent functionalization, graphene also exhibits non-covalent bonding via π-π stacking, cation-π or van der Waals interactions on the sp^2 networks (where present) that are not oxidized or engaged in hydrogen bonding. Via these non-covalent attachments, functional species can be anchored on the surface of graphene sheets without chemical bonding, but able to render external forces to disperse graphene in various media. Moreover, the non-covalent functionalization, comparing to covalent functionalization, is considered to have less impact on the structure and properties of graphene. Ruoff et al. first used poly(sodium 4-styrenesulfonate) (PSS), a ionic polymer with abundant aromatic structures, to stabilize ReG solution in water.[245] The strong π-π interaction between graphene plane and PSS prevents ReG from reaggregation during the reduction step and therefore, form a very stable aqueous dispersion of ReG with concentration up to 1 mg/mL. Similar effect was also observed when aromatic molecules or polymers were applied as surfactant (such as Phospholipid-PEG,[303]

pyrene salts,[304] TCNQ,[305] pyrene diimide salts[27] and sulfonated polyaniline[306] (Figure 28).

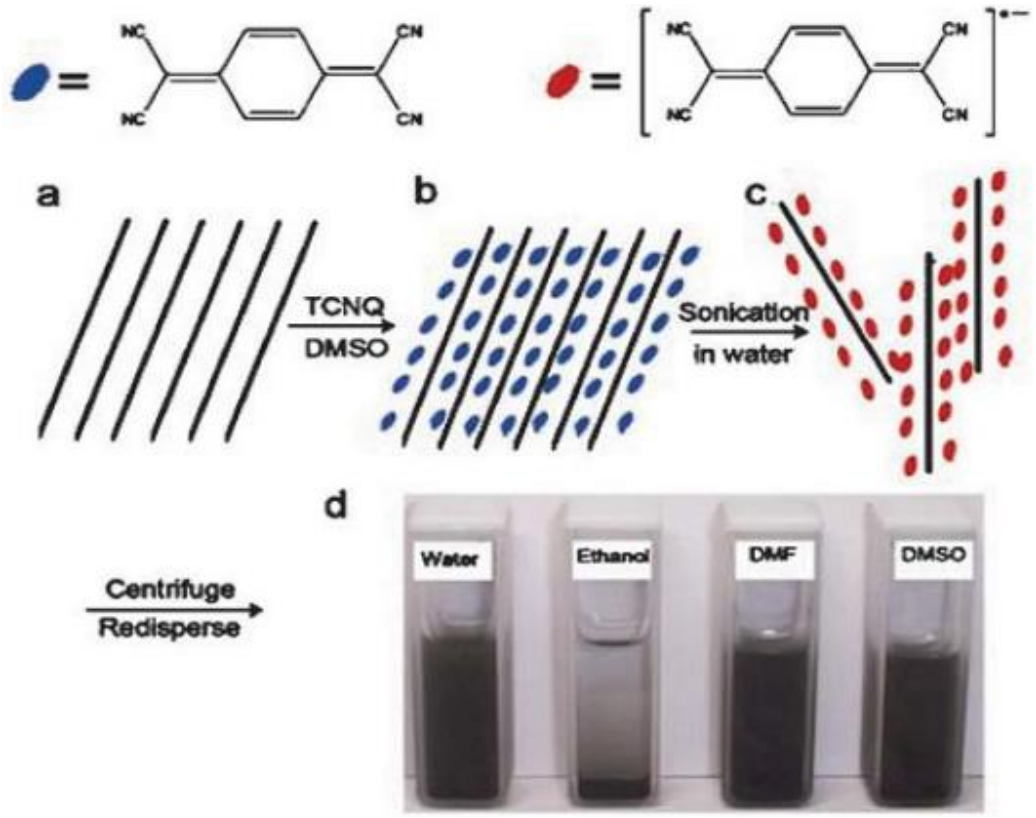

Figure 28. Schematic illustration of aqueous graphene dispersions stabilized with TCNQ anion. a) Pristine expanded graphite b) TCNQ insertion into graphite by the aid of DMSO c) after durative sonication, TCNQ-anion-stabilized graphene in water d) photograph of TCNQ anion adsorbed graphene dispersed in different solvents: water, ethanol, DMF, DMSO.[305]

Later on, it has been discovered that carboxylic acids were not affected by chemical reduction of GO, and these groups would remain intact on the edge of graphene sheets after hydrazine reduction and, if deprotonated, would provide sufficient electrostatic repulsion (zeta potential is about –30 mV) to overcome the aforementioned van der Waals attraction.[257]

By adding ammonia to raise the pH of the suspension to ~10 during the hydrazine reduction of graphene oxide, a stable aqueous dispersion of graphene was obtained. Unfortunately, this suspension was fairly sensitive to both pH and the presence of ‘‘hard’’ electrolytes such as sodium chloride. Furthermore, graphene sheets were successfully transferred into organic solution (such as chloroform) via ionic interaction with the assistance of amphiphilic alkyl ammonia salt (NR_4^+).[123]

The properties of ReG in graphene-based composite materials are greatly limited by the functionalization processes and the defects left during the processes. How to increase the electrical/thermal conductivity as well as the mechanical strength of graphene-based composite materials remains a big challenge.

2.2 Applications of graphene-based materials in organic solar cells[307]

The unique properties, i.e., highly optical transparence, highly electrical conduction, and mechanical flexibility, graphene and its derivatives have been investigated extensively in the field of solar cells. Lots of impressive results have been reported, where graphene was used as the electrodes, i.e., transparent electrodes[19,21,36,308,309,310,311,312,313,314,315] transparent cathodes, as well as where graphene was used as the active layer, i.e., light harvesting material,[293,316,317] Schottky junction,[318,319,320] electron transport layer,[321,322,323,324,325] hole transport layer,[259,326,327,328,329] both hole and electron transport layer,[3288] and interfacial layer in the tandem configuration.[330,331,332]

a) Conductive Electrodes

Recently, graphene has been successfully used as the transparent conductive anode for the flexible organic photovoltaic (OPV) cell with the configuration graphene/poly(3,4-ethylenedioxythiophene):poly(styrenesulfonate) (PEDOT:PSS)/copper phthalocyanine (CuPc)/C_{60}/bathocuproine(BCP)/Al (Figure 29a).[21] Graphene was first deposited onto the Si/SiO_2/Ni film by chemical vapor deposition (CVD) and then transferred onto the transparent glass or polyethylene terephthalate (PET) substrates (Figure 29b). The obtained graphene/PET film showed its sheet resistance down to 230 Ω/sq with transparency of 72 %. The solar cell incorporating CVD-grown graphene (referred to here as CVD-graphene) as the transparent conductive anode exhibited a power conversion efficiency (η) of 1.8%, which is comparable to the performance (1.27%) obtained in the device with the commonly used ITO electrode. Obviously, the flexibility of CVD-graphene device surpasses that of the ITO device because the former device can operate under bending up to 138° (Figure 29c), whereas the latter one degraded

rapidly and irreversibly even under bending of 60° (Figure 29d). Consistently, the decay/decrease rate of the initial fill factor in the CVD-graphene device was much slower than that in the ITO one as the bending angle increased, and the fill factor of the ITO device rapidly decayed to 0 when it was bent to around 60° (Figure 29e). The lower performance under bending, i.e., lower flexibility, of the ITO device was caused by the generation of microcracks in the ITO film under mechanical stress, while no such microcracks were observed on the CVD graphene device (Figure 29f).

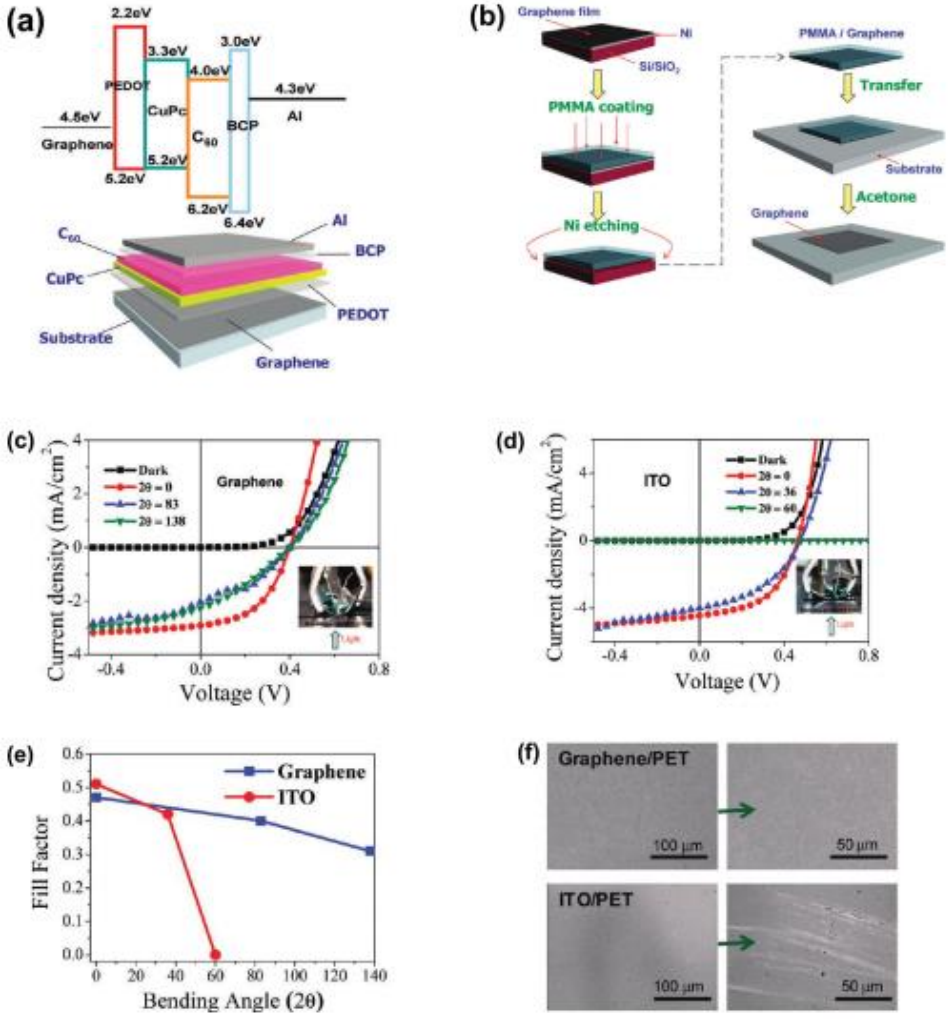

Figure 29. a) Schematic representation of the energy level alignment (top) and the construction of heterojunction organic solar cell fabricated with graphene as anodic electrode: graphene/PEDOT/CuPc/C_{60}/BCP/Al. b) Schematic illustration of the transfer process of CVD-graphene onto transparent substrate. The plots of current density vs voltage for c) graphene and d) ITO devices under 100 mW cm^{-2} AM1.5G spectral illumination at different bending angles. Insets show the experimental setup used in the experiments. e) The plot of fill factor vs bending angle for the graphene and ITO devices. f) Scanning electron microscopy (SEM) images of the surface structure of CVD-graphene (top) and ITO (bottom) devices after being subjected to the bending angles described in panels (c,d).[21]

In the area of flexible OPV devices, Zhang's group has used chemically reduced graphene oxide (rGO) as the transparent conductive anode in the device with configuration of rGO/PEDOT:PSS/poly(3-hexylthiophene):phenyl-C_{61}-butyric acid methyl ester (P3HT:PCBM)/TiO_2/Al. The performance of the OPV devices mainly depends on the charge transport efficiency and the transparency of the rGO electrodes, when the optical transmittance of rGO is above and below 65%, respectively. Impressively, the fabricated OPV device on rGO can sustain a thousand bending cycles at 2.9% tensile strain.[308]

Iijima and co-workers reported a roll-to-roll method to transfer the 30-inch CVD-graphene monolayer film from the copper foil onto a flexible substrate, such as PET.[36] The graphene film exhibited 97.4% optical transmittance with sheet resistance as low as 125 Ω/sq. After a four-layer graphene film was achieved by layer-by-layer stacking, it was doped with HNO_3, showing the further decreased sheet resistance (≈30 Ω/sq at ≈90% transparency), which is superior to the commercial transparent ITO electrode. Furthermore, such graphene electrode was capable of withstanding high strain.[36]

All of the aforementioned reports have demonstrated the highly flexible nature of graphene, which shows its potential application as the transparent conductive anode electrode for flexible solar panels, since both CVD-graphene and solution-processed rGO have exhibited superior mechanical performance over ITO. For the flexible CVD-graphene based thin film, which is compatible with the roll-to-roll fabrication process developed by Iijima and co-workers,[166] it possesses not only better mechanical properties than ITO, but also superior sheet resistance and transparency compared to ITO when used as a transparent electrode.

In addition to the OPV devices, graphene also shows potential as the transparent anode electrode for dye sensitized solar cells (DSSCs). In a recent report,[19] the graphene thin film, prepared by dip coating aqueous graphene oxide (GO) solution on quartz followed by temperature-controlled film drying and subsequent thermal reduction, exhibited a high conductivity of 550 S cm^{-1} and transparency of more than 70% in the wavelength range of 1000–3000 nm. A solid-state DSSC with configuration of graphene/TiO_2/dye/spiro-OMeTAD/Au has been fabricated using the graphene film as the transparent anode (Figure 30a). The corresponding energy level diagram of the DSSC device is shown in Figure 30b. This is the first demonstration of a solid-state

DSSC based on a graphene electrode with the power conversion efficiency (PCE) of 0.26%, which is still lower compared to the fluorine tin oxide (FTO)-based solid-state DSSC (0.84 %, Figure 30c).

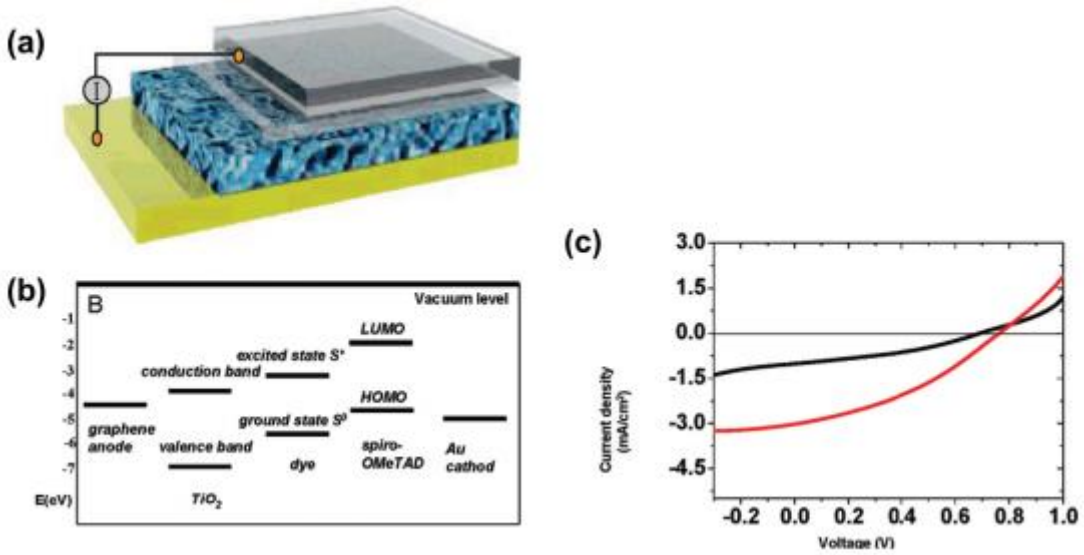

Figure 30. Illustration and performance of DSSC based on graphene electrodes. a) Schematic illustration of DSSC using graphene film as electrode. The four layers from bottom to top are Au, dye-sensitized heterojunction, compact TiO_2, and graphene film. b) The energy level diagram of the DSSC with the configuration of graphene/TiO_2/dye/spiro-OMeTAD/Au. c) Current density–voltage curves of the graphene-based cell (black) and FTO-based cell (red) illuminated under AM solar light (1 sun).[19]

Graphene has also been developed as the transparent conductive cathode electrode for solar cells. Recently, has been reported that rGO was used as the working electrode for electrochemical deposition of functional materials, which was further used as the cathode electrode for the hybrid solar cell application.[308]

Briefly, the rGO thin film on quartz was obtained by two-step reduction of GO, i.e., using hydrazine vapor and then thermal annealing. It exhibited a sheet resistance of 420 Ω/sq at 61 % transmittance. The n-type ZnO nanorods (NRs) were electrochemically deposited on the obtained rGO electrode. Then, the p-type poly(3-hexylthiophene) (P3HT) layer was spin-coated on the top of ZnO NRs to form an inorganic–organic material based hybrid solar cell. In addition, we found that the electrochemical deposition of ZnO strongly depends on the thickness, i.e., the sheet resistance, of the rGO film. The thicker rGO film with lower sheet resistance has advantages for the growth of high quality crystalline ZnO nanorods. The device with a layered structure

of quartz/rGO/ZnO NRs/P3HT/PEDOT:PSS/Au was fabricated with a PCE of around 0.31% (Figure 31a).

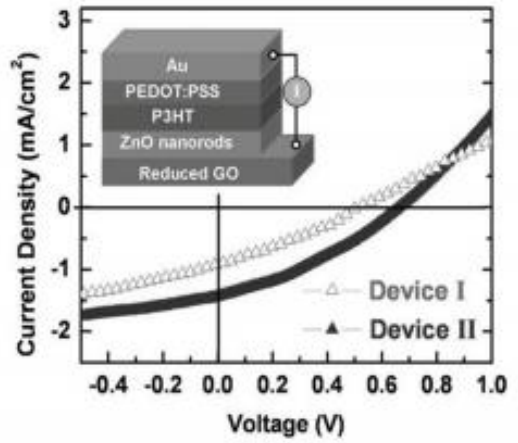

Figure 31. Current density-voltage (J-V) characteristics of ZnO/P3HT hybrid solar cells with rGO film as electrode. Inset: schematic illustration of the fabricated solar cell.[309]

b) Active Layers

The facile chemical functionalization enables graphene as a new candidate for active material in photovoltaic device applications.[293,316,317] Moreover, the work function of graphene can be adjustable by doping with another semiconductor to form a Schottky junction if their energy band structures match.[318,319,320,333,334] With high charge mobility, graphene and rGO are good candidates for the electron transport layer,[321,322,323,324,325] hole transport layer,[259,326,327,328,329] both hole and electron transport layer,[328] and interfacial layer for tandem solar cells in the photovoltaic field.[330,331,332]

Light-Harvesting Materials

GO is easy to be functionalized based on various requirements since it has various functional groups. For example, Chen and co-workers functionalized GO sheets with phenyl isocyanate, which changed hydrophilic GO surface to hydrophobic one.[293] The resultant solution-processed functionalized graphene (SPF-Graphene) was mixed with poly(3-octylthiophene) (P3OT) to form the P3OT/SPF-Graphene composites, which were then used as the active layer material in the bulk heterojunction (BHJ) OPV device (Figure 32 a–d). The annealing conditions are critical for better performance of the device, since annealing can remove the functional groups from graphene sheets and enhance the crystallinity of P3OT. Based on their result, the optimized annealing

condition, 160 °C for 20 min, was applied for fabrication of the OPV device, which achieved the best power conversion efficiency of 1.4%. This work indicated that the functional graphene can serve as a competitive alternative to [6,6]-phenyl C_{61}-butyric acid methyl ester (PCBM) as the electron acceptor for high-performance OPV devices.

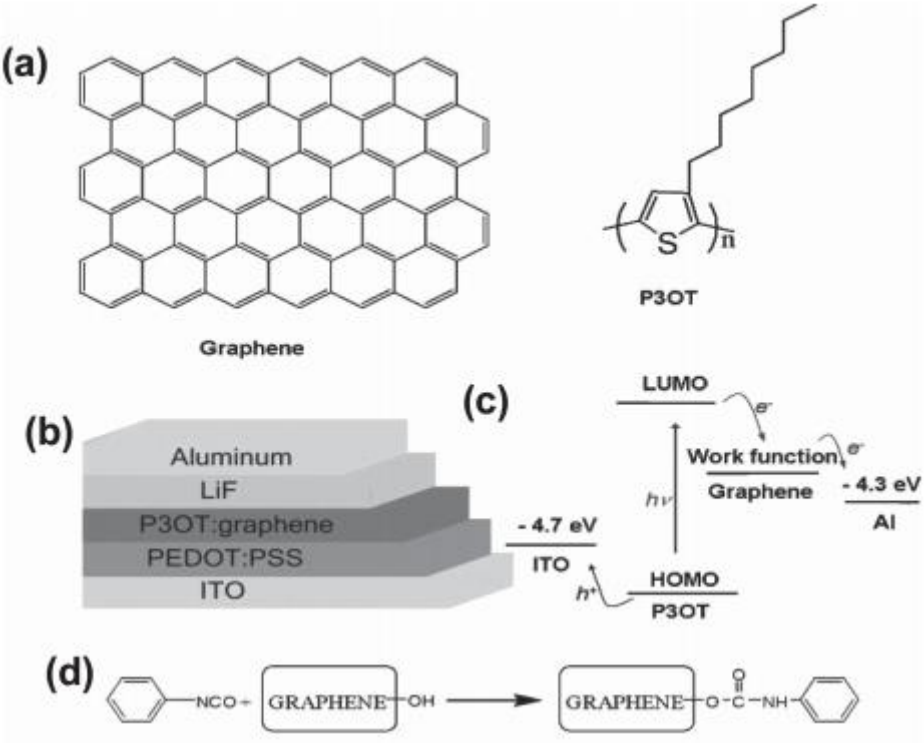

Figure 32. a) The idealized chemical structures of graphene and P3OT. b) Schematic illustration of the device with P3OT/graphene thin fi lm as the active layer and the structure ITO (ca. 17 Ω/sq)/PEDOT:PSS (40 nm)/P3OT:graphene (100 nm)/LiF (1 nm)/Al (70 nm). c) Energy level diagram of P3OT and SPF-Graphene. d) Schematic representation of the reaction of phenyl isocyanate with GO to form SPF-Graphene.[293]

Importantly, the effect of graphene with different lateral size in OPV devices was studied.[316] In this work, the active layer of OPV device was composed of aniline-functionalized graphene (used as electron acceptor) and P3HT (used as electron donor). It was found that after optimization, the device with aniline-functionalized graphene quantum dots (ANI-GQDs) and P3HT showed enhanced efficiency as compared to the one with aniline-functionalized graphene sheets (ANI-GS) and P3HT. The corresponding current density versus voltage curves of ANI-GQDs-P3HT and optimized ANI-GS-P3HT based devices are plotted in Figure 33. The maximum power conversion efficiency is 1.14 % obtained from ANI-GQDs with 1 wt% of ANIGQD and P3HT, which is much higher than 0.65 % obtained from the optimized ANI-GS

devices with 10 wt% ANI-GSs and P3HT. This is attributed to the improved morphological and the optical characteristics in ANI-GQDs. The performance of GQD-based devices is expected to be further improved by choosing other proper functionalization systems.

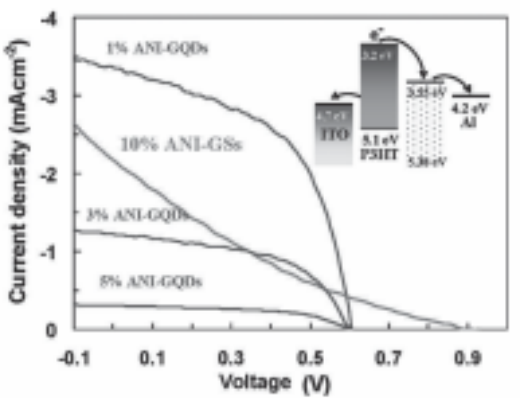

Figure 33. J–V characteristics of the photovoltaic devices based on ANI-GQDs with different amount of GQDs in ANI and ANI-GS with 10 wt% GS in ANI (under optimized condition) annealed at 160 °C for 10 min.[316]

In addition, Li and co-workers presented a novel solubilization strategy for synthesis of graphene nanostructures through a bottom-up method instead of the common top-down method based on the exfoliation of graphite.[317] Solution-processable black GQDs with uniform size were synthesized through solution chemistry, which were then used as a sensitizer for solar cells. However, a much low current density was observed, which was attributed to the low affinity of GQDs on TiO_2 surface due to the physical adsorption, and the consequent poor charge injection. In the future, synthesis of hydrophilic graphene nanostructures or realization of the chemical bonding between graphene nanostructures and TiO_2 surface is expected to improve the device performance.

c) Charge Transport Layers

Electron Transport Layer

Taking the advantage of high electron mobility of graphene, Jiang and co-workers reported that rGO can be used as the 2D electron transport channel in rGO-TiO_2 nanocomposite based DSSCs, showing better performance than 1D CNT-TiO_2 composite based DSSCs (Figure 34a–d). In graphene composite electrodes, the

particles can anchor onto graphene better, and the photogenerated electrons can be easily captured and transferred by the graphene. However, when the composite of TiO_2 with 1D CNT is formed, there is less contact/connection between them. Therefore, the transfer barrier is large, resulting in the severe recombination of electrons and holes. Based on the operational principle of the device (Figure 34e), the introduced 2D graphene performs as an electron transport layer, i.e., accepts electrons from TiO_2 and then transfers them quickly to the FTO electrode. Therefore, the recombination of electrons and holes is suppressed.

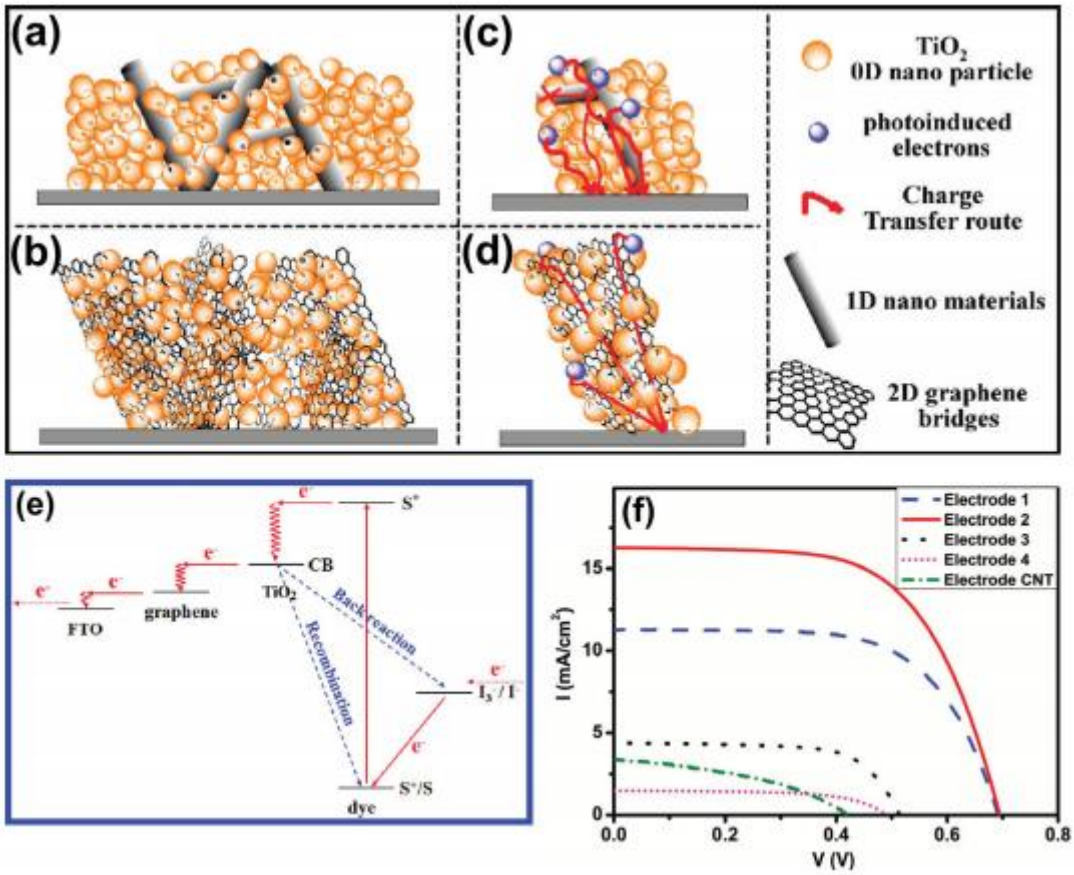

Figure 34. Schematic illustrations of a,c) 1D and b,d) 2D nanomaterial composite electrodes. e) Operational principle of the device in term of charge transfer behavior in the DSSC. f) Photocurrent–voltage characteristics of different electrodes. The sensitizer is N3 (ruthenium dye). The cell active area is 0.20 cm2. The light intensity is 100 mW cm^{-2}. Electrodes 1–4 are pure TiO_2, TiO_2 with loading of 0.6% GO, TiO_2 loading of with 2.5% GO, and TiO_2 loading of with 8.5% GO, respectively.[324]

In Figure 34f, the photocurrent–voltage characteristics of DSSCs with different electrodes are presented. The best performance is demonstrated by the device with the photoanode layer of TiO_2 with loading of 0.4 % rGO (i.e., ≈0.6% GO loading since GO will lose weight after reduction).[324] It means there is an optimal rGO loading window

in terms of the PCE of the devices because too little graphene loading weakens its electron transporting effect, while too much graphene loading reduces the dye adsorption onto TiO_2. Moreover, the excessive graphene can act as a kind of recombination center instead of providing an electron pathway, thus easily triggering the short circuit.

As another example, graphene as the electron transport layer (ETL) in OPV has been reported by Heeger and co-workers.[335] Instead of the usual solution-processed coating to prepare graphene film, they developed a novel facile stamping process to directly transfer graphene onto the bulk heterojunction (BHJ) layer prior to the top Al cathode deposition. Such stamping nanotechnology is able to transfer large-area, single-layer CVD-graphene onto specific regions of a substrate. In this work, the graphene was first doped/oxidized by HNO_3, which is also called graphene oxide (GO). In order to compare with the traditional TiO_x ETL used in OPV, the pure GO, pure TiO_x, and GO/TiO_2 double layer used as the ETL in OPV and the device without the ETL were all studied. Consistently, the OPV with ETL has much higher power conversion efficiency (PCE) than that without the ETL. Importantly, the PCE of a device based on a GO/TiO_2 ETL was increased by 6.8% compared to the pure TiO_2 ETL based device. The improved BHJ device performance is attributed to the fact that introduction of the GO/TiO_2 ETL layer, as compared to the pure TiO_2 or GO ETL layer, increases the hole blocking barrier (Φ_h) and simultaneously shifts E_{vac} downwards, thereby decreasing the electron injection barrier in the BHJ device. The larger hole blocking barrier facilitates the photogenerated hole to transport towards the ITO anode. The smaller electron injection barrier enables the photogenerated electron to transport efficiently towards the Al cathode. Hence, such a synergistic effect enhances the short-circuit current density (Jsc) and thus the PCE of GO/TiO_2 ETL-based BHJ devices.

Hole Transport Layer

Different from graphene, which is a highly efficient electron transporter, the functionalized GO and GO-based composites showed excellent hole transport properties in photovoltaic devices. Huang and co-workers have combined GO and SWCNTs as the hole transport layer for P3HT:PCBM-based polymer solar cells (Figure 35a). They found that the addition of the proper amount of SWCNTs into GO can significantly improve the conductivity of the GO film as the hole transport layer. Such

GO:SWCNT composite films reduce the hole transport resistance and facilitate the hole transport from the active layer to the anode. The results shown in Figure 35b demonstrate that the GO:SWCNTs composite film based device exhibits higher performance than the pure GO film based one. Note that the GO:SWCNT composite can offer comparable performance to the conventional PEDOT:PSS based devices.[329] At the same time, Chhowalla and co-workers also reported that the thin GO film with thickness of ≈2 nm on ITO can work as an effective hole transport layer in polymer solar cells (Figure 35c), showing the comparable values of efficiency to devices fabricated with PEDOT:PSS. They also found a clear trend of decreasing PCE with increasing GO film thickness (Figure 35d). As a result, the thinnest GO film yielded the best performance. This is mainly attributed to the increased serial resistance in the thicker GO film, which decreases J_{sc} and FF and also slightly lowers its transmittance.

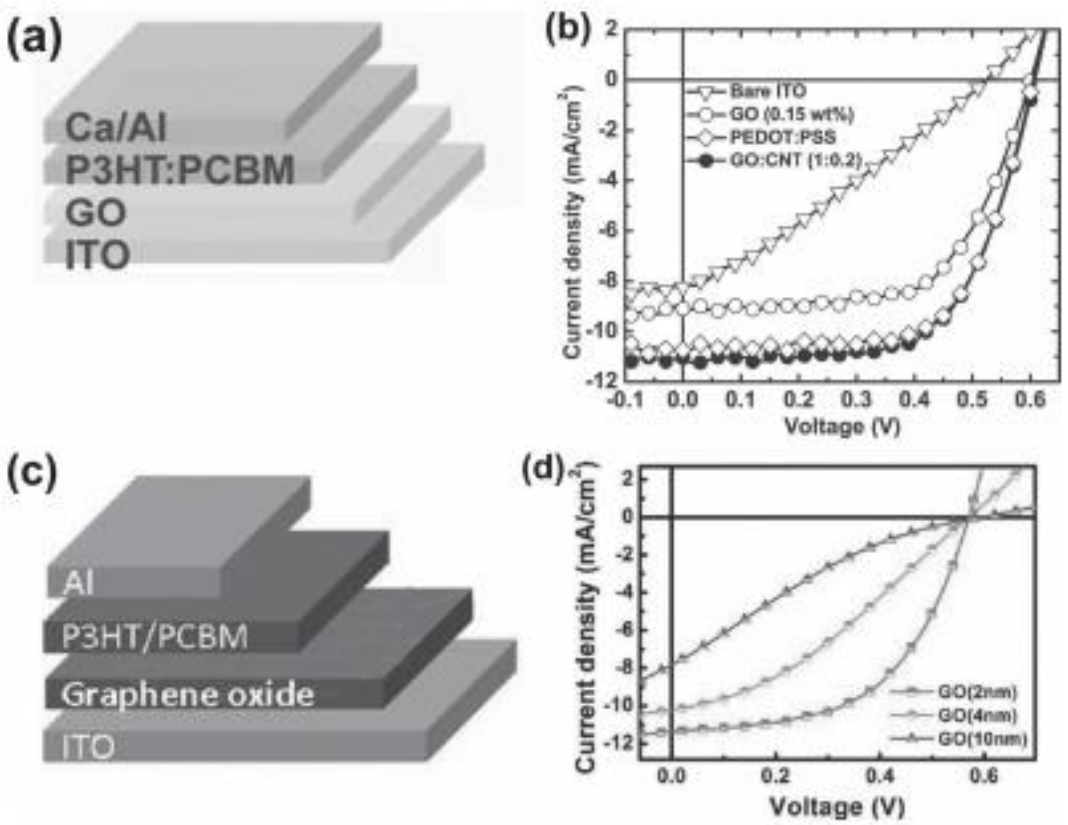

Figure 35. a) Schematic illustration and b) current density–voltage characteristics of ITO/GO/ P3HT:PCBM/Ca/Al device based on unmodified ITO (inverted triangle), GO layer (open circle, spin coated from 0.15 wt% dispersion), PEDOT:PSS layer (diamond), and GO:SWCNT layer (solid circle, spin coated from 0.15 wt% GO dispersion, GO:SWCNTs =1:0.2, w/w).[329] c) Schematic illustration and d) current density–voltage characteristics of ITO/GO/P3HT:PCBM/Al devices with different GO thickness.[326]

Hole and Electron Transport Layer

The work function of GO can be easily tuned by simple chemical modification. Dai and co-workers recently reported GO and modified GO as hole and electron transport layers, respectively, in the single solar cell configuration.[328] As shown in Figure 36a,b, by replacing the periphery –COOH groups with –COOCs groups, the work function of the cesium-neutralized GO (GO-Cs) can be reduced to 3.9–4.1 eV from 4.6–4.8 eV for pure GO. As a result, the work function of GO matches both the ITO anode and the HOMO level of P3HT for efficient hole extraction, while the work function of GO-Cs matches both Al and the LUMO level of PCBM for efficient electron extraction (Figure 36b).

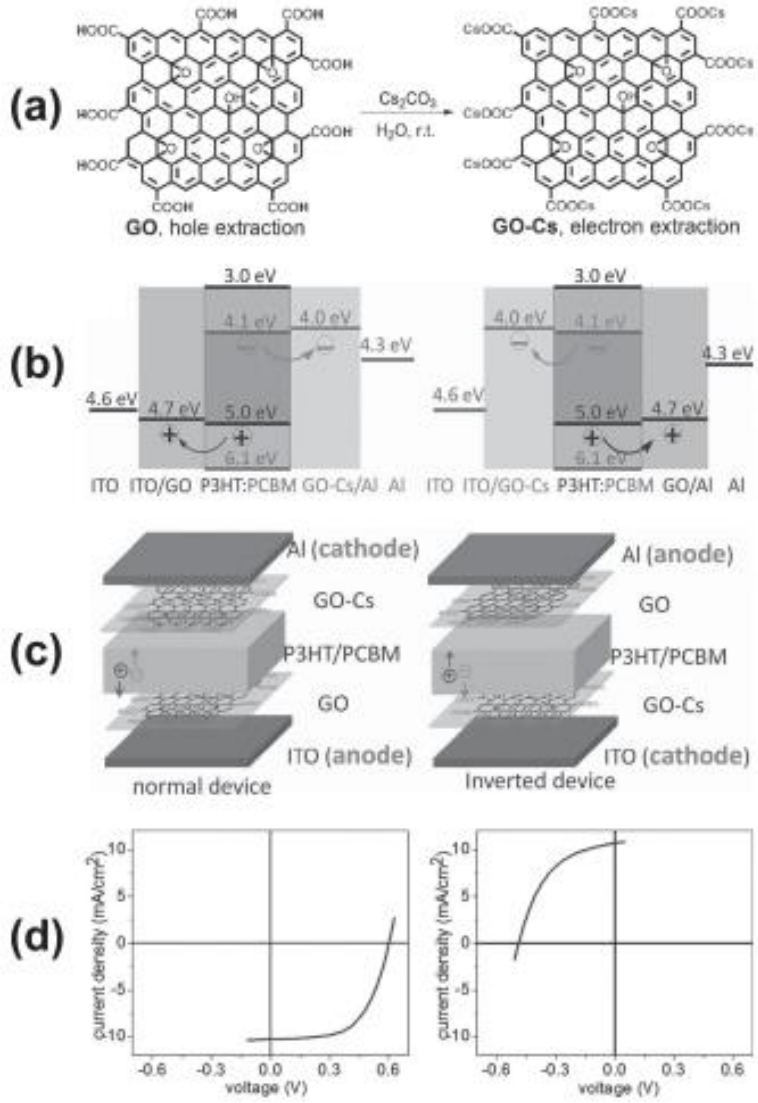

Figure 36. a) Chemical structures and synthetic route of GO and GO-Cs. b) Energy level diagrams and c) device structures of the normal device and the inverted device with GO as hole-extraction layer and GO–Cs as the electron-extraction layer. d) Current density-voltage curves of the normal device (left) and inverted device (right) with GO as the hole-extraction layer and GO–Cs as the electron-extraction layer.[328]

Excellent hole/electron extraction capabilities have been demonstrated for GO/GO-Cs based polymer solar cells. Both the normal device with the configuration of ITO(anode)/GO/P3HT:PCBM/GO-Cs/Al(cathode) and inverted device of ITO(cathode)/GO–Cs/P3HT:PCBM/GO/Al(anode) were investigated (Figure 36c). The observed good performance for both the normal and inverted devices containing GO and GO–Cs demonstrates the capability of hole and electron extraction from GO and GO–Cs, respectively. The slightly lower performance from the inverted device, compared with the normal device, is mainly due to its smaller open-circuit voltage (V_{oc}) (Figure 36d). This study implies that the chemically engineered GO is promising for both hole and electron transport materials in solar cells.

References

[1] R. Saito, G. Dresselhaus, M. S. Dresselhaus. Physical Properties of Carbon Nanotubes (Imperial College Press, London, 1998).

[2] B. T. Kelly. Physics of graphite (Applied Science Publishers, London, 1981).

[3] H. W. Kroto, J. R. Heath, S.C. O'Brien, R.F. Curl, R.E. Smalley, Nat. 1985, 318, 162.

[4] S. Iijima, Nat. 1991, 354, 56.

[5] K. S. Novoselov, A. K. Geim, S. V. Morozov, D. Jiang, Y. Zhang, S. V. Dubonos, I. V. Grigorieva, A. A. Firsov, Science 2004, 306, 666.

[6] Y. Li, L. Xu, H. Liu, y. Li, Chem. Soc. Rev., 2014,43, 2572.

[7] V. C. Tung, M. J. Allen, Y. Yang, R. B. Kaner, Nat. Nanotechnol. 2009, 4, 25.

[8] C. Gomez-Navarro, R. T. Weitz, A. M. Bittner, M. Scolari, A. Mews, M. Burghard, K. Kern, Nano Lett. 2007, 7, 3499.

[9] K. S. Kim, Y. Zhao, H. Jang, S. Y. Lee, J. M. Kim, K. S. Kim, J.H. Ahn, P. Kim, J. Y. Choi, B. H. Hong, Nat. 2009, 457, 706.

[10] T. O. Wehling, K. S. Novoselov, S. V. Morozov, E. E. Vdovin, M. I. Katsnelson, A. K. Geim, A. I. Lichtenstein, Nano Lett. 2008, 8, 173.

[11] P. K. Ang, W. Chen, A. T. S. Wee, K. P. Loh, J. Am. Chem. Soc. 2008, 130, 14392.

[12] R. Bogue, Sensor Review 2008, 28, 344.

[13] S. Stankovich, D. A. Dikin, G. H. B. Dommett, K. M. Kohlhaas, E. J. Zimney, E. A. Stach, R. D. Piner, S. T. Nguyen, R. S. Ruoff, Nature 2006, 442, 282.

[14] Y. X. Xu, W. J. Hong, H. Bai, C. Li, G. Q. Shi, Carbon 2009, 47, 3538.

[15] A. K. Geim, Science 2009, 324, 1530.

[16] R. R. Nair, P. Blake, A. N. Grigorenko, K. S. Novoselov, T. J. Booth, T. Stauber, N. M. R. Peres, A. K. Geim, Science 2008, 320, 1308.

[17] A. W. W. Ludwig, M. P. A. Fisher, R. Shankar, G. Grinstein, Phys. Rev. B 1994, 50, 7526.

[18] P. Blake, P. D. Brimicombe, R. R. Nair, T. J. Booth, D. Jiang, F. Schedin, L. A. Ponomarenko, S. V. Morozov, H. F. Gleeson, E.W. Hill, A. K. Geim, K. S. Novoselov, Nano Lett. 2008, 8, 1704.

[19] X. Wang, L. J. Zhi, K. Mullen, Nano Lett. 2008, 8, 323.

[20] D. I. Son, T. W. Kim, J. H. Shim, J. H. Jung, D. U. Lee, J. M. Lee, W. Il Park, W. K. Choi, Nano Lett. 2010, 10, 2441.

[21] L. G. De Arco, Y. Zhang, C. W. Schlenker, K. Ryu, M. E. Thompson, C. W. Zhou, ACS Nano 2010, 4, 2865.

[22] F. Gunes, G. H. Han, K. K. Kim, E. S. Kim, S. J. Chae, M. H. Park, H. K. Jeong, S. C. Lim, Y. H. Lee, Nano 2009, 4, 83.

[23] S. P. Pang, H. N. Tsao, X. L. Feng, K. Mullen, Adv. Mater. 2009, 21, 3488.

[24] C. A. Di, D. C. Wei, G. Yu, Y. Q. Liu, Y. L. Guo, D. B. Zhu, Adv. Mater. 2008, 20, 3289.

[25] E. Kymakis, K. Savva, M. M. Stylianakis, C. Fotakis, E. Stratakis, Adv. Funct. Mater. 2013, 23, 2742.

[26] E. Kymakis, E. Stratakis, M. M. Stylianakis, E. Koudoumas, C. Fotakis, Thin Solid Films 2011, 520, 1238.

[27] Q. Su, S. P. Pang, V. Alijani, C. Li, X. L. Feng, K. Mullen, Adv. Mater. 2009, 21, 3191.

[28] X. Wang, L. J. Zhi, N. Tsao, Z. Tomovic, J. L. Li, K. Mullen, Angew. Chem. Int. Ed. 2008, 47, 2990.

[29] E. Stratakis, K. Savva, D. Konios, C. Petridis, E. Kymakis, Nanoscale 2014, 6, 6925.

[30] E. Stratakis, M. M. Stylianakis, E. Koudoumas, E. Kymakis, Nanoscale 2013, 5, 4144.

[31] M. M. Stylianakis, E. Kymakis, Applied Phys. Lett. 2012, 100, 093301.

[32] M. M. Stylianakis, G. D. Spyropoulos, E. Stratakis, E. Kymakis, Carbon 2012, 50, 5554.

[33] M. M. Stylianakis, E. Stratakis, E. Koudoumas, E. Kymakis, S. H. Anastasiadis, ACS Applied Mater. Interfaces 2012, 4, 4864.

[34] P. Matyba, H. Yamaguchi, G. Eda, M. Chhowalla, L. Edman, N. D. Robinson, ACS Nano 2010, 4, 637.

[35] J. B. Wu, M. Agrawal, H. A. Becerril, Z. N. Bao, Z. F. Liu, Y. S. Chen, P. Peumans, ACS Nano 2010, 4, 43.

[36] S. Bae, H. Kim, Y. Lee, X. F. Xu, J. S. Park, Y. Zheng, J. Balakrishnan, T. Lei, H. R. Kim, Y. I. Song, Y. J. Kim, K. S. Kim, B. Ozyilmaz, J. H. Ahn, B. H. Hong, S. Iijima, Nat. Nanotechnol. 2010, 5, 574.

[37] G. Viskadouros, M. M. Stylianakis, E. Kymakis, E. Stratakis, ACS Applied Mater. Interf. 2014, 6, 388.

[38] G. Viskadouros, A. Zak, M. M. Stylianakis, E. Kymakis, R. Tenne, E. Stratakis, Small 2014 10, 2398.

[39] K. Savva, A. Y.-H. Lin, C. Petridis, E. Kymakis, T. H. Anthopoulos, E. Stratakis, J. Mater. Chem. C 2014, 2, 5931-5937.

[40] E. Kymakis, C. Petridis, T. D. Anthopoulos, E. Stratakis, IEEE J. Select. Top. Quant. Electron. 2014, 20, 6573325.

[41] W. Liu, B. L. Jackson, J. Zhu, C. Q. Miao, C. H. Chung, Y. J. Park, K. Sun, J. Woo, Y. H. Xie, ACS Nano 2010, 4, 3927.

[42] Y. Cao, Z. M. Wei, S. Liu, L. Gan, X. F. Guo, W. Xu, M. L. Steigerwald, Z. F. Liu, D. B. Zhu, Angew. Chem. Int. Ed. 2010, 49, 6319.

[4343] Y. Cao, S. Liu, Q. Shen, K. Yan, P. J. Li, J. Xu, D. P. Yu, M. L. Steigerwald, C. Nuckolls, Z. F. Liu, X. F. Guo, Adv. Funct. Mater. 2009, 19, 2743.

[44] C. M. Weber, D. M. Eisele, J. P. Rabe, Y. Liang, X. Feng, L. Zhi, K. Muellen, J. L. Lyon, R. Williams, D. A. V. Bout, K. J. Stevenson, Small 2010, 6, 184.

[45] Francesco Bonaccorso, Antonio Lombardo, Tawfique Hasan, Zhipei Sun, Luigi Colombo, Andrea C. Ferrari, Mater. Today 2012, 15, 564.

[46] R. A. Schultz, M. C. Jensen, R. C. Bradt, Int. J. Fracture 1994, 65, 291.

[47] R. Romero, M. Robert, F. Elsass, C. Garcia, Clay Minerals 1992, 27, 21.

[48] X. Lu, M. Yu, H. Huang, R. S. Ruoff, Nanotechnology 1999, 10, 269.

[49] K. S. Novoselov, D. Jiang, F. Schedin, T. J. Booth, V. V. Khotkevich, S. V. Morozov, A. K. Geim, PNAS 2005, 102, 10451.

[50] A. K. Geim, Science 2009, 324, 1530.

[51] C. Casiraghi, A. Hartschuh, E. Lidorikis, H. Qian, H. Harutyunyan, T. Gokus, K. S. Novoselov, A. C. Ferrari, Nano Lett 2007, 7, 2711.

[52] A. C. Ferrari, J. C. Meyer, V. Scardaci, C. Casiraghi, M. Lazzeri, F. Mauri, S. Piscanec, D. Jiang, K. S. Novoselov, S. Roth, A. K. Geim, Phys. Rev. Lett. 2006, 97, 187401.

[53] C. Casiraghi, S. Pisana, Appl. Phys. Lett. 2007, 91, 233108.

[54] S. Pisana, M. Lazzeri, C. Casiraghi, K. S. Novoselov, A. K. Geim, A. C. Ferrari, F. Mauri, Nat. Mater. 2007, 6, 198.

[55] A. Das, S. Pisana, B. Chakraborty, S. Piscanec, S. K. Saha, U. V. Waghmare, K. S. Novoselov, H. R. Krishnamurthy, A. K. Geim, A. C. Ferrari, A. K. Sood, Nat. Nanotech. 2008, 3, 210.

[56] A. C. Ferrari, J. Robertson, Phys. Rev. B 2000, 61, 14095.

[57] A. C. Ferrari, J. Robertson, Phys. Rev. B 2001, 64, 075414.

[58] A. C. Ferrari, J. Robertson, Phil. Trans. Roy. Soc. A 2004, 362, 2477.

[59] L. G. Cancado, A. Jorio, E. H. Martins Ferreira, F. Stavale, C. A. Achete, R. B. Capaz, M. V. O. Moutinho, A. Lombardo, T. S. Kulmala A. C. Ferrari, Nano Lett. 2011, 11, 3190.

[60] N. Ferralis, R. Maboudian, C. Carraro, Phys. Rev. Lett. 2008, 101, 156801.

[61] T. M. G. Mohiuddin, A. Lombardo, R. R. Nair, A. Bonetti, G. Savini, R. Jalil, N. Bonini, D. M. Basko, C. Galiotis, N. Marzari, K. S. Novoselov, A. K. Geim, A. C. Ferrari, Phys. Rev. B 2009, 79, 205433.

[62] A. C. Ferrari, Solid State Comm. 2007, 143, 47.

[63] D. C. Elias, R. R. Nair, T. M. G. Mohiuddin, S. V. Morozov, P. Blake, M. P. Halsall, A. C. Ferrari, D. W. Boukhvalov, M. I. Katsnelson, A. K. Geim, K. S. Novoselov, Science 2009, 323, 610.

[64] C. Casiraghi, A. Hartschuh, H. Qian, S. Piscanec, C. Georgi, A. Fasoli, K. S. Novoselov, D. M. Basko, A. C. Ferrari, Nano Lett. 2009, 9, 1433.

[65] D. M. Basko, S. Piscanec, A. C. Ferrari, Phys. Rev. B 2009, 80, 165413.

[66] K. B. Albaugh, J. Electrochem. Soc. 1991, 138, 3089.

[67] H. Henmi, S. Shoji, Y. Shoji, K. Yoshimi, M. Esashi, Sens. Act. A 1994, 43, 243.

[68] A. Shukla, R. Kumar, J. Mazher, A. Balan, Solid State Commun. 2009, 149, 718.

[69] T. Moldt, A. Eckmann, P. Klar, S. V. Morozov, A. A. Zhukov, K. S. Novoselov, C. Casiraghi, ACS Nano 2011, 5, 7700.

[70] D. B. Chrisey, G. K. Hubler, Pulsed Laser Deposition of Thin Films, by Douglas B. Chrisey, Graham K. Hubler (Editor), 648 Wiley-VCH, May 2003.

[71] Y. Miyamoto, H. Zhang, D. Tomanek, Phys. Rev Lett. 2010, 104, 208302.

[72] S. Dhar, A. R. Barman, G. X. Ni, X. Wang, X. F. Xu, Y. Zheng, S. Tripathy, Ariando, A. Rusydi, K. P. Loh, M. Rubhausen, A. H. Castro Neto, B. Ozyilmaz, T. Venkatesan, AIP Adv. 2011, 1, 022109.

[73] M. Reininghaus, D. Wortmann, J. Finger, O. Faley, R. Poprawe, C. Stampfer, Appl. Phys. Lett. 2012, 100, 151606.

[74] S. Lee, M. F. Toney, W. Ko, J. C. Randel, H.-J. Jung, K. Munakata, J. Lu, T. H. Geballe, M. R. Beasley, R. Sinclair, H. C. Manoharan, A. Salleo, ACS Nano 2010, 4, 7524.

[75] M. Qian, Y.-S. Zhou, Y. Gao, J.-B. Park, T. Feng, S. M. Huang, Z. Sun, L. Jiang, Y.-F. Lu, Appl. Phys. Lett. 2011, 98, 173108.

[76] S. Z. Mortazavi, P. Parvin, A. Reyhani, Laser Phys. Lett. 2012, 9, 547.

[77] Y. Hernandez, V. Nicolosi, M. Lotya, F. M. Blighe, Z. Sun, S. De, I. T. Mc Govern, B. Holland, M. Byrne, Y. K. Gun'ko, J. J. Boland, P. Niraj, G. Duesberg, S. Krishnamurthy, R. Goodhue, J. Hutchison, V. Scardaci, A. C. Ferrari, J. N. Coleman, Nat. Nanotech. 2008, 3, 563.

[78] M. Lotya, Y. Hernandez, P. J. King, R. J. Smith, V. Nicolosi, L. S. Karlsson, F. M. Blighe, S. De, Z. Wang, I. T. Mc Govern, G. S. Duesberg, J. N. Coleman, J. Am. Chem. Soc. 2009, 131, 3611.

[79] T. Hasan, F. Torrisi, Z. Sun, D. Popa, V. Nicolosi, G. Privitera, F. Bonaccorso, A. C. Ferrari, Phys. Status Solidi B 2010, 247, 2953.

[80] A. A. Green, M. C. Hersam, Nano Lett. 2009, 9, 4031.

[81] O. M. Maragó, F. Bonaccorso, R. Saija, G. Privitera, P. G. Gucciardi, M. A. Iatı, G. Calogero, P. H. Jones, F. Borghese, P. Denti, V. Nicolosi, A. C. Ferrari, ACS Nano 2010, 4, 7515.

[82] F. Torrisi, T. Hasan, W. Wu, Z. Sun, A. Lombardo, T. S. Kulmala, G.-W. Hsieh, S. Jung, F. Bonaccorso, P. J. Paul, D. Chu, A. C. Ferrari, ACS Nano 2012, 6, 2992.

[83] P. Blake, P. D. Brimicombe, R. R. Nair, T. J. Booth, D. Jiang, F. Schedin, L. A. Ponomarenko, S. V. Morozov, H. F. Gleeson, E. W. Hill, A. K. Geim, K. S. Novoselov, Nano Lett. 2008, 8, 1704.

[84] T. J. Mason, Sonochemistry; Oxford (1999).

[85] T. Svedberg, K. O. Pedersen, The Ultracentrifuge, Oxford 1940.

[86] M. Z. Behrens, Hoppe-Seyler's Z Physiol. Chem. 1939, 258, 27.

[87] U. Khan, A. O'Neill, M. Lotya, S. De, J. N. Coleman, Small (2010) 6, 864.

[88] V. Alzari, D. Nuvoli, S. Scognamillo, M. Piccinini, E. Gioffredi, G. Malucelli, S. Marceddu, M. Sechi, V. Sanna, A. Mariani, J. Mater. Chem. 2011, 21, 8727.

[89] Z. S. Wu, W. C. Ren, L. B. Gao, B. L. Liu, J. P. Zhao, H. M. Cheng, Nano Res. 2010, 3, 16.

[90] J. Israelachvili, Intermolecular and surface force. Boston: Academic Press third edition (2011).

[91] M. H. Ghatee, L. Pakdel, Fluid Phase Equil. 2005, 234, 101.

[92] J. Lyklema, J. Colloids Surf. A 1999, 156, 413.

[93] H. M. Solomon, B. A. Burgess, G. L. Kennedy, R. e. Staples, Drug Chem. Toxicol. 1995, 18, 271.

[94] G. L. Kennedy, H. Sherman, Drug Chem. Toxicol. 1986, 9, 147.

[95] A. O'Neill, U. Khan, P. N. Nirmalraj, J. Boland, J. N. Coleman, J. Phys. Chem. C 2011, 115, 5422.

[96] S. Wang, Y. Zhang, N. Abidi, L. Cabrales, Langmuir 2009, 25, 11078.

[97] J.-W. T. Seo, A. A. Green, A. L. Antaris, M. C. Hersam, J. Phys. Chem. Lett. 2011, 2, 1004.

[98] P. N. Nirmalraj, T. Lutz, S. Kumar, G. S. Duesberg, John J. Boland, Nano Lett., 2011, 11, 16.

[99] W. S. Hummers, R. E. Offeman, J. Am. Chem. Soc. 1958, 80, 1339.

[100] T. Nakajima, Y. Matsuo, Carbon 1994, 32, 469.

[101] B. C. Brodie, Ann. Chim. Phys. 1860, 59, 466.

[102] L. V. Staudenmaier, Ber. Deut. Chem. Ges. 1898, 31, 1481.

[103] D. R. Dreyer, S. Park, C. W. Bielawski, R. S. Ruoff, Chem. Soc. Rev. 2010, 39, 1.

[104] F. S. Hyde, J. Soc. Chem. Ind. 1904, 23, 300.

[105] V. Kohlschtter, P. Z. Haenni, Anorg. Allg. Chem. 1918, 105, 121

[106] G. Ruess, F. Vogt, Monatsh für Chemie 1948, 78, 222.

[107] C. Gomez-Navarro, J. C. Meyer, R. S. Sundaram, A. Chuvilin, S. Kurasch, M. Burghard, K. Kern, U. Kaiser, Nano Lett. 2010, 10, 1144

[108] K. Erickson, R. Erni, Z. Lee, N. Alem, W. Gannett, A. Zettl, Adv. Mater. 2010, 22, 4467.

[109] X. Li, X. Wang, L. Zhang, S. Lee, H. Dai, Science 2008, 319, 1229.

[110] S. Stankovich, D. A. Dikin, R. D. Piner, K. A. Kohlhaas, A. Kleinhammes, Y. Jia, Y. Wu, S. T. Nguyen, R. S. Ruoff, Carbon 2007, 45, 1558.

[111] J. R. Lomeda, C. D. Doyle, D. V. Kosynkin, W.-F. Hwang, J. M. Tour, J. Am. Chem. Soc. 2008, 130, 16201.

[112] H. C. Schniepp, J.-L. Li, M. J. McAllister, H. Sai, M. Herrera-Alonso, D. H. Adamson, R. K. Prud'homme, R. Car, D. A. Saville, I. A. Aksay, J. Phys. Chem. B 2006, 110, 8535.

[113] X. L. Li, H. L. Wang, J. T. Robinson, H. Sanchez, G. Diankov, H. J. Dai, J. Am. Chem. Soc. 2009, 131, 15939.

[114] S. Niyogi, E. Bekyarova, M. E. Itkis, J. L. McWilliams, M. A. Hamon, R. C. Haddon, J. Am. Chem. Soc. 2006, 128, 7720.

[115] D. Konios, M. M. Stylianakis, E. Stratakis, E. Kymakis, J. Col. Interf. Sci. 2014, 430, 108.

[116] J. I. Paredes, S. Villar-Rodil, A. Martınez-Alonso, J. M. D. Tascon, Langmuir 2008, 24, 10560.

[117] C. Y. Su, Y. P. Xu, W. J. Zhang, J. W. Zhao, X. H. Tang, C. H. Tsai, L. J. Li, Chem. Mater. 2009, 21, 5674.

[118] X. F. Zhou, Z. P. Liu, Chem. Commun. 2010, 46, 2611.

[119] Z. T. Luo, Y. Lu, L. A. Somers, A. T. C. Johnson, J. Am. Chem. Soc. 2009, 131, 898.

[120] Y. Y. Liang, J. Frisch, L. J. Zhi, H. Norouzi-Arasi, X. L. Feng, J. P. Rabe, N. Koch, K. Mullen, Nanotech. 2009, 20, 43.

[121] V. Lopez, R. S. Sundaram, C. Gomez-Navarro, D. Olea, M. Burghard, J. Gomez-Herrero, F. Zamora, K. Kern, Adv. Mater. 2009, 21, 4683.

[122] S. Gilje, S. Han, M. Wang, K. L. Wang, R. B. Kaner, Nano Lett. 2007, 7, 3394.

[123] G. X. Wang, J. Yang, J. Park, X. L. Gou, B. Wang, H. Liu, J. Yao, J. Phys. Chem. C 2008, 112, 8192.

[124] Y. Si, E. T. Samulski, Nano Lett. 2008, 8, 1679.

[125] R. Muszynski, B. Seger, P. V. Kamat, J. Phys. Chem. C 2008, 112, 5263.

[126] N. Liu, F. Luo, H. X. Wu, Y. H. Liu, C. Zhang, J. Chen, Adv. Funct. Mater. 2008, 18, 1518.

[127] M. J. McAllister, J. L. Li, D. H. Adamson, H. C. Schniepp, A. A. Abdala, J. Liu, M. Herrera-Alonso, D. L. Milius, R. Car, R. K. Prud'homme, I. A. Aksay, Chem. Mater. 2007, 19, 4396.

[128] T. Kobayashi, N. Kimura, J. B. Chi, S. Hirata, D. Hobara, Small 2010, 6, 1210.

[129] M. Zhou, T. Tian, X. Li, X. Sun, J. Zhang, P. Cui, J. Tang, L.-C. Qin, Int. J. Electrochem. Sci.2014, 9, 810.

[130] L. M. Viculis, J. J. Mack, O. M. Mayer, H. T. Hahn, R.B. Kaner, J. Mater. Chem. 2005, 15, 974.

[131] J. H. Lee, D. W. Shin, V. G. Makotchenko, A. S. Nazarov, V. E. Fedorov, Y. H. Kim, J. Y. Choi, J. M. Kim, J. B. Yoo, Adv. Chem. 2009, 21, 4383.

[132] W. T. Gu, W. Zhang, X. M. Li, H. W. Zhu, J. Q. Wei, Z. Li, Q. Shu, C. Wang, K. L. Wang, W. Shen, F. Y. Kang, D. H. Wu, J. Mater. Chem. 2009, 19, 3367.

[133] E. H. L. Falcao, R. G. Blair, J. J. Mack, L. M. Viculis, C. W. Kwon, M. Bendikov, R. B. Kaner, B. S. Dunn, Carbon 2007, 45, 1367.

[134] W. Qian, R. Hao, Y. L. Hou, Y. Tian, C. M. Shen, H. J. Gao, X. L. Liang, Nano Res. 2009, 2, 706.

[135] C. Berger, Z. Song, T. Li, X. Li, A. Y. Ogbazghi, R. Feng, Z. Dai, A. N. Marchenkov, E. H. Conrad, P. N. First, W. A. de Heer, J. Phys. Chem. B 2004, 108, 19912.

[136] E. G. Acheson, US patent 1896, 615, 648.

[137] D. V. Badami, Nature 1962, 193, 569.

[138] K. V. Emtsev, A. Bostwick, K. Horn, J. Jobst, G. L. Kellogg, L. Ley, J. L. McChesney, T. Ohta, S. A. Reshanov, J. Röhrl, E. Rotenberg, A. K. Schmid, D. Waldmann, H. B. Weber, T. Seyller, Nat. Mater. 2009, 8, 203.

[139] C. Riedl, C. Coletti, T. Iwasaki, A. A. Zakharov, U. Starke, Phys. Rev. Lett. 2009, 103, 246804.

[140] A. J. Van Bommel, J. E. Crombeen, and A. Van Tooren, Surf. Sci. 1975, 48, 463.

[141] W. A. de Heer, C. Berger, M. Ruan, M. Sprinkle, X. Li, Y. Hu, B. Zhang, J. Hankinson, E. Conrad, PNAS, 2011, 108, 16900.

[142] H.-C. Kang, H. Karasawa, Y. Miyamoto, H. Handa, T. Suemitsu, M. Suemitsu, T. Otsuji, Sol. State Electron. 2010, 54, 1010.

[143] J. S. Moon, D. Curtis, S. Bui, T. Marshall, D. Wheeler, I. Valles, S. Kim, E. Wang, X. Weng, M. Fanton, Electr. Dev. Lett., IEEE 2010, 31, 1193.

[144] H. Lipson, A. R. Stokes, Proc. R. Soc. Lond. A 1942, 181, 101.

[145] J. Biscoe, B. E. Warren, J. Appl. Phys. 1942, 13, 364.

[146] J. C. Shelton, H. R. Patil, J. M. Blakely, Surf. Sci. 1974, 43, 493.

[147] S. M. Winder, D. Liu, J. W. Bender, Carbon 2006, 44, 3037.

[148] P. L. Walker, G. Imperial, Nat. 1957, 180, 1184.

[149] F. J. Derbyshire, A. E. B. Presland, D. L. Trimm, Carbon 1975, 13, 111.

[150] T. B. Massalski, et al., in: Massalski, Th. B., Okamoto, H., Subramanian, P. R., Kacprzak, L., (Eds.), Binary Alloy Phase Diagrams, ASM International, (1990).

[151] X. Li, W. Cai, J. An, S. Kim, J. Nah, D. Yang, R. Piner, A. Velamakanni, I. Jung, E. Tutuc, S. K. Banerjee, L. Colombo, R. S. Ruoff, Science 2009, 324, 1312.

[152] H. Okamoto, C-Hf (Carbon-Hafnium), Binary Alloy Phase Diagrams, II Ed., Ed. T. B. Massalski, 1990, 1, 849.

[153] I. Cadoff, J. F. Nielsen, Trans. Am. Inst. Min. Metal. Pet. Eng. 1953, 197, 248.

[154] A. Fernandez Guillermet, J. Alloys Comp. 1995, 217, 69.

[155] H. Okamoto, Phase Diagrams for Binary Alloys, Desk Handbook, 1, (2000)

[156] L. Kaufman, Calphad 1979, 3, 45.

[157] G. Ruan, Z. Sun, Z. Peng, J. M. Tour, ACS Nano 2011, 5, 7601.

[158] Z. Sun, Z. Yan, J. Yao, E. Beitler, Y. Zhu, J. M. Tour, Nat. 2010, 468, 549.

[159] A. Guermoune, T. Chari, F. Popescu, S. S. Sabri, J. Guillemette, H. S. Skulason, T. Szkopek, M. Siaj, Carbon 2011, 49, 4204.

[160] Y. Miyasaka, A. Nakamura, J. Temmyo, Jpn. J. Appl. Phys. 2011, 50, 04DH12.

[161] Y. Miyata, K. Kamon, K. Ohashi, R. Kitaura, M. Yoshimura, H. Shinohara, Appl. Phys. Lett. 2010, 96, 263105.

[162] A. E. Karu, M. Beer, J. Appl. Phys. 1966, 37, 2179.

[163] K. R. Peters, J. Microsc. Oxford 1984, 133, 17.

[164] C. F. Powell, et al., Vapour Deposition edited by Powell, C. F., Joseph, H. O., John, M. B., Blocher, M., New York Wiley, (1966).

[165] A. Reina, X. Jia, J. Ho, D. Nezich, H. Son, V. Bulovic, M. S. Dresselhaus, J. Kong, Nano Lett. 2009, 9, 30.

[166] K. S. Kim, Y. Zhao, H. Jang, S. Y. Lee, J. M. Kim, K. S. Kim, J.-H. Ahn, P. Kim, J.-Y. Choi, B. H. Hong, Nat. 2009, 457, 706.

[167] R. Rosei, M. De Crescenzi, Phys. Rev. B 1983, 28, 1161.

[168] Q. Yu, J. Lian, S. Siriponglert, H. Li, Y. P. Chen, S.-S. Pei, Appl. Phys. Lett. 2008, 93, 113103.

[169] M. E. Ramon, A. Gupta, C. Corbet, D. A. Ferrer, H. C. P. Movva, G. Carpenter, L. Colombo, G. Bourianoff, M. Doczy, D. Akinwande, E. Tutuc, S. K. Banerjee, ACS Nano 2011, 5, 7198.

[170] A. T. N'Diaye, S. Bleikamp, P. J. Feibelman, T. Michely, Phys. Rev. Lett. 2006, 97, 215501.

[171] J. C. Hamilton, J. M. Blakely, Surf. Sci. 1980, 91, 199.

[172] F. J. Himpsel, Surf. Sci. 1982, 115, L159.

[173] Y. Pan, D.-X. Shi, H.-J. Gao, Chin. Phys. 2007, 16, 3151.

[174] R. B. Little, J. Cluster Sci. 2003, 14, 135.

[175] P. W. Sutter, J.-I. Flege, E. A. Sutter, Nat. Mater. 2008, 7, 406.

[176] Y. Pan, H. Zhang, D. Shi, J. Sun, S. Du, F. Liu, H.-J Gao, Adv. Mater. 2009, 21, 2777.

[177] K. F. McCarty, P. J. Feibelman, E. Loginova, N. C. Bartelt, Carbon 2009, 47, 1806.

[178] E. Loginova, S. Nie, K. Thürmer, N. C. Bartelt, K. F. McCarty, Phys. Rev. B 2009, 80 085430.

[179] A. L. Vazquez de Parga, F. Calleja, B. Borca, M. C. G. Passeggi, Jr., J. J. Hinarejos, F. Guinea, R. Miranda, Phys. Rev. Lett. 2008, 100, 056807.

[180] J. Coraux, A. T. N′Diaye, C. Busse, T. Michely, Nano Lett. 2008, 8, 565.

[181] S. Yoshii, K. Nozawa, K. Toyoda, N. Matsukawa, A. Odagawa, A. Tsujimura, Nano Lett. 2011, 11, 2628.

[182] J. Vaari, J. Lahtinen, P. Hautojarvi, Catal. Lett. 1997, 44, 43.

[183] T. A. Land, T. Michely, R. J. Behm, J. C. Hemminger, G. Comsa, Surf. Sci. 1992, 264, 261.

[184] C. Busse, P. Lazic, R. Djemour, J. Coraux, T. Gerber, N. Atodiresei, V. Caciuc, R. Brako, A. T. N'Diaye, S. Blugel, J. Zegenhagen, T. Michely, Phys. Rev. Lett. 2011, 107, 036101.

[185] D.-E. Jiang, Z. Chen, J. Chem. Phys. 2009, 130, 074705.

[186] H. Zhang, Q. Fu, Y. Cui, D. Tan, X. Bao, J. Phys. Chem. C 2009, 113, 8296.

[187] H. Ago, Y. Ito, N. Mizuta, K. Yoshida, B. Hu, C. M. Orofeo, M. Tsuji, K.-I. Ikeda, S. Mizuno, ACS Nano 2010, 4, 7407.

[188] B. Dai, L. Fu, Z. Zou, M. Wang, H. Xu, S. Wang, Z. Liu, Nat. Comm. 2011, 2, 522.

[189] P. W. Sutter, P. M. Albrecht, E. A. Sutter, Appl. Phys. Lett. 2010, 97, 213101.

[190] Z. Peng, Z. Yan, Z. Sun, J. M. Tour, ACS Nano 2011, 5, 8241.

[191] A. Reina, S. Thiele, X. Jia, S. Bhaviripudi, M. S. Dresselhaus, J. A. Schaefer, J. Kong, Nano Res. 2010, 2, 509.

[192] A. Y. Cho, J. R. Arthur, Prog. Solid State Chem. 1975, 10, 157.

[193] A. Al-Temimy, C. Riedl, U. Starke, Appl. Phys. Lett. 2009, 95, 231907.

[194] S. K. Jerng, D. S. Yu, Y. S. Kim, J. Ryou, S. Hong, C. Kim, S. Yoon, D. K. Efetov, P. Kim, S. H. Chun, J. Phys. Chem. C 2011, 115, 4491.

[195] Z. Liu, J. Tang, C. Kang, C. Zou, W. Yan, P. Xu, Solid State Commun. 2012, 152, 960.

[196] O. Seifarth, G. Lippert, J. Dabrowski, G. Lupina, W. Mehr, M. C. Lemme, IEEE 2011, 12344834, 1.

[197] G. Lippert, J. Dabrowski, M. C. Lemme, C. M. Marcus, O. Seifarth, G. Lupina, Phys. Stat. Solidi B 2011, 248, 2619.

[198] J. M. Garcia, R. He, M. P. Jiang, J. Yan, A. Pinczuk, Y. M. Zuev, K. S. Kim, P. Kim, K. Baldwin, K. W. West, L. N. Pfeiffer, Solid State Commun. 2010, 150, 809.

[199] J. Hackley, D. Ali, J. Di Pasquale, J. D. Demaree, C. J. K. Richardson, Appl. Phys. Lett. 2009, 95, 133114.

[200] J. M. Garcia, U. Wurstbauer, A. Levy, L. N. Pfeiffer, A. Pinczuk, A. S. Plaut, L. Wang, C. R. Dean, R. Buizza, A. M. Van Der Zande, J. Hone, K. Watanabe, T. Taniguchi, Solid State Commun. 2012, 152, 975.

[201] S. K. Jerng, J. H. Lee, D. S. Yu, Y. S. Kim, J. Ryou, S. Hong, C. Kim, S. Yoon, S. H. Chun, J. Phys. Chem. C 2012, 116, 7380.

[202] X. Li, W. Cai, L. Colombo, R. S. Ruoff, Nano Lett. 2009, 9, 4268.

[203] X. Li, Y. Zhu, W. Cai, M. Borysiak, B. Han, D. Chen, R. D. Piner, L. Colombo, R. S. Ruoff, Nano Lett. 2009, 9, 4359.

[204] X. Li, C. W. Magnuson, A. Venugopal, R. M. Tromp, J. B. Hannon, E. M. Vogel, L. Colombo, R. S. Ruoff, J. Am. Chem. Soc. 2011, 133, 2816.

[205] W. T. Tsang, Appl. Phys. Lett. 1984, 45, 1234.

[206] K. Y. Lee, W. C. Lee, Y. J. Lee, M. L. Huang, C. H. Chang, T. B. Wu, M. Hong, J. Kwo, Appl. Phys. Lett. 2006, 89, 222906.

[207] T. Suntola, Mater. Sci. Rep. 1989, 4 261.

[208] M. Ritala, P. Kalsi, D. Riihelä, K. Kukli, M. Leskelä, J. Jokinen, Chem. Mater. 1999, 11, 1712.

[209] H. Kim, P. C. McIntyre, K. C. Saraswat, J. Mater. Res. 2004, 19, 643.

[210] S. Aisemberg, R. Chabot, J. Appl. Phys. 1971, 42, 2953.

[211] Y. Kim, W. Song, S. Y. Lee, C. Jeon, W. Jung, M. Kim C.-Y. Park, Appl. Phys. Lett. 2011, 98, 091502.

[212] T.-O. Terasawa, K. Saiki, Carbon 2012, 50, 869.

[213] G. Eda, Solution-Processed Thin Films for Electronics from Single-Walled CNTs & Graphene, PhD thesis 2009.

[214] X. Wu, M. Sprinkle, X. Li, F. Ming, C. Berger, W. A. d. Heer. Phys. Rev. Lett. 2008, 101, 026801.

[215] S. Wang, P.-J. Chia, L.-L. Chua, L.-H. Zhao, R.-Q. Png, S. Sivaramakrishnan, M. Zhou, R. G. S. Goh, R. H. Friend, A. T. S. Wee, P. K. H. Ho. Adv. Mater. 2008, 20, 3440.

[216] C. Lay-Lay, W. Shuai, C. Perq-Jon, C. Lan, Z. Li-Hong, C. Wei, T.S.W. Andrew, K. H. H. Peter, J. Chem. Phys. 2008, 129, 114702.

[217] I. Jung, D. A. Dikin, R. D. Piner, R. S. Ruoff, Nano Lett. 2008, 8, 4283.

[218] V. Georgakilas, Functionalization of Graphene, June 2014, 1st Ed., Ch. 2, 21.

[219] D. V. Kosynkin, A. L. Higginbotham, A. Sinitskii, J. R. Lomeda, A. Dimiev, B. K. Price, J. M. Tour, Nature 2009, 458, 872.

[220] A. Sinitskii, A. Dimiev, D. A. Corley, A. A. Fursina, D. V. Kosynkin, J. M. Tour, ACS Nano 2010, 4, 1949.

[221] S. Niyogi, E. Bekyarova, M. E. Itkis, H. Zhang, K. Shepperd, J. Hicks, M. Sprinkle, C. Berger, C. Ning Lau, W. A. de Heer, E. H. Conrad, R. C. Haddon, Nano Lett. 2010, 10, 4061.

[222] Z. Jin, J. R. Lomeda, B. K. Price, W. Lu, Y. Zhu, J. M. Tour, Chem. Mater. 2009, 21, 3045.

[223] E. Bekyarova, M. E. Itkis, P. Ramesh, C. Berger, M. Sprinkle, W. A. de Heer, R. C. Haddon, J. Am. Chem. Soc. 2009, 131, 1336.

[224] R. Sharma, J. H. Baik, C. J. Perera, M. S. Strano, Nano Lett. 2010, 10, 398.

[225] M. Z. Hossain, M. A. Walsh, M. C. Hersam, J. Am. Chem. Soc. 2010, 132, 15399.

[226] M. Fang, K. Wang, H. Lu, Y. Yang, S. J. Nutt, Mater. Chem. 2009, 19, 7098.

[227] H. Liu, S. Ryu, Z. Chen, M. L. Steigerwald, C. Nuckolls, L. E. Brus, J. Am. Chem. Soc. 2009, 131, 17099.

[228] V. Georgakilas, A. B. Bourlinos, D. Gournis, T. Tsoufis, C. Trapalis, A. M. Alonso, M. J. Prato, J. Am. Chem. Soc. 2008, 130, 8733.

[229] V. Georgakilas, D. M. Guldi, R. Signorini, R. Bozio, M. Prato, J. Am. Chem. Soc. 2003, 125, 14268.

[230] K. Kordatos, T. Da Ros, S. Bosi, E. Vazquez, M. Bergamin, C. Cusan, F. Pellarini, V. Tomberli, B. Baiti, D. Pantarotto, V. Georgakilas, G. Spalluto, M. Prato, J. Org. Chem. 2001, 66, 4915.

[231] C. Cioffi, S. Campidelli, F. G. Brunetti, M. Meneghetti, M. Prato, Chem. Commun.2006, 2129.

[232] R. Singh, D. Pantarotto, L. Lacerda, G. Pastorin, C. Klumpp, M. Prato, A. Bianco, K. Kostarelos, Proc. Natl. Acad. Sci. U.S.A. 2006, 103, 3357.

[233] K. Kostarelos, L. Lacerda, G. Pastorin, W. Wu, S. Wieckowski, L. Luangsilivay, S. Godefroy, D. Pantarotto, J. P. Briand, S. Muller, M. Prato, A. Bianco, Nat. Nanotechnol. 2007, 2, 108.

[234] A. B. Bourlinos, V. Georgakilas, R. Zboril, T. A. Steriotis, A. K. Stubos, Small 2009, 5, 1841.

[235] V. Georgakilas, A. B. Bourlinos, R. Zboril, T. A. Steriotis, P. Dallas, A. K. Stubos, C. Trapalis, Chem. Commun. 2010, 46, 1766.

[236] X. Zhang, L. Hou, A. Cnossen, A. C. Coleman, O. Ivashenko, P. Rudolf, B. J. van Wees, W. R. Browne, B. L. Feringa, Chem. Eur. J. 2011, 17, 8957.

[237] M. Quintana, K. Spyrou, M. Grzelczak, W. R. Browne, P. Rudolf, M. Prato, ACS Nano 2010, 4, 3527.

[238] L. H. Liu, M. M. Lerner, M. Yan, Nano Lett. 2010, 10, 3754.

[239] T. A. Strom, E. P. Dillon, C. E. Hamilton, A. R. Barron, Chem. Commun. 2010, 46, 4097.

[240] S. Vadukumpully, J. Gupta, Y. Zhang, C. Q. Xu, S. Valiyaveettil, Nanoscale 2011, 3, 303.

[241] J. Choi, K. Kim, B. Kim, H. Lee, S. Kim, J. Phys. Chem. C 2009, 113, 9433.

[242] X. Zhong, J. Jin, S. Li, Z. Niu, W. Hu, R. Li, J. Ma, Chem. Commun. 2010, 46, 7340.

[243] S. Huh, J. Park, Y. S. Kim, K. S. Kim, B. H. Hong, J. M. Nam, ACS Nano 2011, 5, 9799

[244] D. R. Dreyer, S. Park, C. W. Bielawski, R. S. Ruoff, Chem. Soc. Rev.2010, 39, 228.

[245] S. Stankovich, R. D. Piner, X. Q. Chen, N. Q. Wu, S. T. Nguyen, R. S. Ruoff, J. Mater. Chem. 2006, 16, 155.

[246] A. B. Bourlinos, D. Gournis, D. Petridis, T. Szabo, A. Szeri, I. Dekany, Langmuir 2003, 19, 6050.

[247] Y. Y. Liang, D. Q. Wu, X. L. Feng, K. Müllen, Adv. Mater. 2009, 21, 1679.

[248] S. Watcharotone, D. A. Dikin, S. Stankovich, R. Piner, I. Jung, G. H. B. Dommett, G. Evmenenko, S. E. Wu, S. F. Chen, C. P. Liu, S. T. Nguyen, R. S. Ruoff, Nano Lett. 2007, 7, 1888.

[249] G. Chen, W. Weng, D. Wu, C. Wu, Eur. Polym. J.2003, 39, 2329.

[250] R. Verdejo, F. Barroso-Bujans, M. A. Rodriguez-Perez, J. A. D. Saja, M. A. Lopez-Manchado, J. Mater. Chem. 2008, 18, 2221.

[251] A. J. Patil, J. L. Vickery, T. B. Scott, S. Mann, Adv. Mater. 2009, 21, 3159.

[252] E. C. Salas, Z. Sun, A. Lüttge, J. M. Tour, ACS Nano 2010, 8, 4852.

[253] Y. Zhu, S. Murali, M. D. Stoller, A. Velamakanni, R. D. Piner, R. S. Ruoff, Carbon 2010, 48, 2106.

[254] I. K. Moon, J. Lee, R. S. Ruoff, H. Lee, Nat. Commun. 2010, 1, 73.

[255] Z. Wang, X. Zhou, J. Zhang, F. Boey, H. J. Zhang, Phys. Chem. C 2009, 113, 14071.

[256] S. Dubin, S. Gilje, K. Wang, V. C. Tung, K. Cha, A. S. Hall, J. Farrar, R. Varshneya, Y. Yang, R. B. Kaner, ACS Nano 2010,4, 3845.

[257] D. Li, M. B. Muller, S. Gilje, R. B. Kaner, G. G. Wallace, Nat. Nanotechnol. 2008, 3, 101.

[258] Y. Liu, J. Zhou, X. Zhang, Z. Liu, X. Wan, J. Tian, T. Wang, Y. Chen, Carbon 2009, 47, 3113.

[259] D. Yu, Y. Yang, M. Durstock, J. B. Baek, L. Dai, ACS Nano 2010, 4, 5633.

[260] M. Melucci, E. Treossi, L. Ortolani, G. Giambastiani, V. Morandi, P. Klar, C. Casiraghi, P. Samorı, V. Palermo, J. Mater. Chem. 2010, 20, 9052.

[261] Y. Xu, Z. Liu, X. Zhang, Y. Wang, J. Tian, Y. Huang, Y. Ma, X. Zhang, Y. Chen, Adv. Mater. 2009, 21, 1275.

[262] N. Karousis, A. S. D. Sandanayaka, T. Hasobe, S. P. Economopoulos, E. Sarantopoulou, N. Tagmatarchis, J. Mater. Chem. 2011, 21, 109.

[263] Z. B. Liu, Y. F. Xu, X. Y. Zhang, X. L. Zhang, X. L. Chen, J. G. Tian, J. Phys. Chem. B 2009, 113, 9681.

[264] X. Zhang, Y. Feng, D. Huang, Y. Li, W. Feng, Carbon 2010, 48, 3236.

[265] Z. Liu, J. T. Robinson, X. Sun, H. Dai, J. Am. Chem. Soc. 2008, 130, 10876.

[266] K. Yang, S. Zhang, G. Zhang, X. Sun, S. T. Lee, Z. Liu, Nano Lett. 2010, 10, 3318.

[267] C. Shan, H. Yang, D. Han, Q. Zhang, A. Ivaska, L. Niu, Langmuir 2009, 25, 12030.

[268] S. Park, D. A. Dikin, S. T. Nguyen, R. S. Ruoff, J. Phys. Chem. C 2009, 113, 15801.

[269] H. J. Salavagione, M. A. Gomez, G. Martınez, Macromolecules 2009, 42, 6331.

[270] L. M. Veca, F. S. Lu, M. J. Meziani, L. Cao, P.Y. Zhang, G. Qi, L. W. Qu, M. Shrestha, Y. P. Sun, Chem. Commun. 2009, 2565.

[271] Y. Lin, B. Zhou, K. A. S. Fernando, P. Liu, L. F. Allard, Y. P. Sun, Macromolecules 2003, 36, 7199.

[272] Y. Lin, M. J. Meziani, Y. P. Sun, J. Mater. Chem. 2007, 17, 1.

[273] Y. P. Lin, J. Jin, M. Song, J. Mater. Chem. 2011, 21, 3455.

[274] S. H. Lee, D. R Dreyer, J. H. An, A. Velamakanni, R. D. Piner, S. Park, Y. W. Zhu, S. O. Kim, C. W. Bielawski, R. S. Ruoff, Macromol. Rapid Commun. 2010, 31, 281.

[275] H. Kong, C. Gao, D. Yan, J. Am. Chem. Soc. 2004, 126, 412.

[276] G. Gonçalves, P.A. A. P. Marques, A. B. Timmons, I. Bdkin, M. K. Singh, N. Emami, J. Grácio, J. Mater. Chem. 2010, 20, 9927.

[277] K. P. Pramoda, H. Hussain, H. M. Koh, H. R. Tan, C. B. He, J. Polym. Sci., Part A: Polym. Chem.2010, 48, 4262.

[278] T. Ramanathan, A. A. Abdala, S. Stankovich, D. A. Dikin, M. Herrera-Alonso, R.D. Piner, D. H. Adamson, H. C. Schniepp, X. Chen, R. S. Ruoff, S. T. Nguyen,; I. A. Aksay, R. K. Prud'Homme, L. C. Brinson, Nat. Nanotechnol. 2008, 3, 327.

[279] B. Das, K. Eswar Prasad, U. Ramamurty, C. N. R. Rao, Nanotechnology 2009, 20, 125705.

[280] S. Sun, Y. Cao, J. Feng, P. Wu, J. Mater. Chem. 2010, 20, 5605.

[281] T. A. Pham, N. A. Kumar, Y. T. Jeong, Synth. Met. 2010, 160, 2028.

[282] B. Zhang, Y. Chen, X. Zhuang, G. Liu, B. Yu, E. T. Kang, J. Zhu, Y. Li, J. Polym. Sci., Part A: Polym. Chem. 2010, 48, 2642.

[283] A. V. Raghu, Y. R. Lee, H. M. Jeong, C. M. Shin, Macromol. Chem. Phys.2008, 209, 2487.

[284] H. Kim, Y. Miura, C. W. Macosko, Chem. Mater.2010, 22, 3441.

[285] C. E. Hamilton, J. R. Lomeda, Z. Sun, J. M. Tour, A. R. Barron, Nano Lett. 2009, 9, 3460.

[286] Y. Cao, J. Feng, P. Wu, Carbon 2010, 48, 1670.

[287] Y. Chen, X. Zhang, P. Yu, Y. Ma, Chem. Commun.2009, 4527.

[288] Y. Liu, D. Yu, C. Zeng, Z. Miao, L. Dai, Langmuir 2010, 26, 6158.

[289] X. Zhang, Y. Huang, Y. Wang, Y. Ma, Z. Liu, Y. Chen, Carbon 2008, 47, 313.

[290] A. G. Nasibulin, P. V. Pikhitsa, H. Jiang, D. P. Brown, A. V. Krasheninnikov, A. S. Anisimov, P. Queipo, A. Moisala, D. Gonzalez, G. Lientschnig, A. Hassanien, S. D. Shandakov, G. Lolli, D. E. Resasco, M. Choi, D. Tomanek, E. I. Kauppinen, Nat. Nanotechnol. 2007, 2, 156.

[291] J. L. Delgado, P. de la Cruz, A. Urbina, J. T. Lopez Navarrte, J. Casado, F. Langa, Carbon 2007, 45, 2250.

[292] H. Yang, C. Shan, F. Li, D. Han, Q. Zhang, L. Niu, Chem. Commun. 2009, 3880.

[293] Z. Liu, Q. Liu, Y. Huang, Y. Ma, S. Yin, X. Zhang, W. Sun, Y. Chen, Adv. Mater. 2008, 20, 3924.

[294] Q. Liu, Z. Liu, X. Zhang, N. Zhang, L. Yang, S. Yin, Y. Chen, Appl. Phys. Lett. 2008, 92, No. 223303.

[295] Q. Liu, Z. Liu, X. Zhang, L. Yang, N. Zhang, G. Pan, S. Yin, Y. Chen, J. Wei, Adv. Funct. Mater. 2009, 19, 894.

[296] M. B. Avinash, K. S. Subrahmanyam, Y. Sundarayya, T. Govindaraju, Nanoscale 2010, 2, 1762.

[297] S. Gilje, S. Dubin, A. Badakhshan, J. Farrar, S. A. Danczyk, R. B. Kaner, Adv. Mater. 2010, 22, 419.

[298] D. W. Boukhvalov, M. I. Katsnelson, J. Am. Chem. Soc. 2008, 130, 10697.

[299] X. Gao, J. Jang, S. J. Nagase, J. Phys. Chem. C 2010, 114, 832.

[300] N. Ghaderi, M. Peressi, J. Phys. Chem. C 2010, 114, 21625.

[301] M. C. Hsiao, S. H. Liao, M. Y. Yen, P. I. Liu, N. W. Pu, C. A. Wang, C. C. M. Ma, ACS Appl. Mater. Interfaces 2010, 2, 3092.

[302] J. Shen, Y. Hu, C. Li, C. Qin, M. Ye, Small 2009, 5, 82.

[303] X. L. Li, G. Y. Zhang, X. D. Bai, X. M. Sun, X. R. Wang, E. Wang, H. J. Dai, Nat. Nanotech. 2008, 3, 538.

[304] Y. X. Xu, H. Bai, G. W. Lu, C. Li, G. Q. Shi, J. Am. Chem. Soc. 2008, 130, 5856.

[305] R. Hao, W. Qian, L. Zhang, Y. Hou, Chem. Comm. 2008, 6576.

[306] H. Bai, Y. Xu, L. Zhao, C. Li, G. Shi, Chem. Comm. 2009, 1667.

[307] Z. Yin, J. Zhu, Q. He, X. Cao, C. Tan, H. Chen, Q. Yan, H. Zhang, Adv. Energy Mater. 2014, 4, 1300574.

[308] Z. Y. Yin, S. Y. Sun, T. Salim, S. X. Wu, X. A. Huang, Q. Y. He, Y. M. Lam, H. Zhang, ACS Nano 2010, 4, 5263.

[309] Z. Yin, S. Wu, X. Zhou, X. Huang, Q. Zhang, F. Boey, H. Zhang, Small 2010, 6, 307.

[310] V. C. Tung, L.-M. Chen, M. J. Allen, J. K. Wassei, K. Nelson, R. B. Kaner, Y. Yang, Nano Lett. 2009, 9, 1949.

[311] Y. Wang, S. W. Tong, X. F. Xu, B. Özyilmaz, K. P. Loh, Adv. Mater. 2011, 23, 1514.

[312] Y.-Y. Lee, K.-H. Tu, C.-C. Yu, S.-S. Li, J.-Y. Hwang, C.-C. Lin, K.-H. Chen, L.-C. Chen, H.-L. Chen, C.-W. Chen, ACS Nano 2011, 5, 6564.

[313] H. Bi, F. Huang, J. Liang, X. Xie, M. Jiang, Adv. Mater. 2011, 23, 3202.

[314] D. Zhang, F. X. Xie, P. Lin, W. C. H. Choy, ACS Nano 2013, 7, 1740.

[315] H. Park, S. Chang, J. Jean, J. J. Cheng, P. T. Araujo, M. S. Wang, M. G. Bawendi, M. S. Dresselhaus, V. Bulovic, J. Kong, S. Gradecak, Nano Lett. 2013, 13, 233.

[316] V. Gupta, N. Chaudhary, R. Srivastava, G. D. Sharma, R. Bhardwaj, S. Chand, J. Am. Chem. Soc. 2011, 133, 9960.

[317] X. Yan, X. Cui, B. Li, L.-S. Li, Nano Lett. 2010, 10, 1869.

[318] X. Miao, S. Tongay, M. K. Petterson, K. Berke, A. G. Rinzler, B. R. Appleton, A. F. Hebard, Nano Lett. 2012, 12, 2745.

[319] J. Song, Z. Yin, Z. Yang, P. Amaladass, S. Wu, J. Ye, Y. Zhao, W.-Q. Deng, H. Zhang, X.-W. Liu, Chem. Eur. J. 2011, 17, 10832.

[320] X. Li, H. Zhu, K. Wang, A. Cao, J. Wei, C. Li, Y. Jia, Z. Li, X. Li, D. Wu, Adv. Mater. 2010, 22, 2743.

[321] S. Wang, B. M. Goh, K. K. Manga, Q. Bao, P. Yang, K. P. Loh, ACS Nano 2010, 4, 6180.

[322] C. X. Guo, H. B. Yang, Z. M. Sheng, Z. S. Lu, Q. L. Song, C. M. Li, Angew. Chem. Int. Ed. 2010, 49, 3014.

[323] W. Zhou, J. Zhu, C. Cheng, J. Liu, H. Yang, C. Cong, C. Guan, X. Jia, H. J. Fan, Q. Yan, C. M. Li, T. Yu, Energy Environ. Sci. 2011, 4, 4954.

[324] N. Yang, J. Zhai, D. Wang, Y. Chen, L. Jiang, ACS Nano 2010, 4, 887.

[325] Y.-B. Tang, C.-S. Lee, J. Xu, Z.-T. Liu, Z.-H. Chen, Z. He, Y.-L. Cao, G. Yuan, H. Song, L. Chen, L. Luo, H.-M. Cheng, W.-J. Zhang, I. Bello, S.-T. Lee, ACS Nano 2010, 4, 3482.

[326] S.-S. Li, K.-H. Tu, C.-C. Lin, C.-W. Chen, M. Chhowalla, ACS Nano 2010, 4, 3169.

[327] J.-M. Yun, J.-S. Yeo, J. Kim, H.-G. Jeong, D.-Y. Kim, Y.-J. Noh, S.-S. Kim, B.-C. Ku, S.-I. Na, Adv. Mater. 2011, 23, 4923.

[328] J. Liu, Y. Xue, Y. Gao, D. Yu, M. Durstock, L. Dai, Adv. Mater. 2012, 24, 2228.

[329] J. Kim, V. C. Tung, J. Huang, Adv. Energy Mater. 2011, 1, 1052.

[330] S. W. Tong, Y. Wang, Y. Zheng, M.-F. Ng, K. P. Loh, Adv. Funct. Mater. 2011, 21, 4430.

[331] V. C. Tung, J. Kim, J. Huang, Adv. Energy Mater. 2012, 2, 299.

[332] V. C. Tung, J. Kim, L. J. Cote, J. X. Huang, J. Am. Chem. Soc. 2011, 133, 9262.

[333] H. Wang, Y. Yang, Y. Liang, L.-F. Cui, H. Sanchez Casalongue, Y. Li, G. Hong, Y. Cui, H. Dai, Angew. Chem. Int. Ed. 2011, 50, 7364.

[334] Y. X. Lin, X. M. Li, D. Xie, T. T. Feng, Y. Chen, R. Song, H. Tian, T. L. Ren, M. L. Zhong, K. L. Wang, H. W. Zhu, Energy Environ. Sci. 2013, 6, 108.

[335] D. H. Wang, J. K. Kim, J. H. Seo, I. Park, B. H. Hong, J. H. Park, A. J. Heeger, Angew. Chem. Int. Ed. 2013, 52, 2874.

Experimental Part

Chapter 3

Organic bulk heterojunction photovoltaic devices based on polythiophene-graphene composites

Abstract: A solution-processed graphene content was synthesized by treatment of graphite oxide (GO) with phenyl isothiocyanate (PITC) by taking advantage of the functional carboxyl groups of graphene oxide. The GO was prepared by the oxidation of natural graphite powder and was expanded by ultrasonication in order to exfoliate single or/and few-layered graphene oxide sheets. The functionalized graphene oxide, GO-PITC, can be dispersed within poly-(3-hexylthiophene) (P3HT) and can be utilized as the electron acceptor in bulk heterojunction polymer photovoltaic cells. When P3HT is doped with GO-PITC, a great quenching of the photoluminescence of the P3HT occurred, indicating a strong electron transfer from the P3HT to the GO-PITC. The utilization of GO-PITC as the electron acceptor material in poly-(3-hexylthiophene) (P3HT) bulk heterojunction photovoltaic devices was demonstrated, yielding in a power conversion efficiency enhancement of two orders of magnitude compared with that of pristine P3HT.

KEYWORDS: graphene, photovoltaic, functionalization, solution-processed, bulk heterojunction

1. INTRODUCTION

Novel carbon-based structures, such as carbon nanotubes and graphene, have emerged in recent years as integrative materials for organic photovoltaic devices.[1−9] The most recent building block of intriguing actual scientific and technological interest is graphene, best described as a two-dimensional (2D) single atom-thick sheet of sp^2 - hybridized carbon atoms arranged in a honeycomb lattice with outstanding electronic, mechanical, thermal, and chemical properties.[10,11] However, the liquid phase production of graphene-based materials is severely hampered by the low yield of graphene exfoliation (a few graphene monolayers per square millimeter of substrate area) and its poor solubility in common organic solvents,[12] which is mainly due to the attractive van der Waals forces between the graphene sheets.[13,14] So far, the response to the problem of low yield has been the exfoliation of chemically modified forms of graphene, such as graphene oxide (GO), or functionalized graphene,[15−17] or the exfoliation of graphene from graphite under intense sonication in water or organic solvents.[18] On the other hand, graphene sheets are functionalized by covalent or noncovalent coupling modifications in order to increase their solubility in organic solvents or within a polymer matrix.[19−21] The advantage of using noncovalent functionalization via π−π* stacking and hydrophobic interactions instead of covalent functionalization is that the intrinsic properties of graphene are preserved.[22−25] Furthermore, since the pristine graphene is zero bandgap, the introduction of the functional groups opens up the bandgap of the functionalized graphene. Therefore, graphene-based materials are anticipated to be utilized for the effective exciton separation and charge transport when blended with conjugated polymers, because of the large surface area for donor/acceptor interfaces and continuous pathway for the electron transfer, as in the case of carbon nanotubes.[26−30]

Chemical routes, such as those based on Hummers' oxidation method, have been explored as means to introduce a large number of abundant functional groups within the graphene structure, such as hydroxyl (−OH), aldehyde (−CHO), carboxyl (−COOH) or epoxyl ones, thus reducing the interplane forces and imparting hydrophilic character.[31] Moreover, many different functional moieties (amino, bromine, long alkyl chain, etc.) as well as polymer chains (e.g., poly(ethylene glycol), polystyrene) have been anchored onto the graphene oxide sheets by various chemical approaches.[32]

In this paper, a facile method is described that allows the chemical treatment of GO sheets with phenyl isothiocyanate (PITC). This results in a solution processable graphene based material, namely GO-PITC, which can be integrated in organic photovoltaic devices, due to its unique structural and photophysical properties. GO-PITC displays increased solubility in common organic solvents as compared to that of the untreated GO. The synthesized GO-PITC is blended with the conjugated polymer poly(3-hexylthiophene), P3HT, in different concentrations. The structure and morphology of the polythiophene-graphene composites are characterized by X-ray diffraction (XRD) and field-emission scanning electron microscopy (FE-SEM), whereas their spectroscopic properties are investigated by fluorescence, UV/vis and Raman spectroscopies. It is demonstrated that the utilization of GO-PITC in photovoltaic devices with the structure glass/ITO/PEDOT:PSS/P3HT:GO-PITC/Al lead to devices that exhibit photovoltaic performance, significantly better (power conversion efficiency 2 orders of magnitude higher) than that of the pristine P3HT device, indicating the potential of utilizing GO-PITC as an electron acceptor material.

2. EXPERIMENTAL SECTION

2.1 Preparation of graphene oxide (GO)

GO was prepared from purified natural graphite powder (Alfa Aesar, ~200 mesh) according to a modified Hummers' method[33] and purified by a controlled centrifugation method;[34] the procedure is schematically depicted in Figure 1a. Specifically, graphite powder (0.5 g) was placed into a cold mixture of concentrated H_2SO_4 (40 mL, 98%) and $NaNO_3$ (0.375 g) under vigorous stirring for 1 h, in an ice bath. During this time $KMnO_4$ (2.25 g) was added in small portions and the ice bath was kept for 2 h more, in order to cool the mixture below 10°C. The green-brown colored mixture remained under stirring for five days. On completion of the reaction, the brick-colored mixture was mixed with an aqueous solution of 5% H_2SO_4 (70 mL). The mixture was stirred for one hour under heating at 98 °C and became gray-black colored. When the temperature decreased to 60°C, 30% H_2O_2 (~2 mL) was added and the mixture was stirred for 2 h at room temperature. The mixture was, then, centrifuged for 5 min at 4200 rpm and washed with ~600 mL of an aqueous solution of 3% H_2SO_4 (~9 mL)/0.5% H_2O_2 (~1.5 mL) in order to remove the acidic anions, especially these of

Mn. Then, it was put in an ultrasonic vibration bath for 10 min so that the ultrasonic vibration would exfoliate the graphite oxide to GO sheets. The process was repeated 10 times. Then, the mixture was washed and purified with 150 mL of aqueous solution 3% HCl (~1.5 mL) for 3 times. Afterward, it was washed thoroughly with deionized water (DI) and acetone, in order to remove any acidic part remaining. Finally, the resulting GO was dried at 60°C under vacuum oven overnight.

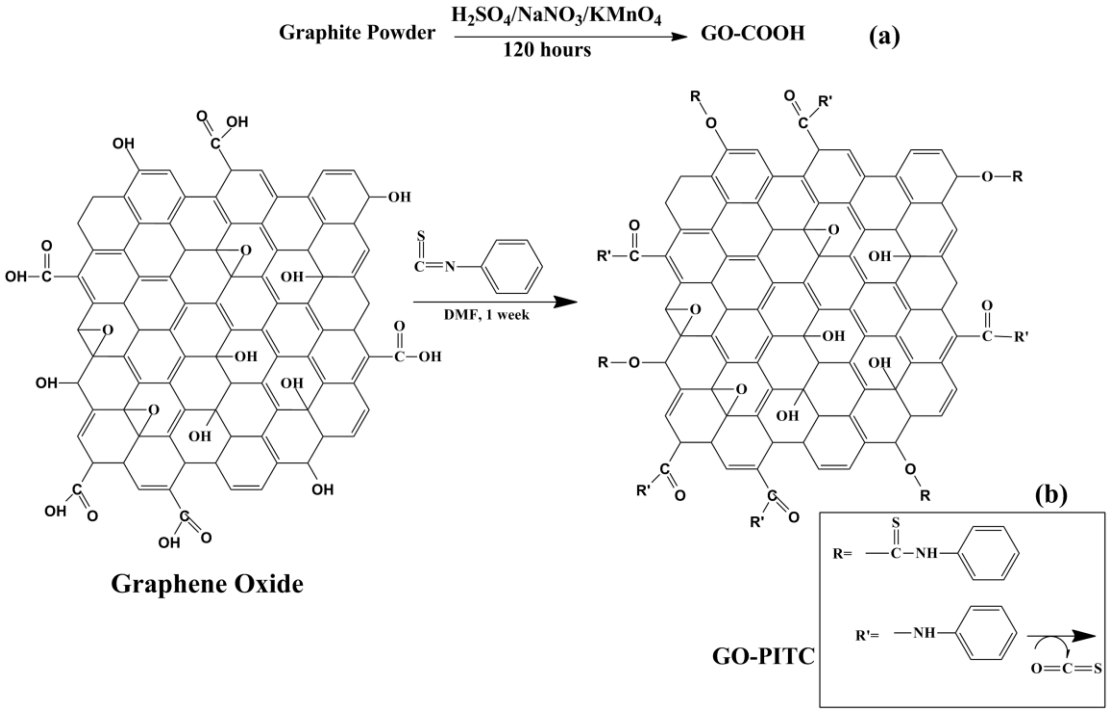

Figure 1. Schematic representation of the chemical synthesis of (a) Graphene Oxide and (b) solution-processed GO-PITC by functionalization of GO.

2.2 Preparation of GO-PITC

GO (200 mg) was placed in a flask with 20 mL of anhydrous dimethylformamide, DMF. The mixture was ultrasonicated for 20 min to give a homogeneous suspension. An amount (20 g) of phenyl isothiocyanate, PITC, was then added to the mixture. The mixture was stirred for one week at room temperature, under nitrogen. The functionalized GO, GO-PITC, was purified and isolated by repeating the procedure below three times, thus, by taking advantage of its hydrophobic nature, in contrast to the hydrophilic GO.35 The suspension was added dropwise to 1,2-orthodichlorobenzene, *o*-DCB, (~30 mL),stirred and centrifuged at 800 rpm for 8 min. The supernatant solution was added dropwise to $CHCl_3$ (~50 mL), stirred and centrifuged at 4200 rpm for 20 min. The resulting GO-PITC was dried overnight in a

vacuum oven (124 mg, yield 62%). The synthesis and the structure of GO-PITC are schematically depicted in the lower part of Figure 1a and in Figure 1b, respectively.

2.3 Fabrication and Characterization of Photovoltaic Devices

All the photovoltaic (PV) devices were fabricated in a sandwich geometry consisting of a bottom indium tin oxide (ITO) coated electrode, a P3HT:GO-PITC thin film, and a top metal (Al) electrode. Indium tin oxide (ITO, 15Ω/sq) coated glass substrates were used for the device fabrication. The substrates were cleaned by 10 min consecutive sonication in detergent, deionized water, acetone and isopropyl alcohol, in an ultrasonic bath (Elma S 30 H Elmasonic). Poly(3,4-ethylenedioxythiophene):poly(styrenesulfonate), PEDOT:PSS, (Clevios P Al 4083,~30 nm thickness) thin film was spin coated onto the clean substrates, which were subsequently dried at 120 °C for 10 min to remove any residual water. Photovoltaic devices were then fabricated, in air, by spin coating a P3HT:GO-PITC thin film (110 nm) from its o-DCB solution (concentration 17 mg/mL), followed by annealing at 160°C for 20 min. Thereafter, an Al electrode (80 nm) was deposited by vacuum evaporation onto the active layer through a shadow mask to define an active area of 18 mm^2 for each device. Current-voltage (J−V) measurements were performed at room temperature using an Agilent B1500A Semiconductor Device Analyzer. For photovoltaic characterization the devices were illuminated with 100 mW/cm^2 power intensity of white light by an Oriel solar simulator with an AM1.5 filter through the glass/ITO side. All measurements were made in air immediately after device fabrication.

2.4 Microscopic and Spectroscopic Characterization

The samples were characterized by Raman spectroscopy at room temperature utilizing a Nicolet Almega XR Raman spectrometer (Thermo Scientific) with a 473 nm blue laser as an excitation source. Fourier transform infrared (FTIR) spectra were measured on a Bruker FTIR spectrometer IFS 66v/F (MIR). The photoluminescence (PL) measurements were carried out in the wavelength range from 500 to 1000 nm using a He-Cd cw laser (325 nm) with a full power of 35 mW as the excitation source. UV-vis absorption spectra were recorded using a Shimadzu UV-2401 PC spectrophotometer over the wavelength range of 300-800 nm. The morphology of the surfaces was

examined by field emission scanning electron microscopy (FE-SEM JEOLJSM-7000F) and by atomic force microscopy (AFM-Digital Instruments NanoScope IIIa). X-ray diffraction patterns were collected on a Panalytical Expert Pro X-ray diffractometer, using Cu Kα radiation (λ=1.5406 Å). Thermogravimetric analysis (TGA) was performed on 5-10 mg samples over the temperature range from 40°C to 800°C at a heating rate of 10 °C/min utilizing a Perkin Elmer Diamond Pyris model under nitrogen atmosphere.

3. RESULTS AND DISCUSSION

GO and GO-PITC powders are analyzed by means of FT-IR spectroscopy and the results are shown in Figure 2. The O-H stretching vibration appears as a broad peak at 3440 cm^{-1}. The most characteristic features in the FT-IR spectrum of GO are the adsorption bands corresponding to the C=O carbonyl stretching at 1670 wavenumbers (cm^{-1}), the C−OH stretching at 1220 cm^{-1}, and the C-O stretching at 1053 cm^{-1}. On the other hand, the peak corresponding to the O-H stretching vibration at 3440 cm^{-1} is decreased while a second peak at ~3330, corresponding to the N–H stretching of the amide is appeared, indicating amides formation in the FT-IR spectrum of GO-PITC. Moreover, the characteristic C=O stretching at 1652 cm^{-1} of the carbonyl groups is exhibited, as well as, the band at ~1600 cm^{-1} can be assigned to the amide carbonyl stretching mode. The new band at 1541 cm^{-1} can originate from either amides or carbamate esters and corresponds to the coupling of the C-N stretching vibration with the CHN deformation vibration.[36] The linking of phenyl isothiocyanate to the hydroxy functional groups of graphene oxide is evaluated from the appeared sharp peak at ~1230 cm^{-1}, which is assigned to the C-O stretching of ethers.

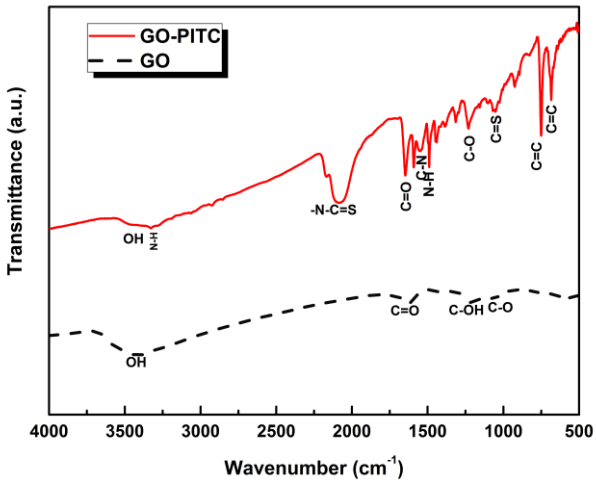

Figure 2. FT-IR spectra of pure GO (black line) and GO-PITC (red line) in transmission mode.

Even more importantly, the FTIR spectrum of GO-PITC displays two characteristic peaks at ~2115 cm^{-1} and at ~1070 cm^{-1} associated with the isothiocyanate group and the C=S stretching vibration, respectively. Thus, the FT-IR spectra of GO and GO-PITC clearly indicate that PITC is chemically linked with GO and not absorbed/intercalated.

In order to investigate the absorption behavior of GO and GO-PITC films, we have prepared thin films by spin-coating onto quartz substrates and the normalized UV−vis absorption spectra of pure GO and GO-PITC are shown in Figure 3. The absorption spectrum of GO-PITC (red line) is red-shifted compared to the pure GO (black line).

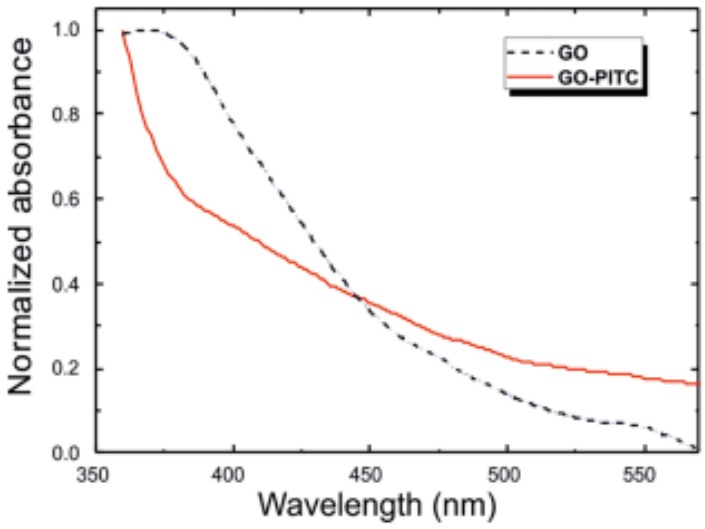

Figure 3. Normalized UV-vis absorption spectra of pure GO (black line) and GO-PITC (red line) in thin solid films prepared by spin coating onto a quartz substrate.

Raman spectroscopy is the most direct and nondestructive technique to characterize the structure and quality of carbon based materials, particularly in order to determine defects, ordered and disordered structures, and the layers of graphene. For the measurement, a laser excitation of 473 nm was used, and powder samples were directly deposited on a Si wafer without using any solvents. Figure 4 shows the Raman spectra of GO and GO-PITC powders, which exhibit two dominant peaks at around 1350 and 1580 cm^{-1} that correspond to the well-defined D and G bands, respectively. The Raman spectra reveal the dramatic changes in the signals of the GO-PITC upon functionalization. GO-PITC exhibits a higher D/G intensity ratio (I_D/I_G) relatively to GO; this attests to the successful functionalization of GO by the formation of covalent bonds between GO and PITC.[37] The Raman shift of the D and for GO-PITC (from 1342 to 1355 cm^{-1}) provides evidence for the charge transfer between the GO sheets and the PITC functional group.

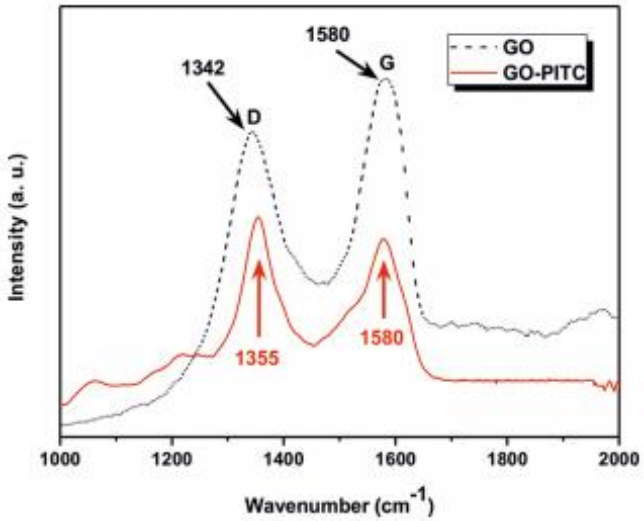

Figure 4. Raman spectra of GO (black line) and GO-PITC (red line), obtained utilizing an incident laser at 473 nm.

The data from the thermogravimetric analysis (TGA), are presented in Figure 5. GO begins to lose mass upon heating even below 100 °C and has resulted in a rapid mass loss commencing at about 200 °C, probably due to pyrolysis of labile oxygen-containing functional groups, such as -OH, -CO and -COOH groups, and a total mass loss of ~40% at 800°C, in agreement with data in the literature.[38]

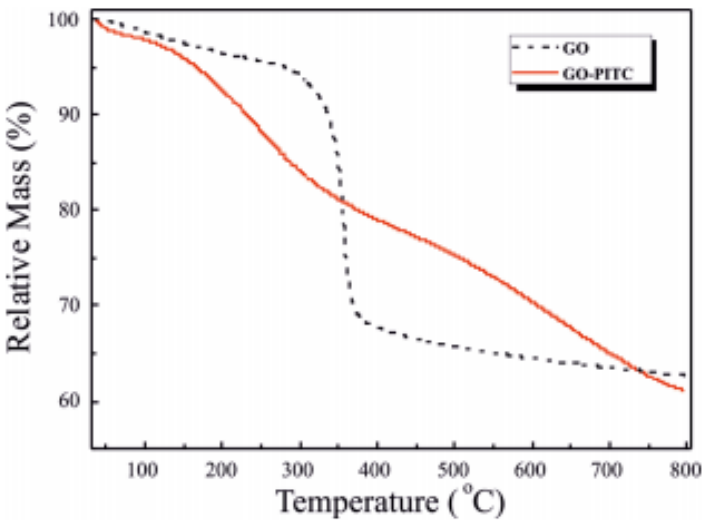

Figure 5. Thermogravimetric (TGA) data of GO (black line) and GOPITC (red line) obtained under an inert nitrogen atmosphere with a heating rate of 10°C/min.

In contrast, GO-PITC displays improved thermal stability until 700 °C. Briefly, the TGA curve of GO-PITC shows a 4% weight loss before 150 °C, due to the humidity and the evaporation of traces of remaining solvent. In the range of 150 to 370°C, a weight loss of ca. 20% occurred due to the decomposition of oxygen containing and isothiocyanate functional groups. From 370 to 800 °C, a weight loss of ~40% was observed, which can be attributed to the removal of the phenyl side rings of the functionalized graphene oxide sheets. The TGA analysis further confirms that GO was successfully functionalized.

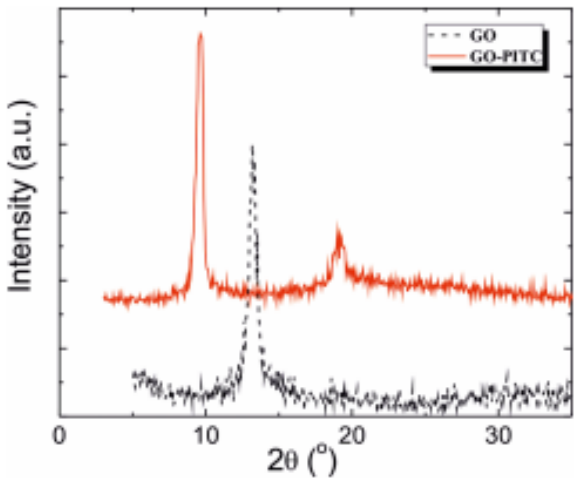

Figure 6. X-ray diffraction patterns of GO (black line) and GO-PITC (red line) powder samples.

The as-prepared GO and GO-PITC samples were also characterized by X-ray diffraction (XRD), Figure 6. The diffraction peak at 2θ = 13.2° has been attributed to

the (002) main reflection of stacks of graphene oxide with a 6.7 Å interlayer distance and a finite number of layers (~18). The diffractogram of GO-PITC does not exhibit the peak at 13.2°; instead peak is observed at 9.5° together with a smaller one at 19.0°; the former should be attributed to the interplanar spacing of the disordered stacking of functionalized graphene oxide sheets,[39,40] i.e., of GO-PITC, with a 9.1 Å interplanar distance and~17 layers. The peak at 19.0° may be due to a partial reduction of GO during the functionalization reaction of GO to GO-PITC. In order to investigate the morphology of GO-PITC, scanning electron microscopy (SEM) and atomic force microscopy (AFM) were used and the images are shown in Figure 7. GO-PITC exhibits a wrinkled and crinkly structure, like plane tree leaves, with a smooth surface. One should note that the network of graphene-based sheets and the individual GO-PITC sheets are electrically conductive since no charging was observed during the SEM imaging. Furthermore, AFM analysis indicated significant exfoliation of the pristine graphene flakes, leading to sheet thicknesses in the 2-20 nm range.

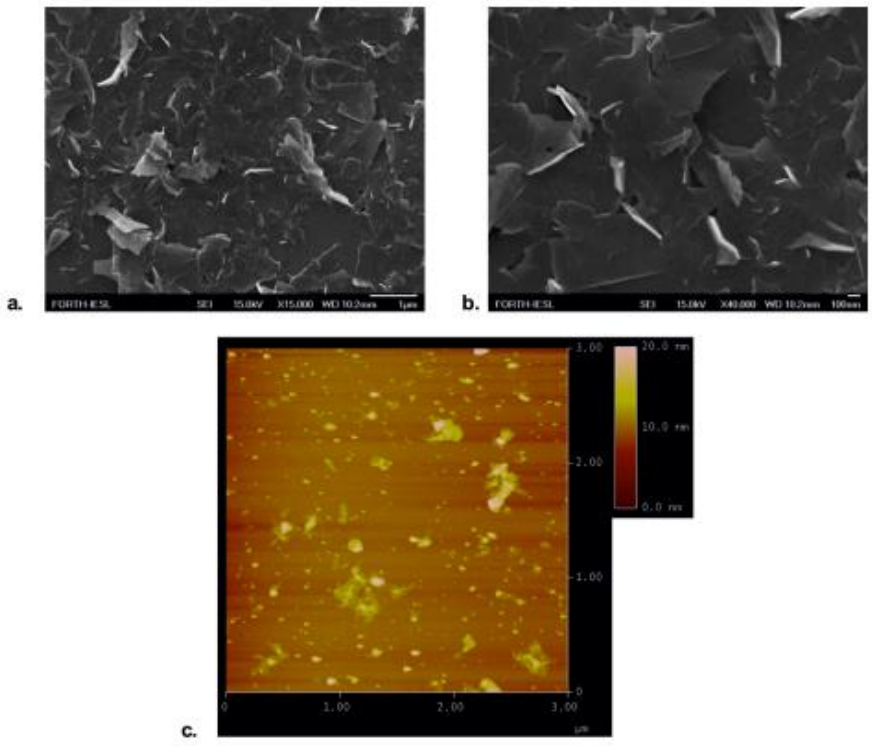

Figure 7. Field-emission scanning electron microscopy (FE-SEM) images of GO-PITC in (a) plane tree leaves, (b) wrapped graphene-based sheets, and (c) AFM image of GO-PITC.

Figure 8 displays the normalized UV-vis absorption spectra of P3HT and of the P3HT:GO-PITC composite in thin films, prepared by spin-coating onto quartz

substrates. The UV-vis spectrum of P3HT:GO-PITC composite is about 35 nm red shifted compared with that of the pristine P3HTfilm. This shift is due to a sufficiently increased chain motion, indicating an increase in the crystalline ordering, resulting in a stabilization of the P3HT chains.[41]

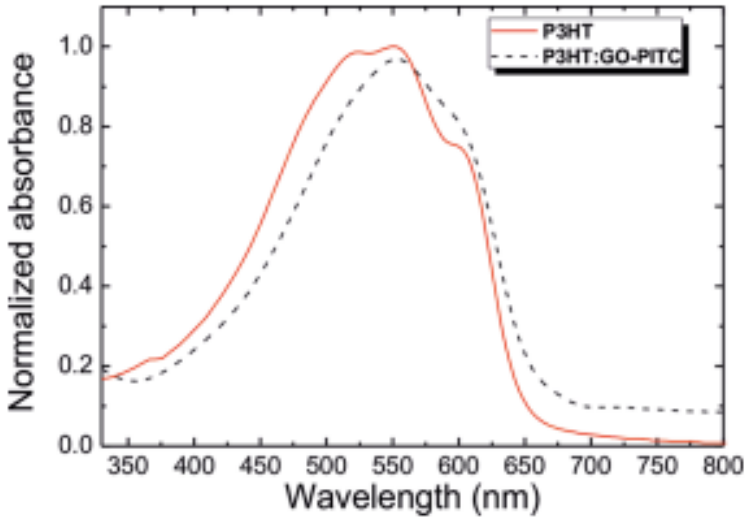

Figure 8. Normalized UV-vis absorption spectra of P3HT (red line) and of the P3HT:GO-PITC (black line) composite in thin films onto quartz substrates.

Also, the presence of GO-PITC in the active layer exhibits a better light-absorbing ability. Therefore, the relatively acceptor content (20%) at which the optimized power-conversion efficiency can be obtained, indicates the great superiority of the GO-PITC used as the electron acceptor material.

Figure 9 depicts the photoluminescence (PL) spectra of pure P3HT and of P3HT:GO-PITC (20%), in thin solid films, on Si substrates, at an excitation wavelength of 325 nm. The data for the film of pure P3HT shows a very strong emission band over the range 650-700 nm, which is apparently extinguished, due to the fluorescence-quenching effect due to the GO-PITC graphene content.[35] This phenomenon illustrates that GO-PITC can be used as a strong electron acceptor moiety in bulk heterojunction (BHJ) devices.

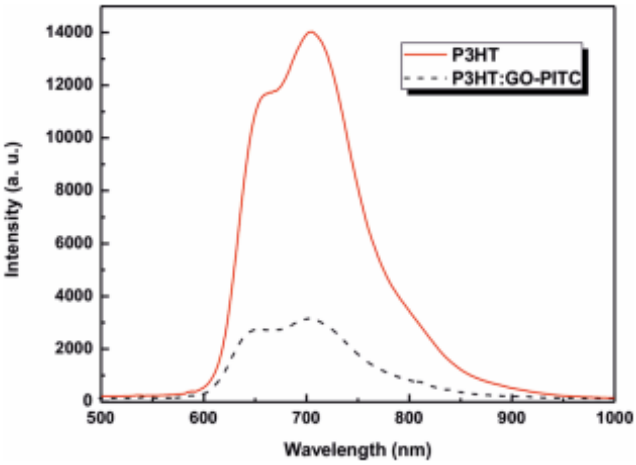

Figure 9. Photoluminescence (PL) spectra of P3HT (red line) and P3HT:GO-PITC 20% (black line) in thin film on a Si substrate at an excitation wavelength of 325 nm.

Figure 10 displays the surface morphology of the P3HT and the P3HT:GO-PITC (20 wt %). composite films by the use of AFM. The GO-PITC is well dispersed in the P3HT matrix, and no agglomerates formed by aggregates sheets are present. Furthermore, the surface of the composite is smoother than the pristine P3HTfilm, and a fine "packaging" of the two blend components can be observed.

Finally, bulk heterojunction photovoltaic devices were fabricated utilizing the GO-PITC as the electron acceptor, and the P3HT as the electron donor. Two different ratios of GO-PITC to P3HT were used (10 and 20 wt %). The structure of the device is, thus, ITO/PEDOT:PSS (30 nm)/P3HT:GO-PITC (110 nm)/Al (80 nm), schematically shown in Figure 11a.

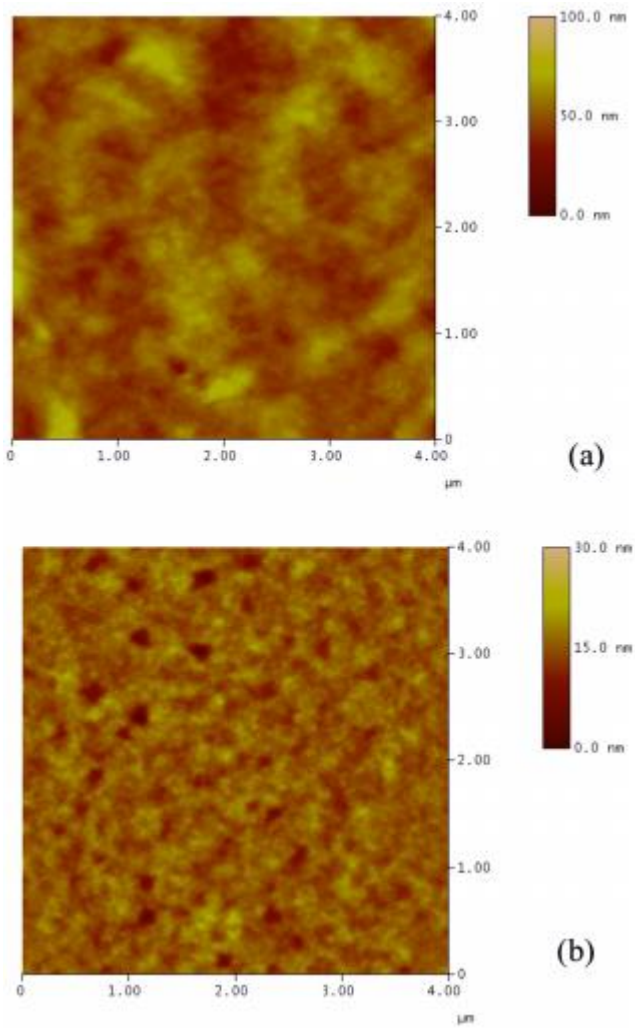

Figure 10. AFM images of (a) P3HT and (b) P3HT:GO-PITC 20% thin films.

A post fabrication annealing of the P3HT:GO-PITC active layer, conducted at 160 °C for 20 min under N_2 atmosphere, improves the morphology of the film and removes residual functional groups linked to the graphene sheet. As a result, the conjugation length increases and the charge transport mobility is enhanced.[42] Figure 11b shows the current voltage (J−V) curves for the photovoltaic devices with GO-PITC content of 10 and 20 wt %. Table 3.1 displays the photovoltaic characteristics and points out that the device containing 20% GO-PITC shows a better photovoltaic performance exhibiting an open-circuit voltage (V_{oc}) of 0.51 V, short-circuit current density (J_{sc}) of 4.34 mA/cm^2, fill factor (FF) of 46%, and power conversion efficiency (η) of 1.02 %, more than 2 orders of magnitude larger than the efficiency of the pristine P3HT device. Moreover, the device with 10% GO-PITC achieved power conversion efficiency (η) of

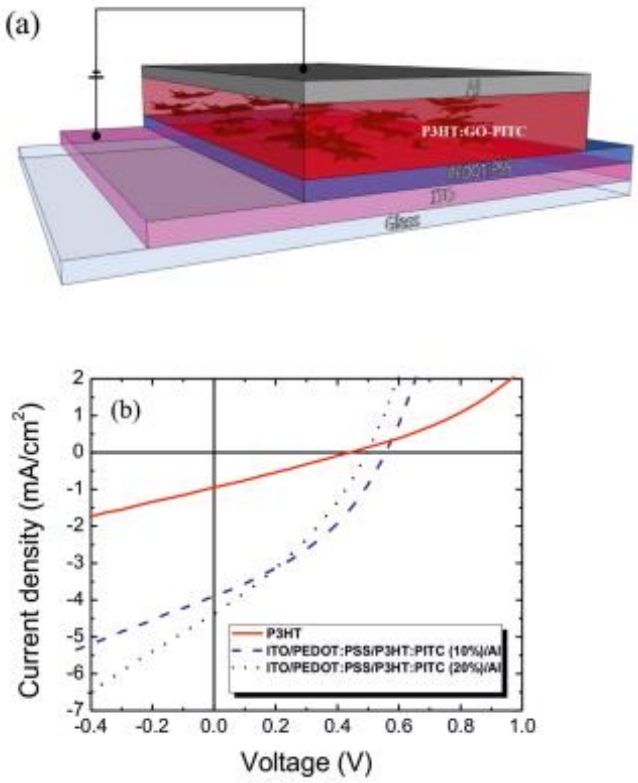

Figure 11. (a) Schematic of the photovoltaic device with P3HT:GO-PITC thin film as the active layer and the structure ITO/PEDOT:PSS(30 nm)/P3HT:GO-PITC(110 nm)/Al(80 nm). (b) Experimental J−V curves of the photovoltaic devices based on P3HT (red curve) and P3HT:GO-PITC composites (blue curve, 10 wt %; black curve, 20 wt %) after post fabrication thermal annealing at 160 °C for 20 min.

0.88% with a V_{oc} of 0.57 V, a J_{sc} of 3.96 mA/cm^2, and a FF of 39%. The efficiency increased when the concentration of the graphene content increased relatively to P3HT. When even higher concentrations of GOPITC were used, large aggregates were formed, which hindered exciton generation and charge separation, thus leading to reduced efficiencies.

GO-PITC (%)	V_{oc} (V)	J_{sc} (mA/cm^2)	FF (%)	η (%)
0	0.40	0.04	0.28	0.004
10	0.57	3.96	0.39	0.88
20	0.51	4.34	0.46	1.02

Table 3.1 Device Performance of Photovoltaic Devices Based on P3HT:GO-PITC Composites with Different GO-PITC Content Following Annealing at 160°C for 20 min.

Despite these promising results, the efficiency of the graphene based OPV devices is still low, about 1 order of magnitude smaller than the fullerene-based devices.[43] However, the polymer-fullerene OPV devices have been extensively optimized for more than a decade. Moreover, the energy level differences of the donor and acceptor materials of the graphene-based system do not match as well as in the polymer-fullerene

case. Therefore, extensive research in the design of new graphene-based materials with tailored bandgap and their corresponding polymer donors is urgently needed.

4. CONCLUSIONS

A novel graphene-based material was synthesized, consisting of GO sheets functionalized with phenyl-isothiocyanate side groups. The resulting GO-PITC, which is soluble in *o*-DCB, was successfully blended with P3HT and used as the photoactive layer in bulk heterojunction organic photovoltaic devices. The device containing 20 wt% GO-PITC blended with P3HT, achieved power conversion efficiency (η) of 1.02 %, after post-fabrication annealing. All the photovoltaic devices were fabricated in air and the measurements were made in air immediately after device fabrication. The sufficient photovoltaic performance of GO-PITC, without any optimization, renders this novel graphene-based material as an alternative electron acceptor for OPVs devices. It can be easily anticipated that its performance would be rather enhanced following the proper optimization.

REFERENCES

1. Borchert, H.; Witt, F.; Chanaewa, A.; Werner, F.; Dorn, J.; Dufaux, T.; Kruszynska, M.; Jandke, A.; Hoeltig, M. Alfere, T.; Boettcher, J. Gimmler, C.; Klinke, C.; Burghard, M.; Mews, A.; Weller, H.; Parisi, J. *J. Phys. Chem. C* 2012, 116, 412-419.
2. Li, S.-S.; Tu, K.-H.; Lin, C.-C.; Chen, C.-W.; Chhowalla, M. *ACS Nano* 2010, 4, 3169-3174.
3. Valentini, L.; Cardinali, M.; Bittolo Bon, S.; Bagnis, D.; Verdejo, R.; Lopez-Manchado, M.-A.; Kenny, J.M. *J. Mater. Chem*. 2010, 20, 995-1000.
4. Kymakis, E.; Amaratunga, G. A. *J. Appl. Phys. Lett*. 2002, 80, 112-114.
5. Yip, H.-L.; Jen, A. K.-Y. Energy & Environ. Sc. 2012, 5, 5994-6011.
6. Kymakis, E.; Servati, P.; Tzanetakis, P.; Koudoumas, E.; Kornilios, N.; Rompogiannakis, I.; Franghiadakis, Y.; Amaratunga, G. A. J. *Nanotech.* 2007, 18, 435702-435707.
7. Stylianakis, M. M.; Mikroyannidis, J. A.; Kymakis, E. *Sol. Energy Mater. Sol. Cells* 2010, 94, 267-274.
8. Po, R.; Carbonera, C.; Bernardi, A.; Tinti, F.; Camaioni, N. *Sol. Energy Mater. Sol. Cells* 2012, 100, 97-114.
9. Stylianakis, M. M.; Kymakis, E. Appl. Phys. Lett. 2012, 100, 093301-093305.
10. Geim, A.K.; Novoselov, K.S. *Nat. Mater.* 2007, 6, 183-191.
11. Geim, A.K. *Science* 2009, 324, 1530-1534.

12. Gomez Navarro, C.; Weitz, R. T.; Bittner, A. M.; Scolari, M.; Mews, A.; Burghard, M.; Kern, K. *Nano Lett.* 2007, 7, 3499-3503.
13. Qi, X. Y.; Pu, K. Y.; Zhou, X. Z.; Li, H.; Liu, B.; Boey, F.; Huang, W.; Zhang, H. *Small* 2010, 6, 663-669.
14. Xu, Y. F.; Liu, Z. B.; Zhang, X. L.; Wang, Y.; Tian, J. G.; Huang, Y.; Ma, Y. F.; Zhang, X. Y.; Chen, Y. S. *Adv. Mater.* 2009, 21, 1275-1279.
15. Dreyer, D. R.; Park, S.; Bielawski, C. W.; Ruoff, R. S. *Chem. Soc. Rev.* 2010, 39, 228-240.
16. Dreyer, D. R.; Jia, H. P.; Bielawski, C. W. Angew. *Chem. Inter. Edit.* 2010, 49, 6813-6816.
17. Swager, T. M. *ACS Macro Lett*. 2012, 1, 3-5.
18. Khan, U.; O'Neill, A.; Lotya, M.; De, S.; Coleman, J. N. *Small* 2010, 6, 864-871.
19. Lomeda, J.; Doyle, C.; Kosynkin, D.; Hwang, W.; Tour, J. *J. Am. Chem. Soc.* 2008, 130, 16201-16206.
20. Xu, Y. X.; Bai, H.; Lu, G. W.; Li, C.; Shi, G. Q. *J. Am. Chem. Soc.* 2008, 130, 5856-5857.
21. Stylianakis, M. M.; Spyropoulos, G. D.; Stratakis, E.; Kymakis, E. *Carbon* 2012, 50, 5554-5561.
22. Su, Q.; Pang, S.; Alijani, V.; Li, C.; Feng, X.; Mullen, K. *Adv. Mater.* 2009, 21, 3191-3195.
23. Englert, J. M.; Rçhrl, J.; Schmidt, C. D.; Graupner, R.; Hundhausen, M.; Hauke, F.; Hirsch, A. *Adv. Mater.* 2009, 21, 4265-4269.
24. Xu, Y.; Zhao, L.; Bai, H.; Hong, W.; Li, C.; Shi, G. *J. Am. Chem. Soc.* 2009, 131, 13490-13497.
25. Ghosh, A.; Rao, K. V.; George, S. J.; Rao, C. N. R. *Chem. A Eur.* J. 2010, 16, 2700-2704.
26. Hill, C. M.; Zhu, Y.; Pan, S. *ACS Nano* 2011, 5, 942-951.
27. Yu, D.; Yang, Y.; Durstock, M.; Baek, J.-B.; Dai, L. *ACS Nano* 2010, 4, 5633-5640.
28. Liu, Q.; Liu, Z.; Zhang, X.; Yang, L.; Zhang, N.; Pan, G.; Yin, S.; Chen, Y.; Wei, J. *Adv. Funct. Mater.* 2009, 19, 894-904.
29. Huang, X.; Qi, X.; Boey, F.; Zhang, H. *Chem. Soc. Rev*. 2012, 41, 666-686.
30. Yu, D.; Park, K.; Durstock, M.; Dai, L. *J. Phys. Chem. Lett*. 2011, 2, 1113-1118.
31. Eda, G.; Fanchini, G.; Chhowalla, M. *Nat. Nanotech*. 2008, 3, 270-274.
32. Sun, S.; Cao, Y.; Feng, J.; Wu, P. J. *Mater. Chem*. 2010, 20, 5605-5607.
33. Becerril, H. A.; Mao, J.; Liu, Z.; Stoltenberg, R. M.; Bao, Z.; Chen, Y. *ACS Nano* 2008, 2, 463-470.
34. Khan, U.; O'Neill, A.; Porwal, H.; May, P.; Nawaz, K.; Coleman, J. N. *Carbon* 2012, 2, 470-475.
35. Liu, Z.; Liu, Q.; Huang, Y.; Ma, Y.; Yin, S.; Zhang, X.; Sun, W.; Chen, Y. *Adv. Mater*. 2008, 20, 3924-3930.
36. Gunzler, H.; Gremlich, H. U. *Winheim: Wiley-VSH* 2002, 223-227.
37. Fang, M.; Wang, K.; Lu, H.; Yang, Y.; Nutt, S. J. *Mater. Chem*. 2009, 19, 7098-7105.
38. Stankovich, S.; Dikin, D. A.; Piner, R. D.; Kohlhaas, K. A.; Kleinhammes, A.; Jia, Y.; Wu, Y.; Nguyen, S. T.; Ruoff, R. S. *Carbon* 2007, 45, 1558-1565.
39. Bourlinos, A. B.; Gournis, D.; Petridis, D.; Szabo, T.; Szeri, A.; Dekany, I. *Langmuir* 2003, 19, 6050-6055.
40. Wang, G. X.; Shen, X. P.; Wang, B.; Yao, J.; Park, J. *Carbon* 2009, 47, 1359-1364.

41. Kymakis, E.; Koudoumas, E.; Franghiadakis, I.; Amaratunga, G. A. J. *J. Phys. D: Appl. Phys*. 2006, 39, 1058-1062.
42. Liang, Y., Xu, Z.; Xia, J.; Tsai, S.-T.; Wu, Y.; Li, G.; Ray C.; Yu, L. *Adv. Mater*. 2010, 22, 135-138.

Chapter 4

Solution-processable graphene linked to 3,5-dinitrobenzoyl as an electron acceptor in organic bulk heterojunction photovoltaic devices

Abstract: 3,5-Dinitrobenzoyl chloride was covalently linked to graphene oxide (GO) nanosheets prepared by a modified Hummers' method, using ethylenediamine as a spacer. The linkage of the GO with the small molecule was confirmed by spectroscopic (e.g., Fourier transform infrared, Raman) and microscopic analyses. The resultant GO-ethylene-dinitro-benzoyl (GO-EDNB) consists of a controlled scale of different graphene structures and is highly dispersable in common organic solvents. The GO-EDNB was used as the electron acceptor material in poly-(3-hexylthiophene) (P3HT) bulk heterojunction photovoltaic devices to significantly improve the performance, yielding a power conversion efficiency improvement of two orders and one order of magnitude compared with the pristine P3HT and the P3HT-GO devices respectively.

1. INTRODUCTION

Though, the silicon (Si) solar cell technology dominates the photovoltaic world market with an over 85% share, the application of solar energy is limited mainly due to the high energy payback time of the Si cells. Organic photovoltaic cells (OPVs) are a promising alternative to Si, due to their mechanical flexibility, low cost and light weight. Also, their high material utilization through low cost printing technologies is an important plus towards commercialization. The most typical OPV structure is based on the bulk heterojunction (BHJ) concept, in which a polymeric electron donor and a fullerene based electron acceptor are mixed in solution and cast into a thin film that is sandwiched between two electrodes.[1] The efficiency of the BHJ is restricted by the random network that is formed through the coating and drying of the photoactive solution due to phase segregation kinetics. This leads to the formation of dead ends and isolated domains that trap charge carriers and prevent them from being extracted.[2] Additionally, due to the low mobility of BHJ materials, there is rivalry between the dissociation and the recombination of the photogenerated carriers within the thin BHJ film.[3] Theoretically, the use of high aspect ratio 1D carbon allotropes, such as the carbon nanotubes should overcome the charge transport setback. But in practice, the presence of impurities and metallic nanotubes, significantly suppresses the charge mobility and favors the formation of recombination pathways, limiting the cells performance.[4,5] Furthermore, the dispersion of nanotubes in the polymer matrix in high concentrations is not possible, since the carbon nanotube length is comparable to the photoactive layer thickness leading to short-circuit effects. Thus, the challenge is to develop an electron acceptor material that is capable to provide a continuous pathway for the electrons to be transported to the metal electrode.

Graphene is a one-atom-thick planar sheet of sp^2-bonded carbon atoms stacked in a two-dimensional (2D) honeycomb lattice, and is the basic building block for carbon allotropes of any dimensionality. It can be stacked into 3D graphite, rolled into 1D nanotubes, or wrapped into 0D fullerenes. Enormous research efforts are devoted to graphene, due to its large surface area, high carrier transport mobility, superior mechanical flexibility, excellent stability and future promise in nanoelectronics.[6–8] Graphene has also the potential to act as an efficient electron acceptor not only due to its morphology but its intrinsic mobility, which can be as high as 70,000 cm^2/V s for mechanical cleaved graphene films[9] and 1–10 cm^2/V s for solution processable

graphene oxide derived graphene films.[10] Likewise, graphene should be highly soluble in organic solvents, such as dichlorobenzene, in order to be effectively blended with the conjugated polymer. A number of works regarding the fabrication of high quality graphene have been reported, such as micromechanical cleaving, epitaxial growth on silicon carbide, liquid-phase exfoliation of graphite and chemical vapor deposition.[11] However, the resulting graphene is insoluble in common organic solvents. Therefore, graphene oxide (GO), a graphene sheet functionalized with oxygen groups in the form of epoxy and hydroxyl groups on the basal plane, produced by the exfoliation of graphite oxide, appears to be the most straightforward approach to obtain a solution processable graphene.[12] Previous works on OPVs utilizing solution processable GO,[13,14] as the electron acceptor material, exhibited significantly lower efficiencies than the fullerene-based devices.[15] The main reason is the poor solubility and dispersion of the graphene in the polymer matrix, as in the case of nanotubes.[4] Therefore, it is vital to implement alternative processing steps, in order to solubilize the GO and at the same time, to properly alter its band structure for OPV applications. In this context, a facile and straightforward approach for the utilization of solution processable graphene, as the electron acceptor material in OPVs, is the linkage of the GO with a suitable small molecule, which contains nitro groups. The attachment of nitro groups at the terminal phenyl rings of the functionalized GO contributes to its absorption broadening,[16] whereas the direct conjugation of the electron-withdrawing nitro group with the GO backbone facilitates enhanced exciton dissociation, due to the presence of the aliphatic linker of EDA.[17] Furthermore, the functional group linked to GO offers the possibility to improve its dispersion within the polymer matrix, and at the same time to limit the large scale of the different graphene structures present.[18]

In this work, a highly solution processable graphene based molecule was prepared by a three-step method, consisting of (a) an oxidation step, (b) an acylation step and (c) a coupling step. GO sheets were linked with small molecule via amide bonds, formed between the acylated COCl groups of GO and 3,5-dinitrobenzoyl chloride with the amino groups of ethylenediamine, aiming at improving the dispersion of graphene in the polymer matrix and thus enhance the interactions between the polymer and the graphene phase. Furthermore, it is expected that the attachment of nitro groups at the terminal phenyls of the molecules, can contribute to absorption broadening as has been observed in the literature.[19] GO-EDNB suspensions were prepared in different organic solvents and were spectroscopic and microscopic analyzed. It should be noted, that the

suspensions remained stable for a time period over than a month. OPV devices were fabricated in various weight ratios, using the GO-EDNB, and the poly(3-hexylthiophene) (P3HT) as the electron acceptor and donor, respectively.

2. EXPERIMENTAL SECTION

2.1 Preparation of graphene oxide (GO)

GO was prepared from purified natural graphite powder (Alfa Aesar,~200 mesh) according to a modified Hummers' method.[20] Specifically, graphite powder (0.5 g) was placed into a cold mixture of concentrated H_2SO_4 (40 mL, 98%) and $NaNO_3$ (0.375 g) under vigorous stirring for 1 h, in an ice bath. During this time KMnO4 (2.25 g) was added in portions and the ice bath was kept for 2 h more, in order to cool the mixture under 10 ^oC. The green-brown colored mixture remained for stirring for 5 days. On completion of the reaction, the brick colored mixture was mixed with an aqueous solution 5% H_2SO_4 (70 mL). The mixture was stirred for 1 h under heating at 98 ^oC and becomes gray-black colored. When the temperature was decreased to 60 ^oC, 30% H_2O_2 (~2 mL) was added and the mixture was stirred for 2 h at room temperature. In order to remove residual acid, derived from the $KMnO_4$, the following process was used. The mixture was centrifuged for 5 min at 4200 rpm and washed with ~600 mL of an aqueous solution of 3% H_2SO_4(~9 mL)/0.5% H_2O_2(~1.5 mL) and then was put in an ultrasonic bath for 10 min (the ultrasonic vibration exfoliates the graphite oxide to GO sheets). The process was repeated for 10 times. Then, the mixture washed and purified with 150 mL of aqueous solution 3% HCl (~1.5 mL) for three times. Afterwards, it is washed thoroughly with distilled water (DI) and acetone, in order to remove any acidic part remaining. Finally, the resulting GO was dried at 60 ^oC in a vacuum oven overnight.

2.2 Preparation of the acylated GO-COCl

GO (30 mg) was dispersed in $SOCl_2$ (20 mL) and a catalytic amount of N,N-dimethylformamide (DMF 0.5 mL) was added. The mixture was sonicated, stirred and refluxed for 24 h at 75 ^oC, under N_2. The excess of thionyl chloride was removed by distillation under reduced pressure.[21] The obtained solid (GO-COCl) was washed with ultra-dried tetrahydrofuran (THF) three times and dried at 40 ^oC in a vacuum oven overnight.

2.3 Preparation of EDNB

3,5-Dinitrobenzoyl chloride (0.5 g, 2.2 mmol) was diluted in THF (15 mL) and cooled to 0-5 ^{o}C in an ice bath, under vigorous stirring. Then, ethylenediamine (0.2 mL, 3 mmol, 1.4 eq) and triethylamine (Et_3N) (~1 mL) were added and the mixture was stirred for 1 h. Thereafter, the heterogeneous solution was centrifuged for 10 min at 4200 rpm and washed twice with water slightly acidified with HCl. Finally, the product was washed with distilled water and methanol respectively, dried at 40 ^{o}C in a vacuum oven for 4 h, and recrystallized several times from ethanol, to afford the white solid ethylenedinitrobenzoyl (EDNB).

2.4 Preparation of GO-EDNB

GO-COCl (26 mg) was dispersed in DMF (15 mL) by ultrasonication (5 min) at room temperature to give a homogenous suspension. EDNB (40 mg) and drops of Et_3N (~2 mL) were added and the mixture was stirred and refluxed for 48 h, under N_2. When the mixture was cooled at room temperature, diethylether (5 mL) was added in order to boost the precipitation of the final product as a brownish solid, which was then collected by filtration. A series of purification steps were subsequently performed, each of which comprised ultrasonication (10 min) and centrifugation (5 min at 4200 rpm) to yield the final GO-EDNB solution. The purification process is important since it affects and determines the size and thickness range of the functionalized sheets which may be critical for the photovoltaic performance. For this purpose, following each step, the size and thickness evolution of the resulting GO-EDNB flakes had been monitored using scanning electron (SEM) and atomic force (AFM) microscopies. Figs. S4 and S5 show that both the average sheet sizes and thicknesses were reduced upon increasing the number of purification steps. The photovoltaic performance results presented in the following correspond to the use of the GO-EDNB solution obtained after five purification steps. Further experiments are in progress to identify the optimum size–thickness combination that gives the best photovoltaic performance. After the purification process, the GO-EDNB washed with MeOH and drying in a vacuum oven at 40 ^{o}C for 6 h.

2.5 Microscopic and spectroscopic characterization

The samples were characterized by Raman spectrometer at room temperature on a Nicolet Almega XR Raman spectrometer (Thermo Scientific) with a 473 nm blue laser as an excitation source. Fourier transform infrared (FT-IR) spectra were measured on a BRUKER FT-IR spectrometer IFS 66v/F (MIR). The photoluminescence (PL) measurements were carried out in the wavelength range from 500 to 1000 nm using a He–Cd cw laser, at 325 nm with a full power of P0= 35 mW, as the excitation source. UV–vis absorption spectra were recorded using a Shimadzu UV-2401 PC spectrophotometer over the wavelength range of 300–800 nm. The morphology of the surfaces was examined by field emission scanning electron microscopy (FE-SEM JEOLJSM-7000F) and by atomic force microscopy (AFM Digital Instruments NanoScope IIIa). X-ray diffraction patterns were collected on a Panalytical Expert Pro X-ray diffractometer, using Cu Ka radiation (k= 1.5406 A˚).

2.6 Fabrication and characterization of photovoltaic devices

Indium tin oxide (ITO, 15X/sq) coated glass substrates were used for the device fabrication. The substrates were cleaned by 10 min consecutive sonication in detergent, deionized water, acetone and isopropyl alcohol, in an ultrasonic bath. (Poly(3,4-ethylenedioxythiophene):poly(styrenesulfonate) (PEDOT:PSS) (Clevios P Al 4083, ~30 nm thickness) was spin coated onto the clean substrates, which were subsequently dried at 120 ^{o}C for 10 min to remove residual water. Photovoltaic devices were then fabricated, in the air, by spin coating a P3HT:GO-EDNB thin film (110 nm) from its 1,2-*o*-dichlorobenzene solution (17 mg/mL), followed by annealing at 160 ^{o}C for 20 min. Thereafter, Al electrode (80 nm) was deposited by vacuum evaporation onto the active layer through a shadow mask to define an active area of 18 mm^2 for each device. Current–voltage (J–V) measurements were performed at room temperature using an Agilent B1500A Semiconductor Device Analyzer. For photovoltaic characterization the devices were illuminated with 100 mW/cm^2 power intensity of white light by an Oriel solar simulator with an AM1.5 filter through the glass/ITO side. All measurements were performed in air immediately after the device fabrication.

3. Results and discussion

The synthetic route and the structure of the GO-EDNB are shown in Figure 1a and b respectively. The resulting GO-EDNB was isolated after centrifugation (5000 rpm, 10 min) and washed thoroughly with ethanol in order to remove the excess of any unbound 3,5-dinitrobenzoyl chloride. The final GO-EDNB was found to be easily dispersable in common organic solvents such as 1,2-*o*-dichlorobenzene, toluene and chloroform, under sonication, as can be clearly seen in Fig. 1c.

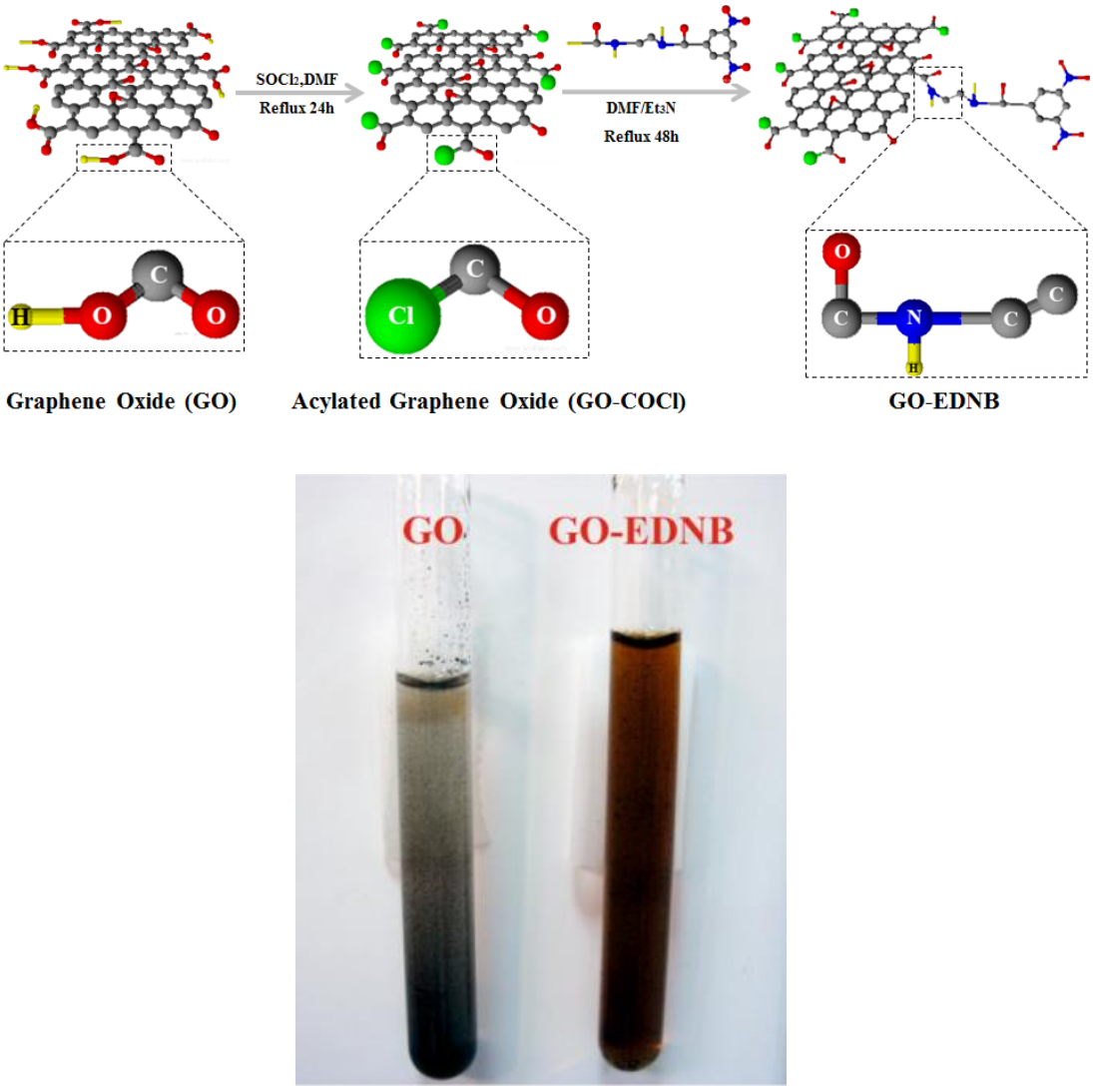

Figure 1. (Top) The chemical synthesis of solution-processed GO-EDNB by functionalization of GO and (bottom) presentation of pure GO and GO-EDNB solutions in *o*-DCB after a week. The GO-EDNB (brown) remains as solution, while the pure GO (gray) precipitates.

The amide linkage between dinitrobenzoyl and graphene in GO-EDNB is confirmed by FT-IR spectroscopy. Figure 2 shows the FT-IR spectra of pure GO and resulting GO-

EDNB. The pure GO (black line) shows the peaks of OH (O-H stretching vibrations) at ~3400 cm^{-1}, C–O (carboxylic acid and carbonyl moieties) at ~1700 cm^{-1} and the graphitic domains of C–C at ~1580 cm^{-1}. The band from 980-1250 contains the C-O (1010 cm^{-1}) and the O-H (1220 cm^{-1}) deformation, respectively, of carboxylic acid groups. GO-EDNB (red line) shows a broad peak at ~3362 cm^{-1} (N–H stretching) and an aliphatic C–H stretching at ~2870 cm^{-1}, which confirms the presence of EDA. The peaks of C–O (amide carbonyl moieties) and C–N (stretching) are displayed at ~1735 and ~1132 cm^{-1}, respectively. While, the bending and waging peaks of N–H are displayed at ~1600 and ~752 cm^{-1}, respectively. Finally, the bands at ~1350 and ~1530 cm^{-1} are characteristic of the nitro groups of GO-EDNB.

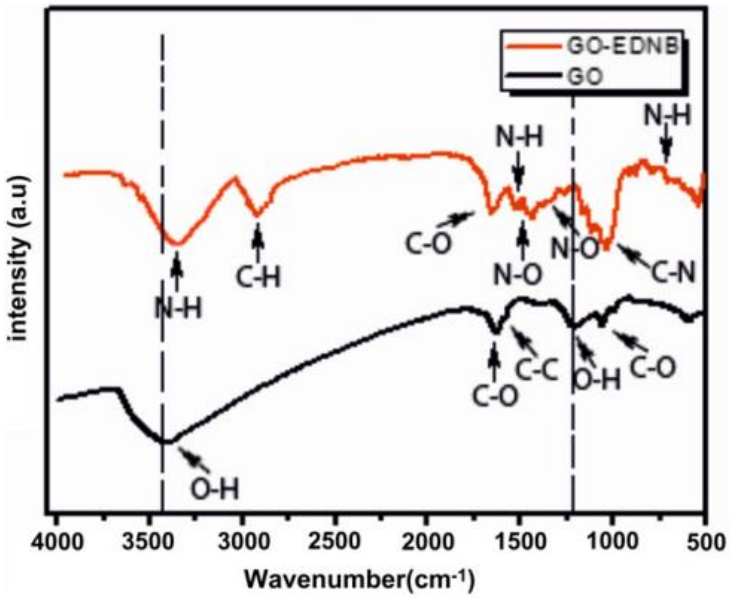

Figure 2. FT-IR spectra of pure GO and GO-EDNB in transmission mode.

Figure 3 displays the normalized UV–vis absorption spectra of pure GO and GO-EDNB in thin solid films prepared by spin-coating on quartz substrates. The absorption spectrum of GO-EDNB (red line) is red-shifted compared to the pure GO (black line). The graphene-induced enhancement in electron delocalization along the chemically linked EDNB moieties was observed in the GO-EDNB film, as evidenced by about 90 nm red-shift in the absorption band of the GO-EDNB with respect to that of GO. This result indicates that a strong interaction exists, due to the enhanced electron delocalization through the chemically conjugated graphene oxide sheet and the EDNB functional group. This interaction reduces the band gap energy; an advantage for the photovoltaic application.[19,20]

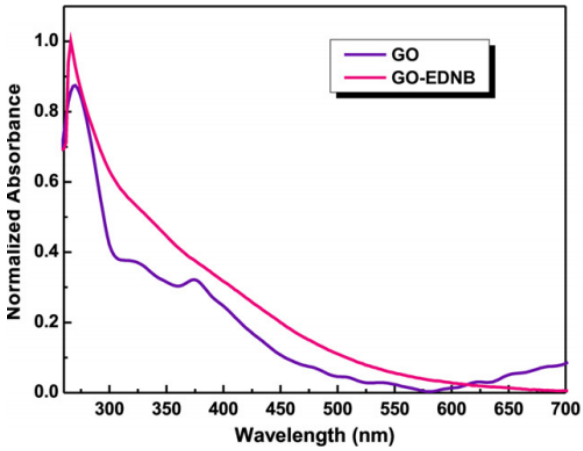

Figure 3. Normalized UV–vis absorption spectra of pure GO and GO-EDNB in solid thin film prepared by spin-coating on quartz substrate.

Figures 4a and b present also the normalized UV–vis absorption spectra of P3HT and the mixture of P3HT and GO-EDNB in DCB solution (10^{-5} M) and in thin films spin coated on quartz substrates, respectively. Both figures indicate that the simple mixture of P3HT and GO-EDNB in the same solvent cause no significant change in the P3HT absorption band.

Finally, Figure 5 shows the photoluminescence (PL) spectra, at an excitation wavelength of 325 nm, of P3HT and P3HT:GO-EDNB in thin films spin-coated on Si substrate. It is observed that, the pure P3HT shows a strong emission band over 650-700 nm, which was remarkably reduced for P3HT:GO-EDNB due to the PL quenching effect caused by graphene.[22] This is an additional advantage for using the GO-EDNB as an acceptor in BHJ photovoltaic devices.

Raman spectroscopy is a powerful tool for identifying carbonaceous materials because of their high Raman intensities. The Raman spectra of GO and GO-EDNB are depicted in Figure 6. For the measurement, a laser excitation of 473 nm was used, and powder samples were directly deposited on a Si wafer in the absence of solvents. In both samples studied, two prominent peaks are clearly visible, corresponding to the so-called D and G bands. In particular the Raman spectrum of GO exhibited a D band peak at 1348 cm^{-1}, while that of GO-EDNB at 1363 cm^{-1}, that corresponds to the breathing mode of j point phonons of A_{1g} symmetry and a G band peak at 1575 cm^{-1} due to the first-order scattering of the E_{2g} phonons.[23]

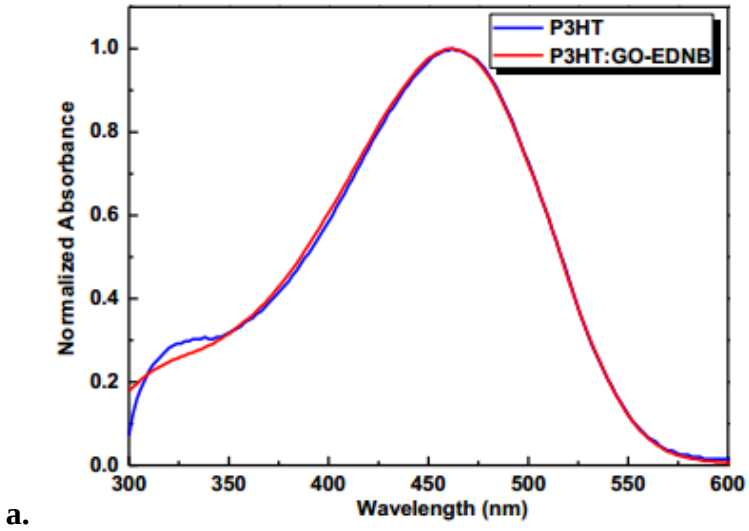

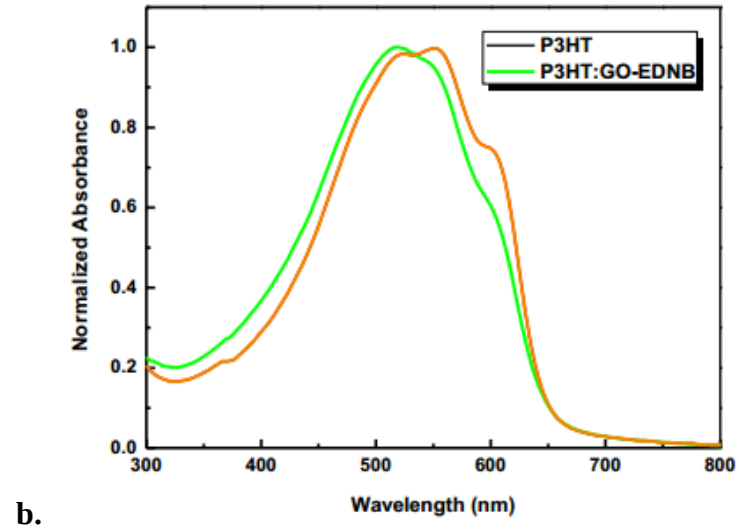

Figure 4. (a) Normalized UV-Vis absorption spectra of P3HT and P3HT:GO-EDNB blend in *o*-DCB solution (10^{-5} M) and (b) in thin film on a quartz substrate.

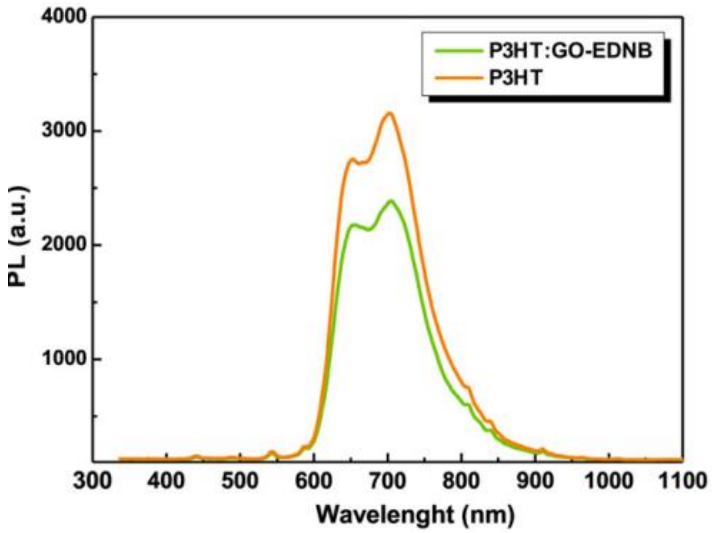

Figure 5. PL spectra of P3HT and P3HT:GO-EDNB thin films on Si.

Generally, the D band is relatively weak or nearly invisible for perfect graphene lattices, which arises primarily from symmetry breaking at the edge.[24] The intensity ratio (I_D/I_G) of D and G bands expresses the sp^2/sp^3 carbon ratio, a measure of the extent of disorder.[23,25] Comparing the G bands of GO and GO-EDNB, it is clear that G band of GO-EDNB occurs at 1585 cm^{-1}, which is upshifted by 10 cm^{-1} compared to that of GO.

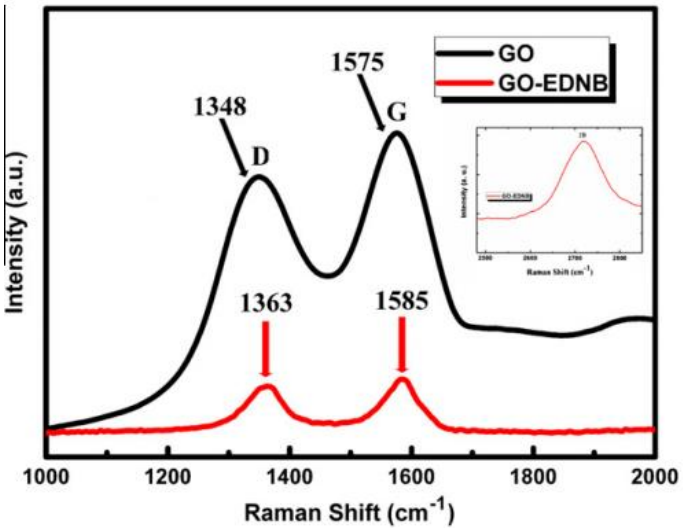

Figure 6. Raman spectra of GO and GO-EDNB. The inset shows the 2D peak of GO-EDNB.

Upon calculation, the intensity ratios I_D/I_G of GO and GO-EDNB were found to be 0.73 and 0.92 respectively, reflecting the increase in disorder. The change in the I_D/I_G ratio can be at least partly attributed to the formation of covalent bonds between GO and EDNB.[26] The inset of Figure 6 shows the 2D peak of GO-EDNB. The Raman shift of the G band for GO-EDNB provides evidence for the charge transfer between the GO sheets and EDNB, which suggests a strong interaction between the EDNB and the GO sheet.

Figure 7 shows thermogravimetric curves from the graphene oxide and the GO-EDNB sample as well as, the inset displays the TGA graph of the initial EDNB. The samples were loaded into an alumina pan for TGA under constant nitrogen flow. The temperature ceiling was set at 800 ^oC from room temperature, with a slow heating rate (10 ^oC/min) to ensure a regular and integrated decomposition of GO and GO-EDNB. GO is thermally unstable and starts to lose mass upon heating even below 100 ^oC and has resulted in a rapid mass loss commencing at about 200 ^oC, presumably due to pyrolysis of labile oxygen-containing functional groups, such as OH, CO and COOH

groups, and a total mass loss of ~40% at 800 ºC. Similar results were reported by Stankovich et al.[27]

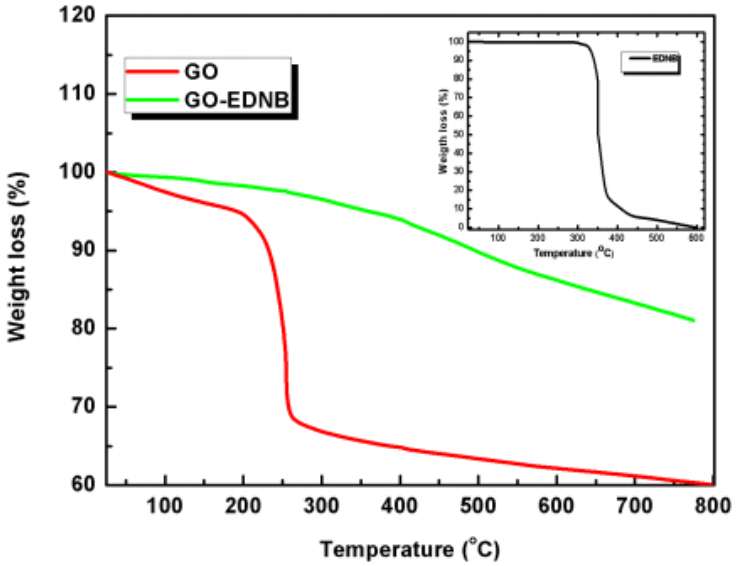

Figure 7. The TGA graphs of GO and GO-EDNB obtained under inert atmosphere of N_2, with heating rate 10 °C/min. The inset displays the TGA graph of the initial EDNB.

In comparison to GO, GO-EDNB exhibits improved thermal stability, due to the amino-functionalization.[28] It is stable over a wide temperature range, with only about 20% weight loss at 800 ºC. Specifically, TGA of GO-EDNB shows 3% weight loss in a nitrogen atmosphere at ~250 ºC, due to the lower ‘‘oxygen’’ concentration than GO. Finally, our sample displays a second significant mass loss at ~400 ºC, because of the decomposition of the nitro groups.[29]

To further confirm the structures, XRD patterns are presented in Figure 8 from GO and GO-EDNB powder. A strong, at 26.5º, and a weak, at 46.3º, peaks appear in the GO-EDNB pattern that were not present in the GO spectrum which showed a strong peak at 12.6º.

GO and GO-EDNB were morphologically characterized by SEM and AFM to determine sheet size and thickness distributions. AFM has also been employed to quantitate the degree of exfoliation after the dispersion of the powder in a solvent.

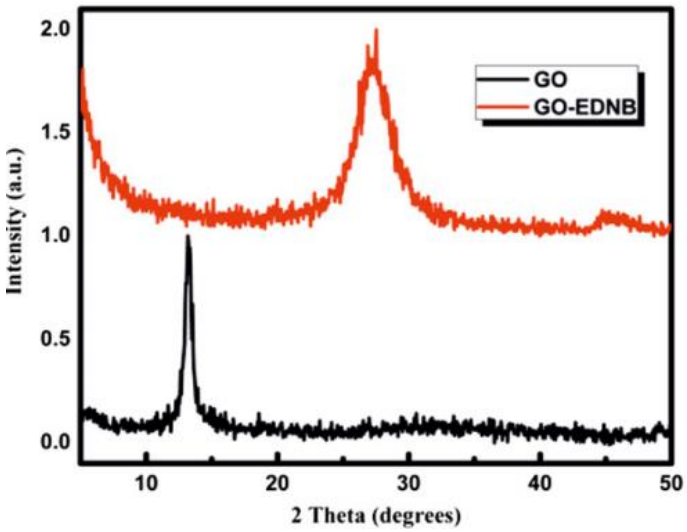

Figure 8. X-ray diffraction patterns from GO and GO-EDNB samples.

SEM and AFM results indicate that the morphological features of GO were not altered significantly upon functionalization. Representative SEM images of the dry, as-produced sheets, deposited on Si substrates are shown in Fig. 9a–c. A closely packed ‘‘tiling’’ of graphene oxide sheets with a uniform contrast was observed. Such flakes exhibit lateral dimensions ranging from several hundreds of nanometers to several micrometers and are arranged in an edge-to-edge configuration (Fig. 9a and b).

a)

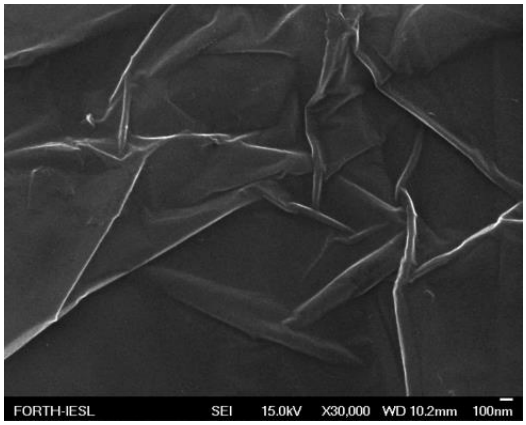

b)

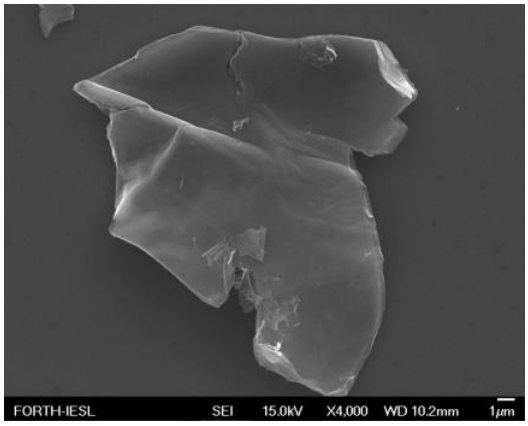

c)

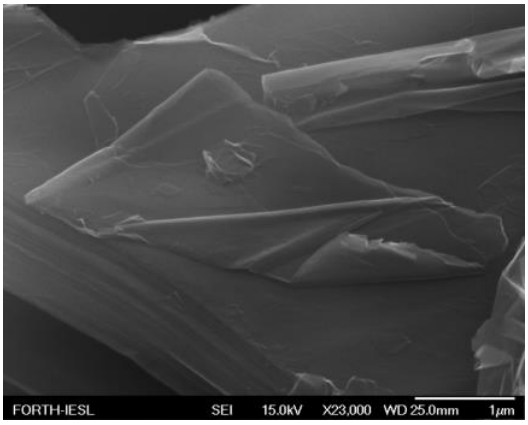

d)

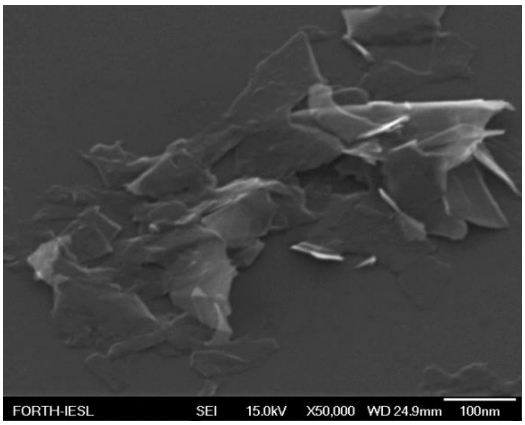

e)

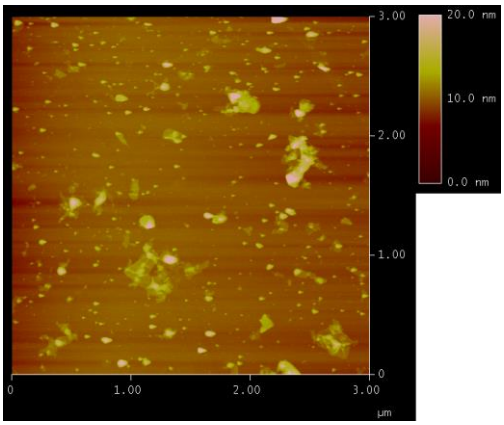

Figure 9. SEM images of unpurified GO-EDNB a) in a graphene neurons structure, b) and c) wrapped graphene-based sheets, (d) a vermiculite-like structure; SEM and (e) AFM images of purified GO-EDNB graphene sheets.

Moreover, the SEM image of larger-scale particles presents the ‘‘as wrapped’’ functionalized graphene oxide sheets (Fig. 9b and c). SEM and AFM images of the GO-EDNB sheets obtained after the series of five purification steps are presented in Figure 9d and e respectively, both showing that the sheet size is significantly reduced compared to the initial one. The absence of charging during the SEM imaging indicates that the network of graphene-based sheets and the individual sheets were electrically

conductive. Figure 10 presents the dependence of the most probable sheet size (a) and maximum sheet thickness (b) on the number of purification steps. Figure 11 shows the sheet size distribution, determined statistically using a number of SEM and AFM images. The purified sheets exhibit lateral dimensions ranging from several tens to several hundreds of nanometers. Furthermore, AFM analysis indicated significant exfoliation of the pristine flakes, leading to sheet thicknesses in the 2–20 nm range. An AFM image of a single GO-EDNB sheet is presented in Figure 12.

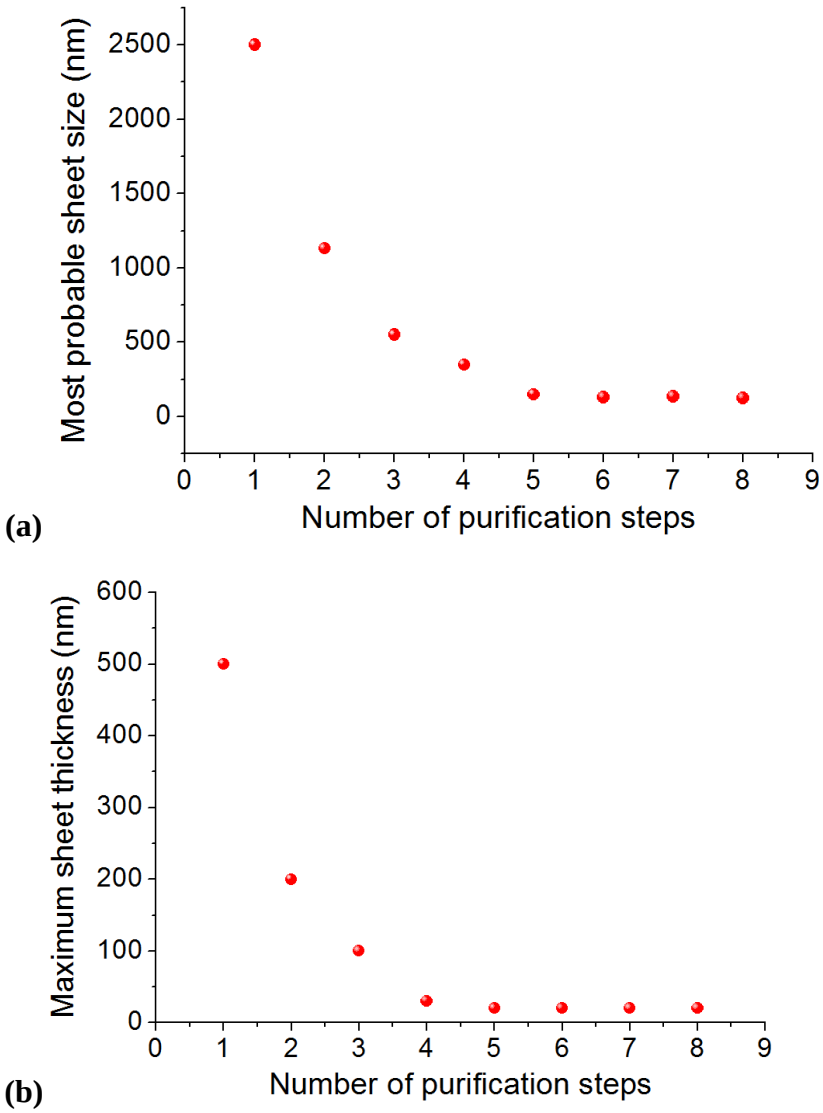

Figure 10. Dependence of the most probable sheet size (a) and maximum sheet thickness (b) on the number of purification steps.

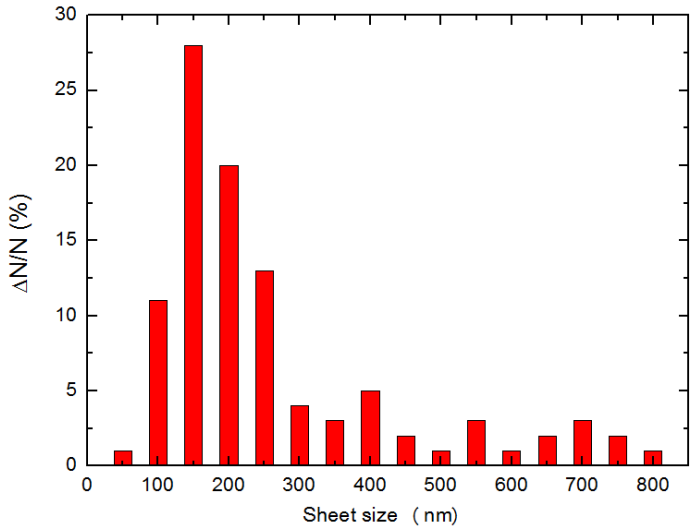

Figure 11. GO-EDNB sheet size distribution following a series of five purification steps. Sheet sizes were determined using a number of SEM and AFM images.

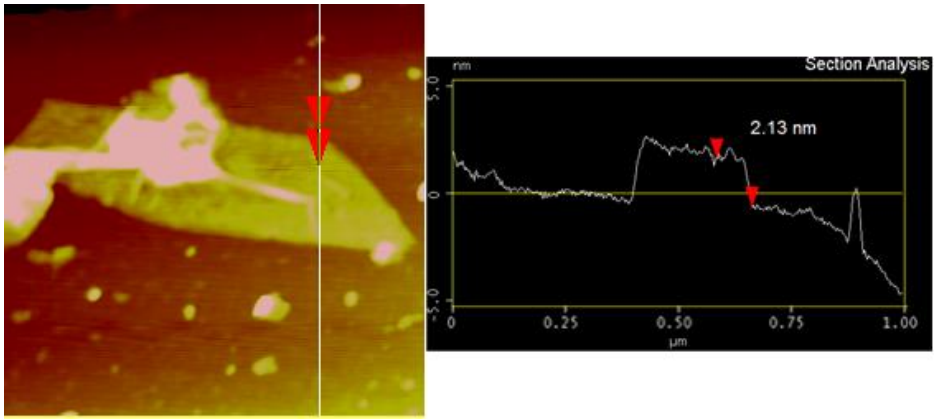

Figure 12. AFM image of a single GO-EDNB sheet.

The basal planes of graphene sheets in GO-EDNB are terminated mostly with epoxide and hydroxyl groups, in addition to parietal dinitrobenzoyl substituted groups connected via aliphatic chains. As a consequence, GO-EDNB readily forms stable colloidal dispersions of thin GO-EDNB sheets in organic solvents, such as *o*-DCB and chloroform, commonly used to prepare organic photovoltaic blends. Solar cells using the GO-EDNB molecules as electron acceptors were consequently fabricated. A solution of 17 mg mL^{-1} P3HT in *o*-DCB with GO-EDNB of 5, 10 and 15 wt% was spin-coated onto indium tin oxide (ITO) glass substrate, which was modified with poly(ethylene dioxythiophene) doped with polystyrene sulfonic acid (PEDOT:PSS). Al was then vacuum-deposited as the top contact to form a PV device with the structure of

ITO/PEDOT:PSS (30 nm)/P3HT:GO-EDNB (110 nm)/Al (80 nm), shown in Figure 13a. A post-fabrication annealing of the P3HT:GO-EDNB active layer, conducted at 160 ^{o}C for 20 min under N_2 atmosphere, has played an important role in the improvement of the device performance. The morphology of the film has been improved, residual functional groups linked to the graphene sheet have been removed and thus the conductivity of the graphene sheet has increased.[30] As a result, the conjugation length increases and the charge transport mobility is enhanced.[31]

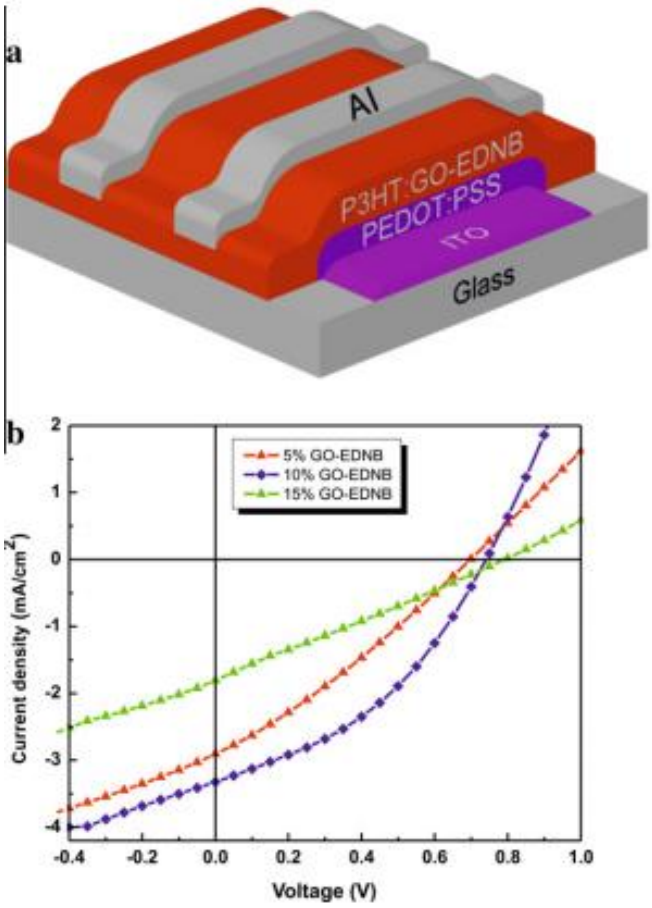

Figure 13. (a) Schematic of the device with P3HT/GO-EDNB thin film as the active layer and the structure ITO/PEDOT:PSS (30 nm)/P3HT:GO-EDNB (110 nm)/Al (80 nm) (b) J–V curves of PV devices based on P3HT:GO-EDNB active layer with different graphene content (5, 10, and 15 wt%) after annealing at 160 ^{o}C for 20 min.

Figure 13b shows the current voltage (J–V) curves for P3HT:GO-EDNB for the devices with GO-EDNB content of 5%, 10% and 15 wt%. The illumination source was a simulated, AM 1.5, solar irradiation of 100 mW/cm^2 intensity. The detailed photovoltaic characteristics are listed in Table 4.1 indicating that the best photovoltaic performance was achieved by the P3HT:(10%) GO-EDNB device, exhibiting an open-

circuit voltage (V_{oc}) of 0.72 V, short-circuit current density (J_{sc}) of 3.3 mA cm^{-2}, fill factor (FF) of 40 % and power conversion efficiency (n) of 0.96 %, more than two orders of magnitude larger than the efficiency of the pristine P3HT device. A control device [ITO/PEDOT:PSS (30 nm)/P3HT:GO (110 nm)/Al (80 nm)] using the as-synthesized GO (10% content) was also prepared for comparison. As presented in Table 1 the power conversion efficiency measured for this device was lower by more than one order of magnitude. It should also be mentioned, that the photocurrent value obtained is one order of magnitude higher than that measured in optimized carbon nanotubes-based photovoltaic devices.[32]

Device	J_{sc} (mA/cm^2)	V_{oc} (V)	FF (%)	η (%)
ITO/PEDOT: PSS/P3HT/Al	0.04	0.40	28	0.004
ITO/PEDOT: PSS/P3HT: GO-EDNB (5%)/Al	2.90	0.67	32	0.622
ITO/PEDOT: PSS/P3HT: GO-EDNB (10%)/Al	3.32	0.72	40	0.956
ITO/PEDOT:PSS/P3HT: GO-EDNB (15%)/Al	1.78	0.76	28	0.379
ITO/PEDOT:PSS/P3HT: GO (10%)/Al	0.16	0.47	25	0.019

Table 4.1 Device performances of PV devices based on P3HT:GO-EDNB composites with different graphene content (5, 10, and 15 wt%) after annealing at 160 °C for 20 min.

The J_{sc} and the FF increase with increasing GO-EDNB concentration of up to 10% and then decay. The maximum efficiency is obtained from the composite containing 10% of GO-EDNB. This efficiency enhancement is attributed to the formation of internal polymer/graphene junctions resulting in higher exciton dissociation and balanced charge transport throughout the entire volume of the P3HT:GO-EDNB composite. The observed strong PL quenching (Figure 5) of the composite films confirms the enhanced charge transfer processes in the films. For concentrations higher than 10 wt%., the photocurrent is believed to be limited due to a lower photogeneration rate, due to aggregation effects. The increase in Voc from 0.4 V for the pristine P3HT, to 0.72 V for the P3HT:GO-EDNB device with 10 wt% can be explained as in the case of polymer–carbon nanotube devices.[32] The upper limit of V_{oc} of single layer devices is explained by the metal–insulator–metal (MIM) model, and is easily calculated from an estimate of the difference of the two electrodes work functions. The V_{oc} of the pristine

P3HT is 0.4 V, perfect matching the work function difference of the ITO and Al electrodes. While, for the P3HT:GO-EDNB device, the V_{oc} is determined by the difference of the GO-EDNB lowest unoccupied molecular orbital (LUMO) and the P3HT highest occupied molecular orbital (HOMO) energy levels. Therefore, the V_{oc} of the optimum device is increased to 0.72 V, which is in accordance with the difference between the HOMO level (5.25 eV) of P3HT, determined by cyclic voltammetry and the work function of graphene (4.5 eV). The photovoltaic properties of our GO-EDNB devices are rather satisfactory considering that these devices use a new type of electron-acceptor material, different from the most-studied fullerene system. Indeed, the performance of those devices was reached without any attempt to optimize the morphology of the active layer which is the significant extrinsic factor that impacts all the device characteristics. Also, the GO-EDNB can be utilized as an additive in both the active layer and the hole transport layer, as in the case of carbon nanotubes.[33] Further studies concentrating on the graphene particle size and layer structure influence on the photovoltaic characteristics are needed for the device optimization.

5. Conclusions

A new high solution-processed graphene based material, was synthesized by linking graphene oxide (GO) sheets with small molecule via peptide bonds between the acylated COCl groups of GO and 3,5-dinitrobenzoyl chloride with the amino groups of ethylenediamine. The resulting GO-EDNB was efficiently mixed with P3HT in the ratio of 5%, 10%, 15%, and used as the photoactive layer in BHJ OPV devices. After the post-fabrication annealing process, we get efficiency of 0.96% for the device containing 10% GO-EDNB in the active layer. Considering that remarkable and reproducible performance is obtained for the GO-EDNB based devices without any optimization of the blend morphology it is expected that our new organic solution-processable functionalized graphene material will serve as a competitive alternative to PCBM for high-performance OPV devices.

References

1. Dennler G, Scharber MC, Brabec CJ. Polymer–fullerene bulk heterojunction solar cells. Adv Mater 2009;21:1323–38.
2. Yang X, Loos J. Toward high-performance polymer solar cells: the importance of morphology control. Macromolecules 2007;40:1353–62.
3. Blom PWM, Mihailetchi VD, Koster LJA, Markov DE. Device physics of polymer:fullerene bulk heterojunction solar cells. Adv Mater 2007;19:1551–66.
4. Kymakis E, Amaratunga GAJ. Single-wall carbon nanotube/conjugated polymer photovoltaic devices. Appl Phys Lett 2002;80:112–4.
5. Kymakis E, Servati P, Tzanetakis P, Koudoumas E, Kornilios N, Rompogiannakis I, et al. Effective mobility and photocurrent in carbon nanotube–polymer composite photovoltaic cells. Nanotechnology 2007;18:435702–7.
6. Lin YM, Dimitrakopoulos C, Jenkins KA, Farmer DB, Chiu HY, Grill A, et al. 100-GHz transistors from wafer-scale epitaxial graphene. Science 2010;327:662.
7. Bolotin KI, Ghahari F, Shulman MD, Stormer HL, Kim P. Observation of the fractional quantum Hall effect in graphene. Nature 2009;462:196–9.
8. Stratakis E., Eda G., Kymakis E., Fotakis C., Chhowalla M. Freestanding graphene on microstructured silicon vertices for enhanced field emission. Nanoscale 2012;4:3069–74.
9. Chen F, Xia JL, Tao NJ. Dielectric screening enhanced performance in graphene field effect transistor. Nano Lett 2009;9:2571–4.
10. Kymakis E, Stratakis E, Stylianakis MM, Koudoumas E, Fotakis C. Spin coated graphene films as the transparent electrode in organic photovoltaic devices. Thin Solid Films 2011;520:1238–41.
11. Avouris P. Dimitrakopoulos graphene: synthesis and applications. Mater Today 2012;15:86–97.
12. Hernandez Y, Nicolosi V, Lotya M, Blighe FM, Sun Z, De S, et al. High-yield production of graphene by liquid-phase exfoliation of graphite. Nat Nanotech 2008;3:563–8.
13. Yu D, Yang Y, Durstock M, Baek JB, Dai L. Soluble P3HT-grafted graphene for efficient bilayer-heterojunction photovoltaic devices. ACS Nano 2010;4:5633–40.
14. Hill CM, Zhu Y, Pan S. Fluorescence and electroluminescence quenching evidences of interfacial charge transfer in poly (3-hexylthiopene): graphene oxide bulk heterojunction organic photovoltaic device. ACS Nano 2011;2:942–51.
15. Troshin PA, Hoppe H, Peregudov AS, Egginger M, Shokhovets S, Gobsch G, et al. [70]Fullerene-based materials for organic solar cells. Chem Sus Chem 2011;4:119–24.
16. Suresh P, Balraju P, Sharma GD, Mikroyannidis JA, Stylianakis MM. Effect of the incorporation of a low-band-gap small molecule in a conjugated vinylene copolymer: PCBM blend for organic photovoltaic devices. ACS Appl Mater Interfaces 2009;1:1370–4.
17. Mikroyannidis JA, Stylianakis MM, Balraju P, Suresh P, Sharma GD. Novel p-phenylenevinylene compounds containing thiophene or anthracene moieties and cyanovinylene bonds for photovoltaic applications. ACS Appl Mater Interfaces 2009;1:1711–8.
18. Khan U, Porwal H, O'Neill A, Nawaz K, May P, Coleman JN. Solvent-exfoliated graphene at extremely high concentration. Langmuir 2011;27:9077–82.

19. He Y, Wang X, Zhang J, Li Y. Low bandgap polymers by copolymerization of thiophene with benzothiadiazole. Macromol Rapid Commun 2009;30:45–51.
20. Becerril HA, Mao J, Liu Z, Stoltenberg RM, Bao Z, Chen Y. Evaluation of solution-processed reduced graphene oxide films as transparent conductors. ACS Nano 2008;2:463–70.
21. Stylianakis MM, Mikroyannidis JA, Kymakis E. A facile, covalent modification of single-wall carbon nanotubes by thiophene for use in organic photovoltaic cells. Sol Energy Mater Sol Cells 2010;94:267–74.
22. Liu Z, Liu Q, Huang Y, Ma Y, Yin S, Zhang X, et al. Organic photovoltaic devices based on a novel acceptor material: graphene. Adv Mater 2008;20:3924–30.
23. Alwarappan S, Erdem A, Liu C, Li CZ. Probing the electrochemical properties of graphene nanosheets for biosensing applications. J Phys Chem C 2009;113:8853–7.
24. Kudin KN, Ozbas B, Schniepp HC, Prud'homme RK, Aksay IA, Car R. Raman spectra of graphite oxide and functionalized graphene sheets. Nano Lett 2008;8:36–41.
25. Ferrari AC, Robertson J. Interpretation of Raman spectra of disordered and amorphous carbon. Phys Rev B 2000;61:14095–107.
26. Fang M, Wang K, Lu H, Yang Y, Nutt S. Covalent polymer functionalization of graphene nanosheets and mechanical properties of composites. J Mater Chem 2009;19:7098–105.
27. Stankovich S, Dikin DA, Piner RD, Kohlhaas KA, Kleinhammes A, Jia Y, et al. Synthesis of graphene-based nanosheets via chemical reduction of exfoliated graphite oxide. Carbon 2007;45:1558–65.
28. Hu Y, Shen J, Li Na, Shi M, Ma H, Yan B, Wang W, et al. Amino-functionalization of graphene sheets and the fabrication of their nanocomposites. Polym Compos 2010;31:1987–94.
29. Mikroyannidis JA, Stylianakis MM, Suresh P, Balraju P, Sharma GD. Low band gap vinylene compounds with triphenylamine and benzothiadiazole segments for use in photovoltaic cells. Org Electron 2009;10:1320–33.
30. Liu Q, Liu ZF, Zhang XY, Yang LY, Zhang N, Pan GP, et al. Polymer photovoltaic cells based on solution-processable graphene and P3HT. Adv Funct Mater 2009;19:894–904.
31. Kymakis E, Koudoumas E, Franghiadakis I, Amaratunga GAJ. Post-fabrication annealing effects in polymer–nanotube photovoltaic cells. J Phys D Appl Phys 2006;39:1058–62.
32. Kymakis E, Alexandrou I, Amaratunga GAJ. High open-circuit voltage photovoltaic devices from carbon-nanotube–polymer composites. J Appl Phys 2003;93:1764–8.
33. Stylianakis MM, Kymakis E. Efficiency enhancement of organic photovoltaics by addition of carbon nanotubes into both active and hole transport layer. Appl Phys Lett 2012;100:093301.

Chapter 5

Photochemical Synthesis of Solution-Processable Graphene derivatives with Tunable Band-gap for Organic Solar Cells

Abstract: A photochemical route for the facile synthesis of tunable bandgap graphene-based derivatives from graphene oxide (GO) through controlled laser irradiation in liquid phase is presented. The method is facile and fast, yielding these materials within 2 hours and with excellent long-term stability. It makes use of photogenerated solvated electrons that give rise to GO reduction, accompanied by preferential attachment of the desired functional unit, intentionally dispersed into the precursor GO solution. As a proof of concept, Graphene Oxide-Ethylene-DiNitro-Benzoyl (LGO-EDNB) was photochemically synthesized and utilized as the electron acceptor material in organic bulk heterojunction solar cells (OSCs) with the poly[*N*-9′-heptadecanyl-2,7-carbazole-alt-5,5-(4′,7′-di-2-thienyl-2′,1′,3′-benzothiadiazole)] (PCDTBT) as the electron donor. The graphene derivatives are highly dispersible in organic solvents used in OSCs, while their energy levels can be readily tuned upon fine-tuning of the bandgap, which is directly related to the irradiation dose applied during the synthesis process. The utilization of LGO-EDNB with a bandgap of 1.7 eV, and a resultant lowest unoccupied molecular orbital (LUMO) level of 4.1 eV, leads to maximum open-circuit voltage of 1.17 V and to power conversion efficiency (PCE) of 2.41%, which is the highest PCE for graphene-based electron acceptors to date.

Keywords: Solution-Processable, graphene-based OPVs, band-gap, photochemical synthesis

1. INTRODUCTION

Graphene functionalization has received considerable attention as a suitable mean to tailor its chemical, structural and optoelectronic properties.[1],[2],[3],[4] As a result, a wide range of novel graphene-based functional materials and derivatives has been developed.[5],[6],[7],[8] One of the most extensively studied chemical modification approach, is via exfoliation of oxidized graphite to graphene oxide (GO)[9] followed by interaction of the functional unit with reactive oxygen groups located at the basal plane and edges of the GO lattice. In this concept, covalent functionalization of GO poses considerable challenges and great potential for future applications.[10],[11],[12] For instance, small molecules and polymers have been covalently attached to GO to realize novel polymer composites, paper-like materials, sensors and drug-delivery systems.[13],[14],[15]

Currently there are intense research efforts focusing on the application graphene-based derivatives as light-harvesting materials in OSCs.[5],[16] Indeed, Yong et al., predicted that the single-cell efficiency of functionalized graphene-based OSCs can exceed 12% attributed to its tunable bandgap and band-position features, as well as its superior carrier mobility, thermal stability and mechanical integrity.[17] Therefore, graphene-based materials are anticipated to be utilized for the effective exciton separation and charge transport when blended with conjugated polymers, because of their large surface area for donor/acceptor interfaces and continuous pathway for the electron transfer, as in the case of carbon nanotubes.[18],[19] Previous works on OSCs utilizing functionalized GO, as the electron acceptor material[20],[21],[22] exhibited significantly lower efficiencies than the fullerene-based devices.[23],[24] The main reason is the poor solubility[25],[26] of GO in common organic solvents, which results in its poor dispersion in the polymer matrix. The second and more important reason is that, contrary to fullerene acceptors,[27],[28] to date no graphene-based electron acceptor system with tunable energy levels has been demonstrated. As a result, the energy levels of the polymer donor and currently available graphene-based acceptor systems cannot be tuned to provide ideal band offsets for both hole and electron transport. Indeed, taking into account the energy levels of the most efficient and well known narrow band gap donors, such as the poly[(4,4′-bis(2-ethylhexyl)dithieno[3,2-b:2′,3′-d]-silole)-2,6-diyl-alt-(2,1,3-benzothiadiazole)-4,7-diyl] (PDTSBT),[29] poly[2,6-(4,4-bis-(2-ethylhexyl)-4H-cyclopen-ta[2,1-b;3,4-b′]dithiophene)-alt-4,7-(2,1,3-benzothiadiazole)

(PCPDTBT),[30] poly[(4,4′-bis(2-ethylhexyl)dithieno[3,2-b:2′,3′-d]silole)-2,6-diyl-alt-(2,1,3-benzothiadiazole)-4,7-diyl] (PSBTBT)[31] and the poly[*N*-9′-heptadecanyl-2,7-carbazole-alt-5,5-(4′,7′-di-2-thienyl-2′,1′,3′-benzothiadiazole)] (PCDTBT)[32] the favorable LUMO and HOMO levels of the electron acceptor material should be higher than 3.6 eV and 5.5 eV respectively in order to facilitate efficient excitons dissociation and electron and hole transport to the opposite electrodes. In our previous work, chemically synthesized GO-EDNB[20] has been used as the electron acceptor material in P3HT based bulk heterojunction (BHJ) photovoltaic devices. However, the utilization of the GO-EDNB as a universal electron acceptor is not possible, since its LUMO is at 3.4 eV, providing an energetic offset for excitons dissociation only in the P3HT case ($LUMO_{P3HT}$=3 eV), and with none of the above mentioned polymers. Therefore, it is vital to develop alternate functionalization routes towards improving solubility and at the same time, properly tune the bandgap of the graphene derivatives, in order to achieve an ideal energy offset between the polymer and the graphene for enhanced OSC performance.

In this work, a new facile and room temperature methodology to obtain high-performance graphene derivatives for OSCs, based on photochemical functionalization of GO, by pulsed laser irradiation in solution (see Figure 1) is demonstrated. Using this method, a bandgap tunable electron acceptor system, named as Laser Graphene Oxide-Ethylene-DiNitro-Benzoyl (LGO-EDNB), was successfully synthesized. It is found that the attachment of nitro groups at the terminal phenyl rings of GO contributes to its absorption broadening, whereas the direct grafting of the electron-withdrawing nitro group with the GO backbone gives rise to enhanced exciton dissociation, due to the presence of the aliphatic linker of ethylenediamine, which also affects the optical properties of the attached molecules and the degree of quenching.[33] At the same time, GO electronic properties can be substantially influenced by the presence of the small molecule, due to charge-transfer effects.[34] Moreover, the functional group linked to GO offers the possibility to improve its dispersion within the polymer matrix and thus facilitate efficient blending between the donor/acceptor phases. More importantly, it is demonstrated that depending on the irradiation conditions the bandgap of the LGO-EDNB acceptor can be readily tuned with respect to the energy levels of the polymer donor used, in order to provide desirable energy offsets for both hole and electron

transport. The method relies on precise photochemical reactions initiated by pulsed laser irradiation in the presence of a precursor solution.

Compared with the commonly used chemical functionalization approaches, our photochemical approach is much faster, since a few pulses are sufficient to yield functionalized material with excellent long-term stability. Furthermore, during the photochemical synthesis, a simultaneous photoreduction of the GO lattice takes place [35],[36] enabling tunability of the functionalization degree. Finally, the technique negates the need for high temperature steps and can provide access to the synthesis of large quantities of functionalized graphene dispersions with good control over the functional unit levels, which is not readily realized by existing methods.

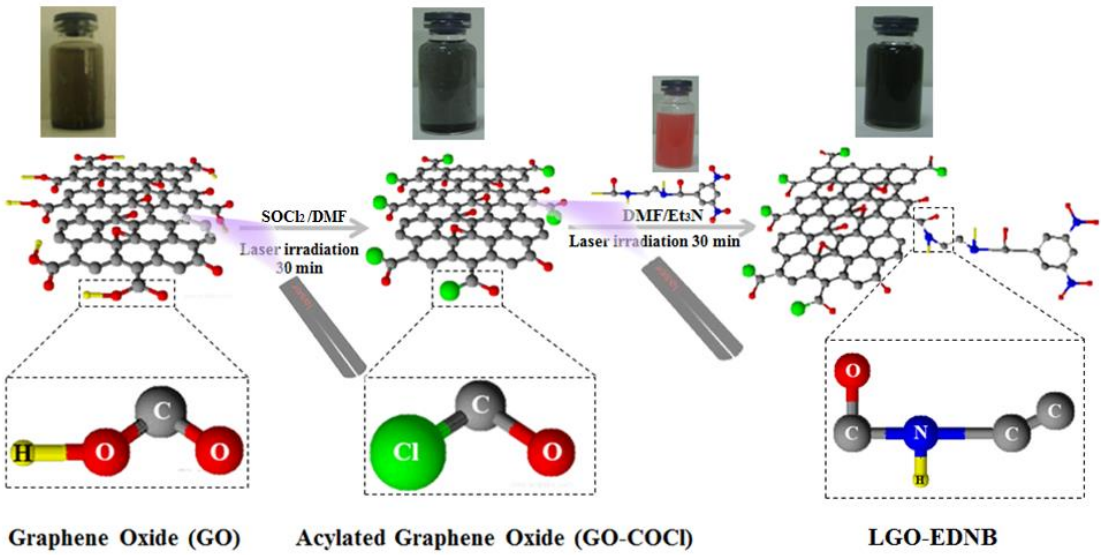

Figure 1. Schematic display of the spontaneous acylation of graphene oxide and (Bottom) the spontaneous grafting of ethylenediaminedinitrobenzoyl (EDNB), induced by pulsed laser.

2. RESULTS AND DISCUSSION

All the reactions took place into a quartz reactor (Figure 2), containing the initial GO dispersion into which the precursor molecules were dissolved. Figures 1, 2 and 3 outline the overall reaction process; no mechanistic details are implied. We found that laser excitation is required for the reaction (see below).

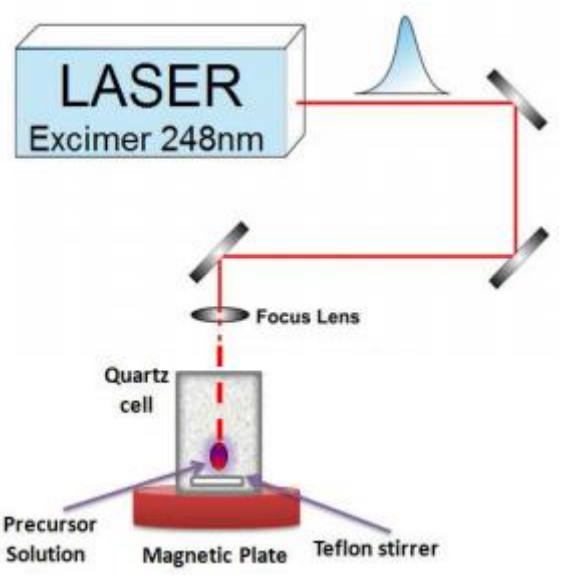

Figure 2. Schematic of the experimental setup used for the photochemical synthesis of LGO-EDNB.

In particular, as shown in Figure 1, the synthesis of LGO-EDNB comprises two distinct photochemical steps, an acylation and a coupling one. During the first step, UV laser irradiation of GO in the presence of $SOCl_2$ gives rise to acylation of the -COOH side groups to -COCl. This reaction is highly exothermic and above a critical laser intensity cracking of the quartz tube was observed. Figure 3 illustrates a proposed reaction mechanism where thionyl chloride interacts in a nucleophilic fashion with a carboxylic group.[37]

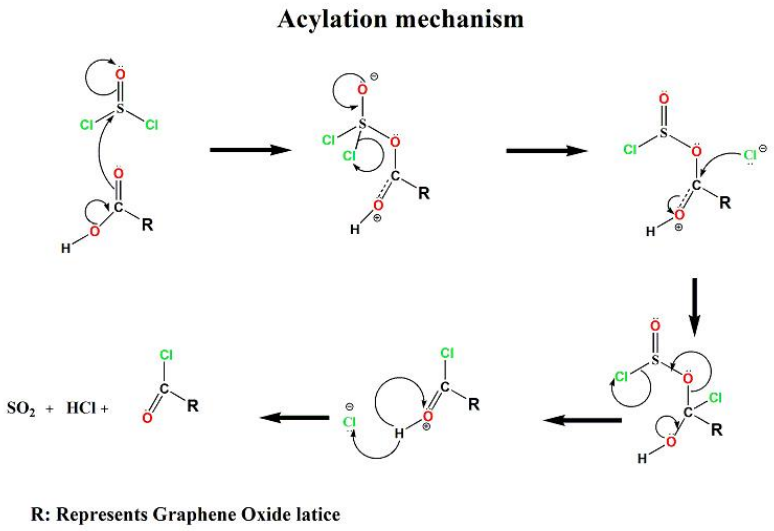

a)

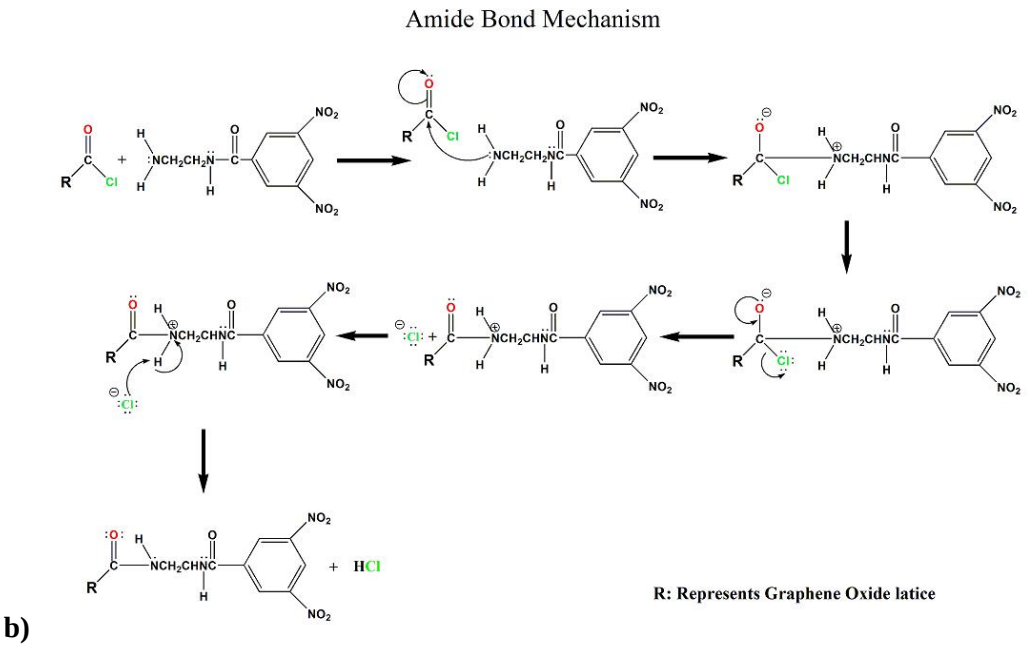

b)

Figure 3. The Proposed Reaction Mechanisms of (a) Acylation (b) Amide bond Mechanism.

Light excitation provides the energy required for displacement of chloride ion and subsequently carbonyl oxygen forms a sulfite ester intermediate which readily reacts with nucleophiles, as it is a good leaving group (Figure 3a). Upon formation of the acyl chloride, the displaced sulfite ion is unstable and decomposes into SO_2^+ and Cl^-. In the second step, the acylated GO sheets were irradiated in the presence of triethylamine (Et_3N) and is linked with small molecule via amide bonds, formed between the COCl groups and 3,5-dinitrobenzoyl chloride with the amino groups of Et_3N (Figure 3b). During the different reaction steps notable changes in the coloration of the irradiated solution were observed (Figure 1). The efficiency of the photochemical process is unexpectedly high; the final product can be delivered within a couple of hours, which is much faster than the commonly used synthetic routes.

Following irradiation, spectroscopy (XPS) was used to probe the chemical modifications introduced into the GO lattice. Figure 4a compares typical XPS spectra of GO and LGO-EDNB respectively. From these data it can be seen that the intensity of the O1s peak relative to that of C1s is reduced while the characteristic N1s peak appears after irradiation. These results indicate laser-induced simultaneous reduction and N-based functionalization of the GO sheets. The Na peaks visible in the XPS scans are contributions from the sample mounting procedure and can therefore be ignored.

Analysis of the core level characteristic peaks allowed insight to be gained into the nature of the chemical bonds in each case. Figure 4b presents in high resolution the respective C1s of GO (top) and LGO-EDNB (bottom) produced upon irradiation with 10 pulses of 10 mW power, respectively. In particular, the XPS spectrum of GO showed a second peak at higher binding energies, corresponding to large amounts of sp^3 carbon with C-O bonds, carbonyls (C=O), and carboxylates (O-C=O), resulted from harsh oxidation and destruction of the sp2 atomic structure of graphene.[38] After irradiation, the C-O/C-C intensity ratio decreases from 1.09 to 0.71 indicating reduction of the GO lattice. Photo-excitation is a well-established method for GO reduction, mediated by photogenerated solvated electrons.[39] At the same time the N1s/C1s intensity ratio becomes equal to 0.15.

We investigated the bonding configurations in laser synthesized derivative based on high-resolution N1s XPS spectra; a typical example is presented in Figure 4c. It comprises two peaks, one of higher binding energy, corresponding to N-O bonding[40] and one of lower, corresponding to N-C bonds.[41] In particular, the peak at 399.8 eV is likely to be associated with various reduced forms of nitrogen such as NH_2 (399.4 eV), NHOH (400.3 eV), NH-pyrrolic (400.5 eV) and azoxy (399.98 eV) groups,[42] while that of 405.7 eV corresponds to the NO_2 groups bound to aromatic carbon within the EDNB functionalized unit.[20],[43]

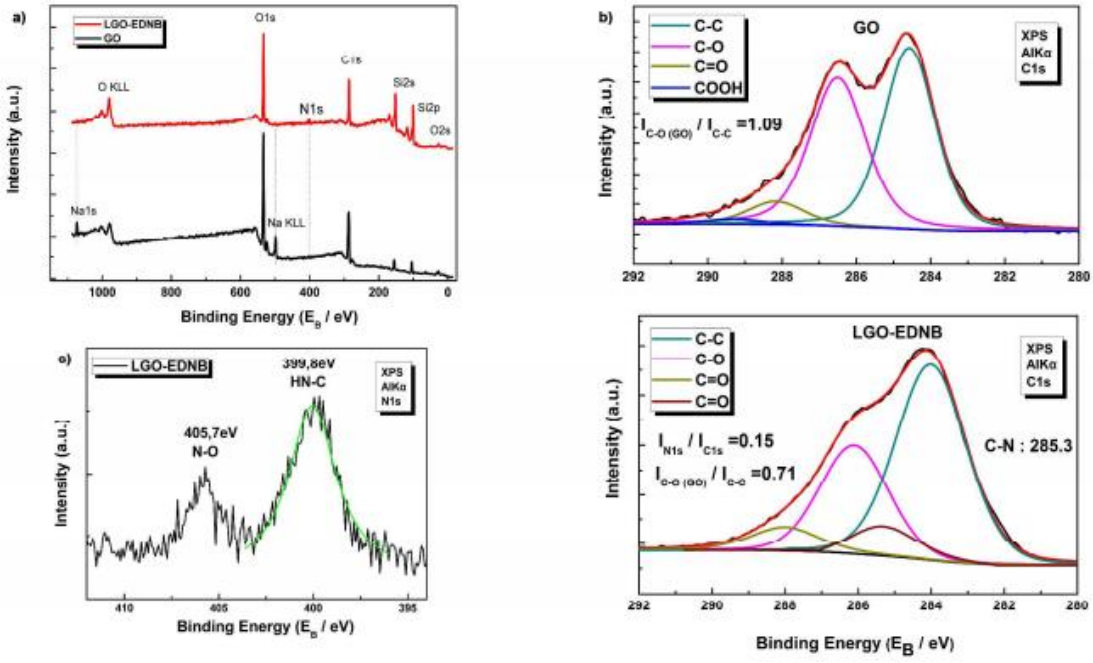

Figure 4. (a) XPS survey spectra of GO and LGO-EDNB; (b) high-resolution XPS C1s spectra of GO (top) and LGO-EDNB (bottom); (c) high-resolution N1s XPS spectra.

The attachment of EDNB moieties to GO was also confirmed by ^{1}H NMR spectroscopy. Figure 5a presents the ^{1}H NMR spectrum of LGO-EDNB displayed upfield signals at 9.06 and 8.92 ppm assigned to the aromatic protons ortho and meta to nitro groups, labeled ‘‘c’’ and ‘‘b’’, respectively. The aliphatic protons ‘‘a’’ gave signals at 4.00 ppm, associated with the alkyl -CH_2-CH_2- linking groups. LGO-EDNB was further checked by Fourier transform infrared (FT-IR) spectroscopy (Figure 5b), showing two new bands at 1543 and 1345 cm^{-1} compared to pristine GO, which are characteristic of the symmetric and asymmetric stretching modes of the NO_2 group.[44] Compared to the FT-IR spectrum of the pristine GO dispersion, it is clear that the -OH characteristic peak at ~3400 cm^{-1} is significantly reduced, denoting that there is a partial reduction of the GO lattice during the irradiation process, in accordance to the XPS results. Figure 6 also depicts the Raman spectra of GO and LGO-EDNB. GO displays characteristic peaks at 1581 and 1346 cm^{-1}, corresponding to G and D bands, respectively. These peaks were shifted to 1572 and 1352 cm^{-1} respectively in the spectrum of LGO-EDNB. Furthermore, the I_D/I_G intensity ratio is increased from 0.84 in pristine GO to 0.94 in LGO-EDNB. Notably, the spectrum of LGO-EDNB appears an additional weak shoulder at 1433 cm^{-1} that can be attributed to the deoxygenation of GO,[45] due to the grafting of the parietal EDNB moieties to the COOH groups of the GO sheets. All these observations confirm the substantial modification of the GO lattice due to the laser-induced functionalization process.

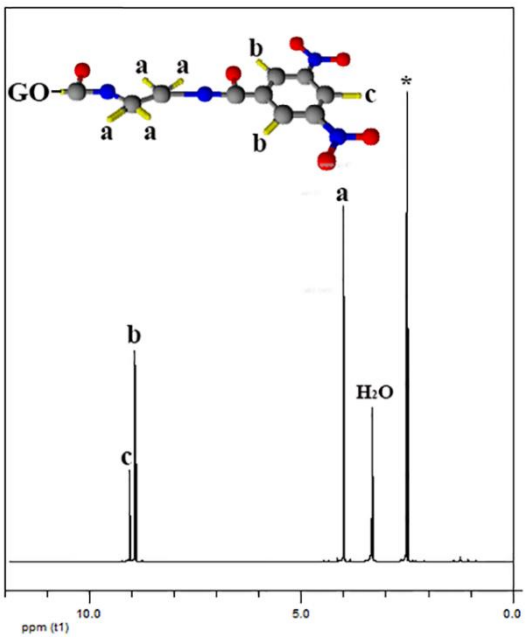

a)

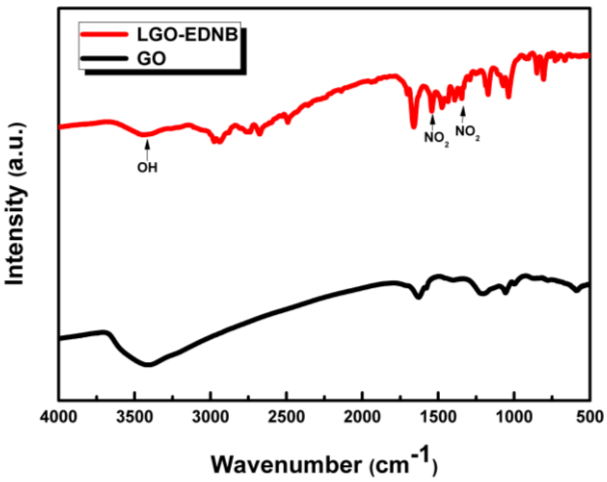

b)

Figure 5. (a) The ^{1}H NMR spectra in DMSO d_6 solution of GO-EDNB. The solvent peak is denoted by an asterisk. The spectrum displays upfield signals at 9.06 and 8.92 ppm assigned to the aromatic protons ortho and meta to nitro groups, labeled ‘‘c’’ and ‘‘b’’, respectively. The aliphatic protons ‘‘a’’ gave signals at 4.00 ppm, associated with the alkyl -CH_2-CH_2- linking groups. (b) Fourier transform infrared (FT-IR) spectra of LGO-EDNB. The spectrum of the functionalized dinitro graphene-based material exhibits two new bands at 1543 and 1345 cm^{-1}, which are characteristic of the symmetric and asymmetric stretching modes of the NO_2 group. The observed lowering of the OH characteristic peak at ~3400 cm^{-1} indicates reduction of the initial GO lattice.

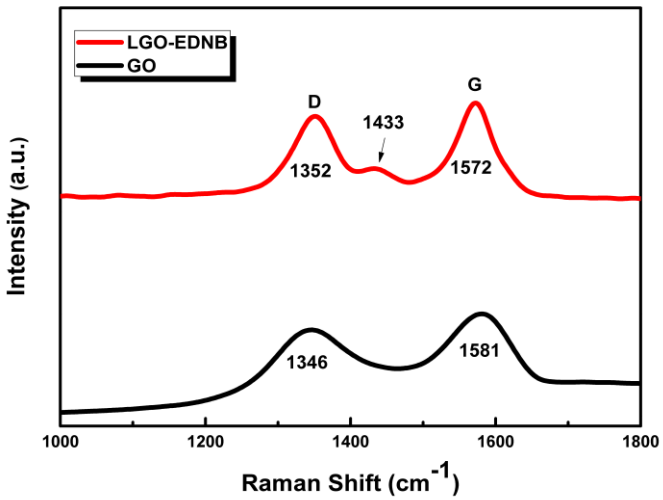

Figure 6. Raman spectra of GO (black) and LGO-EDNB (red).

In our technique, by carefully tuning key laser parameters, the lattice reduction degree and, in series, the functionalization level could be readily controlled. In particular, it is observed that an increase of P in the range from 10 mW to 50 mW or an increase of Np at a certain P, gives rise to a corresponding decrease of the respective N1s peak intensity. Accordingly, as shown in Figure 7a, there is a rapid decrease of the N1s/C1s intensity ratio upon increasing Np at a constant P=10 mW, while at the same

time a sharp increase in the GO reduction ratio is evident. This effect was further studied by UV-vis spectroscopy.

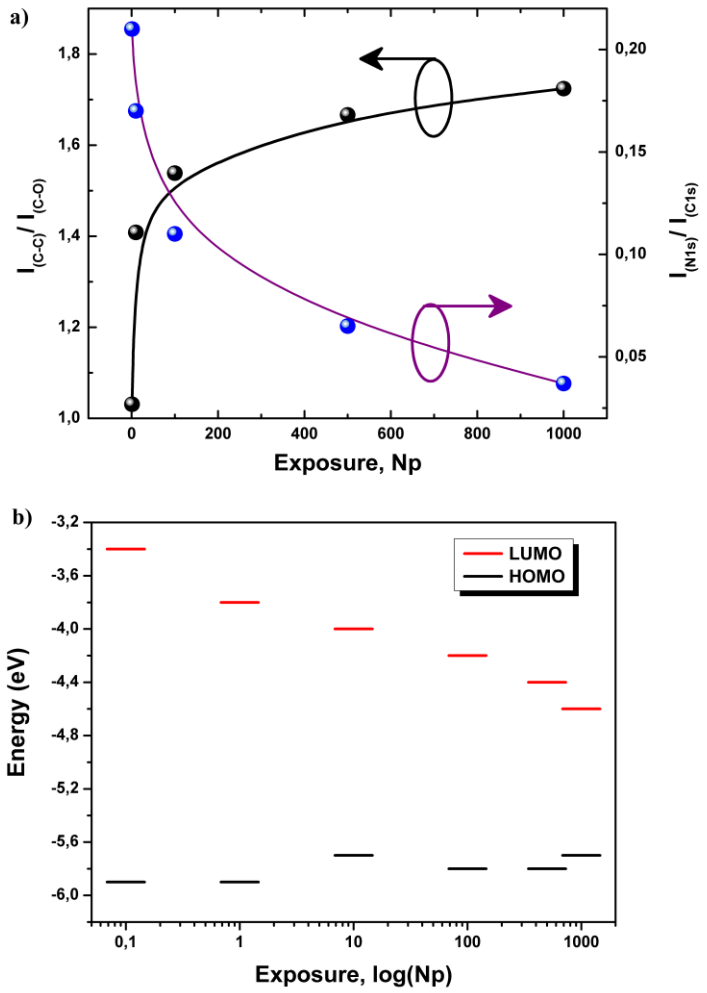

Figure 7. (a) GO reduction and functionalization levels as a function of Np (b) the evolution of the HOMO and LUMO levels as a function of irradiation time. The HOMO-LUMO levels of GO-EDNB are also shown for comparison.

Figure 8 presents the respective absorption spectra showing that, as the exposure time increases, the LGO-EDNB absorption is enhanced in the whole spectral range. At the same time, the absorption band becomes progressively broader, indicating laser mediated bandgap modulation[46] of the LGO-EDNB derivatives. To further explore potential changes in the electronic bandgap, CV measurements were carried out on LGO-EDNB derivatives produced at different exposure times.

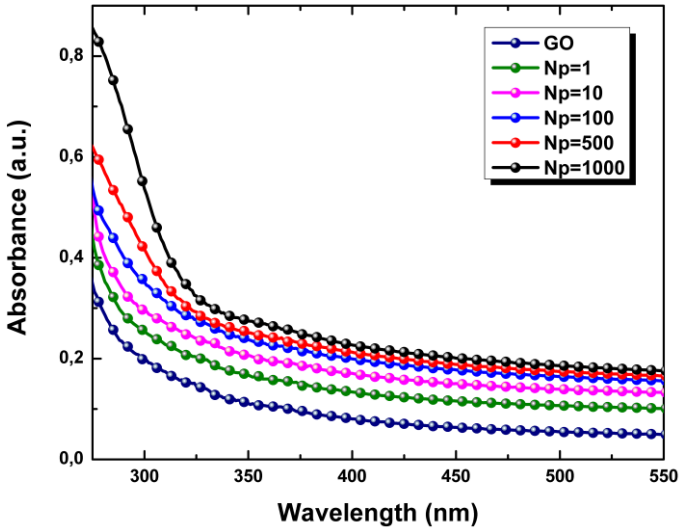

Figure 8. The absorption UV-vis spectra of LGO-EDNB as a function of irradiation time.

The results revealed well-defined oxidation and reduction peaks (Figure 9), the position of which changes with the exposure time. From the onset of oxidation ($E_{[onset, ox\ vs.\ Fc+/Fc]}$) and reduction ($E_{[onset, red\ vs.\ Fc+/Fc]}$) potentials, the highest occupied and lowest unoccupied molecular orbitals (HOMO and LUMO, respectively) can be calculated (see experimental section). The obtained electrochemical data are summarized in Figure 7b that presents the evolution of the HOMO and LUMO levels as a function of irradiation time. It is evident that the HOMO-LUMO level separation, and thus the bandgap, decreases with increased exposure time most likely due to a synergetic effect of the EDNB-functionalization and the partial reduction processes (see also Figure 10). It can be postulated that the large-scale coupling between EDNB and GO sheets facilitates charge transfer interaction, giving rise to the decreased bandgap observed for LGO-EDNB.[47,48] Time-resolved pump-probe experiments are currently in progress to understand the dynamics of this interaction during laser irradiation.

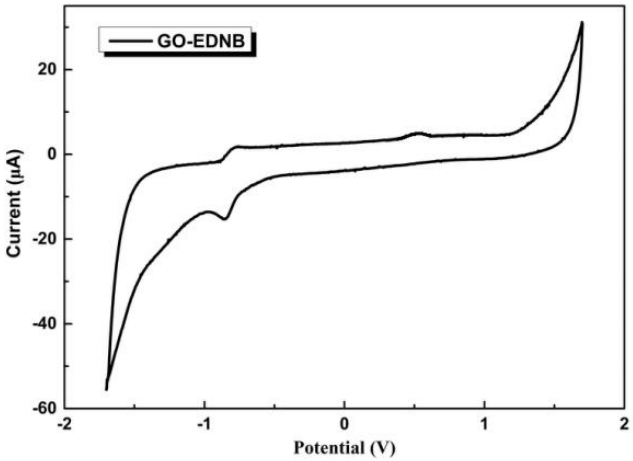

Figure 9. The voltammetric behavior of LGO-EDNB (prepared at 10mw, 100 pulses) in CH_3CN using 0.1 M Tetrabutylammonium hexafluorophosphate ($TBAPF_6$) as the electrolyte, at a scan rate of 10 mV s^{-1}, between the potential sweep window of 1.7 V to −1.7 V. A well-defined reversible reduction peak was observed at −1.0 V (R1) and −0.8 V (R2), while an oxidation peak was appeared at 0.7 V.

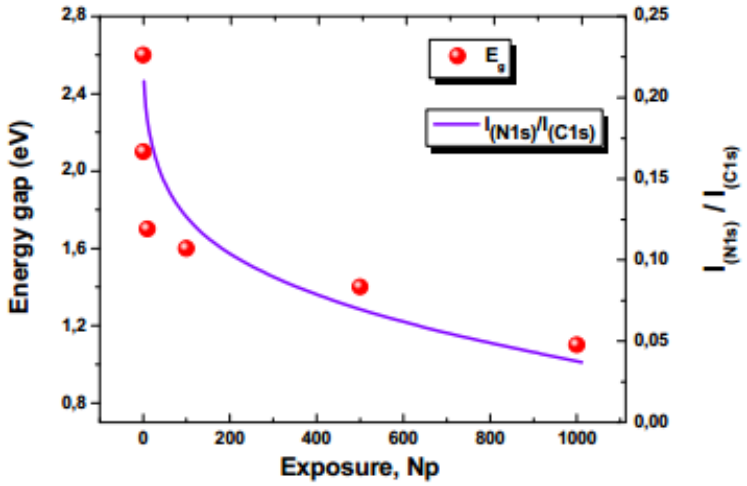

Figure 10. The HOMO-LUMO levels separation of LGO-EDNB as a function of irradiation time. The corresponding evolution of the N_{1s}/C_{1s} intensity ratio is also shown. The bandgap, decreases with increased exposure time most likely due to a synergetic effect of the EDNB-functionalization and the partial reduction processes.

The bandgap tunability of the laser-functionalized graphene derivatives demonstrates potential application of LGO-EDNB in solution processed electronics. In addition to this, the direct linking of the electron-withdrawing nitro group with the GO backbone facilitates enhanced exciton dissociation, due to the presence of the aliphatic linker of ethylenediamine, which demonstrates its potential application as electron acceptor in OSCs. On the other hand, we found that the LGO-EDNB flakes produced are extremely soluble in common organic solvents compared to the starting GO material as well as the chemically synthesized GO-EDNB.[20] Indeed, thermogravimetric

measurements performed on LGO-EDNB and GO-EDNB (Figure 11) indicate the higher degree of functionalization in case of LGO-EDNB; more amide bonds are formed, as well as more chromophores nitro groups are linked at the edges of GO sheets. Owing to the higher degree of functionalization and the presence of excess aliphatic groups (-CH_2-), the dispersibility within the polymer matrix is facilitated and thus the interactions between the polymer and graphene phases are enhanced. All the above properties are desirable towards the structure/property characterization and OSC device fabrication by solution processing.

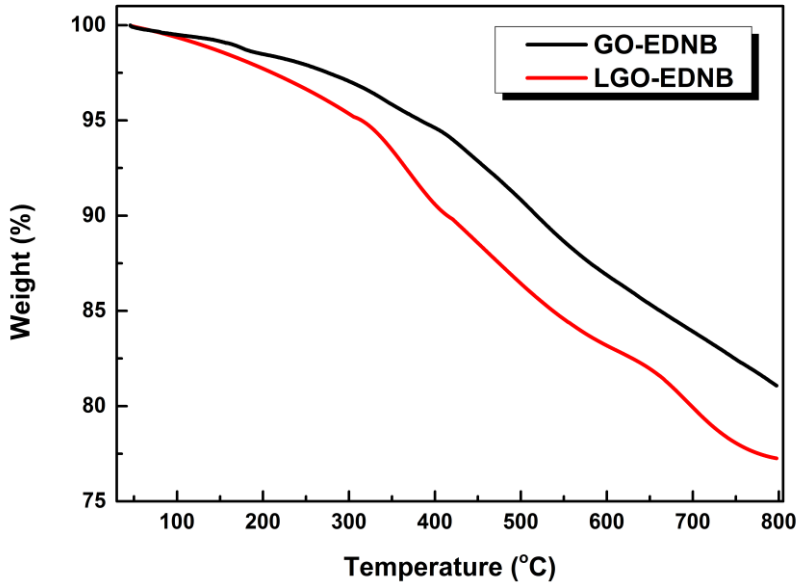

Figure 11. The TGA graphs of LGO-EDNB, prepared using Np=10 pulses, and GO-EDNB obtained under inert atmosphere of N_2, with heating rate 10 °C/min.

More specifically, for the experiments, the samples were loaded into an alumina pan for TGA under constant nitrogen flow. The temperature ceiling was set at 800 ^oC from room temperature, with a slow heating rate (10 ^oC/min) to ensure a regular and integrated decomposition of GO-EDNB and LGO-EDNB. The presence of more aliphatic groups render LGO-EDNB thermally unstable, compared to GO-EDNB and starts to lose mass upon heating even below 100 ^oC and has resulted in a rapid mass loss commencing at about 190 ^oC. Moreover, LGO-EDNB shows 6 % weight loss in a nitrogen atmosphere at ~300 ^oC, due to the lower ‘‘oxygen’’ concentration than GO-EDNB, as resulted from the reduction, during the photochemical process. Finally, a

second significant mass loss at ~410 ºC is observed, since the nitro groups are decomposed,[49] consolidating a total 24 % weight loss at 800 ºC.

In order to investigate the electron accessible nature of LGO-EDNB, BHJ photovoltaic devices were fabricated utilizing the LGO-EDNB as the electron acceptor and the PCDTBT as the electron donor. For this purpose, OSCs with the conventional device structure glass /indium tin oxide ITO/PEDOT:PSS/PCDTBT:LGO-EDNB/Al, where fabricated. The corresponding OSC structure and the energy level diagram of the different materials comprising the devices are shown in Figure 12a and 12b. Before analyzing the photovoltaic characteristics, it is important to describe the functionality of the electron acceptor component of the BHJ during the device operation. The solar light irradiates the photoactive layer through the PEDOT:PSS/ITO electrode side, while the donor molecules absorbs photons to produce excitons. The photo-induced excitons dissociate at the donor-acceptor interface into electrons in the lowest unoccupied molecular orbital (LUMO) of the acceptor, and holes in the highest occupied molecular orbital (HOMO) of the polymer donor. Therefore, the LUMO level of the acceptor should be ideally below that of the donor so that the electrons can be readily transported to the Al electrode. At the same time its HOMO level should be above that of the donor to facilitate holes' transport.

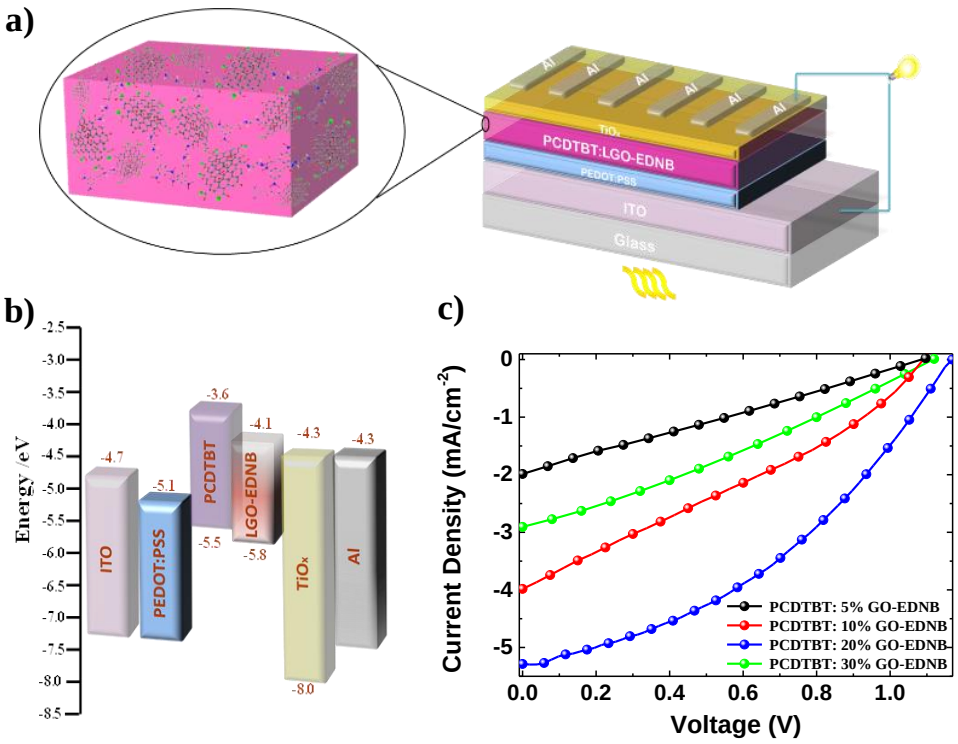

Figure 12. (a) Schematic illustration of BHJ OSC device with LGO-EDNB as the electron acceptor (b) The energy level diagram depicting the relevant energy levels under flat conditions of all materials used in OSCs c) J-V characteristics of OSCs with different LGO-EDNB concentrations.

Initially, a series of devices using LGO-EDNB acceptors obtained at different exposure times and exhibit different HOMO-LUMO levels (Figure 7b), were tested. It is found that the best photovoltaic performance was measured for the OSCs incorporating the LGO-EDNB derivative obtained for Np=10 pulses, regardless the polymer-donor ratio. This can be attributed to the best matching between the energy levels of this derivative and the polymer donor that facilitates efficient exciton dissociation, as indeed can be observed in Figure 12b. Besides this, the lower HOMO level of LGO-EDNB acts as an efficient barrier to hole extraction, through the acceptor material, minimizing charge recombination. It is important to note that devices fabricated with chemically synthesized GO-EDNB[20] as electron accepting materials failed to produced photovoltaic effect, apparently because its LUMO level ($LUMO_{GO\text{-}EDNB}$=3.4 eV), shown in Figure 7b, is lower that of PCDTBT ($LUMO_{PCDTBT}$=3.6 eV).

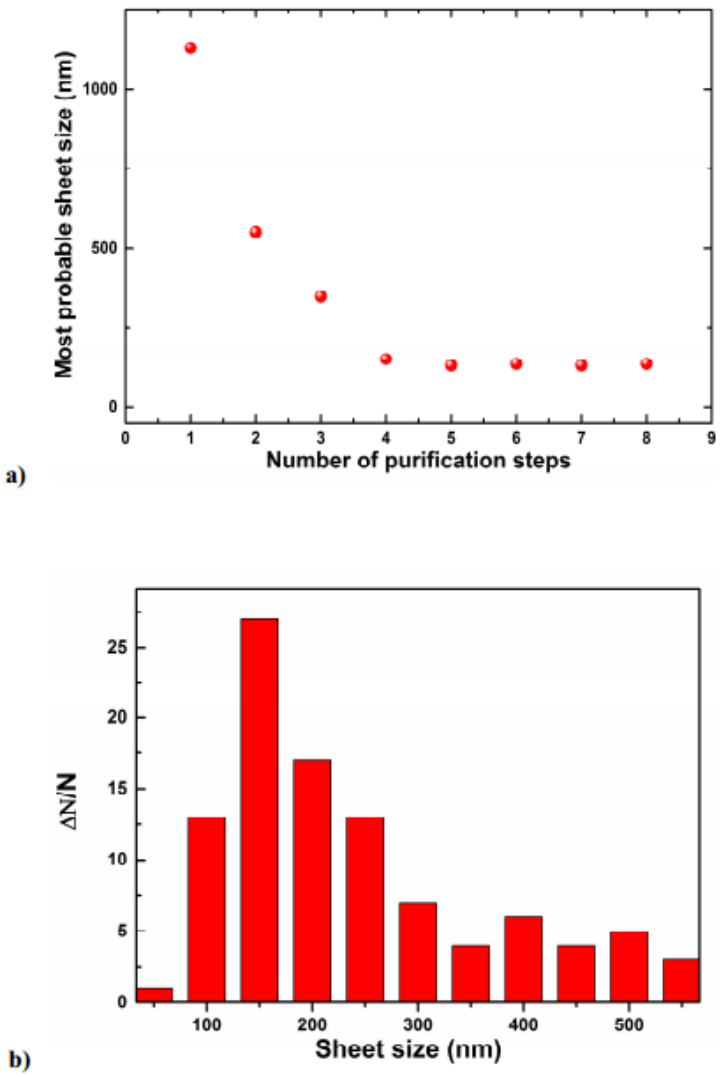

Figure 13. (a) Dependence of the most probable sheet size on the number of purification steps; (b) LGO-EDNB sheet size distribution following a series of five purification steps. Sheet sizes were determined using a number of TEM a representative of which is shown in Figure 14.

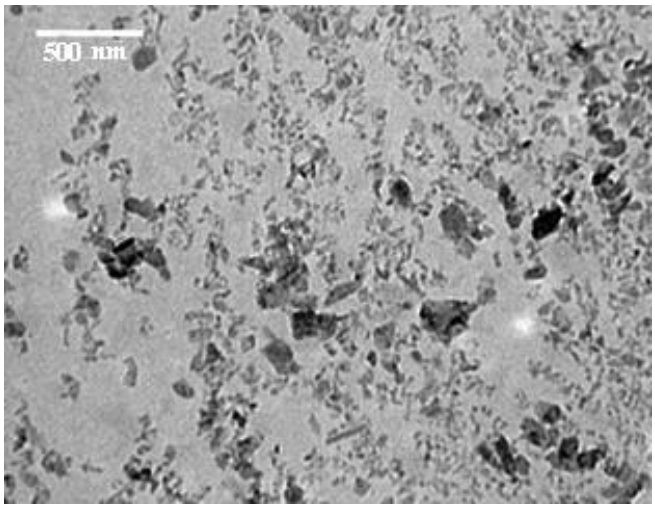

Figure 14. Representative TEM image of LGO-EDNB flakes.

In a next step, OSCs fabricated using different blend ratios of the best performed PCDTBT:LGO-EDNB BHJ were compared. As it can be seen in the respective *J–V* curves of Figure 12c and the summarized photovoltaic parameters in Table 5.1, device performance strongly depends on the donor-acceptor ratio. Indeed, the maximum efficiency is attained using the composite BHJ blend containing 20% of LGO-EDNB. For concentrations higher than 20% w.t., the photocurrent is believed to be limited due to increased aggregation of graphene sheets leading to a lower photogeneration rate. The measured of V_{oc} of 1.17 V for PCDTBT:LGO-EDNB OSC showed the best efficiency, can be explained as the difference between the LGO-EDNB LUMO (-4.1 eV) and the PCDTBT HOMO (-5.8 eV) energy levels.[50] The above results show the importance of the tunability of the LGO-EDNB acceptor HOMO-LUMO levels, suggesting the applicability of our technique to practically any polymer donor system.

Device Structure	J_{sc}(mA/cm^2)	V_{oc}(V)	FF(%)	PCE(%)
ITO/PEDOT:PSS/PCDTBT:LGO EDNB(5%)/TiO_x/Al	1.99±0.22	1.10±0.05	25.5±0.4	0.55±0.11 (0.66)
ITO/PEDOT:PSS/PCDTBT:LGO-EDNB(10%)/TiO_x /Al	3.98±0.20	1.09±0.06	31.1±0.3	1.34±0.17 (1.51)
ITO/PEDOT:PSS/PCDTBT:LGO-EDNB(20%)/TiO_x /Al	5.29±0.25	1.17±0.06	39.2±0.5	2.42±0.29 (2.71)
ITO/PEDOT:PSS/PCDTBT:LGO-EDNB(30%)/TiO_x /Al	2.91±0.19	1.12±0.03	29.0±0.3	0.95±0.09 (1.04)

Table 5.1. Average photovoltaic characteristics and standard deviations for OPV devices based on PCDTBT:LGO-EDNB composites with different LGO-EDNB content (5, 10, 20 and 30 wt%). The numbers in parentheses represent the values obtained for the champion OPV cells. To account for experimental errors, the reported averages and deviations for each device are taken for 10 identical devices, consisting of 6 cells each.

The best performed PCDTBT:LGO-EDNB based device showed a J_{sc} of 5.29 mA/cm^2 and PCE 2.41 %, which is the highest than the previously reported which incorporated covalently-modified graphene[51],[52],[53] and 71% higher than the state of

the art graphene-based electron acceptor materials.[21] Such efficiency enhancement can be attributed to the formation of internal polymer/graphene junctions giving rise to higher exciton dissociation and balanced charge transport throughout the entire volume of the PCDTBT:LGO-EDNB composite. The photovoltaic properties of our LGO-EDNB-based devices are rather satisfactory considering that these OSCs use a new type of electron-acceptor material, different from the most-studied fullerene system. Indeed, the performance of those devices was reached without any attempt to optimize the morphology of the active blend which is the significant extrinsic factor that impacts all the device characteristics. Further studies focusing on the graphene sheet size and blend structure effects on the OSC characteristics are required for further optimization.

3. CONCLUSIONS

In brief, we have demonstrated the successful synthesis of a novel graphene-based derivative, through laser-induced covalent grafting of GO nanosheets with EDNB molecules. The LGO-EDNB derivative attained exhibited improved processability, physicochemical and electronic properties compared to the pristine GO nanosheets. More importantly, it is shown that our technique enables bandgap tunability of LGO-EDNB, a property that paves the way for its application as efficient electron acceptor in OSCs, opening new avenues for the realization of all graphene based OSCs. The photochemical synthesis presented here is fast, facile, is performed at room temperature and can provide adequate control over the functional unit levels, which is not readily realized by existing methods. The combination of different irradiation parameters and precursor materials with various attaching molecules could yield a virtually unlimited number of graphene nanoconjugates, in terms of composition, electronic structure and electrochemical properties, making this method very appropriate for the production of extraordinary types of nanomaterials that cannot be attained via traditional chemical routes. These conjugates can be obtained directly in solution, without the use of supplementary chemical reagents and thus they can be used for applications without further purification.

4. EXPERIMENTAL SECTION

Synthesis of Graphite oxide (GO)

Graphite oxide was prepared from purified natural graphite powder (Alfa Aesar, ~200 mesh), by a modified Hummers method.[54] Briefly, graphite powder (0.5 g) was placed into a cold mixture of concentrated H_2SO_4 (40 mL, 98 %) and $NaNO_3$ (0.375 g) under vigorous stirring for 1h, in an ice bath. $KMnO_4$ (3.0 g) was slowly added into the reaction mixture over 1h. The mixture was then stirred at room temperature for 4h. Afterwards, the reaction mixture was allowed to reach room temperature before being heated to 35 ^oC for 30 min, forming a thick paste. It was then poured into a beaker containing 50 mL of deionized water and further heated to 90 ^oC for 30 min. 200 mL of distilled water was added, followed by a slow addition of H_2O_2 (3 mL, 30%), turning the color of the solution from dark brown to yellow. The reaction mixture was then allowed to settle down and decanted. The graphite oxide obtained was then purified by repeated high-speed centrifugation (4200 rpm, 3 min) and redispersing in deionized water to neutralize the pH (~10 times needed). Finally, the resulting GO was dried at 60 °C in a vacuum oven for 48h.

Preparation of the GO dispersions

GO was exfoliated to give a brown dispersion of GO under ultrasonication.[37],[55],[56] The resulting GO was negatively charged over a wide pH condition, as the GO sheet had chemical functional groups of carboxylic acids.

Experimental setup

Figure 2 presents a schematic of the experimental setup used. Before each irradiation stage precursor molecules were dissolved into the pristine GO dispersions. The resulting solution was subsequently placed into a quartz cell and then it was subjected to irradiation by a KrF excimer laser source emitting 20 ns pulses of 248 nm at 1 Hz repetition rate. For uniform exposure of the whole irradiated volume, a top-hat beam profile was obtained using a beam homogenizer. Different combinations of laser powers (P) and the number of pulses (Np) were tested in an effort to optimize the photochemical functionalization processes. In a typical experiment, the sample was irradiated at a constant P with Np =1, 10, 100, 500 and 1000, corresponding to different photochemical reaction times.

Photoacylation of GO (GO-Cl)

The acylation process took part into the quartz tube, exposed to laser beam, while the dispersion was under magnetic stirring. Specifically, GO sheets (6 mg), were dispersed in $SOCl_2$ (4 mL), through ultrasonication for 10 min and adding a small catalytic amount of N,N-dimethylformamide (DMF 0.2 mL). After 30 min of irradiation the dispersion was isolated by centrifugation and the black precipitate was washed with THF, in order to take off the excess of $SOCl_2$. The yielded GO-COCl was dried for 3h at 80 ^oC.

Photochemical synthesis of LGO-EDNB

The final step of the reaction, took also part into the quartz tube. In particular, GO-COCl was dispersed in THF (~2 mL) via ultrasonication for 10 min. Then, EDNB (6 mg) is added, as well as a few drops of triethylamine (Et_3N) (0.3 mL). After the addition of Et_3N the dispersion gets a pink hue. Following irradiation by pulsed laser for 30 min the dispersion darkens. The final LGO-EDNB is yielded by centrifugation (5 min at 4200 rpm), washed with MeOH and dried in a vacuum oven at 40 ^oC for 6h. The total time for the photochemical synthesis of LGO-EDNB is ~2 h, while for that obtained via chemical synthesis is 4 days.[20]

^1H NMR (500 MHz, DMSO-d_6, ppm): 9.06 (s, 1H, Ar H); 8.92 (s, 2H, Ar 2H); 4.00 (s, 4H, CH_2); IR (KBr): ν = 3400, 1543, 1345 cm^{-1};

Characterization of GO derivatives

Fourier transform infrared (FT-IR) spectra were recorded on a BRUKER FTIR spectrometer IFS 66v/F (MIR). Raman spectroscopy was performed using a Nicolet Almega XR Raman spectrometer (Thermo Scientific) with a 473 nm blue laser as an excitation source. X-ray photoelectron spectroscopy (XPS) measurements were carried out in a Specs LHS-10 UltrahighVacuum (UHV) system. The XPS spectra were recorded at room temperature using unmonochromatized Al Ka radiation under conditions optimized for the maximum signal (constant DE mode with a pass energy of 36 eV giving a full width at half maximum (FWHM) of 0.9 eV for the Au 4f7/2 peak). The analyzed area was an ellipsoid with dimensions 2.5 x 4.5 mm^2. The XPS core level spectra were analyzed using a fitting routine, which allows the decomposition of each spectrum into individual mixed Gaussian–Lorentzian components after a Shirley

background subtraction. NMR spectrum was carried out using a Bruker AMX-500 spectrometer. Electrochemical experiments were carried out by using a model PGSTAT302N (Autolab). The experiments were performed with a conventional three electrode electrochemical cell. The three electrode system consisted of Ag/AgCl (SCE) as the reference electrode, Pt-disc as the working electrode and Pt-wire as the counter electrode. The chemical reagents used for those experiments were, Ferrocene (Aldrich, 98%), Tetrabutylammonium hexafluorophosphate >99.0% (TBAPF6, Fluka, electrochemical analysis >99%) and acetonitrile (Acros Organics, extra dried and distilled >99.9%). The HOMO and LUMO levels were measured by the voltammographs from the onset potential of the reduction and oxidation process.[57] Therefore, we have endorsed the formula $E_{HOMO} = -(E_{[onset,\ ox\ vs.\ Fc+/Fc]} + 5.1)$ (eV) and $E_{LUMO} = -(E_{[onset,\ red\ vs.\ Fc+/Fc]} + 5.1)$ (eV).

A series of purification steps were subsequently performed, each of which comprised ultrasonication (10 min) and centrifugation (5 min at 4200 r.p.m) to yield the final LGO-EDNB solution used for the fabrication of OSCs. The purification process is important since it affects and determines the size and thickness range of the functionalized sheets (Figures 12a and b), which may be critical for the photovoltaic performance. For this purpose, following each step, the size evolution of the resulting LGO-EDNB flakes had been monitored using Transmission Electron (TEM) Microscopy (Figure 13). Figure 12a shows that the average sheet sizes were reduced upon increasing the number of purification steps. The photovoltaic performance results presented in the following correspond to the use of the LGO-EDNB solution obtained after 5 purification steps (Figure 12b). Further experiments are in progress to identify the optimum size that gives the best photovoltaic performance. After the purification process, the LGO-EDNB washed with MeOH and drying in a vacuum oven at 40 ˚C for 6h.

Preparation of Titanium suboxide (TiO_x) solution[58]

TiO_x solution preparation: Titanium(IV) isopropoxide ($Ti[OCH(CH_3)_2]_4$, 5 mL), 2-methoxyethanol ($CH_3OCH_2CH_2OH$, 20 mL) and ethanolamine ($H_2NCH_2CH_2OH$, 2 mL) were added to a three-necked flask in a nitrogen atmosphere. The solution was then stirred for 1h at room temperature, followed by heating at 80 ºC for 1h and 120 ºC

for another 1h. The solution was then cooled to room temperature and 10 mL of isopropanol (IPA) was added.

Device fabrication and measurements

PCDTBT polymer was purchased from Solaris Chem. Electron donor PCDTBT was dissolved in 1,2-dichlorobenzene:chlorobenzene (3:1) (*o*-DCB:CB) and stirred overnight at 80 ^{o}C to ensure the good dissolution of the polymer. Then, graphene based electron acceptor LGO-EDNB, after vacuum dried overnight, was mixed with PCDTBT with different blend ratios (respect to the polymer) and stirred for at least 2h at 80 ^{o}C before used. The photovoltaic devices reported were fabricated on 20 mm by 15 mm indium–tin-oxide (ITO) glass substrates with a sheet resistance of ~10 Ω sq^{-1}. Patterned ITO-coated glass substrates were cleaned through a 3-step ultrasonication process (deionized water with 10% soap, acetone, IPA). As a hole transport layer, poly(ethylene-dioxythiophene) highly doped with poly(4-styrenesulfonate) (PEDOT:PSS), purchased from Heraeus, was spin-cast from an aqueous solution on the ITO substrate at 6000 rpm for 60 s with an average thickness of 30 nm and then annealed at 120 °C for 15 min. Photoactive layers with different blend ratios were subsequently deposited in ambient conditions by spin coating PCDTBT:LGO-EDNB solution at 1000 rpm on top of PEDOT:PSS layer until the thickness reaches approximately 80 nm, followed by drying at 60 ^{o}C for about 5 min under inert condition, to avoid the intermixing with the next deposited layer. Then, the electron extraction layers were coated by spin casting the solutions on top of the active layer. TiO_x interlayer was dissolved in methanol (1:200) and then spin-coated to a thickness of approximately 10 nm (6000 rpm, 40 s) in air.[59] The samples were heated at 80 ^{o}C for 1 min in air. Lastly, 100 nm of Al was deposited through a shadow mask by thermal evaporation on the devices. The area of each device was 4 mm^2, as determined by the overlap of the ITO and the evaporated Al.

The performances of the devices were measured at room temperature with an Air Mass 1.5 Global (A.M. 1.5 G) solar simulator at an intensity of 100 mW cm^{-2} (1 sun irradiation). A reference monocrystalline silicon solar cell from Newport Corp. was used to calibrate the light intensity. All measurements were carried out in air immediately after device fabrication without encapsulation process.

References

[1] A. Hirsch, J. M. Englert, F. Hauke, *Acc. Chem. Res.* **2013**, *46*, 87.

[2] W. Wei, X. Qu, *Small* **2012**, *8*, 2138.

[3] V. Georgakilas, M. Otyepka, A. B. Bourlinos, V. Chandra, N. Kim, K. C. Kemp, P. Hobza, R. Zboril, K. S. Kim, *Chem. Rev.* **2012**, *112*, 6156.

[4] P. V. Kumar, N. M. Bardhan, S. Tongay, J. Wu, A. M. Belcher, J. C. Grossman, *Nat. Chem.* **2014**, *6*, 151.

[5] J. Englert, A. Hirsch, Z. Feng, K. Mullen, *Angew. Chem. Int. Ed.* **2011**, *50*, A17.

[6] Z. Yin, J. Zhu, Q. He, X. Cao, C. Tan, H. Chen, Q. Yan, H. Zhang, *Adv. Energy Mater.* **2014**, *4*, 1300574.

[7] L. Liao, Z. Song, Y. Zhou, H. Wang, Q. Xie, *Small* **2013**, *9*, 1348.

[8] P. Wick, A. E. Louw-Gaume, M. Kucki, H. F. Krug, K. Kostarelos, B. Fadeel, K. A. Dawson, A. Salvati, E. Vazquez, L. Ballerini, M. Tretiach, F. Benfenati, E. Flahaut, L. Gauthier, M. Prato, A. Bianco, *Angew. Chem. Int. Ed.* **2014**, *53*, 7714.

[9] D. R. Dreyer, S. Park, C. W. Bielawski, R. S. Ruoff, *Chem. Soc. Rev.* **2010**, *39*, 228.

[10] S. Pan, Y. Hernandez, X. Feng, K. Mullen, *Adv. Mater.* **2011**, *23*, 2729.

[11] K. P. Loh, Q. Bao, G. Eda, M. Chhowalla, *Nat. Chem.* **2010**, *2*, 1015.

[12] D. Chen, H. Feng, J. Li, *Chem. Rev.* **2012**, *112*, 6027.

[13] G. Eda, M. Chhowalla, *Adv. Mater.* **2010**, *22*, 2392.

[14] S. Park, R. S. Ruoff, *Nat. Nanotechnol.* **2009**, *4*, 217.

[15] D. Li, R. B. Kaner, *Science* **2008**, *320*, 1170.

[16] Z. Pan, H. Gu, M.-T. Wu, Y. Li, Y. Chen, *Opt. Mater. Express* **2012**, *2*, 814.

[17] V. Yong, J. M. Tour, *Small* **2010**, *6*, 313.

[18] M. M. Stylianakis, J. A. Mikroyannidis, E. Kymakis, *Sol. Energy Mater. Sol. Cells* **2010**, *94*, 267.

[19] E. Kymakis, G. A. J. Amaratunga, *Applied Phys. Lett.* **2002**, *80*, 112.

[20] M. M. Stylianakis, G. D. Spyropoulos, E. Stratakis, E. Kymakis, *Carbon*, **2012**, *50*, 5554.

[21] Z. Liu, Q. Liu, Y. Huang, Y. Ma, S. Yin, X. Zhang, W. Sun, Y. Chen, *Adv. Mater.* **2008**, *20*, 3924.

[22] M. M. Stylianakis, E. Stratakis, E. Koudoumas, E. Kymakis, S. H. Anastasiadis, *ACS Applied Mater. Interfaces* **2012**, *4*, 4864.

[23] J. You, L. Dou, K. Yoshimura, T. Kato, K. Ohya, T. Moriarty, K. Emery, C.-C. Chen, J. Gao, G. Li, Y. Yang, *Nat. Commun.* **2013**, *4*, 1446.

[24] Z. He, C. Zhong, S. Su, M. Xu, H. Wu, Y. Cao, *Nat. Photon.* **2012**, 6, 591.

[25] S. Villar-Rodil, J. I. Paredes, A. Martinez-Alonso, J. M. D. Tascon, *J. Mater. Chem.* **2009**, *19*, 3591.

[26] D. Konios, M. M. Stylianakis, E. Stratakis, E. Kymakis, *J. Col. Interf. Sci.* **2014**, *430*, 108.

[27] C. Yang, J.-Y. Kim, S. Cho, J.-K. Lee, A. J. Heeger, F. Wudl, *J. Am. Chem. Soc*. **2008**, *130*, 6444.

[28] C.-Z. Li, H.-L. Yipa, A. K.-Y. Jen, *J. Mater. Chem.* **2012**, *22*, 4161.

[29] H. Lv, X. Zhao, Z. Li, D. Yang, Z. Wang, X. Yang, *Polym. Chem.*, DOI: 10.1039/c4py00758a.

[30] C. Soci, I.-W. Hwang, D. Moses, Z. Zhu, D. Waller, R. Gaudiana, C. J. Brabec, A. J. Heeger, *Adv. Funct. Mater.* **2007**, *17*, 632.

[31] J. Hou, H.-Y. Chen, S. Zhang, G. Li, Y. Yang, *J. Am. Chem. Soc.* **2008**, *130*, 16144.

[32] S. H. Park, A. Roy, S. Beaupre, S. Cho, N. Coates, J. S. Moon, D. Moses, M. Leclerc, K. Lee, A. J. Heeger, *Nat. Photon.* **2009**, *3*, 297.

[33] A. Kasry, A. A. Ardakani, G. S. Tulevski, B. Menges, M. Copel, L. Vyklicky, *J. Phys. Chem. C*, **2012**, *116*, 2858.

[34] C. N. R. Rao, R. Voggu, *Mater. Today*, **2010**, *13*, 34.

[35] Y.-L. Zhang, L. Guo, H. Xia, Q.-D. Chen, J. Feng, H.-B. Sun *Adv. Opt. Mater.* **2014**, *2*, 120.

[36] E. Kymakis, K. Savva, M.M Stylianakis, C. Fotakis, E. Stratakis, *Adv. Fumc. Mater.* **2013**, *23*, 2742.

[37] J. K. Wassei, K. C. Cha, V. C. Tung, Y. Yang, R. B. Kaner, *J. Mater. Chem.* **2011**, *21*, 3391.

[38] S. Stankovich, D. A. Dikin, R. D. Piner, K. A. Kohlhaas, A. Kleinhammes, Y. Jia, Y. Wu, S. T. Nguyen, Ruoff, R. S. *Carbon* **2007**, *45*, 1558.

[39] R. Y. N. Gengler, D. S. Badali, D. Zhang, K. Dimos, K. Spyrou, D. Gournis, R. J. D. Miller, *Nat. Comm.* **2013**, *4*, 2560.

[40] B. J. Lindberg, J. Hedman, *Chem. Scr.* **1975**, *7*, 155.

[41] N. A. Kumar, H. Nolan, N. McEvoy, E. Reznavi, R. Doyle, M. Lyons, G. Duesberg, *J. Mater. Chem.* **2013**, *1*, 4431.

[42] J. F. Moulder, W. F. Stickle, P. E. Sobol, K. D. Bomben, *Handbook of X-Ray Photoelectron Spectroscopy* ed. J. Chastain (Eden Prairie, MN: Perkin-Elmer Corporation) **1992**.

[43] A. K. Chakraborty, *Nanotech.* **2009**, *20*, 155704.

[44] E. Bekyarova, E. M. Itkis, P. Ramesh, C. Berger, M. Sprinkle, A. W. de Heer, C. R. Haddon, *J. Am. Chem. Soc.* **2009**, *131*, 1336.

[45] Y. Xu, H. Bai, G. Lu, C. Li, G. Shi, *J. Am. Chem. Soc.* **2008**, *130*, 5856.

[46] L. Guo, R.-Q. Shao, Y.-L. Zhang, H.-B. Jiang, X.-B. Li, S.-Y. Xie, B.-B. Xu, Q.-D. Chen, J.-F. Song, H.-B. Sun, *J. Phys. Chem. C* **2012**, *116*, 3594.

[47] V. Bavastrello, S. Carrara, M. K. Ram, C. Nicolini, *Langmuir* **2004**, *20*, 969.

[48] Z. Luo, N. J. Pinto, Y. Davila, A. T. Charlie Johnson, *Applied Phys. Lett.* **2012**, *100*, 253108.

[49] J. A. Mikroyannidis, M. M. Stylianakis, P. Suresh, P. Balraju, G. D. Sharma, *Org. Electron.* **2009**, *10*, 1320.

[50] M. C. Scharber, D. Mühlbacher, M. Koppe, P. Denk, C. Waldauf, A. J. Heeger, C. J. Brabec, *Adv. Mater.* **2006**, *18*, 789.

[51] Z. Yin, S. Sun, T. Salim, S. Wu, X. Huang, Q. He, Y. M. Lam, H. Zhang, *ACS Nano* **2010**, *4*, 5263.

[52] Z. Yin, S. Wu, X. Zhou, X. Huang, Q. Zhang, F. Boey, H. Zhang, *Small* **2010**, *6*, 307.

[53] T. Mahmoudi, W.-Y. Rho, H.-Y. Yang, S. R. P. Silva, Y.-B. Hahn, *Chem. Comm.* **2014**, *50*, 8705.

[54] Q. Su, S. Pang, V. Alijani, C. Li, X. Feng, K. Mullen, *Adv. Mater.* **2009**, *21*, 3191.

[55] A. Ciesielski, P. Samorì, *Chem. Soc. Rev.* **2014**, *43*, 381.

[56] Z. Y. Xia, S. Pezzini, E. Treossi, G. Giambastiani, F. Corticelli, V. Morandi, A. Zanelli, V. Bellani, V. Palermo, *Adv. Funct. Mater.* **2013**, *23*, 4684.

[57] C. M. Cardona, W. Li, A. E. Kaifer, D. Stockdale, G. C. Bazan, *Adv. Mater.* **2011**, *23*, 2367.

[58] Z. He, C. Zhong, X. Huang, W.-Y. Wong, H. Wu, L. Chen, S. Su, Y. Cao, *Adv. Mater.* **2011**, *23*, 4636.

[59] D. H. Wang, S. H. Im, H. K. Lee, J. H. Park, O. O. Park, *J. Phys. Chem. C* **2009**, *113*, 17286.

Chapter 6

Graphene Oxide Porphyrin-based Molecule for Efficient Ternary Blend Organic Solar Cells

Abstract: A graphene oxide porphyrin-based molecule (GO-TPP) was synthesized by covalent linkage of graphene oxide (GO) with 5-(4-aminophenyl)-10,15,20-triphenyl) porphyrin (TPP-NH_2). The yielded graphene-based nanohybrid material is a D-A molecule, exhibiting strong intermolecular interaction between the graphene oxide core (A) and the covalently anchored porphyrin (D), which attributes to the high solubility in common organic solvents. Eventually, ternary blend organic solar cells of the structure glass/ITO/PEDOT:PSS/PCDTBT:PC_{71}BM:GO-TPP/TiO_x/Al have been fabricated, by incorporating GO-TPP in the photoactive layer, which acts as electron-cascade donor material. The addition of GO-TPP into the active layer, forms percolation paths exclusively to electrons through the energy level offset of PCDTBT:PC_{71}BM, improving the photovoltaic performance of the device. More particularly, the short circuit current density (J_{sc}) of the device is raised up to ~33%, leading to the enhancement of the power conversion efficiency (PCE) from 5.40 % to ~6%. The aforementioned increase in PCE certifies (a) the higher exciton generation and (b) the more effective charge separation and transport. Finally, GO-TPP has been characterized by spectroscopic, thermal techniques and electrical measurements.

1. Introduction

Organic solar cells (OSCs) are of tremendous interest as a lightweight and flexible power source, which can be easily integrated in wearable electronics and smart textiles.[1] Bulk heterojunction (BJH).[2] OSCs based on blends of conjugated polymers as the electron donor (D) and fullerenes as the electron acceptor (A) material have dominated the last two decade research efforts, achieving around 9% and 10% power conversion efficiency (PCE) using a single[3,4,5] and a tandem[6] BHJ structure respectively.

This success was mainly due to the utilization of low band gap polymers with deep highest occupied molecular orbital (HOMO) levels[7] as the D material for higher light harvesting and the optimization of the two buffer layers for effective charge collection.[8] Nevertheless, the combination of the polymer short exciton diffusion length (10 nm) with the low charge carrier mobility in the fullerene and polymer phase separated layers within the photoactive layer enhance recombination and trapping of the separated electron and holes before arriving at the respective electrodes.[9,10] In this context, a straightforward approach to reduce the recombination in the photoactive layer is by decreasing the charge transfer energy offsets between the D and the A. This can be accomplished by the addition of a third component in the binary blend, which can act as a bridge between the D and A material, structuring a ternary cascade OSC.[9] In particular, its energy levels must exhibit a proper offset with respect to the polymer and the fullerene, while at the same time it should act as an electron acceptor and transporter when a heterojunction is formed with the D and as an electron donor and hole transporter when it forms a junction with the fullerene.

Graphene flakes were recently identified as a promising additive for assisting the charge transport in the photoactive layer of OSCs[11,12] due to its excellent charger carrier mobility, thermal and chemical stability, and low cost and the facile processing.[13,14,15] Whereas, solution processable graphene oxide (GO) sheets can be prepared by oxidizing graphite.[16] The presence of oxygen functional groups within the graphene structure, such as hydroxyl (-OH), aldehyde (-CHO), carboxyl (-COOH) or epoxyl ones, reduces the interplane forces and imparts hydrophilic character. Thus, GO is highly soluble in water in polar organic solvents, forming stable dispersions.[17,18] Moreover, the functional groups can act as a handle for the chemical functionalization of graphene oxide using known carbon surface chemistry.[19,20]

Porphyrins exhibit a planar and π-aromatic framework, exhibiting high photostability, large extinction coefficients, as well as high susceptibility in electron transfer reactions.[21] Similarly, porphyrins have been utilized as the ternary component of D-A active layer, leading to improvements in light-harvesting efficiency at longer wavelengths, extending into the NIR region.[22] Therefore, the fine control of the GO functionalization with the porphyrin can be advantageous in providing a hybrid with HOMO and LUMO levels between the respective polymer and fullerene ones.

In the present study, GO flakes covalently functionalized with a TPP-NH2 porphyrin, forming GO-TTP hybrids were incorporated in BHJ poly [N-9'-hepta-decanyl-2,7-carbazole-alt- 5,5-(40,70-di-2-thienyl-20,10,30-benzothiadiazole)] (PCDTBT)- [6,6]-phenyl C71-butyric acid methyl ester (PC71BM) OSCs as the cascade material. The fine tuning of its energy levels was achieved by adjusting the reaction time of GO-TPP synthesis, which affected the functionalization degree of the resulting GO-COCl.

A PCE enhancement of ~10% was achieved compared to the binary OSC, mainly due to an increase in the hole mobility, which balances the hole to electron mobility ratio and therefore increases the photocurrent.

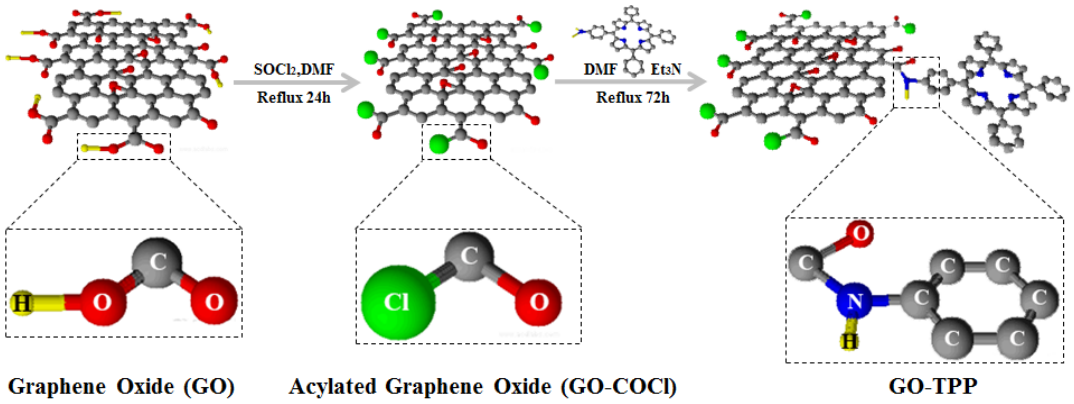

Figure 1. Schematic representation of the chemical synthesis

2. Experimental Section

Instruments and Measurements

Mid-infrared spectra in the region 500-4000 cm^{-1} were obtained on a Fourier transform infrared (FT-IR) spectrometer (Equinox 55 from Bruker Optics) equipped with a single reflection diamond attenuated-total-reflectance (ATR) accessory (DuraSamp1IR II by

Sens IR Technologies). Thermogravimetric analysis (TGA) was performed on 5 mg samples over the temperature range from 40 °C to 800 °C at a heating rate of 10 °C/min utilizing a Perkin Elmer Diamond Pyris model under nitrogen atmosphere. UV-vis absorption spectra were recorded using a Shimadzu UV-2401 PC spectrophotometer over the wavelength range of 270-800 nm. The emission spectra were measured on a JASCO FP-6500 fluorescence spectrophotometer equipped with a red-sensitive WRE-343 photomultiplier tube (wavelength range 200-850 nm). The samples were characterized by Raman spectroscopy at room temperature utilizing a Nicolet Almega XR Raman spectrometer (Thermo Scientific) with a 473 nm blue laser as an excitation source. X-ray diffraction patterns were collected on a Panalytical Expert Pro X-ray diffractometer, using Cu K_α radiation (λ=1.5406 Å). Current-voltage (J-V) measurements were performed at room temperature using an Agilent B1500A Semiconductor Device Analyzer. All electrochemical experiments were carried out by using a model PGSTAT302N (Autolab). The experiments were done with a conventional three electrode electrochemical cell. The three electrode system consisted of Ag/AgCl (SCE) as the reference electrode, Pt-disc as the working electrode and Pt-wire as the counter electrode. The photovoltaic devices were illuminated with 100 mW/cm^2 power intensity of white light by an Oriel solar simulator with an AM1.5 filter.

Synthesis of Graphene oxide (GO)

GO was prepared from purified natural graphite powder (Alfa Aesar, ~200 mesh) according to a modified Hummers' method.[23] Specifically, graphite powder (0.5 g) was placed into a cold mixture of concentrated H_2SO_4 (40 mL, 98%) and $NaNO_3$ (0.375 g) under vigorous stirring for 1h, in an ice bath. $KMnO_4$ (3 g) was slowly added into the reaction mixture over 1h. The mixture was then stirred at room temperature for 4h. Afterwards, the reaction mixture was allowed to reach room temperature before being heated to 35 ^oC for 30 min, forming a thick paste. It was then poured into a beaker containing 50 mL of deionized water and further heated to 90 ^oC for 30 min. 200 mL of distilled water was added, followed by a slow addition of H_2O_2 (3 mL, 30%), turning the color of the solution from dark brown to yellow. The reaction mixture was then allowed to settle down and decanted. The graphite oxide obtained was then purified by repeated high-speed centrifugation (4200 rpm, 3 min) and redispersing in deionized water to neutralize the pH (~10 times needed). Finally, the resulting GO was dried at 60 °C in a vacuum oven for 48h.

Synthesis of TPP-NH_2 (5-(4-aminophenyl)-10,15,20-triphenyl)

TPP-NH_2 was prepared according to the literature.[24]

Acylation of GO (GO-COCl)

GO (60 mg) was dispersed in $SOCl_2$ (40 mL) and a catalytic amount of DMF (1 mL) was added. The mixture was sonicated, stirred and refluxed for 24 h at 75 ^oC, under N_2. The excess of thionyl chloride and solvent was removed by distillation under reduced pressure.[25] The obtained solid (GO-COCl) was washed with ultra-dried tetrahydrofuran (THF) three times and dried at 40 ^oC in a vacuum oven for 30 min (Figure 1).

Synthesis of GO-TPP

An amount of the acylated GO-COCl (40 mg) was dispersed in DMF (20 mL) via ultrasonication treatment for 30 min. Then, TPP-NH_2 (60 mg) in excess was added, in the presence of triethylamine (1 mL) as catalyst. The mixture was stirred and refluxed at 130 ^oC for 72 h, under N_2 atmosphere (Figure 1). After the reaction, the solution was cooled to room temperature and then poured into diethylether (~50 ml) to precipitate the product. The product was isolated from the red-purple supernatant by centrifugation (4200 rpm, 5 min). The slushiness precipitate was dried in a vacuum oven at 50 ^oC for 10 min. Thereafter, it was redispersed in THF (~5 mL) through ultrasonication (10 min), and was centrifuged (4200 rpm, 3 min). The above procedure was repeated 5 times using THF and 5 more using $CHCl_3$, as washing solvents, in order to remove the excess of the unreacted TPP-NH_2. The final product was washed with distilled water (5 times) to remove $Et_3N{\cdot}HCl$ and was left in a vacuum oven for drying (65 ^oC, 48 h), yielded ~ 50%.

TiO_x solution preparation

Titanium(iv) isopropoxide ($Ti[OCH(CH_3)_2]_4$, 5 ml), 2-methoxyethanol ($CH_3OCH_2CH_2OH$, 20 ml) and ethanolamine ($H_2NCH_2CH_2OH$, 2 ml) were added to a three-necked flask under nitrogen atmosphere. The solution was then stirred for 1h at room temperature, followed by heating at 80 ^oC for 1h and 120 ^oC for additional 1h. The solution was then cooled to room temperature and 10 ml of methanol was added.

Fabrication of PCDTBT:$PC_{71}BM$:GO-TPP nanocomposites and Measurements of Photovoltaic Devices

PCDTBT:$PC_{71}BM$ were dissolved in 1,2-dichlorobenzene:chlorobenzene (3:1) (*o*-DCB:CB) with a 1:4 (4mg:16mg) ratio and stirred for at least 72 hours at 80 ^{o}C before used. GO-TPP was dispersed in N-Methyl-2-pyrrolidone (NMP) (1 mg/mL) by ultrasonication for 1h, in an ultrasonic bath (Elma S 30 H Elmasonic). After ultrasonication, the dispersion was left to settle for 24h to allow the heavy GO-TPP sheets (with large diameter) to sediment out. The photovoltaic devices reported were fabricated on 15 mm by 15 mm indium tin-oxide (ITO) glass substrates with a sheet resistance of 8-12 Ω/sq. The impurities are removed from the ITO glass through a 3-step cleaning process. As a buffer layer, poly(ethylenedioxythiophene) doped with poly(4-styrenesulfonate) (PEDOT:PSS), purchased from Heraeus, was spin-cast from an aqueous solution on the ITO substrate at 6000 rpm for 60 seconds and the average thickness of the layer was 30 nm, followed by baking for 15 min at 120 °C inside a nitrogen-filled glove box. Then, GO-TPP dispersion (supernatant) was blended into the PCDTBT:$PC_{71}BM$ solution and mixed for 2h. Composite blends with 0.1, 0.2, 0.3, 0.4 and 0.5% GO-TPP, were prepared. All photoactive layers were subsequently deposited by spin-coating the blend solutions at 1000 rpm on top of PEDOT:PSS layer until the thickness reaches approximately 80nm. The TiO_x interlayer was dissolved in methanol (1:200) and then spin-coated to a thickness of approximately 10 nm (6000 rpm, 40 s) in air.[26] The sample was heated at 80 ^{o}C for 1 min in air. Lastly, 100 nm of Al was deposited through a shadow mask by thermal evaporation on the devices through a shadow mask to define an active area of 18 mm^2 for each device. The performances of the devices were measured at room temperature with an Air Mass 1.5 Global (A.M. 1.5 G) solar simulator at an intensity of 100 mW/cm^2. A reference monocrystalline silicon solar cell from Newport was used to calibrate the lamp. All measurements were made in air immediately after device fabrication.

3. Results and Discussion

Synthesis and characterization

The covalent linking of GO and TPP-NH_2 took place between the carboxyl functional side groups of GO and the porphyrin amino groups, forming amide bonds (CONH).

The synthesis of GO-TPP was carried out by refluxing TPP-NH_2 and GO-COCl in DMF at 130 ^oC for 72 h in presence of triethylamine. It is noted that the acylated GO-COCl is extremely sensitive in ambient conditions and therefore it is immediately used in the next step of the reaction; the covalent linking with the TPP-NH_2 molecule, which is added in excess. The yielded product is washed thoroughly with THF and $CHCl_3$ in order to remove the excess of TPP-NH_2 and deionized water to remove the formed $Et_3N{\cdot}HCl$. The functional groups as well as the bonds of GO and GO-TPP were identified by FT-IR spectroscopy (Figure 2a). Primarily, the spectrum of GO (black) displays that the OH stretching vibration appears as a broad peak at 3390 cm^{-1}.

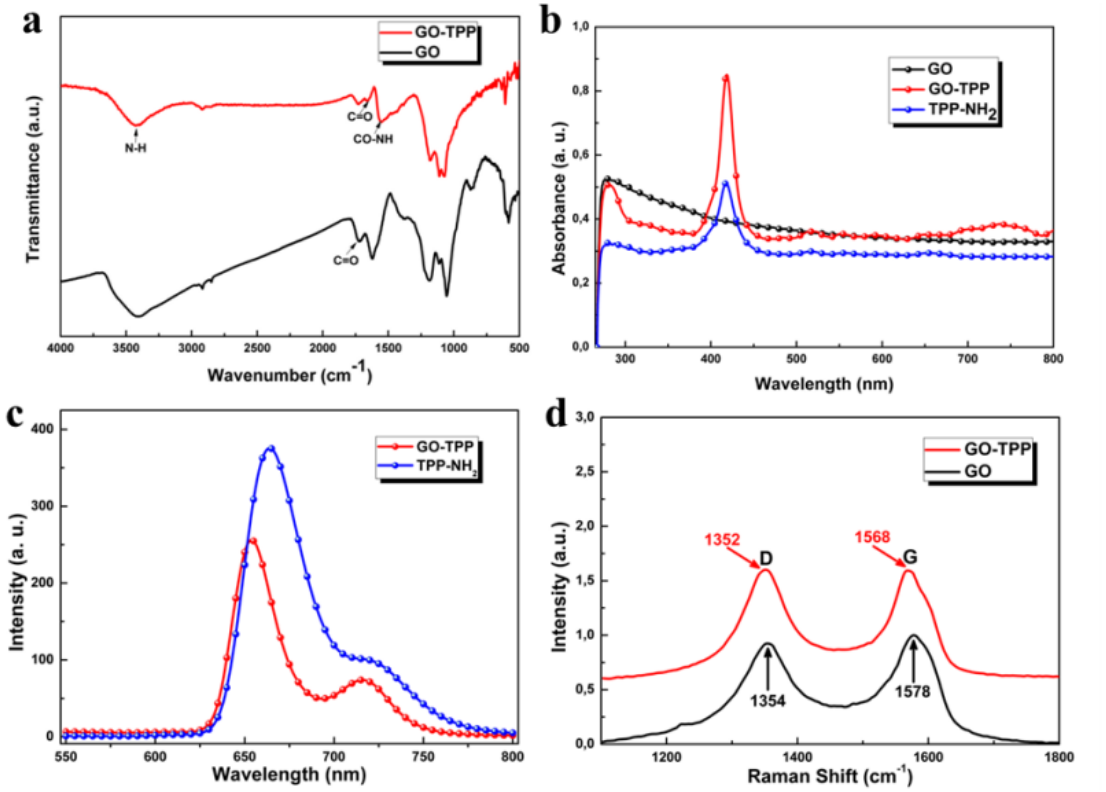

Figure 2. Characterization of GO (black line) and GO-TPP (red line). a) FT-IR spectra, b) UV-vis spectra including the UV-vis spectrum of TPP-NH_2, c) Room-temperature fluorescence spectra of isoabsorbing (A = 0.24) DMF solutions of TPP-NH_2 (blue line) and GO-TPP (red line) after excitation at 419 nm and d) Raman spectra.

Moreover, the most characteristic features in the FT-IR spectrum of GO are the adsorption bands corresponding to the C=O carbonyl stretching at ~1726 wavenumbers (cm^{-1}), the C-OH stretching at 1220 cm^{-1} and the C-O stretching at 1053 cm^{-1}. The spectrum of GO-TPP (red) exhibits a new peak at ~1650 cm^{-1} which corresponds to the C=O characteristic stretching band of the amide group, while the peak at ~1726 cm^{-1}

of GO is significantly quenched.[27] This quenching proves that an important proportion of the carboxyl groups of the GO core is converted to amide bonds. It can be originated from either amides or carbamate esters that correspond to the coupling of the C-N stretching vibration with the CHN deformation vibration which amide stretching band CO-NH occurs at ~1556 cm^{-1}.[28]

Figure 2b shows UV-vis absorption spectra of GO (black), TPP-NH_2 (blue) and GO-TPP (red) in DMF, GO exhibits a characteristic absorption band at λ_{max}(DMF ~0.02 mg/mL)/280 nm. The spectra of TPP-NH_2 and GO-TPP appear strong Soret absorption band for both at 418 nm and weak Q-bands between 500 and 700 nm, which are consistent with that of porphyrins reported.[29]

In order to investigate the electronic interactions of the porphyrin units with the GO sheets in the excited state, fluorescence spectroscopy was applied. Upon excitation of TPP-NH_2 and GO-TPP at the Soret band (419 nm), where the absorbance was adjusted to be identical at the excitation wavelength, the characteristic fluorescence emission of $TPPNH_2$ was significantly quenched in GO-TPP hybrid material as displayed at room-temperature fluorescence spectra of isoabsorbing (A= 0.24) DMF solutions in Figure 2c. Except of the quenching, the emission of the TPP-NH_2 at 664 nm was also blue shifted by 10 nm to 654 nm. It's difficult to quantify the quenching since the GO alone, also absorbs at the excitation wavelength. However, the observed emission quenching of the porphyrin indicates that there is a strong interaction between the singlet excited state of the porphyrin and the GO part in the nano-hybrid material. This quenching may be attributed to either photoinduced electron transfer or energy transfer processes from the porphyrin chromophore to the GO sheets.

An additional proof of functionalization of GO was provided by Raman spectroscopy and can give information on the number and orientation of atomic layers of GO, as well as the presence of doping and defects. Figure 2d depicts the Raman spectra of GO (black line) and GO-TPP (red line). GO Raman spectrum shows two typical broad peaks at 1354 and 1578 cm^{-1}, corresponding to defect-induced D and in-plane vibration of sp^2 carbon G bands, respectively, with I_D/I_G ratio of 0.92. The functionalized GO with various porphyrins results in small changes in the D and G peaks. The I_D/I_G ratio of GO-TPP is increased (1.01) compared to GO, which is attributed to the functionalization of graphene through covalent bonding.[30] Therefore,

the increased intensity ratio of I_D/I_G accounts for a lower degree of crystallinity of graphite materials.[31] In particular, the D and G bands are shifted from 1354 to 1352 cm^{-1} and 1578 to 1568 cm^{-1}, respectively.

Cyclic voltammetry (CV) was used to calculate the energy levels of the graphene oxide-porphyrin hybrid material.

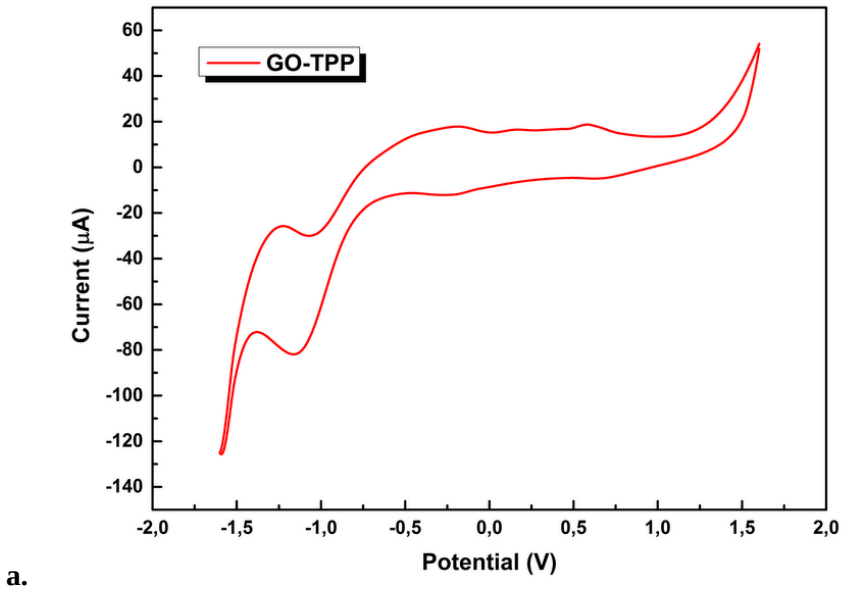

a.

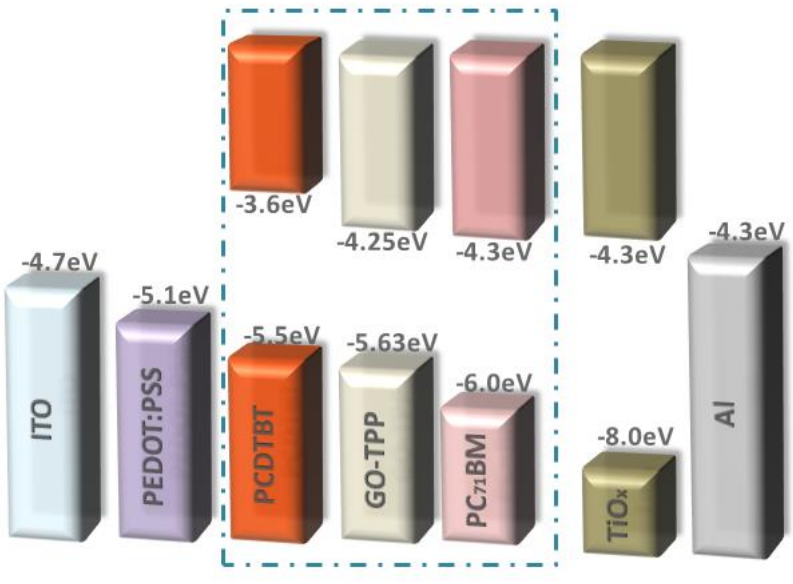

b.

Figure 3. a) Cyclic voltammetry curve of GO-EDNB in CH_3CN using 0.1 M Tetrabutylammonium hexafluorophosphate (TBAPF6) as the electrolyte, at a scan rate of 10 mV s^{-1}. b) Energy levels diagram of photovoltaic device components referenced to the vacuum level.

According to the literature, the molecular orbital energy levels can be measured by the voltammographs from the onset potential of the reduction and oxidation process. Ferrocene (Aldrich, 98%), Tetrabutylammonium hexafluorophosphate >99.0% (TBAPF6, Fluka, electrochemical analysis >99%), acetonitrile (Acros Organics, extra dried and distilled >99.9%), were used as received, without further purification. Figure 3 demonstrates the voltammetric behavior of GO-TPP in CH_3CN using 0.1 M Tetrabutylammonium hexafluorophosphate (TBAPF6) as the electrolyte, at a scan rate of 10 mV s^{-1}, between the potential sweep window of 1.6 V to −1.6 V (Figure 3a) and the energy levels diagram of photovoltaic device components referenced to the vacuum level (Figure 3b). The calculations of HOMO and LUMO levels were based on the following empirical relations from the literature.[32]

$E_{HOMO} = -(E_{[onset,\ ox\ vs.\ Fc+/Fc]} + 5.1)$ (eV) and

$E_{LUMO} = -(E_{[onset,\ red\ vs.\ Fc+/Fc]} + 5.1)$ (eV)

The HOMO level of GO-TPP is approximately 5.63 eV calculated by the oxidation peak onset 0.53 V, while the LUMO level extracted from the onset of the reduction peak (0.85 V) is 4.25 eV.

To evaluate the linked TPP onto the graphene oxide backbone sheet, thermogravimetric analysis (TGA) was used. Figure 4 displays the TGA curves of GO (black) and GO-TPP (red), respectively. GO begins to lose mass upon heating even below 100 °C and has resulted in a rapid mass loss commencing at about 200 °C, probably due to pyrolysis of labile oxygen-containing functional groups, such as -OH, -CO and -COOH groups, and decomposes above 600 ºC, with a total mass loss of ∼40 % at 800 °C, in agreement with data in the literature.[19] The TGA curve of GO-TPP exhibits approximately 23% weight loss, relative to graphene oxide, between 250 and 500 ºC. This weight loss is attributed to the loss of TPP molecules covalently attached to graphene oxide. Accordingly, the degree of functionalization was estimated to be one TPP group per ~170 carbon atoms in GO-TPP.[33]

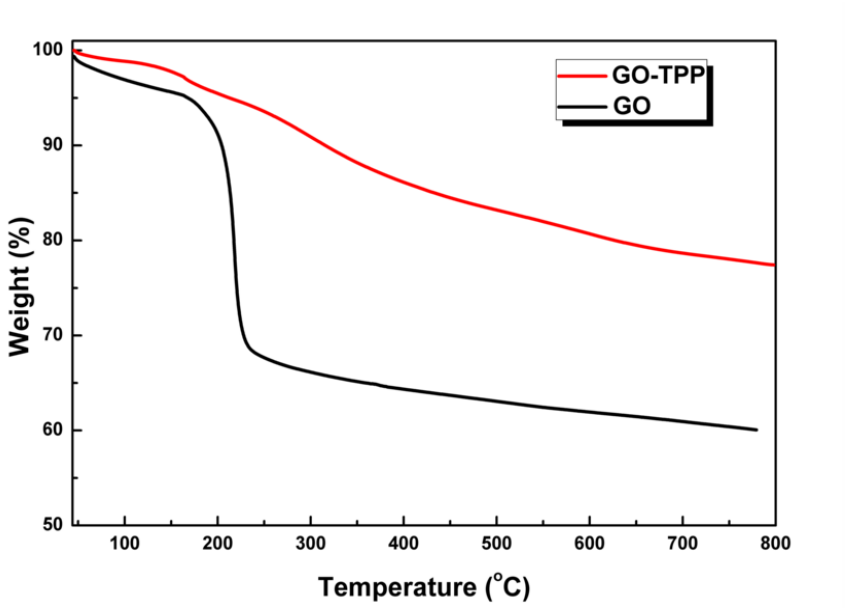

Figure 4. Thermogravimetric Analysis. TGA curves of GO (black) and GO-TPP (red).

Finally, BHJ photovoltaic devices were fabricated by using GO-TPP in the photoactive layer as additive material. Different volume ratios of GO-TPP to the blend PCDTBT:$PC_{71}BM$ were used (0.1, 0.3 and 0.5 %). The structure of the device is thus, ITO/PEDOT:PSS(30 nm)/PCDTBT:$PC_{71}BM$:GO-TPP(80 nm)/ TiO_x(10 nm) /Al (100 nm), schematically shown in Figure 5a, while in Figure 5b are displayed the current voltage (*J*-V) curves for the photovoltaic devices with GO-TPP content.

Table 6.1 displays the photovoltaic characteristics of the fabricated devices and points out that the device containing 0.3 % GO-TPP showed the best photovoltaic performance exhibiting an open-circuit voltage (V_{oc}) of 0.84 V, J_{sc} of 13.81 mA/cm^2, fill factor (FF) of 51 % and a power conversion efficiency (η) of 5.93 %, which was increased by ~10 % compared to the device without the graphene-porphyrin content. Moreover, the device with 0.5 % GO-TPP showed the highest J_{sc} of ~15 mA/cm^2, η of 5.58% with a V_{oc} of 0.81 V and a FF of 46 %.

GO-TPP (%)	J_{sc} (mA/cm^2)	V_{oc} (V)	FF (%)	PCE (%)
0	11.28	0.86	55.7	5.40
0.1	12.76	0.84	53.6	5.77
0.3	13.81	0.84	51.0	5.93
0.5	14.99	0.81	46.2	5.58

Table 6.1 Device Performance of Photovoltaic Devices Based on PCDTBT:$PC_{71}BM$:GO-TPP Composites with Different GO-TPP Content.

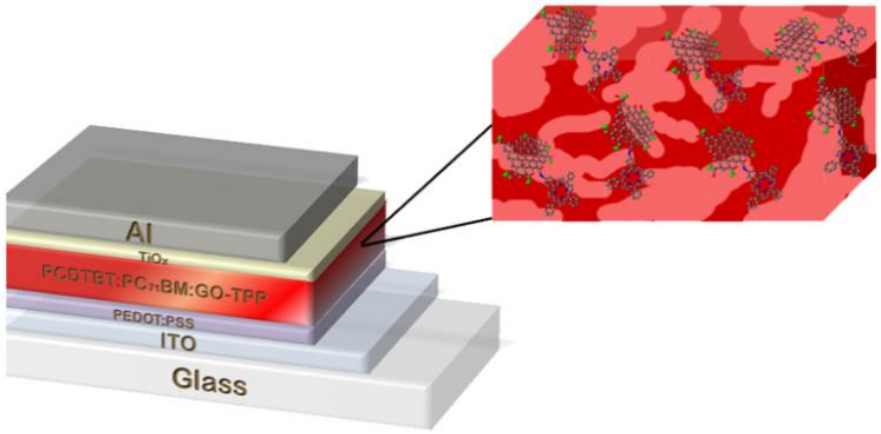

a.

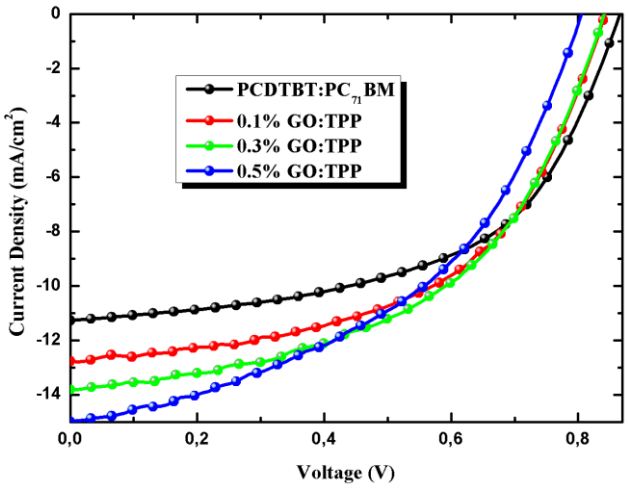

b.

Figure 5. a) Schematic of the photovoltaic device with PCDTBT:$PC_{71}BM$:GO-TPP thin film as the active layer and the structure ITO/PEDOT:PSS/PCDTBT:$PC_{71}BM$:GO-TPP/TiO_x/Al (top). b) Experimental *J*−V curves of the photovoltaic devices based on PCDTBT:$PC_{71}BM$ (black curve) and PCDTBT:$PC_{71}BM$:GO-TPP composites (red curve, 0.1%; green curve, 0.3%); blue curve, 0.5%).

The main observation is that the efficiency was increased when the concentration of the graphene-porphyrin content was increased relatively to the blend (PCDTBT:$PC_{71}BM$). Although, there is a threshold to GO-TPP concentration, when higher concentrations were used, large aggregates were formed, which hindered exciton generation and charge separation and thus leading to reduced efficiencies.

In order to have an insight about the mechanism responsible for the enhanced photocurrent and performance of the devices, we measured the hole and electron-only space-charge-limited current density (SCLC). The electron only devices had the structure: ITO/Al/PCDTBT:$PC_{71}BM$:GO-TPP/TiO_x/Al and the hole only

devices had the structure: ITO/PEDOT:PSS/PCDTBT:$PC_{71}BM$:GO-TPP/MoO_3/Au. The SCLC is modelled using the Mott–Gurney equation:

$$J_{SCLC} = \frac{9}{8}\varepsilon_0\varepsilon_r\mu_e\frac{(V - V_{bi})^2}{d^3}$$

where J_{SCLC} is the current density of SCLC, ε_r is the relative permittivity of the organic active layer, ε_0 is the permittivity of free space, V is the applied voltage, V_{bi} is the built-in voltage, μ is the charge mobility, and d is the thickness of the active layer. Thus, by fitting this equation to the experimental data, the charge mobilities of the devices were calculated (**Table 6.2**). The addition of the GO-TPP as additive in the active layer balance the values of electron and hole mobilities. This mobility balance avoid building up of space charges which is detrimental for device efficiency and thus is responsible for the increase in J_{sc} and photovoltaic performance. This balance in charge mobilities indicate optimized carrier transport.

GO-TPP (%)	μ_h ($cm^2 V^{-1}s^{-1}$)	μ_e ($cm^2 V^{-1}s^{-1}$)	μ_e/μ_h
0	$9.64\ 10^{-5}$	$2.28\ 10^{-4}$	2.36
0.1	$9.72\ 10^{-5}$	2.2110^{-4}	2.27
0.3	$9.86\ 10^{-5}$	2.1110^{-4}	2.14
0.5	$9.68\ 10^{-5}$	$2.25\ 10^{-4}$	2.32

Table 6.2. Hole and Electron Mobilities of PCDTBT:$PC_{71}BM$:GO-TPP based Device with Different GO-TPP Content

4. Conclusion

We have synthesized a graphene-based material, consisting of graphene oxide covalently linked with porphyrin moieties. The resulting material, GO-TPP was thoroughly characterized and incorporated, in different concentrations (0.1, 0.3 and 0.5 %), ratio to the blend volume, into the active layer of PCDTBT:$PC_{71}BM$, forming ternary blends. The addition of GO-TPP tuned the energy levels of D-A, facilitating the electron-cascade effect. The ideal ternary blend of the structure ITO/PEDOT:PSS/PCDTBT:$PC_{71}BM$:GO-TPP/TiO_x/Al has been formed containing 0.3% of GO-TPP, resulted an increased short circuit current density (J_{sc}) about ~33%, achieving PCE of 5.93%, displaying an enhancement of ~10%, compared to the reference blend.

References

1. M. Kaltenbrunner, M. S. White, E. D. Głowacki, T. Sekitani, T. Someya, N. S. Sariciftci and S. Bauer, *Nat. Commun.*, 2012, **3**, 770 doi:10.1038/ncomms1772.
2. C. J. Brabec, N. S. Sariciftci and J. C. Hummelen, *Adv. Funct. Mater.*, 2001, **11**, 15.
3. S. Liu, K. Zhang, J. Lu, J. Zhang, H.-L. Yip, F. Huang and Y. Cao, *J. Am. Chem. Soc.*, 2013, **135**, 15326.
4. S.-H. Liao, H.-J. Jhuo, P.-N. Yeh, Y.-S. Cheng, Y.-L. Li, Y.-H. Lee, S. Sharma and S.-A. Chen, *Sci. Rep.*, 2014, **4**, 6813.
5. S.-H. Liao, H.-J. Jhuo, Y.-S. Cheng and S.-A. Chen, *Adv. Mater.*, 2013, **25**, 4766.
6. J. You, L. Dou, K. Yoshimura, T. Kato, K. Ohya, T. Moriarty, K. Emery, C.-C. Chen, J. Gao, G. Li and Yang Yang, *Nat. Commun.*, 2013, **4**, 1446.
7. Z. He, C. Zhong, X. Huang, W.-Y. Wong, H. Wu, L. Chen, S. Su and Y. Cao, *Adv. Mater.*, 2011, **23**, 4636.
8. Z. He, C. Zhong, S. Su, M. Xu, H. Wu and Y. Cao, *Nat. Photon.*, 2012, **6**, 591.
9. T. Ameri, P. Khoram, J. Min and C. J. Brabec, *Adv. Mater.*, 2013, **25**, 4245.
10. G. Dennler, M. C. Scharber, C. J. Brabec, *Adv. Mater.*, 2009, **21**, 1323.
11. G. H. Jun, S. H. Jin, B. Lee, B. H. Kim, W.-S. Chae, S. H. Hong and S. Jeon, *Energy & Environ. Sci.*, 2013, **6**, 3000.
12. P. Robaeys, F. Bonaccorso, E. Bourgeois, J. D'Haen, W. Dierckx, W. Dexters, D. Spoltore, J. Drijkoningen, J. Liesenborgs, A. Lombardo, A. C. Ferrari, F. Van Reeth, K. Haenen, J. V. Manca and Milos Nesladek, *Appl. Phys. Lett.*, 2014, **105**, 083306.
13. K. S. Novoselov, A. K. Geim, S. V. Morozov, D. Jiang, Y. Zhang, S. V. Dubonos, I. V. Grigorieva, A. A. Firsov, *Science*, 2004, **306**, 666.
14. A. K. Geim and K. S. Novoselov, *Nat. Mater.*, 2007, **6**, 183.
15. M. D. Stoller, S. Park, Y. Zhu, J. An and R. S. Ruoff, *Nano Lett.*, 2008, **8**, 3498.
16. G. Eda, G. Fanchini and M. Chhowalla, *Nat. Nanotech.*, 2008, **3**, 270.
17. J. I. Paredes, S. Villar-Rodil, A. Martinez-Alonso and J. M. D. Tascon, *Langmuir*, 2008, **24**, 10560.
18. D. Konios, M. Stylianakis, E. Stratakis and E. Kymakis, *J. Colloid Interface Sci.*, 2014, **430**, 108.
19. M. M. Stylianakis, E. Stratakis, E, Koudoumas, E. Kymakis and S. H. Anastasiadis, *ACS Appl. Mater. & Interfaces*, 2012, **4**, 4864.
20. M. M. Stylianakis, G. D. Spyropoulos, E. Stratakis and E. Kymakis, *Carbon*, 2012, **50**, 5554.
21. D. M. Guldi and M. Prato, *Acc. Chem. Res.*, 2000, **33**, 695.
22. L. Lu, T. Xu, W. Chen, E. S. Landry and L. Yu, *Nat. Photon.*, 2014, **8**, 716.
23. Q. Su, S. Pang, V. Alijani, C. Li, X. Feng and K. Mullen, *Adv. Mater.*, 2009, **21**, 3191.
24. K. Ladomenou, T. Lazarides, M. K. Panda, G. Charalambidis, D. Daphnomili and A. G. Coutsolelos, *Inorg. Chem.*, 2012, **51**, 10548.
25. M. M. Stylianakis, J. A. Mikroyannidis and E. Kymakis, *Sol Energy Mater. Sol Cells*, 2010, **94**, 267.

26. D. H. Wang, S. H. Im, H. K. Lee, J. H. Park and O. O. Park , *J. Phys. Chem. C*, 2009, **113**, 17286.
27. M. O. Senge, M. Fazekas, E. G. A. Notaras, W. J. Blau, M. Zawadzka, O. B. Locos and E. M. Ni Mhuircheartaigh, *Adv. Mater.*, 2007, **19**, 2737.
28. H. Gunzler and H. U. Gremlich, *Winheim: Wiley-VSH*, 2002, 223.
29. Z.-B. Liu, Y.-F. Xu, X.-Y. Zhang, X.-L. Zhang, Y.-S. Chen and J.-G. Tian, *J. Phys. Chem. B*, 2009, **113**, 9681.
30. M. Quintana, K. Spyrou, M. Grzelczak, W. R. Browne, P. Rudolf and M. Prato, *ACS Nano*, 2010, **4**, 3527.
31. M. Bala Murali Krishna, N. Venkatramaiah, R. Venkatesan and D. Narayana Rao, *J. Mater. Chem.*, 2012, **22**, 3059.
32. C. M. Cardona, W. Li, A. E. Kaifer, D. Stockdale and G. C. Bazan, *Adv. Mater.*, 2011, **23**, 2367.
33. X. Zhang, L. Hou, A. Cnossen, A. C. Coleman, O. Ivashenko, P. Rudolf, B. J. van Wees, W. R. Browne and B. L. Feringa, *Chem. Eur. J.*, 2011, **17**, 8957.

Conclusions and suggested future works

In this dissertation, the design and synthesis of novel solution-processed graphene-based materials are presented. Different small molecules have been attached to the basal graphene sheets with simple chemical and photochemical synthetic routes and their structures were extensively confirmed by various spectroscopic and microscopic methods. Our successful attempt managed to combine the unique properties of graphene with the optical, mechanical and electrical properties of the small molecules attached. Furthermore, the opportunity to control their properties upon fine-tuning by different processes (irradiation time, degree of functionalization etc), renders the resulting solution-processed graphene-based materials ideal perspectives for organic photovoltaic applications. Specifically, graphene-based materials have been introduced into the photoactive layer, as electron-acceptor materials, alternative to the state of the art fullerene derivatives ($PC_{60}BM$, $PC_{71}BM$). In addition, they have been used as electron-cascade donor materials, constituting the third component to a ternary organic blend, along with polymer/fullerene composites. In both cases, this study demonstrates the fabrication of high performance OPVs, yielding efficiencies higher or comparable to the literature.

During my thesis preparation, various conclusions have been put under consideration. New ideas and suggestions have been emerged to extend beyond my present research horizon. Some of my ideas are collocated in the following paragraph and are provided for future work.

The most important concept proposed is emanated from the photochemical synthesis of the above mentioned LGO-EDNB in Chapter 5, where the energy levels of the graphene-based material could be readily tuned upon irradiation by a laser beam. This opportunity opens new avenues for graphene engineering, since new graphene-based materials can be synthesized with selective HOMO and LUMO levels. Highly efficient ternary blend organic solar cells can be fabricated, introducing graphene-based electron-cascade donor/acceptor materials. Matching the energy levels of the two main components of the active layer, ideal band offsets can be provided, facilitating the excitons dissociation for both hole and electron transport to the opposite electrodes.

Finally, besides this very challenging and promising project, the bandgap tuning associated with their properties regulation (transmittance, conductivity, etc) upon laser

irradiation, could be crucial for the realization of all graphene-based OSCs. Graphene-based materials, in dependence on the irradiation dose, can be exploited as buffer layers, as well as transparent, conductive electrodes.

Acknowledgement of previous publications

This thesis dissertation is composed in part of independent articles that have been published previously, are currently in submission, or under review. Specifically, the materials presented in Chapter 3 and 4 are results from (Stylianakis et al. *ACS Applied Materials & Interfaces* 2012, 4, 4864) and (Stylianakis et al. *Carbon* 2012, 50, 5554), respectively. All results and materials presented in Chapter 5 are in part of (Stylianakis et al. *Advanced Optical Materials* 2014 (accepted), DOI: 10.1002/adom.201400450). Similarly, all materials and part of the results described in Chapter 6 are under submission (Stylianakis et al. 2015, *under Submission*).

Curriculum Vitae

Minas Stylianakis

Research assistant

Chemistry Department,

University of Crete,

Centre of Materials Technology & Photonics,

Technological Educational Institute (TEI) of Crete,

Heraklion, 71004 Crete, Greece.

Tel./Fax: +30-2810-379775

Mob: +30-6932541404

E-mail: stylianakis@staff.teicrete.gr

Website: http://nano.teicrete.gr/

Education:

University of Crete, Chemistry dept., Heraklion, Crete, Greece.

PhD candidate in Chemistry, October 2014.

University of Patras, Chemistry dept., Patras, Greece.

Master of Science in Chemistry, October 2009.

University of Patras, Chemistry dept., Patras, Greece.

Bachelor of Science in Chemistry, December 2007.

Work Experience:

Teaching Assistant, Assisted in instruction of the undergraduate laboratory course in "Analytical Chemistry" (Chem. Dept., Univ. of Patras 2007-2009).

Adjunct laboratory assistant, Dept. of Sciences, TEI of Crete, Greece (Sep 2010-today).

Teaching duties:

i) Laboratory courses in Advanced Materials
ii) Biochemistry

Publications

1. **Novel blue-greenish electroluminescent poly(fluorenevinylene-alt dibenzothiophenevinylene)s and their model compounds**
   Journal of Polymer Science Part A: Polymer Chemistry 2006, 44, 6790-6800.
   John A. Mikroyannidis, Helen A. Moshopoulou, John A. Anastasopoulos, **Minas M. Stylianakis**, Larysa Fenenko, Chihaya Adachi.

2. **Alternating phenylenevinylene and thienylenevinylene copolymers with cyano groups: Synthesis, photophysics and photovoltaics**
   Synthetic Metals 2009, 159, 142-147.
   John A. Mikroyannidis, **Minas M. Stylianakis**, Kai Yin Cheung, Man Kin Fung, Aleksandra B. Djurišić.

3. **A Novel Alternating Phenylenevinylene Copolymer with Perylene Bisimide Units: Synthesis, Photophysical, Electrochemical, and Photovoltaic Properties**
   J. Phys. Chem. C, 2009, *113*, 7904-7912.
   John A. Mikroyannidis, **Minas M. Stylianakis**, G. D. Sharma, P. Balraju, M. S. Roy.

4. **New 4,7-dithienebenzothiadiazole derivatives with cyano-vinylene bonds: Synthesis, photophysics and photovoltaics**
   Synthetic Metals 2009, 159, 1471-1477.
   John A. Mikroyannidis, **Minas M. Stylianakis**, Qingfeng Dong, Yinhua Zhou, Wenjing Tian.

5. **Synthesis, photophysical and photovoltaic properties of star-shaped molecules with triphenylamine as core and phenylethenylthiophene or dithienylethylene as arms**
   Solar Energy Materials & Solar Cells 2009, 93, 1952-1958.
   Minas M. Stylianakis, John A. Mikroyannidis, Qingfeng Dong, Jianing Pei, Zhaoyang Liu, Wenjing Tian.

6. **Alternating Phenylenevinylene-Copolymers with Dithienbenzothiadiazole Moieties: Synthesis, Photophysical and Photovoltaic Properties**
   Journal of Applied Polymer Science 2009, 114, 2740-2750.
   John A. Mikroyannidis, **Minas M. Stylianakis**, Qingfeng Dong, Wenjing Tian.

7. **Synthesis, photophysics of two new perylene bisimides and their photovoltaic performances in quasi solid state dye sensitized solar cells**
   Journal of Power Sources 2009, 194, 1171-1179.
   John A. Mikroyannidis, **Minas M. Stylianakis**, M.S. Roy, P. Suresh, G. D. Sharma.

8. **Efficient Hybrid Bulk Heterojunction Solar Cells Based on Phenylenevinylene Copolymer, Perylene Bisimide and TiO_2**
   Solar Energy Materials & Solar Cells 2009, 93, 1792-1800.
   John A. Mikroyannidis, **Minas M. Stylianakis**, P. Suresh and G. D. Sharma.

9. **Low Band Gap Vinylene Compounds with Triphenylamine and Benzothiadiazole Segments for Use in Photovoltaic Cells**
   Organic Electronics 2009, 10, 1320-1333.
   John A. Mikroyannidis, **Minas M. Stylianakis**, P. Suresh, P. Balraju and G. D. Sharma.

10. **A facile, covalent modification of single-wall carbon nanotubes by thiophene for use in organic photovoltaic cells**
    Solar Energy Materials and Solar Cells 2010, 94, 267-274.
    Minas M. Stylianakis, John A. Mikroyannidis, Emmanuel Kymakis.

11. **Novel p-Phenylenevinylene Compounds Containing Thiophene or Anthracene Moieties and Cyano-Vinylene Bonds for Photovoltaic Applications**
    ACS Applied Materials & Interfaces 2009, 1, 1711-1718.
    John A.Mikroyannidis, **Minas M. Stylianakis**, P. Balraju, P. Suresh, G. D. Sharma.

12. **Effect of Incorporation of a Low Band Gap Small Molecule in Conjugated Vinylene Copolymer : PCBM Blend for Organic Photovoltaic Devices**
    ACS Applied Materials & Interfaces 2009, 1, 1370-1374.
    P. Suresh, P. Balraju, G. D. Sharma, John A. Mikroyannidis, **Minas M. Stylianakis**.

13. **Bulk heterojunction organic photovoltaic devices based on low band gap small molecule BTD-TNP and perylene-anthracene diimide**
    Solar Energy Materials & Solar Cells 2009, 93, 2025-2028.
    G. D. Sharma, P. Balraju, John A. Mikroyannidis, **Minas M. Stylianakis**.

14. **Synthesis of perylene monoimide derivative and its use for quasi-solid-state dye-sensitized solar cells based on bare and modified nano-crystalline ZnO photoelectrodes**
    Energy & Environmental Science 2009, 2, 1293-1301.
    John A. Mikroyannidis, **Minas M. Stylianakis**, P. Suresh, M. S. Roy, G. D. Sharma.

15. **Efficient Bulk Heterojunction Devices based on Phenylenevinylene Small Molecule and Perylene-Pyrene Bisimide**
    Journal of Materials Chemistry 2010, 20, 561-567.
    G. D. Sharma, P. Suresh, John A. Mikroyannidis, **Minas M. Stylianakis**.

16. **Plasmonic organic photovoltaics doped with metal nanoparticles**
    Photonics and Nanostructures-Fundamentals and Applications 2011, 9, 184-189.
    G. D. Spyropoulos, **Minas M. Stylianakis**, E. Stratakis, E. Kymakis.

17. **Spin coated graphene films as the transparent electrode in organic photovoltaic devices**
Thin Solid Films 2011, 520, 1238-1241.
E. Kymakis, E. Stratakis, **M. M. Stylianakis**, E. Koudoumas, C. Fotakis.

18. **Spin coated carbon nanotubes as the hole transport layer in organic photovoltaics**
Solar Energy Materials and Solar Cells 2012, 96, 298-301.
E. Kymakis, **M. M. Stylianakis**, G. D. Spyropoulos, E. Stratakis, E. Koudoumas, C. Fotakis.

19. **Efficiency enhancement of organic photovoltaics by addition of carbon nanotubes into both active and hole transport layer**
Applied Physics Letters 2012, 100, 093301/1-093301/5.
M. M. Stylianakis, E. Kymakis.

20. **Organic bulk heterojunction photovoltaic devices with surfactant-free Au nanoparticles embedded in the active layer.**
Applied Physics Letters 2012, 100, 213904/1-213904/5.
G. D. Spyropoulos, **M. M. Stylianakis**, E. Stratakis, E. Kymakis.

21. **Solution-processable graphene linked to 3,5-dinitrobenzoyl as an electron acceptor in organic bulk heterojunction photovoltaic devices**
Carbon 2012, 50, 5554-5561.
Stylianakis M. M., Spyropoulos G. D., Stratakis, E., Kymakis, E.

22. **Organic bulk heterojunction photovoltaic devices based on polythiophene-graphene composites.**
ACS Applied Materials & Interfaces 2012, 4, 4864-4870.
Stylianakis M. M., Stratakis E., Koudoumas E., Kymakis E, Anastasiadis S. H.

23. **Flexible Organic Photovoltaic Cells with In Situ Nonthermal Photoreduction of Spin-Coated Graphene Oxide Electrodes**
Advanced Functional Materials 2013, 23, 2742-2749.
Emmanuel Kymakis, Kyriaki Savva, **Minas M. Stylianakis**, Costas Fotakis, Emmanuel Stratakis.

24. **Plasmonic organic photovoltaic devices with graphene based buffer layers for stability and efficiency enhancement**
Nanoscale 2013, 5, 4144-4150.
Stratakis E., **Stylianakis M. M.**, Koudoumas E., Kymakis E.

25. **Optical limiting action of few layered graphene oxide dispersed in different solvents**
Optical Materials 2013, 36, 112-117.
Liaros N., Iliopoulos K., **Stylianakis M. M.**, Koudoumas E., Couris S.

26. **Enhanced Field Emission from Reduced Graphene Oxide Polymer Composites**
ACS Applied Materials & Interfaces 2014, 6, 388-393.
Georgios M. Viskadouros, **Minas M. Stylianakis**, Emmanuel Kymakis, Emmanuel Stratakis.

27. **Enhanced Field Emission from Reduced Graphene Oxide Polymer Composites**
Small 2014, 10, 2398-2403.
Georgios M. Viskadouros, A. Zak, **M. Stylianakis**, E. Kymakis, R. Tenne, E. Stratakis.

28. **Dispersion behavior of graphene oxide and reduced graphene oxide**
Journal of Colloid & Interface Science 2014, 430, 108-112.
Konios D., **Stylianakis M. M.**, Stratakis E., Kymakis E.

29. **Photochemical synthesis of Solution-Processable Graphene derivatives with Tunable Band-gap for Organic Solar Cells**
Advanced Optical Materials 2014, DOI: 10.1002/adom.201400450.
Minas M. Stylianakis, Maria Sygletou, Kyriaki Savva, George Kakavelakis, Emmanuel Kymakis, Emmanuel Stratakis.

30. **Functionalized Graphene as an Electron Cascade Acceptor for Air Processed Organic Ternary Solar Cells**
Advanced Functional Materials 2015, DOI: 10.1002/adfm.201501052.
Francesco Bonaccorso, Nikolaos Balis, **Minas M. Stylianakis**, Marika Savarese, Carlo Adamo, Mauro Gemmi, Vittorio Pellegrini, Emmanuel Stratakis, Emmanuel Kymakis.

31. **Rational design of graphene/polymer photovoltaic interfaces from atoms to devices**
Under Submission, 2015.
Keian Noori, Dimitrios Konios, **Minas M. Stylianakis**, Emmanuel Kymakis and Feliciano Giustino.

32. **Graphene Oxide Porphyrin-based Molecule for Efficient Ternary Blend Organic Solar Cells**
Under Submission, 2015.
M. M. Stylianakis, D. Konios, G. Kakavelakis, G. Charalambidis, E. Stratakis, A. G. Coutsolelos, E. Kymakis, S. H. Anastasiadis.